CANCER HYPERTHERMIA USING GOLD AND MAGNETIC NANOPARTICLES

Anil Pravin Patel

(BSc, Mres)

Submitted in fulfilment of requirements for the degree of Doctor of Philosopy (PhD)

Centre for Cell Engineering
Institute of Molecular, Cell and System Biology
School of Medical, Veterinary and Life Sciences
University of Glasgow
Glasgow, G12 8QQ
December 2016

Abstract

An estimated 12 million people worldwide are diagnosed with cancer every year, with around 17 million cancer-related deaths per year predicted by 2030 (Thun et al. 2010). Contemporary clinical treatments include surgery, chemotherapy and radiotherapy, however all vary in success and exhibit unpleasant side effects. Localised tumour hyperthermia is a moderately new cancer treatment envisaged by researchers, which exploits exclusive tumour vulnerabilities to specific temperature profiles (42-45°C) leading to cancer cell apoptosis, whilst normal tissue cells are relatively unaffected. Hyperthermia is therefore proposed as an alternative potential therapy for cancer, by delivering localised treatment to cancer cells, without the severe side effects associated with traditional therapies.

This project aimed to investigate potential hyperthermic treatment of cancer cells *in vitro* by adopting nanomedicine principles. Inorganic nanoparticles, such as gold or iron oxide, are both capable of generating heat when appropriately stimulated, therefore both have been suggested as candidates for inducing localised tumour heating following their internalisation into cells. In this project, both gold (GNPs) and magnetic (mNPs) were individually assessed for their potential to deliver toxic thermal energy to bone cancer cells (MG63) and breast cancer cells (MCF-7). Studies were carried out both in standard 2D monolayer and in 3D tumour spheroids.

When considering use *in vivo*, it is essential that both GNPs and mNPs are biocompatible, therefore initial studies characterised the cell viability and metabolic activity following incubation with the NPs. The NP internalisation was subsequently verified, prior to hyperthermic studies. Following hyperthermic treatment, both GNPs and mNPs were confirmed as inducing cancer cell death. Further studies were carried out using the GNPs, to identify the cell death pathways activated, where mitochondrial stress was evident following 2D culture tests. Gene and protein expression analysis indicated that cell death occurred predominantly *via* several apoptotic pathways, through increased fold expression changes in apoptotic markers. Interestingly, cell protective mechanisms were simultaneously switched on, as cells were also observed to exhibit thermotolerance with a number of heat shock proteins (Hsps) being substantially increased during hyperthermic treatments.

Table of Contents

Table of Figures

Table of Tables

Acknowledgments

I would like to thank my supervisor; Catherine Berry for all her support, help and guidance during my PhD, her continuous encouragement and patience has helped me tremendously and I am extremely grateful for having Catherine as my supervisor.

I wish to take this opportunity to thank all my friends at the Centre for Cell Engineering, I cannot have asked for a better group of people to work alongside and call my friends. Both professionally and socially I think the 'CCE family' has evolved over the years and I consider myself very fortunate to have been part of this team. I'm also extremely grateful to everyone who has ever helped me during my PhD and I would like to say a special thanks to Ross Gurden, for all his time and effort he used helping me with large data sets and answering the more difficult statistical queries I had! Also a very big thank you to my close friend, Rikki Unadkat who helped design and create the 3D chambers, as well as being a great friend!

I wish to thank my best friend Shabana Hudda, who has been a source of positivity, strength and support during my time in Glasgow. It will never be taken for granted how much you took care of me during my knee surgeries and how balanced you kept me during difficult periods, for encouraging me to do my best and always supporting me during my time in Glasgow. Words cannot express how grateful I am for everything you have done for me. This also extends to my long-term friends Nabeel Hussain and Umar Azram who have been ever-present figures throughout my college years and hopefully, for many more years to come!

Finally, I would to say thank you to my incredible family, these have been truly difficult times for all of us but you all have individually made sure I prioritised my PhD and always encouraged me to focus, keep strong and stay positive. I am truly blessed to have you all and I could not have been in, and stayed in this position if it wasn't for all the help you have all given me during the years. A special, special thank you to my unbelievable mom. I've never met a stronger and more dedicated mother and I'm truly blessed to have your constant wisdom, faith and unconditional love. I'd like to dedicate this PhD to you, for everything you have done for this family and for me.

Author's declaration

I hereby declare the research conducted in this thesis is my own work, unless otherwise stated, and at the time of submission, is not being considered elsewhere for any other academic qualification

Anil Patel

8th December, 2016

Definitions/Abbreviations

2D	Two-Dimensional
3D	Three-dimensional
A549 cells	Human hepatocellular liver carcinoma
AC	Alternating current
AgNO3	Silver nitrate
AIF	Apoptosis inducing factor
Akt	Protein kinase B
AMF	Alternating magnetic field
APAF-1	Apoptotic protease activating factor 1
ATP	Adenosine triphosphate
ATP5B	ATP synthase subunit beta
Bak	Bcl-2 homologous antagonist/killer
Bax	BCL2 Associated X
Bcl-XL	B-cell lymphoma-extra large
BCL2L15	BCL2 Like 15
BHK21	baby hamster kidney
Bid	BH3 interacting-domain death agonist
Bim	Bcl-2-like protein 11
BLC-2	B-cell lymphoma 2
BMF	Bcl-2-modifying factor
BSA	Bovine serum albumin
c-IAP1	Apoptosis Inhibitor 1
c-IAP2	Apoptosis Inhibitor 2
CD40	Cluster of differentiation 40
CD95	also known as FAS receptor
cIAP2	cellular inhibitor of apoptosis proteins 2
CO_2	Carbon dioxide
CT	computed tomography
CTAB	cetyltrimethylammonium bromide
CW	centiwatt
DAPI	4',6-diamidino-2-phenylindole
SMAC	second mitochondria-derived activator of caspases
DISC	death-inducing signaling complex
DMEM	Dulbecco's modified Eagle's medium
DMSO	Dimethyl sulfoxide
DR5	death receptor 5
DR6	death receptor 6
EPR	enhanced permeability and retention
ER	endoplasmic reticulum
ERK	extracellular signal–regulated kinases
EthD-1	ethidium homodimer
FADD	FAS-associated DEATH domain protein
FAS-L	Fas Cell Surface Death Receptor ligand
Fe2O3	Iron(III) oxide
Fe3O4	Iron(II,III) oxide

FITC	Fluorescein isothiocyanate
GNPs	Gold nanoparticles
GRP78	78 kDa glucose-regulated protein
H_2O	water
H_2O_2	Hydrogen peroxide
HAuCl4	tetrachloroauric acid,TCCA
HCL	Hydrochloric acid
HeLa cells	human cervical cancer cells
HepG3	human hepatocellular
HSE	Heat shcok element
HSF1	Heat shock factor 1
Hsp	Heat shock protein
HTRA	High-Temperature Requirement A Serine Peptidase 1
IAPs	inhibitors of apoptosis proteins
ICP-MS	Inductively coupled plasma mass spectrometry
IGF-I	Insulin Like Growth Factor 1
IGF-II	Insulin Like Growth Factor 2
IGFBP-1	Insulin Like Growth Factor Binding Protein 1
IGFBP-2	Insulin Like Growth Factor Binding Protein 2
IGFBP-3,	Insulin Like Growth Factor Binding Protein 3
IGFBP-4	Insulin Like Growth Factor Binding Protein 4
IGFBP-5	Insulin Like Growth Factor Binding Protein 5
IGFBP-6	Insulin Like Growth Factor Binding Protein 6
JNK	c-Jun N-terminal kinases
kDa	Kilodalton
kHz	kilohertz
log_2	logarithm 2
LSPR	localised surface plasmon resonance
MCF-7 cells	breast cancer cell line
Mcl-1	Induced myeloid leukemia cell differentiation protein 1
MF	Magnetic Field
$mg.ml^{-1}$.	Milligram per millilitre
MG63 cells	Human osteosarcoma cells
MitoSox	mitochondrial superoxide indicator
mL	Mililitre
mM	Millimolar
MNPs	Magnetic nanoparticles
MOM	mitochondrial outer membrane
MOMP	mitochondrial outer membrane permeabilisation
MPT	mitochondrial permeability transition
MRI	magnetic resonance imaging
mRNA	Messenger RNA
$Na_2S_2O_3$	Sodium thiosulfate
$NaBH_4$	Sodium borohydride
NaOH	Sodium hydroxide
NF-κB	nuclear factor kappa-light-chain-enhancer of activated B cells

NIR	near infrared
NO	Nitric oxide
PMAIP1 (NOXA)	Phorbol-12-myristate-13-acetate-induced protein 1
NPs	Nanoparticles
PARP	Poly (ADP-ribose) polymerase
PBS	Phosphate-buffered saline
PEG	polyethylene glycol
PKB	Protein kinase B
PUMA	p53 upregulated modulator of apoptosis
RES	reticulo-endothelial system
RME	receptor-mediated endocytosis
RNA	Ribonucleic acid
ROS	Reactive oxygen species
SAMs	self-assembled monolayers
SAR	specific absorbance rate
SBD	substrate-binding domain
SCCA1	Squamous Cell Carcinoma Antigen
SEM	Scanning electron microscopy
SMAC	second mitochondria-derived activator of caspases
SOD-1	superoxide dismutase
SPIONs	Superparamagnetic nanoparticles
SPR	surface plasmon resonance
sTNF-R1	Soluble tumor necrosis factor Receptor 1
sTNF-R2	Soluble tumor necrosis factor Receptor 2
TEM	Transmission electron microscopy
TNF	Tumour necrosis factor
TNFSF10	Tumour Necrosis Factor Superfamily Member 10
TNFα	Tumor necrosis factor-α
TRAIL	TNF related apoptosis inducing ligand
TRAIL-R4	TNF-related apoptosis-inducing ligand- receptor 4
TRITC	Tetramethylrhodamine
UV	Ultraviolet
W	Watt
XIAP	X-linked inhibitor of apoptosis protein
µg	Microgram
µL	Microlitre
µM	Micromolar

Chapter 1

1. General Introduction:

1.1 Cancer

Cancer is defined as a range of diseases, which originate from the unregulated proliferation of cells (Trosko 2009). The resultant cancerous tumours are malignant, which means they are able to spread, by invading neighbouring tissues, and/or distant tissues (*via* the bloodstream, or lymph system). The spread of the disease from one tissue or organ to another non-adjacent tissue or organ is referred to as metastasis, and it is this capability, which accounts for such high mortality rates in cancer patients (Geiger and Peeper 2009; Seyfried and Huysentruyt 2013). Cancer-related deaths are projected to increase in the future, with the World Health Organization (WHO) estimating about 13.1 million cancer-related deaths by the year 2030. An estimated ten million people are diagnosed with the disease annually, with disease progression characterised by a multistep process involving various physiological systems, such as cell signalling and apoptosis, making it a highly complex disease (Misra et al. 2010). In humans, cancer refers to at least 100 versions of a disease capable of developing in almost any tissue in the body (Masoudi-Nejad et al. 2015). Although different cancers show various characteristics, all develop in a common system of progression, involving genetic and epigenetic incidences in addition to a complex network of interactions between cells and the extracellular matrix (Masoudi-Nejad et al. 2015). Cancer arises as a result of alterations to DNA, enabling cells to avoid regulatory mechanisms that control normal cell growth and proliferation (Hyndman 2016). In this state, cells display unique traits or 'hallmarks' – including genome instability; inhibition of apoptosis and growth suppression; proliferation and immortality; induction of angiogenesis and inflammation; invasion and metastasis (Hanahan and Weinberg 2000; Hyndman 2016).

1.1.1 Carcinogenesis

At its core, genomic instability is a characteristic feature of almost all human cancers (Negrini et al. 2010). DNA is vulnerable to a variety of stimuli, which can lead to DNA lesions and sites of damage. When referring to cancer, such stimuli are termed 'carcinogens', and include those in the environment such as UV

radiation, ionising radiation, drugs and dietary chemicals. Carcinogens may also be present at the cellular level through metabolism, free radical production and gut microbiota (Roos et al. 2016). It is estimated that 95% of cancers occur through the interaction of environmental factors (such as tobacco smoke, dietary constituents, pollutants, drugs, radiation, and infectious agents) with genes, while the remaining 5% are attributed to hereditary mutations (Hyndman 2016).

DNA lesions can cause significant structural and chemical alterations and eventual transcriptional mutagenesis (T. Gong et al. 2014). Damaged DNA can lead to cell death or survival based on DNA recognition repair mechanism and damage tolerance (Roos et al. 2016). Affected genes are broadly separated into proto-oncogenes and tumour suppressor genes. Proto-oncogenes are a group of genes that usually encode for proteins involved in stimulating cell division and inhibiting differentiation and apoptosis. Oncogene activation can lead to replication stress and DNA double strand breaks as well as further genomic instability (Miron et al. 2015). Onocogene activation and abnormal high expression can also cause the hyperactivation of signalling pathways that may be integral to control cell growth, proliferation, motility, and can have down stream implications of wider signalling networks that incite cancer progression, including the tumour microenvironment, angiogenesis, and inflammation (Sever and Brugge 2015).

Tumour suppressor genes, meanwhile, generally encode for proteins involved in inhibiting cell proliferation and include proteins involved in cell cycle checkpoint controls, apoptosis, and DNA repair (Velez and Howard 2015). If these genes are mutated, a loss-of-function occurs and an accumulation of genetic damage and double stranded breaks can arise (Broustas and Lieberman 2014; Sun and Yang 2010; J. Zhang and Powell 2005). Also at this genomic level, continuous faulty DNA maintenance machinery and disruption to epigenetic modifiers can result in potentially thousands of sequence alterations and anomalies causing extreme difficulties in identifying global markers for various cancers (Du and Elemento 2015).

1.1.2 Current Treatment Plans

The need for early and effective detection, diagnosis and treatment is of upmost importance in treatment success. The most common cancer treatments to date are restricted to chemotherapy, radiation and surgery, however hyperthermia is emerging as a strong contender (Misra et al, 2010).

1.1.2.1 Surgery

Surgery is the oldest oncological discipline and involves the surgical removal of the primary tumour from the patient (Pagani et al. 2010; Wyld et al. 2015). In the case of breast cancer, the overall success of these procedures are debatable (Pagani et al. 2010). The removal of the primary tumour can inhibit the metastatic spread of cancer cells, while animal studies have shown the removal of tumours can restore immune function as primary tumours have been shown to compromise the immune system through release of immunosuppressive factors (Gnerlich et al. 2007; P. Sinha et al. 2005; Wood 2007). The removal of necrotic tumour tissue and overall reduction in cancer cells can also facilitate increased chemotherapeutic drug delivery within tumour sites (P. Sinha et al. 2005). Despite its relative success, major problems are associated with this treatment plan, including the fast-tracked relapse of the tumour, in response to its initial removal (Retsky et al. 2004). While the invasive nature of surgeries can lead to further complications such as infections and associated side effects of anaesthesia (Andreae and Andreae 2012; D. J. Jones et al. 2014).

1.1.2.2 Chemotherapy

Chemotherapy is a type of cancer treatment that uses specific drugs to kill cancer cells, by slowing the growth and proliferation of the rapidly dividing cells and is usually given in combination with surgery and/or radiotherapy (Pérez-Herrero and Fernández-Medarde 2015; Untch et al. 2014). Chemotherapy is an aggressive form of treatment and due to its non-localised method of administration (e.g. by injection or oral tablet), has a global effect on the patient (Carr et al. 2014; Numico et al. 2015; Wissing 2015). The drugs used are toxic not only to cancerous cells but also to other rapidly proliferating normal cells, such as those of the bone

marrow, the intestinal epithelium and hair follicles, leading to severe side effects that can further hinder the recovery time and prognosis of the patient, as well as potentially leading to treatment failure (B. Yu et al. 2010). There are several different types of chemotherapeutics currently used in clinic, which are varied depending on the type of cancer, these are summarised in table 1-1.

Table 1-1: A summary of the various types of chemotherapeutics available for cancer therapy.

Drug Type	Examples	Mode of Action
Alkylating agents	Cisplatins; Mitomycin C	Cell-cycle independent drugs. Typically, these chemotherapeutics alkylate (bind) DNA bases leading to the cross-linking of DNA strands and/or proteins, eventually leading to single and double stranded DNA breaks, leading to apoptosis (Puyo et al. 2014).
Antimetabolites	Methotrexate; pemetrexed.	Cell cycle dependent. Small molecules that closely resemble critical metabolites and are capable of interfering with the normal function of metabolic enzymes including those involved in DNA, RNA and protein synthesis (Bobrovnikova-Marjon and Hurov 2014).
Anti-microtubule agents	Vinca alkaloids (vincristine, vinblastine etc); taxanes (paclitaxel, docetaxel).	Cell cycle specific (s-phase). Inhibit microtubule function causing mitotic arrest and subsequent apoptosis (Klute et al. 2014).
Topisomerase inhibitors	Irinoteacan/topotecan (I);etoposide, doxorubicin, mitoxantrone, novobiocin, aclarubicin (II).	Cell cycle dependent. Inhibit enzymes (topoisomerase I and II) involved in DNA unwinding, therefore DNA replication and transcription; leading to apoptosis (Khadka and Cho 2013).
Cytotoxic antibiotics	actinomycin, doxorubicin, epirubicin, mitoxantrone.	Cell cycle dependent. Generally act to interrupt cell division by intercalating with DNA and preventing the resealing of the DNA double helix, triggering the apoptotic pathway (Tahover et al. 2015)

1.1.2.3 Radiotherapy

Radiotherapy is a type of cancer treatment that utilises focused radiation in order to kill cancer cells. The exposure of radiation in tissue leads to the ionisation of molecules and eventually, DNA damage (Minniti et al. 2012). Radiation energy can be absorbed directly, in vital cellular components such as membranes, organelles, and importantly, DNA, while indirect radiation absorption through the ionisation of water and oxygen molecules leads to the formation of free radicals, further disrupting DNA integrity and eventually leading to apoptosis (Baskar et al. 2012; Willers et al. 2013). Radiotherapy is utilised ubiquitously in a wide variety of cancers with around 50% of cancer patients expected to receive radiotherapy as a form of cancer treatment (Baskar et al. 2012). As with chemotherapy, radiotherapy poorly discriminates between normal functional cells and cancerous cells, with both cell types susceptible to radiation therapy. However these effects have been somewhat alleviated, due to the efficiency of DNA repair in normal cells, upon radiation exposure, thus providing a small therapeutic window for successful treatment (Begg et al. 2011). Furthermore, due to variations in the tumour microenvironment, cancer cells are often characterised in oxygen deplete states (hypoxia) (J. M. Brown 2007). As radiotherapy primarily relies on the increased production of free radicals to kill cancer cells, a low concentration of oxygen molecules thus translates to a lower concentration of free radical production, thus lowering the impact of radiation therapy on cancer cells leading to the phenomenon of radioresistance (Willers et al. 2013).

1.1.2.4 Malignant Hyperthermia

Hyperthermia is defined as a rise in temperature within the body. When considered as a cancer therapy, the increase in temperature is induced intentionally and results in cell death. The potential for localised treatments that will produce fewer side effects, yet accurately and effectively target cancerous cells for destruction, has led to the renewed interest in hyperthermia. The term ‘hyperthermia’ in a cancer setting refers to a variety of techniques that utilise heat to treat cancer. It is considered that there is no intrinsic difference between the hyperthermia sensitivity of normal and cancerous cells, however it has been demonstrated that hyperthermia can lead to specific cancer cell apoptosis, while

normal tissues remain undamaged even after treatment for 1 hour at a temperature of up to 44°C (van der Zee 2002). Normal cells appear to exhibit thermotolerance and recovery upon hyperthermia exposure compared to cancer cells. However the susceptibility of cancer cells to hyperthermia is likely due to the actual biophysical nature of tumours themselves, rather than inherent differences between normal cell and cancerous cells (Behrouzkia et al. 2016; Hegyi et al. 2013). This includes the disorganised and compact vascular structure often presented during tumour development, which leads to difficulty in dissipating heat, while healthy tissues can more easily maintain a normal temperature (Hegyi et al. 2013). Additionally, tumour environments are often hypoxic and exhibit a low pH that contribute to their sensitivity to hyperthermia (van der Zee 2002).

“Those who cannot be cured by medicine can be cured by surgery. Those who cannot be cured by surgery can be cured by fire. Those who cannot be cured by fire, they are indeed incurable.”—Hippocrates (479–377 B.C.).

The concept of treating cancer cells using hyperthermia dates back at least 5000 years (K. Ahmed et al. 2015a). Before any knowledge of the molecular basis for cancer, there was an understanding that unexpected mass or growth lesions could be burned off as a form of treatment; this concept of using heat for cancer treatment is being revisited and explored more appropriately as hyperthermia (Glazer and Curley 2011).

The effectiveness of the technique is predominantly dependent on the temperature range and exposure time (Raaphorst and Feeley 1990). However recent studies have also shown that the method of heat application to cells/tumours is also a significant variable in treatment success (Burke et al. 2012; Hegyi et al. 2013). Indeed, the recent resurgence in hyperthermic treatment is attributed to the rapid development of technology, with the delivery of controlled thermal energy to tumours and cancer sites in the body in a non-invasive fashion.

At present, hyperthermia is used as an adjunct to traditional cancer therapies such as chemotherapy and radiotherapy, as it further renders cancer cells more vulnerable to such treatments, thus increasing their effectiveness (R. D. Issels 2008; Jacoba van der Zee et al. 2000). In the case of chemotherapy, a temperature-dependent enhancement has been documented, including increased

cellular uptake of chemotherapeutic drugs upon exposure to hyperthermia (R. D. Issels 2008; Miyahara et al. 1993). The denaturation of proteins and inhibition of DNA repair by heat were also shown to increase the efficacy of certain chemotherapeutic drugs (Z. G. Cui et al. 2014d; DeNardo and DeNardo 2008). Hyperthermia also increases the local blood and interstitial fluid flow to facilitate chemotherapeutic delivery into tumour sites (L. Li et al. 2014). Although the exact mechanisms of action for the increased efficacy observed in chemotherapy/hyperthermia still remains unclear, it has been proposed that hyperthermia may affect sodium/potassium-ATPase activity, transmembrane conductivity, glutathione metabolism and P-gp activity (Hildebrandt et al. 2002; Y. Tang and McGoron 2013). Despite this lack of knowledge, clinical trials do support the use hyperthermia in conjunction to chemotherapy (Chicheł et al. 2007; Colombo et al. 2011; R. D. Issels 2008).

For radiotherapy treatments, hyperthermia has radiosensitising properties that render cancer cells more susceptible to radiotherapy through multiple mechanisms, including cancer cells deemed resistant to radiotherapy effects (Datta et al. 2015; Horsman and Overgaard 2007). For example, hyperthermia affects cells in S phase - a phase where radiation is less effective – this also holds potential to increase treatment potency. As aforementioned, tumour cells have low oxygen concentration and therefore the effect of radiation and the production of reactive oxygen species that leads to the downstream effect of apoptosis are limited. The addition of hyperthermia counters this hypoxic effect by increasing blood flow and its clinical application has been greatly explored (E. L. Jones et al. 2005; Kampinga and Dikomey 2001; Mallory et al. 2015; Zagar et al. 2010). However as explained previously, both chemotherapy and radiotherapy have challenging side effects for the patient and this has led to hyperthermia being evaluated as a sole mediator for cancer cell apoptosis, where it is being explored as a viable therapeutic alternative in its own right.

1.2 Hyperthermia at the Molecular Level

A number of reviews have outlined the significant effects of hyperthermia on cells both *in vitro* and *in vivo* (M. Ahmed and Douek 2013; DeNardo and DeNardo 2008; Mallory et al. 2015). Broadly, hyperthermia has a variety of effects at both the cellular and molecular level as summarised in figure 1-1, which can inhibit cancer cell growth, function and ultimately viability, by promotion of apoptosis (Hildebrandt et al. 2002; C. H. Hou et al. 2014a).

1.2.1 Apoptosis

Apoptosis is an essential process and has multiple functions in ontogenetic development and tissue remodeling (Kerr et al. 1972). There are two major protein families that regulate apoptotic pathways; the caspase family and the Bcl-2 family. Once activated, these molecules determine the fate of the cell. Caspase proteins are a group of cysteine-aspartic proteases that either falls into the subcategories of pro inflammatory caspases (caspase -1, -4, 5 and 12), initiator caspases (caspase -2, -8, -9 and -10) and executioner caspases (caspase -3, -6 and -7) (D. R. McIlwain et al. 2013a; Perez-Hernandez et al. 2015). The caspase family thus provides critical links in cell regulatory networks and are integral components in supervising inflammation and cell death (David R. McIlwain et al. 2013b). Caspase proteins are enzymes produced by cells as inactive zymogens (Shi 2004). The activation of caspase proteins are tightly controlled by the inactivation or activation of substrates and signalling events promoting their aggregation into dimers or macromolecular complexes, leading to their catalytic activation and the downstream demolition of cellular components and finally, apoptosis (David R. McIlwain et al. 2013b).

The Bcl-2 proteins (B-cell lymphoma 2) are believed to negotiate whether the cell commits to apoptosis or aborts the process (Elmore 2007). It is thought that the main mechanism of action of the Bcl-2 family is the regulation of cytochrome c release from the mitochondria *via* alteration of mitochondrial membrane permeability. The Bcl-2 family therefore govern mitochondrial membrane permeability and can be either pro-apoptotic or antiapoptotic. Bcl-2 proteins thus regulate the permeabilisation of mitochondria, which leads to the activation of the

downstream caspase cascade events (J. H. Zheng et al. 2015). The Bcl-2 family is subdivided into pro-apoptotic proteins (e.g. Bak, Bax, Bid, Bim, Noxa, PUMA) and anti apoptotic proteins (e.g. Bcl-2, Mcl-1, Bcl-XL, etc) (Adams and Cory 2007).

1.2.2 Mitochondrial Stress

Hyperthermia has been shown to compromise the permeability of the mitochondrial membrane, although the exact mechanisms have not been fully realised (Z. G. Cui et al. 2014c). Caspase 2 has been shown to become active after hyperthemic exposure and once active can cleave and activate the pro-apoptotic protein Bid (Bonzon et al. 2006). The active Bid subsequently compromises mitochondrial permeability, leading to the release of a variety of proteins including cytochrome c into the cytosol, which disturbs the homeostasis of additional pro- and anti- apoptotic, Bcl-2 proteins (Bonzon et al. 2006; Saelens et al. 2004). Cytochrome c can also be released from the mitochondria *via* Bax activation in response to various death stimuli. Here, Bax undergoes a conformational change and consequently translocates to the mitochondria, leading to the eventual release of Cytochrome c (X. Yang et al. 2012a). Cytochrome c then interacts with the pro-caspase 9 on the scaffold protein, Apoptotic protease activating factor 1 (Apaf-1) and deoxyadenosine triphosphate (dATP) to form an apoptosome, leading to the activation of pro-caspase 9. This activation can initiate caspases that can then cleave and activate executioner caspases -3, -6 and -7. Executioner caspases are capable of cleaving critical proteins and leading the cell towards apoptosis (Adams and Cory 2007). Hyperthermia has also been reported to lead to the oligomerization of Bax and/or Bak. This conformational change leads to pore formation on the outer mitochondrial membrane and thus, the subsequent release of cytochrome c and the associated downstream effects (Pagliari et al. 2005; Subburaj et al. 2015).

1.2.3 Reactive Oxygen Species

Apoptosis can also be induced by an increase in reactive oxygen species (ROS) (Chun et al. 2010; Slimen et al. 2014; Z. Wang et al. 2013c). ROS are by-products generated during oxygen metabolism within mitochondria. An overproduction of ROS can stimulate oxidative stress and damage macromolecules, proteins, lipids and DNA (Ott et al. 2007). Antioxidant systems help neutralise ROS generation,

however a strong imbalance between antioxidants and elevated ROS concentration, upon hyperthermic exposure, can render the cell defenceless to the effects of oxidative stress (C.-H. Hou et al. 2014b; Mari et al. 2009). Hyperthermia has been demonstrated to cause an increase in ROS in the form of hydrogen peroxide, superoxide anion and hydroxyl radical (Kikusato and Toyomizu 2013; Mujahid et al. 2006; Slimen et al. 2014). Hyperthermia has also been shown to decrease crucial antioxidant levels such as superoxide dismutase, thus promoting the cell into apoptosis (El-Orabi et al. 2011).

1.2.4 Cellular Damage

The morphological changes of mammalian cells exposed to hyperthermia have been well documented (Andocs et al. 2016; Luchetti et al. 2002; Villanueva et al. 2010; Vlad et al. 2010; Vlad et al. 2013; Welch and Suhan 1985). Hyperthermia has been demonstrated to cause disruption and fragmentation of the Golgi complex – an essential organelle involved in lipid and protein intracellular and extracellular transport as well as lysosome formation in response to hyperthermic temperatures (Welch and Suhan 1985). The cytoskeleton microtubule polymerisation can also be directly altered by hyperthermia, compromising not only the integrity of the cell, but also cell proliferation through the lack of mitotic spindle structure, a crucial component to chromosome alignment during mitosis (S. H. Huang et al. 1999).

Perhaps the most damaging cellular effect of hyperthermia is the resultant unfolding and aggregation of proteins (J. L. Roti Roti 2008a). Hyperthermia can denature proteins, leading to the exposure of hydrophobic regions in polypeptides that can engage non-specific intermolecular interactions with additional proteins, promoting the aggregation of various proteins. This not only inhibits their function but can also have a consequential effect on cell function and viability at a molecular level (Taipale et al. 2010).

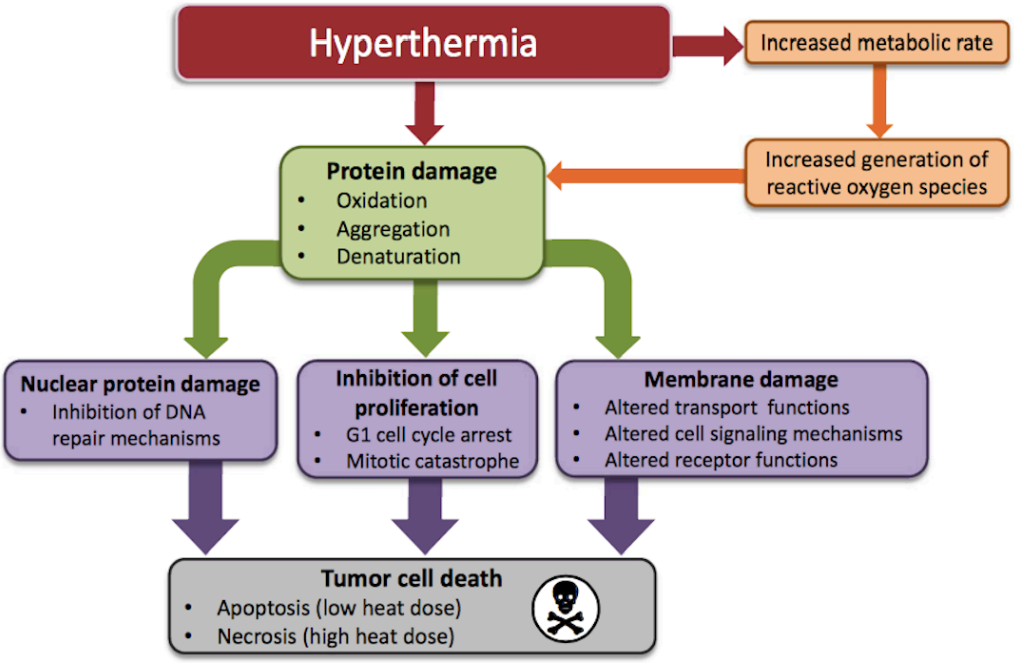

Figure 1-1: Cellular damage initiated by hyperthermia (adapted from Rangel et al., 2013).

1.3 Thermotolerance and Heat Shock Proteins

The direct impact of hyperthermia on cells is dependent on temperature levels and exposure times. However cells do maintain a form of thermotolerance, allowing the cell to resist heat stress and this is strongly associated with an increase in heat shock protein expression (Hsp) (H.-Y. Wang et al. 2013a). Hsps are a specific family of proteins produced by cells in response to stressful conditions that govern resistance to heat, as well as other environmental insults such as UV exposure and cold environments. Hsps both assist in the recovery of the cell and inhibit apoptosis (Yanting Cui et al. 2013; Kalmar and Greensmith 2009; Lanneau et al. 2008b). Hsps are found in various locations in the cell, including the endoplasmic reticulum, lysosomes, and the mitochondria, but are predominantly concentrated in the cytosol and nucleus (Venojärvi et al. 2013). Although continually expressed at basal levels in cells, Hsps are induced and up regulated in response to cellular stress and have various functions in order to recreate a homeostatic environment and thus preserve the cell.

Hsps are highly conserved and ubiquitous in all organisms, from plants, bacteria and animals (Jolly and Morimoto 2000). In mammalian cells, five major Hsps exist; these highly conserved proteins are grouped accordingly based on their molecular weight and further subdivided to large ATP dependent Hsp110, Hsp90, Hsp70, Hsp60 and small ATP independent Hsps (15–30 kDa) including Hsp27. Hsps are also overexpressed in cells exposed to environmental insults such as oxidative stress (Y. Cui et al. 2014a), heavy metals (B. M. Kim et al. 2014) and inflammation (Batulan et al. 2016). The heat shock response was first demonstrated in 1962 and since this original report, many groups have investigated Hsps for their function in normal cell viability, in particular, protein synthesis and management as well as associated pathologies (Adachi et al. 2009; Ou et al. 2014; Venojärvi et al. 2013).

Hsps have various roles but predominantly function as “molecular chaperones” aiding in the maintenance of protein homeostasis and protein quality control (C.-J. Park and Seo 2015). Hsps are capable of repairing and refolding denatured proteins, which have exposed hydrophobic residues that can lead to protein miss folding and aggregation with other proteins. Hsps are also fundamental for the destruction of misfolded/dysfunctional proteins, binding and guiding them for destruction *via* ubiquitination or lysosomal degradation (Bozaykut et al. 2014).

Hsps are synthesised in response to cell stress, and are transcriptionally regulated to produce a rapid response, occurring within minutes of cell stress, such as elevated temperature exposure (Åkerfelt et al. 2010; K. J. Kelly et al. 2001). In response to hyperthermic stress, the inactive complex of Hsp and heat shock factor 1 (HSF1) dissociates, with the former able to bind to denatured proteins. HSF1 meanwhile can trimerise with other free HSF1 within the cytoplasm and translocate into the nucleus. Once in the nucleus the trimeric HSF1 complexes can bind to heat shock elements (HSE), which are specific DNA sequences in the heat shock gene promoters. Once bound to DNA, HSF1 becomes phosphorylated, thereby initiating the transcription and translation of Hsps, as shown in figure 1-2 (Horowitz and Robinson 2007; Kalmar and Greensmith 2009; Stetler et al. 2010; Venojärvi et al. 2013).

The response times of these events have been well documented with Boehm et al, 2003 showing the rapid activation of Hsp70 in drosophila flies within minutes from

heat shock stimuli *in vivo* (Boehm et al. 2003). As the synthesis of Hsps increases, Hsp70 localises to the nucleus and inactivates HSF1 leading to dissociation of trimmers back to their inert monomeric state, thereby repressing Hsp gene transcription (Santoro 2000). Of these Hsps, Hsp -90, -70, and -27 have been predominantly demonstrated to increase expression in response to hyperthermia (Sajjadi et al. 2013; Samali et al. 2001; Tedeschi et al. 2015).

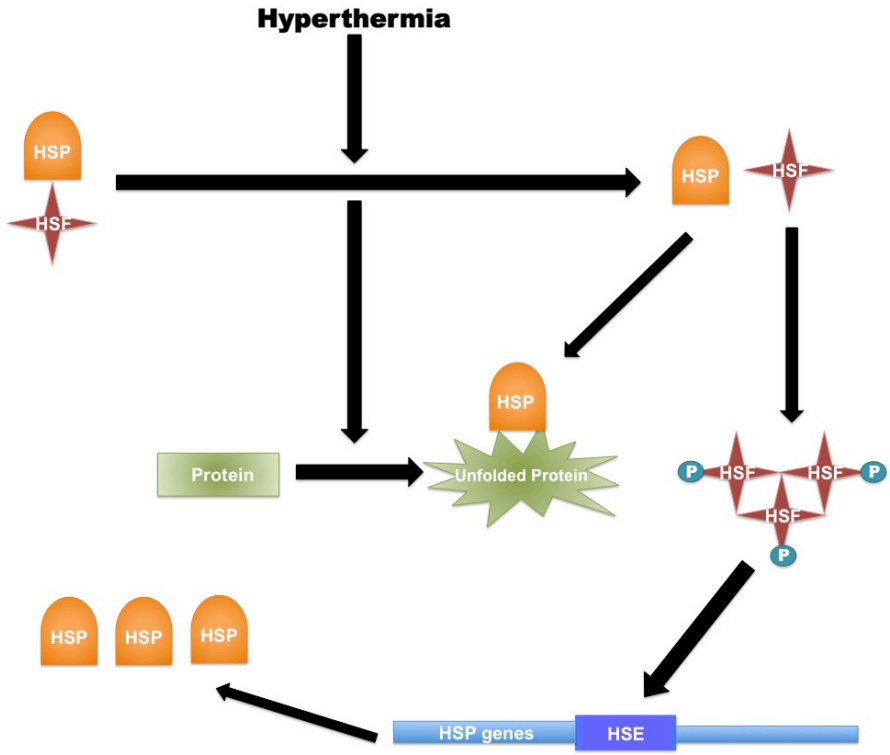

Figure 1-2: Activation of the heat shock response. Hyperthermia leads to the denaturation of proteins, and the dissociation of Hsp and HSF-1. Hsps begin refolding damaged proteins while free HSF-1 monomers, trimerise and become activated and translocate to the nucleus, binding to the heat shock element (HSE) located on the genes of Hsps. The activation of HSE mediates the upregulation of Hsps, orchestrating thermotolerance (personal image).

1.3.1 Hsp90

The importance of Hsp90 is apparent, due its highly ubiquitous and conserved nature within all kingdoms of life, with the exception of archaea (Taipale et al. 2010). Hsp90 is a large dimeric protein found in almost every compartment of eukaryotic cells and has a range of functions including cell signalling, myelination of neuronal cells and predominantly, acting as chaperones for steroid and hormone receptors (Taipale et al. 2010; Tedeschi et al. 2015). Hsp90 relies on

ATP activity in order to fold proteins and is particularly aimed at a set pool of proteins involved in cell signalling, but in contrast to other Hsps, Hsp90 is responsible for maintaining proteins in a functional folded state rather than binding unfolded proteins and preventing aggregation (Karagoz and Rudiger 2015). Its chaperone activity has been shown to be dependent upon the interaction of a network of proteins or co-chaperones as well as an interaction with Hsp70, where Hsp70 members deliver protein substrates to the Hsp90 and co-chaperone complex (Richter et al. 2010). Although a comprehensive understanding of this process remains yet to be fully realised, several recent studies have demonstrated hyperthermia inducing Hsp90 expression (Eng et al. 2014; Kalamida et al. 2015; T. Miyagawa et al. 2014a).

1.3.2 Hsp70

The most widely understood heat shock family member, Hsp70 has been extensively studied in diabetes (Barbosa-Sampaio et al. 2015), chemo-resistance (Stope et al. 2016), radio-resistance (Lauber et al. 2015) as well as its possible role in the pathogenesis of various diseases such as inflammatory bowel disease (Samborski and Grzymislawski 2015). Hsp70 is highly conserved and ubiquitous in most prokaryotes and eukaryotes and has been heavily investigated for its role in cell thermotolerance for a number of years (Beckham et al. 2004; De Maio 2014; Jolesch et al. 2012; Manjari et al. 2015; Marquez et al. 1994; Sharma and Masison 2009). The role of Hsp70 is clearly established under normal physiological conditions and involves the facilitation of protein synthesis, protein translocation, and protein homeostasis. During cellular stress Hsp70 is accountable for protein refolding and preventing protein aggregation, thus protecting the cell against heat-induced apoptosis (Bozaykut et al. 2014). Hsp70 is possibly the most well known Hsp, known to be induced by minimum increases in temperature; a recent publication by Dangi et al (2014) demonstrated high Hsp70 protein expression compared to other Hsps in heat shocked barbari goats (Dangi et al. 2015).

The mechanistic chaperone activities of Hsp70 have been well characterised (Duncan et al. 2015). The ATP dependent chaperone is capable of binding to target proteins through its substrate-binding domain (SBD) while its affinity is grossly determined by the presence of either ATP (low substrate affinity) or ADP (high substrate affinity) (Clerico et al. 2015). The high versatility of Hsp70 allow it

to interact with nearly all proteins in their unfolded, misfolded, or aggregated states (Mayer 2013). Besides its protein homeostatic functions, Hsp70 has also been demonstrated to directly interact with members of the Bcl-2 family and can inhibit the activity of Bax proteins, resulting in the inhibition of apoptosis (X. Yang et al. 2012a). Hsp70 has also been credited with the inhibition of the caspase pathway, the JNK stress signalling pathway, apoptosome formation and AIF (Apoptosis inducing factor) release, thus encouraging cell survival, as shown in figure 1-3 (Evans et al. 2010).

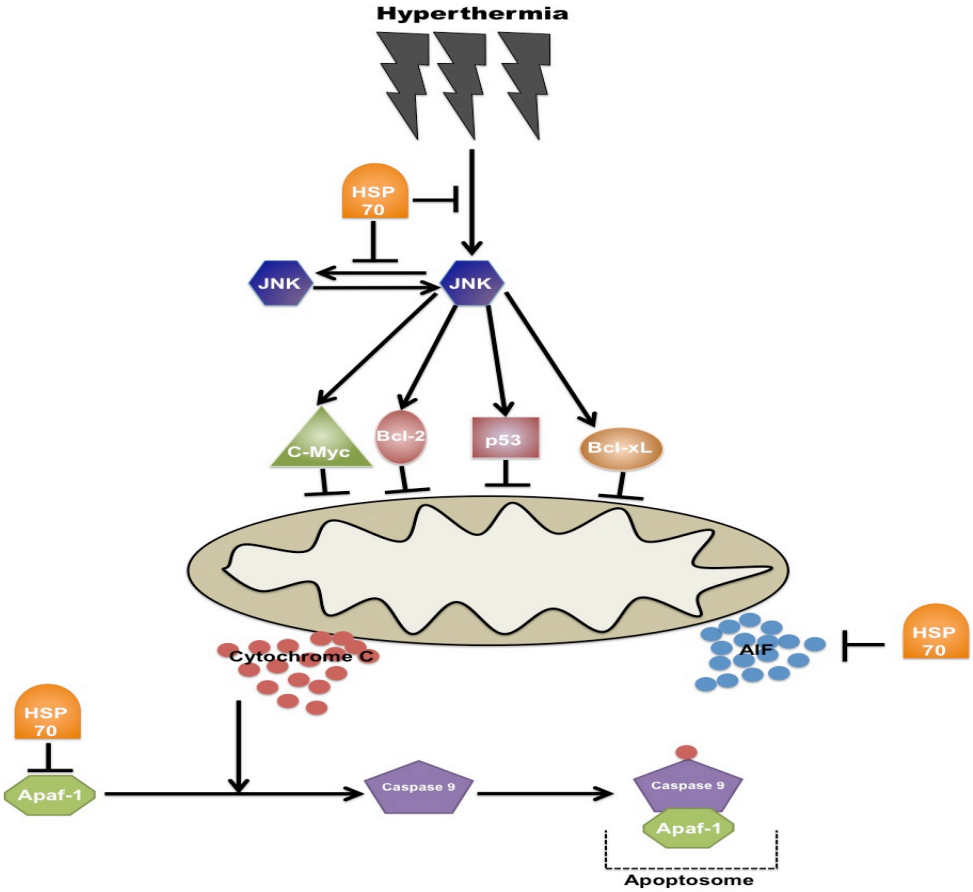

Figure 1-3: Pathways inhibited by Hsp70 to prevent apoptosis *via* hyperthermia. Hyperthermia leads to the activation of pro-apototic molecules orchestrated by the activation of the JNK pathway leading to the downstream release of cytochrome c and AIF. Hsp70 inhibits JNK activation, apoptosome formation and AIF activation, which are all integral components to the apoptosis pathway, thus preserving cell viability (personal image).

1.3.3 Hsp27

Hsp27 is typically expressed at low basal levels within the cytosol of human cells and studies have shown that overexpression of Hsp27 protects cells from subsequent stress (Bechtold and Brown 2000; Rylander et al. 2010). Unlike the larger Hsps, Hsp27 is an ATP independent chaperone and has the capacity to be phosphorylated and oligomerise to form complexes up to 1000 kDa (Jego et al. 2013; X. Wang et al. 2014b). The state of the oligomerisation appears to be significant to its cellular functions, with larger oligomers associated with anti-oxidant properties by modulating ROS *via* the glutathione-dependent pathway and displaying potent chaperoning function (Rylander et al. 2010). Smaller oligomers are known to play a role in favoring the ubiquitination and degradation of selected proteins under stress conditions as well as stabilising actin filaments (Jego et al. 2013). Hsp27 has been shown to interact with and to inhibit key apoptotic proteins and is also involved in the negative regulation of cytochrome c (Bruey et al. 2000). A study by Bruey et al (2000) indicated that Hsp27 binds to cytochrome c released from damaged mitochondria and inhibit its interaction with Apaf-1 and procaspase-9, thus preventing the formation of the apoptosome and the downstream activation of executor caspases (Samali et al. 2001). Hsp27 expression during hyperthermia has been evaluated both *in vitro* (Samali et al. 2001) and *in vivo* (Madersbacher et al. 1998) with Rylander et al (2010) observing the expression levels of Hsp27 almost double that of Hsp70 at various hyperthermic profiles in prostate cells (Rylander et al. 2010).

1.4 Nanomedicine

Nanotechnology is the understanding and manipulation of matter at dimensions between approximately 1 and 100 nanometres. At these dimensions, materials produce unique phenomena that enable novel applications that have been fundamentally explored in areas of research and medicine. This exploaration has opened the relatively new field of nanomedicine, dealing with the detection, control, construction, repair, defence and improvement of all human biological systems (Boisseau and Loubaton 2011). The use of nanotechnology is not a new concept; indeed evidence suggests the use of nanocrystal-containing hair dyes by Egyptians, Greeks and Romans (Cole et al. 2011a). However it was not until 1959

when renowned physicist Richard Feynman presented his talk ‘There’s plenty room at the bottom’ where he discussed the possibilities and potential benefits of the manipulation of materials at the atomic level. This led to discussions with his peers about how we could begin ‘manipulating and controlling things on a small scale’. At its core, nanotechnology involves materials that have arrangements and structures of atoms at the nanoscale, whereby they display enhanced quantum level phenomena (Cherukuri et al. 2010).

It has however, only been in the last three decades that researchers have begun to understand and subsequently exploit the unique properties materials demonstrate at the nanoscale (Sainz et al. 2015). In recent years, the field of nanotechnology has broadened to include expertise from material science, cell biology, chemistry, physics, engineering, computing, electronics energy, and biomedicine (Cherukuri et al. 2010).

The application of nanotechnology within medicine has been termed ‘nanomedicine’ (Rizzo et al. 2013), with a particular emphasis of nanosystems designed for therapeutics, diagnostics, and imaging (Boisseau and Loubaton 2011; Langer and Weissleder 2015). Nanoscale particles, or nanoparticles (NPs), can be synthesised to a size compatible with biological molecules such as proteins and nucleic acids, as shown in figure 1-4, and can thus be appropriately developed for use as potential probes, delivery platforms, carriers and devices giving unique opportunities for improvements in disease detection, therapy and prevention (S. Tong et al. 2014). Furthermore, NPs can ultimately improve the pharmacokinetic and pharmacodynamic profiles of established and characterised therapeutics, making them very attractive vehicles for traditional anti-cancer compounds (Wicki et al. 2015). Indeed, nanomedicine has led to recent developments of nanoparticle-carriers for drug/gene delivery (W. Gao and Zhang 2015; Look et al. 2015), imaging (Mu et al. 2016), and theranostics (diagnostics and therapeutics) (S. Tong et al. 2014).

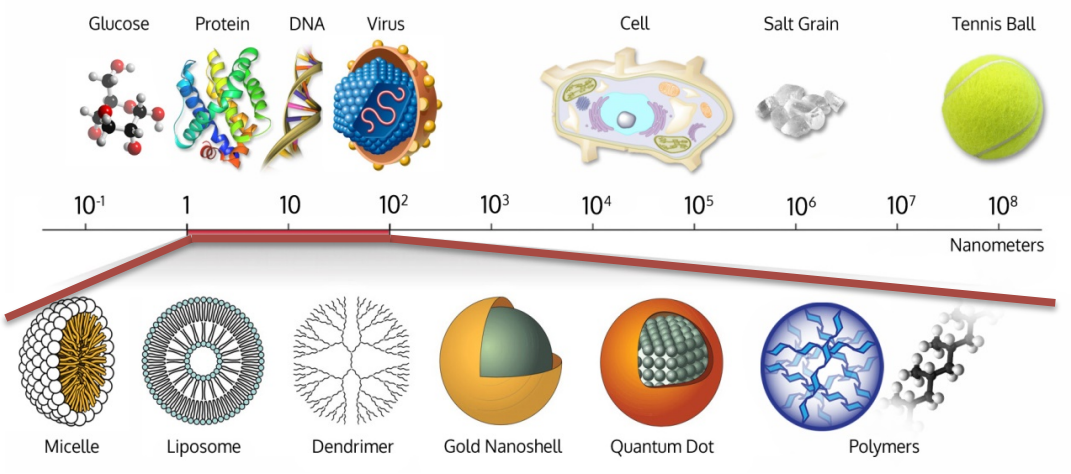

Figure 1-4: Scale of materials in nanometer range Image adapted from WhichLab; http://www.wichlab.com/research).

1.4.1 Nanoparticles

Nanoparticles (NPs) are generally considered to be microscopic particles with at least one dimension less than 100 nm (Cole et al. 2011a). NPs offer a unique advantage over traditional therapies as recent advances in nanotechnology allow researchers to synthesise NPs with dual modalities – integrating diagnostic as well as therapeutic capabilities within a single NP formulation (K. S. Kim et al. 2016b; Mieszawska et al. 2013; J. Park et al. 2015). Therefore, NPs hold great promise for theranostic purposes, and are considered to be highly applicable for personalising nanomedicine-based treatments.

NPs are organic or inorganic in nature, with the latter often being implemented in nanotechnology, in particular nanomedicine as they offer unique inherent properties (Anselmo and Mitragotri 2015). Examples of both are shown in figure 1-5. Inorganic NPs can be synthesised *via* bottom-up or top-down approaches, however bottom-up apporaches allow for a large degree of flexibility and control of size distributions (nm to μm scale), surface chemistry and physical properties the materials may infer; synthesis typically favours a co-precipitation technique, especially in the case of magnetic nanoparticle synthesis (Santhosh and Ulrih 2013). The most popular method for gold nanoparticle synthesis involves the reduction of $HAuCl_4$ (tetrachloroauric acid, TCCA) by reducing agents. This citrate reduction method was developed by Turkevich et al (1954) and later adapted by Fresn (1973) to produce comparatively monodisperse particles with a controlled

average equivolume diameter (Khlebtsov and Dykman 2010). Inorganic NPs, such as iron oxide and gold, are extensively investigated in both preclinical and clinical studies for the treatment, diagnosis, and detection of diseases (Anselmo and Mitragotri 2015).

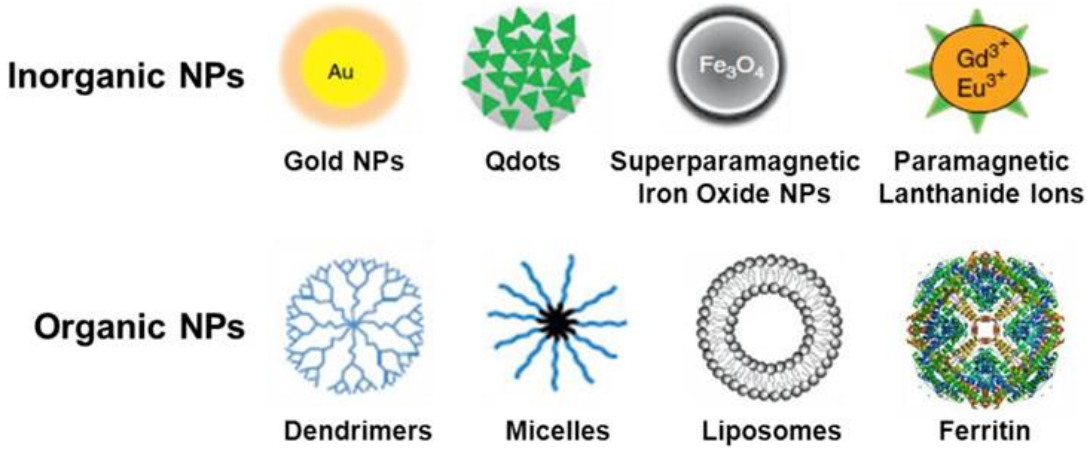

Figure 1-5. Examples of various types of inorganic and organic NPs that have been explored for their potential in nanomedicine (taken from (Xing et al. 2014)).

Nanomedicine is a rapidly growing research field, involving the use of advanced NP design and functionalisation (Chang et al. 2015; Doane and Burda 2012). Currently, NPs are being explored as possible agents for drug (R. Singh and Lillard 2009), gene (G. Lin et al. 2015) and antibiotic (A. N. Brown et al. 2012) delivery due to their nano-scale size, and unique properties allowing for the capacity to cross natural barriers and interact with biomolecules in the blood, organs, tissues or cells (Chang et al. 2015). The use of NPs as delivery agents is promising due to the multivalent properties NPs can exhibit, allowing NPs to deliver therapeutic payloads to target sites *via* ligand or antibody targeting (S. Kumar et al. 2008; R. Singh and Lillard 2009). NPs have also been explored as multifunctional agents with Hao and co-workers recently developing magnetic nanoparticles that were used as both contrasting agents for MRI and hyperthermia (R. Hao et al. 2013). More sophisticated NP synthesis have also been explored, producing multivalent NPs that express various ligands capable of interacting with specific receptors on targeted cells and increasing their internalisation into cells, compared to traditional NPs expressing a monovalent system (Avvakumova et al. 2014).

1.4.2 Nanoparticles *In Vivo*

When using NPs *in vivo*, as with any biomaterial, there are several immediate challenges, such as the host immune system. The immune system helps preserve and maintain tissue homeostasis by protecting the host from foreign environmental insults such as microbes and chemicals (Dobrovolskaia et al. 2016). NPs administered into the bloodstream are identified and subsequently coated by various components of the complement system, namely in the form of plasma proteins such as opsins, as indicated in figure 1-6 (Chaudhari et al. 2012). The NPs coated with these opsins are effectively 'marked' for recognition by the reticulo-endothelial system (RES). The RES is a diffusion system composed of phagocytic cells derived from the connective tissue framework of the liver, spleen and lymph nodes (Berry 2005). Opsonisation aids the process of phagocytosis and thus the destruction of the NPs, it is therefore imperative for researchers to develop NP systems that can resist or avoid opsonisation and therefore avoid the cascade of events that can lead to the destruction of NPs although complete avoidance of the RES is still yet not possible.

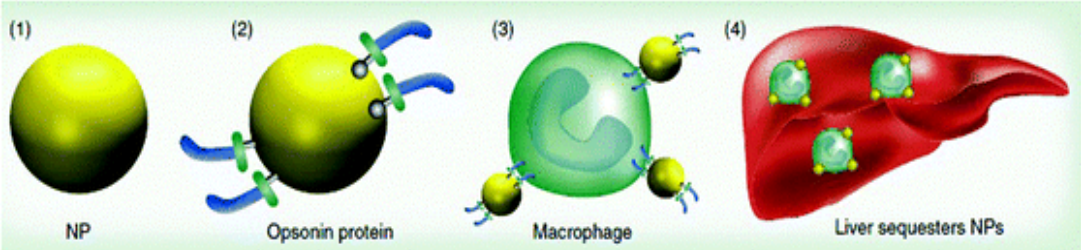

Figure 1-6: The fate of administrated NPs *in vivo*. NPs are coated by blood proteins (2) and sequestered by macrophages (3) upon opsonisation and are transported to the liver to be further metabolised and phagocytised (4). (Taken from (Jokerst et al. 2011)).

There are two major routes for administration of NPs; intravenously, where the blood circulation is used to transport the particles throughout the body, or directly injected into the tissue/organ of interest, where pressure gradients from blood vessels are assumed to aid diffusion to tissue spaces (De Jong et al. 2008; Soni et al. 2014). First generation NPs aimed towards tumour therapy are designed without active targeting systems and instead rely on 'passive targeting' where systemically circulating NPs penetrate the leaky vasculature and poor tissue architecture often associated with tumours and accumulate due to slow clearance

from poor lymphatic drainage, a cumulative consequence termed the enhanced permeability and retention (EPR) effect (Cheng et al. 2015; Maeda et al. 2013; Ngoune et al. 2016; Soni et al. 2014).

To maximise the EPR effect, NPs must be biocompatible within the bloodstream and must also avoid accumulation within the spleen and liver. The surface morphology, surface chemistry, charge and hydrophobicity are all important factors that influence NP pharmacokinetics, biodistribution and overall *in vivo* performance . For example, hydrophilic surfaces tend to resist opsonisation and are thus cleared slowly as opposed to hydrophobic surfaces, which are efficiently coated with plasma components and removed from the circulation at a faster rate (Shah et al. 2013). With regards to NP charge, negatively charged and neutral NPs are more biocompatible compared to their positively charged counterparts due to less protein binding in the blood (Duskey and Rice 2014). NP size distribution and shape are also known to influence NP fate in terms of RES uptake, renal clearance and blood half-life with larger NPs (~100 nm) considered an optimal range for leveraging the EPR effect and minimising clearance in spherical NPs (Ernsting et al. 2013; S.-D. Li and Huang 2008). While more sophisticated geometries, such as rods and stars have shown to enhance circulation time compared to traditional spherical NPs (Ernsting et al. 2013; Toy et al. 2014).

In order to produce the optimum NP performance *in vivo*, the particles are sterically stabilised with either an inorganic or organic coating material, to increase their biocompatibility. The most commonly used coating materials to date are in the form of derivatives of polyethylene glycol (PEG) (Muhammad et al. 2016), dextran (Peng et al. 2015), as well as amphiphilic molecules such as fatty acids or phospholipids (S. J. Soenen et al. 2009). PEG and dextran polymers in particular have been shown to prolong half-blood circulation times by inhibiting opsonisation (Inturi et al. 2015; Suk et al. 2016); coating NPs therefore effectively produces ‘RES-evading’ particles.

New generations of NPs have since been produced with ‘active targeting’ systems in the form of ligands (van der Meel et al. 2013), antibodies (M. Ahmed et al. 2015c), peptides and polysaccharides, as well as specific cell surface receptors (Shah et al. 2013). Researchers therefore design NPs with increased blood half-

life, which can avoid RES interaction and have a high specificity to target sites to increase particle accumulation.

1.4.3 Nanoparticles in Cancer Hyperthermia

Although hyperthermia is a highly regarded therapeutic alternative for cancer treatment, previous attempts before the intervention of NP-assisted hyperthermia, have produced partially satisfactory results (K. Ahmed and Zaidi 2013). One of the crucial factors limiting the use of hyperthermia for clinical use is the means of heat delivery to tumours within patients. Traditional hyperthermia typically involves an external heating source that generates considerable temperature gradients from the external source to the tumour with the maximum heat dissipated on the body's surface that dramatically decreases with distance from the heating source (outside-in hyperthermia) (Beik et al. 2016). Typically this traditional form of hyperthermia means the majority of energy is dissipated in the healthy tissues situated along the path of external radiation which can have toxic affects while also not providing adequate thermal energy within tumours to cause cell death (Beik et al. 2016). The use of NPs has helped alleviate these limitations as they act as the primary heating source and can be intravenously targeted into tumours, while also reversing the direction of heat loss, generating the necessary heating profiles (42-45°C) within tumours and providing minimal damage to the surrounding tissue as the thermal energy dissipates from the tumour (inside-out hyperthermia) (Banobre-Lopez et al. 2013; Beik et al. 2016).

To be an effective candidate for NP-assisted cancer hyperthermia, NPs must exhibit low toxicity, ease of functionalisation, suitable biocompatibility and uptake into cells and importantly, able to generate efficient heating profiles upon exposure to an external non-invasive heating source (Banobre-Lopez et al. 2013; Ganeshlenin Kandasamy and Maity 2015b). Of the plethora of NPs that have been investigated for hyperthermia, both gold nanoparticles and magnetic nanoparticles have been proposed as the ideal candidates due to their low toxicity and inert nature in their inactive states, while their high conversion of energy into heat upon external laser exposure and external alternating magnetic field respectively, has placed them at the forefront for cancer hyperthermia (Chatterjee et al. 2011; Cherukuri et al. 2010; Curry et al. 2014; Giustini et al. 2010; Ingrid Hilger 2013).

1.5 Gold Nanoparticles

The synthesis of Gold nanoparticles (GNPs) was first reported more than 150 years ago however their resurgence in the last few decades has occurred due to the increased development, knowledge and functionalisation, thereby opening up opportunities to enhance and optimise their potential and breadth of their applicability (Alex and Tiwari 2015). In more recent years, GNPs have been investigated for use as drug/gene delivery carriers and diagnostics agents (Robinson et al. 2015). GNPs have also been investigated for cancer hyperthermia due to their unique optical properties when exposed to visible- near infrared (NIR) wavelengths (Wei et al. 2013), where they are capable of efficient conversion of light energy into heat, which is quickly dissipated into the environment. Over the past decade, researchers have concentrated on improving GNP design for hyperthermic treatments, focusing on varying particle shapes such as rods, cubes, stars, and prisms to promote GNP light absorption and thus heat generation (Dykman and Khlebtsov 2011).

There have been several advances in GNP synthetic processes, in particular the ubiquitous and simple citrate reduction method, which allows controllable GNP sizes at high throughput and narrow size distributions (X. Huang and El-Sayed 2010). The use of various coating agents to further increase the biocompatibility of an already deemed inert GNP core includes a variety of organic self-assembled monolayers (SAMs) (e.g. thiolates, dithiolates, amines, carboxylates, cyanides, isothiocyanates, phosphines, etc.) (Connor et al. 2005; Krpetic et al. 2010; Love et al. 2005; X. Wu et al. 2013). Other biomolecules have also been used to increase GNP biocompatibility including, transferrin, lipids, sugars such as dextran, and polymers such as PEG (Dickerson et al. 2008; I. H. El-Sayed et al. 2006; J. L. Li et al. 2009; Nikoobakht 2003; Beatriz Pelaz and del Pino 2012; Pissuwan et al. 2006; Vankayala et al. 2014). These molecules are capable of easily decorating GNPs due to their highly reactive surface chemistry. GNP surfaces can subsequently be further functionalised to allow for increased biocompatibility, targeting and uptake (Bastus et al. 2007; I. H. El-Sayed et al. 2006; Melancon et al. 2008; Pissuwan et al. 2006).

These physiochemical properties make them an attractive candidate for nanomedicine applications, however is it the increased understanding in the last decade of GNP tunable optical properties that has propelled them to the forefront of cancer hyperthermia as photothermal agents. Photothermal therapy is essentially the killing of cells by local hyperthermia, achieved by converting optical energy into thermal energy upon irradiation with light (P. M. Tiwari et al. 2015b). GNPs are efficient converters of light energy into heat, making them promising agents for targeted photothermal effects, while also offering real time diagnostics as imaging agents, therefore making them ideal agents for cancer hyperthermia (X. Huang and El-Sayed 2010, 2011; H. Liu et al. 2012; M. Singh et al. 2015).

1.5.1 Photothermal Properties Of Gold Nanoparticles

GNPs within the size range 10–100 nm, undergo a plasmon resonance with light exposure which leads to surface plasmon resonance (SPR) (Pissuwan et al. 2006). SPR occurs when free electrons oscillating on the surface of the GNPs interact with electromagnetic fields in the form of photons at specific angular momentum and frequency, as shown in the simple schematic in figure 1-7 (Huang et al. 2009). This leads to a collective oscillation of electrons on the surface of the GNP, which greatly increases absorption, or scattering of the photons (Dreaden et al. 2011). Surface plasmon absorption occurs rapidly, dissipating absorbed energy into the environment *via* eventual phonon–phonon relaxation that results in highly localised heat generation (X. Huang and El-Sayed 2010). GNP size and shape are very important factors in determining the absorbance cross-sections and wavelength interaction. Smaller particle sizes (~30 nm) cause absorption at shorter wavelengths while larger particles shift absorption to longer wavelengths and increases the ratio of scattered versus absorbed light (K. L. Kelly et al. 2003; Link and El-Sayed 2003).

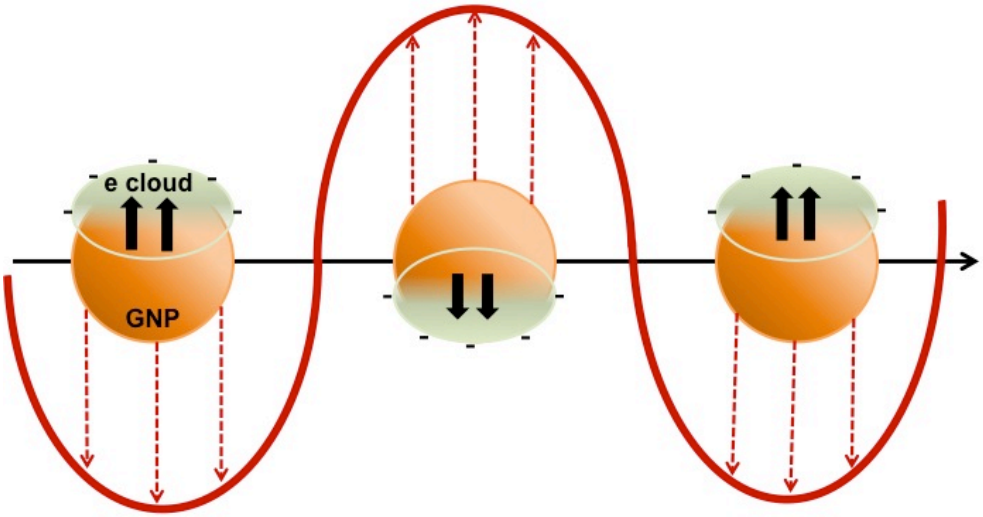

Figure 1-7: A simplified schematic depicting localized surface plasmon resonance (SPR) of gold nanoparticles due to collective oscillation of surface electrons with incident light at a specific wavelength (personal image).

Researchers exploit this SPR phenomenon for cancer hyperthermia. By actively controlling GNP size, they are able to produce GNPs with peak optical absorption cross sections in the near infrared regions (NIR) (Khan et al. 2013; N. G. Khlebtsov and Dykman 2010; Kevin L. Shuford et al. 2005b). NIR spectrum between 750 and 1300 nm provides a 'biological window' for optical absorption through tissue (while shorter and longer wavelengths are attenuated by biological entities such as hemoglobin, pigments, and water) (R. Weissleder 2001a). NIR wavelengths allow for maximum tissue depth penetration without causing significant damage to normal cells (J. Park et al. 2015). The dispersion of heat energy may also be released through photoacoustic effects, if the rate of heat absorption is much faster than the relaxation rate. In this instance, GNP surfaces may exceed many hundreds of degrees leading to cavitation effects and the formation and collapse of microbubbles that can release mechanical shockwaves, which can rupture cell membranes as well as other acoustic associated damage (Lapotko et al. 2006; Wei et al. 2013). Several recent *in vitro* and *in vivo* studies have demonstrated the potential for GNP hyperthermia *via* laser irradiation with a plethora of GNP sizes, geometries and functionalisation (Y. Y. Bai et al. 2014b; Choi et al. 2011; Robinson et al. 2015).

1.5.2 Gold Nanoparticle Size and Shape Influences Optical Properties

The application of GNPs for photothermal therapy *via* laser irradiation does have several shortcomings. In order to synthesis GNPs that have optical absorption towards the NIR region, particles have to be synthesised at a fairly large size distribution, however the increase in size directly correlates to light scattering and absorption ratios. Therefore, GNPs over 40 nm begin to display light scattering characteristics while GNPs over 80 nm diameter the extinction is contributed by both absorption and scattering at similar ratios (X. Huang and El-Sayed 2010). More recently large GNPs (~80 nm) have been identified for use as strong contrast agents due to their high scattering efficiency (P. K. Jain et al. 2006). Gold nanospheres in the size range commonly employed (40 nm) show absorption cross-section 5 orders higher than traditional dyes, while the magnitude of light scattering by 80 nm gold nanospheres is 5 fold higher than the light emission from fluorescing markers. The variation in the plasmon wavelength maximum of nanospheres, i.e., from 520 to 550 nm, is however too limited and reserved for more *in vitro* studies (Panchapakesan et al. 2011).

For photothermal treatment to be fully realised, GNPs must be able to efficiently absorb light energy in the NIR region, however as described above, this involves increasing the size of GNPs. Increasing the size of GNPs has a negative impact on absorbance efficiency, with light energy predominantly scattered rather than absorbed, thus yielding a lower heating output that can not be effectively used for the purpose of hyperthermia (Ivan H. El-Sayed et al. 2005; P. K. Jain et al. 2006). Due to the limitations of spherical GNPs, as described above, researchers began investigating the effects of GNP shape on light absorption and scattering, in order to synthesis GNPs that have optical light absorbance in the NIR region, suitable for laser therapy with low scattering and high absorbance to induce hyperthermia (Hua et al. 2015; Jihye et al. 2011). The more sophisticated geometries have included gold nanorods and gold nanoprisms, which have shown great potential as hyperthermic agents (Mackey et al. 2014; J. E. Millstone et al. 2005; B. Pelaz et al. 2012; Jing Wang et al. 2012a).

Nanorods are cylindrically shaped GNPs containing two distinct plasmon bands (Lakhani et al. 2015). This SPR spectrum split produces a stronger long-wavelength band in the NIR region due to the longitudinal oscillation of electrons,

and a weaker short-wavelength band in the visible region around 520 nm due to the transverse electronic oscillation correlating to the length and width of the nanorods (X. Huang et al. 2008). The absorption spectrum of gold nanorods is dictated by the aspect ratio (length/width) of rods, a feature that can be manipulated by researchers to produce highly absorbing or scattering GNPs. By increasing the nanorod aspect ratio, the SPR absorption wavelength maximum of the longitudinal band significantly shifts toward the NIR region. This easily tuneable characteristic has made nanorods a suitable agent for cancer hyperthermia. Gold nanorods can therefore be synthesised to display the highest absorption peak in the NIR region that correlates well with laser wavelengths during photothermal irradiation both *in vivo* and *in vitro* and is seen as a key modulator for future GNP cancer hyperthermia therapies (A. M. Alkilany et al. 2012; Dickerson et al. 2008; Tanya S. Hauck et al. 2008b; Qin et al. 2015).

Gold nanoprisms represent a more complex nanoarchitecture, typically in the form of a triangular geometry (Alfranca et al. 2016). Gold nanorpisms can be tailored by modifying their aspect ratio, tip sharpness, thickness and length, which can influence and promote enhanced optical properties as well as improve *in vivo* performance (Alfranca et al. 2016; Chenchen Bao et al. 2016). The optical properties of nanoprisms are not governed by diameter but instead are heavily influenced by their aspect ratio and symmetry (Jill E. Millstone, 2004). The aspect ratio is based on the thickness of the nanoprism and edge length, however the three tips of the nanoprisms are also crucial characteristics determining its optical properties (E. Hao et al. 2004; K. L. Shuford et al. 2005a). The absorption spectrum of gold nanoprisms in particular, often presents four frequency modes, which have been confirmed both theoretically and experimentally, namely in-plane and out of- plane modes, both of which in turn can be dipolar and quadrupolar (B. Pelaz et al. 2012; Perez-Hernandez et al. 2015). The major contribution to the UV-vis-NIR spectrum of triangular gold nanoprisms (NPRs) is attributed to the in-plane dipolar mode located in the NIR range (B. Pelaz et al. 2012). The highly anisotropic shape of nanoprisims provides them with strong absorption in the NIR region and makes them highly suitable for biological applications including otpoacoustic imaging (C. Bao et al. 2013), bioesensing (Z. Guo et al. 2010a) and photothermal therapy (X. Ma et al. 2015).

1.6 Magnetic Nanoparticles

In 1957, Gilchrist et al proposed the use of magnetic nanoparticles for cancer hyperthermia owing to their capacity to convert magnetic energy into thermal energy (C. S. Kumar and Mohammad 2011). Magnetic nanoparticles (mNPs) are composed of a magnetic metal core, very often in the form of magnetite, a potent magnetic material (Fe_3O_4), or its oxidised form, maghemite (Fe_2O_3), with an outer coating of a biocompatible material (e.g. dextran) (C. S. Kumar and Mohammad 2011). Synthesis is predominantly *via* a bottom up approach, allowing the generation of mNPs in the nanometre range that infer enhanced magnetic properties. In the presence of an alternating magnetic field, iron oxide mNPs generate heat and can induce hyperthermia.

The current biomedical applications of mNPs have been outlined in several reviews (Catherine and Adam 2003; Gobbo et al. 2015; Yallapu et al. 2011), which detail the potential use of mNPs for cancer imaging, when used as contrast agents to enhance the contrast in magnetic resonance imaging (MRI) scans. A further potential use is with magnetic drug targeting, whereby the possibility of attaching various ligands (eg anti-cancer drugs) to the mNPs (figure 1-8) as well as the particles inherent magnetic properties are capitalised upon (Berry 2009). Once inside the body, the mNPs can be attracted to external magnetic fields, allowing accumulation at specific sites where they can subsequently deliver their cancer therapeutic payloads. In 1996, the first clinical trial using magnetic drug targeting was performed in patients with advanced solid tumours (Lubbe et al. 1996).

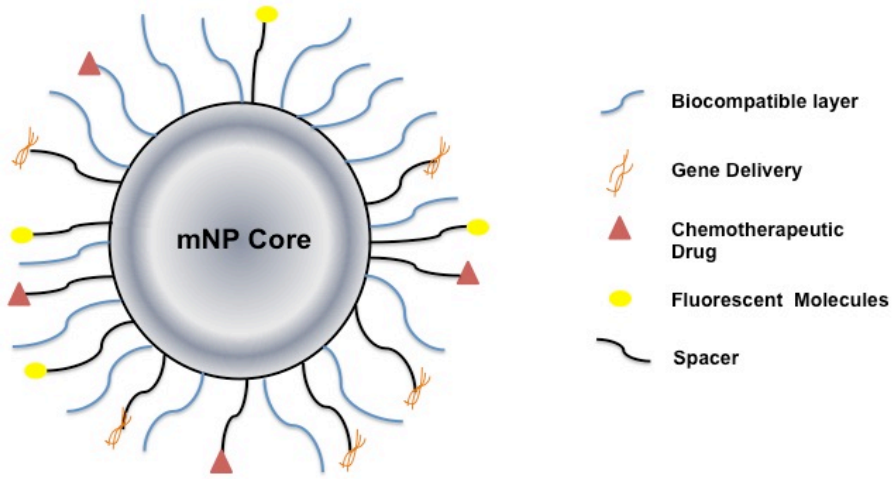

Figure 1-8: Schematic of a multifunctional mNP. MNPs can be functionalised with various biocompatible coatings including PEG and can also be further functionalised to act as a drug/gene chaperones or used as contrast agents with the addition of fluorescent molecules/dyes (personal image).

Based on magnetic resonance tomographic techniques and histological detection, mNPs functionalised with epirubicin could be directed to tumours using magnetic fields localised outside the tumour surface. Magnetic nanoparticles are usually well physiologically tolerated within the body due to their external biocompatible coating with organic polymers (usually dextran), which have a very low toxicity index, while excess mNPs are cleared from the body *via* the aforementioned RES. Briefly, the RES, orchestrated mainly by the kuppfer cells within the liver, ingests the iron oxide mNPs *via* phagocytosis and the resultant products are stored within cellular compartments such as endosomes (Santhosh and Ulrih 2013). The iron oxide is then metabolised into iron and oxygen with the former stored within storage proteins such as ferritin (Santhosh and Ulrih 2013).

1.6.1 Magnetically-Mediated Hyperthermia

Magnetic hyperthermia is dependent on two fundamental points (1) that the cancer cells uptake mNPs into the cell body, and (2) that the mNPs used are capable of generating heat when exposed to an alternating magnetic field. Gilchrist's work was one of the first to utilise magnetic material for hyperthermia treatment, resulting in the heating of tissue samples using iron oxide nanoparticles ranging from 20-100 nm (1.2 MHz magnetic field exposure)(Gilcrest 1957). Since this

seminal report, many publications have been produced, with researchers attempting to use various metal NPs, including nickel, cobalt and zinc (C. S. Kumar and Mohammad 2011). However, whilst metals such as nickel and cobalt are also highly magnetic, they are also very toxic and can be easily oxidised within the body, causing cellular damage, thus iron oxide magnetic nanoparticles are reserved for biomedical application (S. Laurent et al. 2011). The effectiveness of mNP-hyperthermia relies on its inert, biocompatibility during inactivity and crucially, its ability to generate adequate heating profiles upon activation. The heating efficiency of mNPs is determined by the magnetic energy absorbed by mNPs and converted into thermal energy and is notably described as the specific absorbance rate (SAR). The SAR is expressed as an equation and is equal to the rate at which energy is absorbed per unit mass of the mNPs at a specific frequency, defined by the equation below (Deatsch and Evans 2014; Guardia et al. 2012; Arati G. Kolhatkar et al. 2013b).

$$\text{SAR, W/g} = C\left(\Delta T/\Delta t\right) = (\text{Area of hysteresis loop} \times (\text{Frequency, f}))$$

Where C is the specific heat capacity of water, and $\Delta T/\Delta t$ is the rate of change of temperature (A. G. Kolhatkar et al. 2013a).

Although SAR is good indicator of heating potential, various groups have adopted different models, producing different degrees of consensus within the literature. For example Suto and co-workers emphasised the impact of the weight of mNPs and the frequency and strength of magnetic fields (Suto et al. 2009). Many groups that attempt to theoretically or experimentally estimate the SAR of mNP based heating highlight the significance of not just the mNP characteristics, but also the variation of the external alternating magnetic field, including field strength, frequency and duration (Deatsch and Evans 2014; C. S. Kumar and Mohammad 2011; L. Yu et al. 2014). In general, the generation of heat produced by iron oxide magnetic nanoparticles is proportional to the square of the applied magnetic field amplitude, thus, as expected; an increase in magnetic field strength coincides with an increase heat generation within mNPs (Mehdaoui et al. 2010). The influence of magnetic field frequency is far more complex although at more physiologically appropriate boundaries, its impact becomes severely limited and is somewhat overlooked for hyperthermia investigations (Deatsch and Evans 2014). However the impact of field frequency itself does influence the size distribution of iron oxide

nanoparticles that can be used for hyperthermia experiments with studies showing the mNPs between 12 and 20 nm showing optimal magnetic field absorbance (Deatsch and Evans 2014). Physiological considerations have proved challenging for effective *in vivo* hyperthermia using mNPs as large amplitude, high frequency magnetic fields may induce uncontrolled local heating in tissues due to induced eddy currents (Gunnar et al. 2006). Despite these limitations to the magnetic field variables, many groups have successfully used mNPs for hyperthermia experiments *in vivo* with promising results (I. Hilger et al. 2002; Thiesen and Jordan 2008).

Table 1-2: A list of clinical trials involving mNP based hyperthermia.

Clinical trials	Key Features	References
Clinical hyperthermia of prostate cancer using magnetic nanoparticles: Presentation of a new interstitial technique	Phase I study Concentration of ferrites in aqueous solution was 120 mg.ml^{-1} 15 nm and were coated with an amino silan-type shell in water Treatments were delivered in the first magnetic field applicator for use in humans (MFH300F, MagForceÕ Nanotechnologies GmbH, Berlin), alternating magnetic field with a frequency of 100 kHz and a variable field strength (0–18kAm^{-1}).	(M. Johannsen et al. 2005)
Intracranial Thermotherapy using Magnetic Nanoparticles Combined with External Beam Radiotherapy: Results of a Feasibility Study on Patients with Glioblastoma Multiforme	Phase I study Aminosilane coated iron oxide nanoparticles 14 patients suffering with recurrent glioblastoma multiforme Used as an adjunct to radiotherapy	(Maier-Hauff et al. 2007)
mNP based hyperthermia combined with radiotherapy	66 patients iron concentration of 112 mg.ml^{-1} 12 nm diameter with an aminosilane coating	(Maier-Hauff et al. 2011)

	Combined treatment with radiotherapy showed more effective therapy	
Neo-adjuvant chemotherapy alone or with regional hyperthermia for localised high-risk soft-tissue sarcoma: a randomised phase 3 multicentre study	Randomised phase 3 trial treatment for high-risk soft-tissue sarcoma (STS) in adults Patients received either neo-adjuvant chemotherapy consisting of etoposide, ifosfamide, and doxorubicin (EIA) alone, or combined with regional hyperthermia (EIA plus regional hyperthermia) in addition to local therapy. 341 patients were enrolled, with 169 randomly assigned to EIA plus regional hyperthermia and 172 to EIA alone. regional hyperthermia increases the benefit of chemotherapy	(Rolf D. Issels et al. 2010)

1.6.2 Superparamagnetic Iron Oxide Nanoparticles (SPIONs)

Superparamagnetic iron oxide NPs (SPIONs) are small particles (1-20 nm) containing an iron oxide magnetic core (Fe2O3 and Fe3O4) which exhibit superparamagnetic behaviour due to their small size and crucially, the subsequent switch from a multi domain structure to a single domain structure (S. Laurent et al. 2011). Bulk magnetic material, such as iron are composed of multiple domains, each containing large numbers of atoms whose magnetic moments (orbital and spin motions of electrons within atoms) are parallel producing a net magnetic moment of the domains in random directions (Bashar Issa et al. 2013b). These randomly distributed domains within the material produce a zero net magnetic moment (Cindi L. Dennis and Ivkov 2013b). When ferromagnetic material are placed in a magnetic field, the magnetic moments of the domains align along the direction of the applied magnetic field forming a large net magnetic moment and a residual magnetic moment, allowing the material to retain its magnetism even after the magnetic field is removed (Bashar Issa et al. 2013b; Santhosh and Ulrih 2013).

The change of SPIONs from a multiple domain structure to a single domain structure greatly alters their magnetic behaviour from ferromagnetic characteristics to superparamagnetic characteristics (B. Issa et al. 2013a; Wahajuddin and Arora 2012b). In this single domain state the material can display either ferromagnetic or

paramagnetic characteristics depending on the presence or absence of an external magnetic field, respectively, leading to the phenomenon described as superparamagnetism (Amtenbrink et al, 2009).However unlike their larger, multi domain bulk, counterparts, single domain, superparamagnetic material do not retain their magnetism after the removal of an external magnetic field (Santhosh and Ulrih 2013). Thus, superparamagnetism is as a form of magnetism exhibited in small ferromagnetic NPs (Hervault and Thanh 2014). This form of magnetism relies on the presence of a magnetic field in order for particles to magnetise, therefore the loss or absence of a magnetic field leads to particles losing their magnetic potential and thus, magnetism and heating capacity (L. S. Wang et al. 2012b).

For biomedical applications, it is of paramount importance to have superparamagnetic behaviour at room temperature to prevent aggregation; aggregation is more common in SPIONs due to their smaller size, increased surface-to-volume ratio as well as magnetic attractive forces and weak Van Der Waals forces (Santhosh and Ulrih 2013). Superparamagnetic materials can flip the direction of their magnetisation under the influence of temperature and the time between these flips is termed the Neel relaxation time. In the absence of an external magnetic field, if the time used to measure the magnetisation of mNPs is longer than the Neel relaxation time, the magnetisation of the material is said to be approximately zero (Arati G. Kolhatkar et al. 2013b).

The Curie temperature is also an important parameter, which researchers can manipulate; the Curie temperature is the temperature at which a materials permanent magnetism changes, above these temperatures, materials lose their magnetism and effectively ‘turn off’ (Sharifi et al. 2012). This process inhibits their ability to heat, thus stopping them from over heating within the body (Rehman et al. 2002). The Curie temperature is therefore fundamental to hyperthermia therapies that can ‘turn off’ once the desired temperature is achieved (Sharifi et al. 2012).

1.6.3 Mechanism Of Heat Generation In Magnetic Nanoparticles

As described above, SPIONs have a size range of 1-20 nm. At this size it is considered that the SPIONs change from a multiple domain structure to a single domain structure and thus change from having ferromagnetic characteristics to superparamagnetic characteristics (Wahajuddin and Arora 2012a). Frenkel and Dorfman first studied single domain theory in 1930 with further studies, identifying the importance of a shift from multiple domain to a single domain in the creation of permanent magnets (Ortega et al. 2010).

When SPIONs are subjected to an alternating magnetic field (AMF) they generate heat by two main mechanisms; hysteresis loss and relaxation (Mamiya and Jeyadevan 2011; Ruta et al. 2015). Hysteresis occurs when an AMF is applied to the particles leading to the atomic dipoles within the particles aligning themselves accordingly with the AMF albeit at a delay and becoming magnetised in response (C. S. Kumar and Mohammad 2011). Single domain SPIONs respond by rotating during the presence of an external AMF and this can create currents within the SPION carrier fluid (usually in the form of a ferrofluid) (C. S. Kumar and Mohammad 2011).

Heat is also produced *via* a delay in the relaxation processes in the form of Brownian and Neel relaxation mechanisms, again producing heat *via* friction causing thermal cytotoxicity to tumour cells (J. Pearce et al. 2013a). Both Neel and Brownian relaxation mechanisms lead to thermal loss *via* an applied MF but both are produced by different phenomenons, as shown in figure 1-9. Neel relaxation mechanism occurs due to the rapid changes in direction of magnetic moments within the particles thus leading to rotation within the particle itself leading to heat loss (J. Bai et al. 2014a). Brownian relaxation meanwhile relies on the actual physical rotation of the particle itself within the carrier media it is suspended in (e.g. ferrofluid) *via* an external AMF (S. Laurent et al. 2011). This mechanism therefore relies on the external environment - the carrier fluid, including density, viscosity and other external dynamic factors which could either inhibit, suppress or resist the particles spinning, thus affecting the generation of heat produced (L. Yu et al. 2014).

Both Neel and Brownian relaxation rely on particle diameter. When particles are exposed to an external AMF, the time of magnetic reversal is less than the magnetic relaxation times of the particles, and heat is dissipated *via* the delay in relaxation of magnetic moments within the particles (Vallejo-Fernandez et al. 2013). By increasing the size of SPIONs it is possible to increase the heating efficacy of these particles, but this must be balanced with the requirement to maintain superparamagnetism (Sharifi et al. 2012).

Other factors also affect SPIONs ability to generate heat, including their shape and crystal structure (linked to domain size). Furthermore, particle internalisation into cells can also cause a shift in heating potential, with mNPs likely to experience inhibition of particle spinning or movement, thus limiting heat to Neel relaxation only (Espinosa et al. 2016). All these parameters need to either be satisfied or at least accounted for in order to estimate the specific absorption rate of the SPIONs and thus their effectiveness *in vivo*.

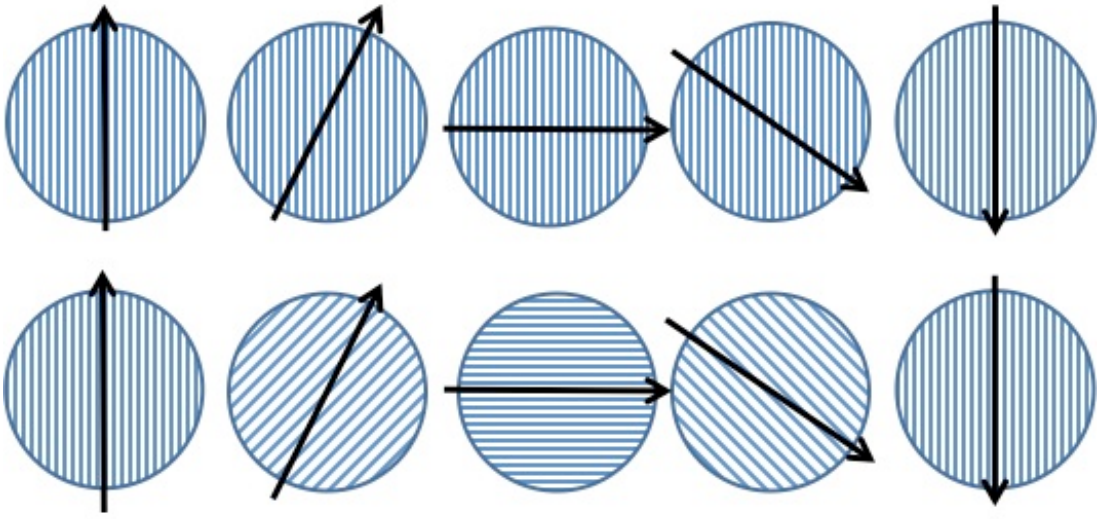

Figure 1-9: Néel rotation and Brownian rotation. (Top) Néel rotation: The magnetic moment rotates while the particle remains fixed. (Bottom) Brownian rotation: The magnetic moment leads to the physical rotation of the particle (personal image).

1.6.4 Clinical Application of Magnetic Nanoparticles

Over the last two decades considerable improvements have been made to magnetically-mediated hyperthermia to enable clinical translation (Cole et al. 2011a). A number of parameters are vital to the success of this application, including (1) the position of the tumour (superficial or deep seated), (2) the half-life of the NPs (avoiding opsonisation), (3) the specific targeting of cancer cells (e.g. by identifying specific molecular markers on cancer cells, such as antibodies), (4) the strength and exposure time of the magnetic field (high enough to excite mNPs, but low enough to not cause any potential localised damage), and (5) general safety considerations (eg. potential toxicity issues). All these factors have to be negotiated in order to produce a mNP that will be safe to use *in vivo* and able to efficiently produce heat when located in a cancer cell and exposed to an alternating magnetic field.

The use of hyperthermia treatment to treat cancer patients was first highlighted in studies from Jordan et al 2001 and Johannsen et al 2005, with both studies focusing on the susceptibility of cancer cells to cell death/apoptosis or necrosis upon exposure to hyperthermia (M. Johannsen et al. 2005; A. Jordan et al. 2001). In 2001, Jordan and colleagues presented the proposals for the manufacturing of a new AC magnetic field therapy system for the clinical application of mNP hyperthermia. The first prototype of a clinical magetic fluid hyperthermia (MFH) therapy system that will be set up at the Charité Medical School, Campus Virchow-Klinikum, Clinic of Radiation Oncology in Berlin. The system was produced to match the limitations given by non-specific eddy current heating in highly conductive tissue as well as monitoring other potential safety concerns. The system was expected to be used for global hyperthermic applications but primarily for regional hyperthermia (A. Jordan et al. 2001). Johannsen and co-workers (2005) conducted a pilot study to evaluate mNP hyperthermia for the treatment of prostate cancer. MNPs were injected transperineally into the prostate. Treatments were conducted in the first magnetic field applicator for human use (MFH300F, MagForceÕ Nanotechnologies GmbH, Berlin), with the system producing an alternating current magnetic field with a frequency of 100 kHz and variable field strength (0–18 kA m^{-1}). Patients were subjected to treatments for 60 minutes for six weekly hyperthermia sessions. CT scans and invasive temperature measurements confirmed mNPs were retained in the prostate during the treatment

interval for six weeks with temperature reaching hyperthermic temperature profiles (42-45°). The study showcased the great potential of mNP hyperthermia highlighted by the low mNP toxicity and distribution within the tumour, however the group did note that a greater concentration of mNP was required than initially calculated in order to generate sufficient hyperthermic profiles while the field strength, even at more moderate conditions still appeared to cause pain and discomfort and was subsequently cut by more than half the original dose (<5kA m^{-1}) (M. Johannsen et al. 2005). In 2007, the same group conducted a prospective phase 1 study on ten prostate cancer patients using aminosilane-type shell SPIONs (MFL AS, MagForce® Nanotechnologies, Berlin, Germany). Not only did the group show more successful hyperthermic temperature profiles hyperthermic to thermoablative temperatures were achieved in the prostates at only 25% of the available magnetic field strength. The group also investigated a noninvasive thermometry method specific for this approach, which shows great potential for future development (Manfred Johannsen et al. 2007).

There are two distinct approaches to magnetic hyperthermia used by research groups; conventional mNP hyperthermia and magnetic thermoblation (Stapf et al. 2015). Conventional mNP hyperthermia typically involves temperature profiles of around 42-45°, and has shown to cause cancer cell death and the shrinkage of tumours in animal models with minimal/no damage associated with normal cells (Elsherbini et al. 2011). Magnetic thermoblation meanwhile is similar in principle to magnetic hyperthermia, however higher temperatures are achieved, ranging from 43-55°C. In this case the increase in temperature not only causes tumour cell death, but also has strong cytotoxic effects for neighbouring healthy cells (I. Hilger et al. 2002). The reason for utilising magnetic thermoblation as opposed to magnetic hyperthermia is that a higher rate of tumour regression is often noted with thermoablation (I. Hilger et al. 2002). Although considered effective, magnetic thermoblation is used precariously as elevated temperatures >50°C is associated with necrosis (Cherukuri et al. 2010). At present, the clinical use of agnetic hyperthermia is being predominantly explored as an adjunct to existing cancer therapy treatments, such as chemotherapy and radiotherapy, particularly as cells show an increased susceptibility to both these treatments when magnetic hyperthermia is also used (Giustini et al. 2010).

1.7 Aims and Objectives

The aim of this project was to assess the potential application of gold nanoparticles and magnetic nanoparticles as hyperthermic agents *in vitro*. In order for any NP to be considered for future *in vivo* use and in clinical settings, they must exhibit low toxicity upon cell exposure, show good biocompatibility and subsequent cellular uptake (Charlton et al. 2016; Mahmoudi et al. 2011; A. Panariti et al. 2012a). Therefore, both NP species were assessed in terms of their biocompatibility. Two cancer cell lines were adopted for the *in vitro* studies representing both hard and soft tissue; bone cancer cells (MG63) and breast cancer cells (MCF-7). The NPs were assessed in standard monolayer culture and 3D tumour spheroid culture.

To be considered as ideal candidates for hyperthermia, NPs must exhibit sufficient heating potential to achieve hyperthermic temperature profiles (42-45°C) when exposed to an appropriate stimulant, such as a NIR laser or an external alternating magnetic field, in the case of GNPs and mNPs, respectively (Hayashi et al. 2013; B. N. Khlebtsov et al. 2012). Following biocompatibility tests, both the NP species employed in this project were also characterised for their respective heating potential.

In this final part of the project, I aim to identify the apoptosis pathways responsible for hyperthermia-induced cell death, as the molecular events of hyperthermia induced cell death have not been fully realised (Joseph L. Roti Roti 2008b). The discrimination between apoptosis and necrosis is often overlooked and the various apoptosis pathways which may be activated are poorly studied, making clinically applicable data untranslatable (Kodiha et al. 2014; Yin et al. 2014).

The following objectives were completed to achieve these aims;

1. **Gold & magnetic NPs** - to assess the effectiveness of both NPs to induce ***hyperthermia*** within cancer cells (42-47°) when exposed to (i) an alternating electromagnetic field (AMF) or (ii) light.

2. **Gold NPs** – to adapt a laser system to allow for NP heating via plasmon excitation.

3. **Gold NPs** - to study the ***mechanism events of cell death*** induced by hyperthermia and how this rate could be increased for cancerous cells as well as aiding non-cancerous cell survival. This may include use of targeted NPs (ie. targeting cancer cells).

4. **Magnetic NPs** - to adapt a magnetherm device to allow testing of the parameters required to induced cancer hyperthermia *in vitro*.

Chapter 2

2. Materials and Methods

Table 2-1: A list of materials, reagents and suppliers used during experiments. (* Preparation methods of solutions are described in detail in section 2.1).

Materials/Reagents	Supplier(s)
1. Cells	
Human breast adenocarcinoma (MCF-7 Cells)	Sigma Aldrich, UK
Human osteosarcoma (MG63 Cells)	Sigma Aldrich, UK
2. Nanoparticles	
~11 nm Superparamagnetic Iron oxide nanoparticles (SPIONs) coated with dextran	Synthesised by collaborators at the Aragón Materials Science Institute, Spain.
Gold nanoprisms & nanorods coated with PEG	Synthesised by collaborators in Zaragoza, Spain
3. Cell Culture	
Dulbecco's modified eagle medium (DMEM)	Sigma-Aldrich, UK
Ethylenediaminetetraacetic acid (EDTA)	Sigma- Aldrich, UK
Foetal bovine Serum (FBS)	Sigma- Aldrich, UK
HEPES	Fisher Scientific
L- Glutamine 200 mM	Invitrogen, UK
Media 199	Sigma- Aldrich, UK
Penicillin-streptomycin	Sigma- Aldrich, UK
Sodium Pyruvate mM	Life Technologies
Trypsin	Sigma-Aldrich
Trypsin/Versene solution	In house
Versene*	In house (see section 2.1)
4. Cell Viability	

3-(4,5-Dimethyl-2-thiazolyl)-2,5-diphenyl-2H-tetrazolium bromide (MTT)	Sigma-Aldrich, UK
Dimethyl sulfoxide	Sigma-Aldrich, UK
LIVE/DEAD® viability/Cytotoxicity kit	Invitrogen, UK
PBS	Sigma-Aldrich, UK
5. Cell Staining	
BSA	Sigma-Aldrich, UK
Formaldehyde (38%)	Fisher Scientific, UK
HEPES	Fisher Scientific, UK
Magnesium Chloride (($MgCl_2$) hexahydrate)	VWR Chemicals, UK
Primary antibodies	Abcam, UK and Santa Cruz biotechnologies, UK
Rhodamine-phalloidin	Invitrogen, UK
Secondary biotin conjugated antibodies	Vector Laboratories, USA
Sodium Chloride (NaCl)	VWR Chemicals, UK
Sucrose	Fisher Scientific, UK
Tertiary streptavidin- FITC	Vector Laboratories, USA
Triton X	Sigma-Aldrich, UK
Tween 20	Sigma-Aldrich, UK
6. Electron Microscopy	
Aqueous uranyl acetate	Agar Scientific Ltd, UK
Epon resin araldite (812 Kit E202)	TAAB Lab Equipment Ltd, UK
Ethanol	VWR Chemicals, UK
Glutaraldehyde (25% aq pure, EM Grade)	Sigma-Aldrich, UK
Methanol	VWR Chemicals, UK
Osmium tetroxide	Agar Scientific Ltd, UK
Propylene oxide	VWR Chemicals, UK
Reynolds lead citrate	Agar Scientific Ltd, UK
Sodium cacodylate	Agar Scientific Ltd, UK

Thermanox Coverslip	ThermoScientific , UK
Uranyl acetate	Sigma-Aldrich, UK
7. Microscopes	
Axiovert 25 fluorescence Microscope	Zeiss, UK
Jeol 6400 SEM	Jeol Ltd, UK
Leo 912AB TEM	Zeiss, UK

2.1 Cell Culture Growth Media and Solutions

Modified DMEM (standard growth media)

MEM	400 mL
Medium 199	100 mL
FBS	50 mL
Penicillin-streptomycin	10 mL
Sodium pyruvate	5 mL

Versene

Water	1000 mL
NaCl	8 g
KCl	0.4 g
Glucose	1 g
HEPES	2.38 g
EDTA	0.2 g
0.5% phenol Red	2 mL
Adjusted to pH 7.5	

Trypsin/versene solution

Versene (in house solution)	20 mL
Trypsin	0.5 mL

PBS Solution

PBS	1 tablet
Water	200 mL

Cell Fixation buffer (fluorescent staining)

PBS solution	90 mL
Formaldehyde (38%)	10 mL
Sucrose	2 g

Cell Permeability buffer (fluorescent staining)

PBS solution	100 mL
Sucrose	10.3 g
NaCl	0.292 g

$MgCl_2$ hexahydrate	0.06 g
HEPES	0.476 g
Adjusted to pH 7.2	
Triton X	0.5 mL

0.5% Tween 20 in PBS

PBS solution	100 mL
Tween 20	0.5 mL

2.2 Monolayer Cell Culture

The human osteosarcoma cell lines (MG63) and human breast adenocarcinoma cell line (MCF-7) were cultured in T75 flasks with Dulbecco's modified Ealges medium (DMEM) supplemented with medium 199 (20%), foetal bovine serum (10%), antibiotics (2%) and sodium pyruvate (1%). Cells were incubated in an atmosphere of 5% CO_2 at a temperature of 37ºC and cultured until 70% confluence. Once cells were confluent they were washed with HEPES solution and detached from the flask surface with 2 mL of trypsin/versene (5 minutes at 37ºC). Fresh media (~8 mL) was added to the cells to neutralise the trypsin/versene solution. The resultant cell suspension was centrifuged for 4 minutes at 1400 g, the supernatant was removed and the remaining cell pellet was re-suspended in 1 mL of fresh media (unless otherwise stated). Cells were then counted using a hemocytometer and seeded into appropriate wells for experiments at a concentration of 1×10^4 per mL.

2.3 Cell Viability

Cells were analysed both for their metabolic activity using the MTT assay and also their viability, using a live/dead fluorescent stains.

2.3.1 MTT Assay

The MTT assay is a colorimetric assay designed to assess cell metabolic activity (when challenged with nanoparticles). The assay relies on the ability of NADPH-dependent cellular oxidoreductase found within mitochondria to reduce yellow MTT (3-(4,5-dimethylthiazol-2-yl)-2,5-diphenyltetrazolium bromide) to purple formazan. Viable cells with an active metabolism will therefore produce a purple

colour at an absorbance near 570 nm. Measurements are recorded using a plate reader, with the concentration of purple (ie. formazan) proportional to the metabolic activity of the cells. The measurements are evaluated against control cell samples containing no nanoparticles (NPs), which are assumed to be 100%.

MG63 and MCF-7 cells were seeded in 96 well plates at $1x10^4$ per well and incubated for 24 hours. The media was then removed and replaced with fresh media containing the specific NPs at desired concentrations and the cells were incubated for a further 24, 48 and 72 hrs (5 replicates for each condition). Subsequently, 10 µL of yellow MTT dye solution (5 $mg.mL^{-1}$ in phosphate buffer pH 7.4) was added to each well. The plates were wrapped in foil and placed into an incubator at 37°C for one hour. After one hour, the media was removed and any resultant formazan crystals were solubilised using 200 µL of DMSO per well. The absorbance of each well was read on a microplate reader (Dynatech MR7000 instruments) at 550 nm.

MTT data analysis: Percentage metabolic activity was calculated using the following equation:

(Absorbance of NP-treated cells / Absorbance of control cells) x 100 = %)

2.3.2 Live/Dead Fluorescent Staining

The LIVE/DEAD® Viability/Cytotoxicity kit was also carried out, to determine cell viability. The assay is a two-colour fluorescence assay that allows simultaneous staining in both live and dead cells (*via* calcein AM and ethidium homodimer respectively). This allowed for the visualisation of cells exposed to NPs (as well as control group, containing no NPs).

The kit contained two compounds, calcein AM and ethidium homodimer (EthD-1). MG63 and MCF-7 cells were seeded at 1 x 10^4 onto 13 mm diameter glass coverslips located in a 24 well plate and cultured for 24 hours to allow cell attachment. The media was then removed and replaced with fresh media containing the specific NPs at desired concentrations and the cells were incubated for a further 24, 48 and 72 hours (3 replicates for each condition). At the relevant time points, the media was removed from each sample, thoroughly washed in

warm PBS (3 times) and 1 mL of fresh media suspension containing 1 µL calcein AM and 1 µL ethidium homodimer was added to each sample. The well plates were foil wrapped and incubated for 1 hour (37°C, 5% CO_2). After incubation, the media was removed and samples were washed twice in warm fresh media and stored in an incubator ready to be viewed. Samples were then imaged under an inverted fluorescence microscope; the excitation/emission wavelengths were 485/515 nm for calcein AM and 525/590 for EthD-1 and were viewed with FITC and TRITC filters, respectively.

2.4 Observation of Cell-NP Interaction and Internalisation

2.4.1 Scanning Electron Microscopy

Scanning electron microscopy (SEM) was used to visualise the interaction of the NPs with the cells. The cells were seeded at 1 x 10^4 on 13 mm glass coverslips and cultured for 24 hours. Samples were then incubated with the NPs diluted in fresh media at the desired concentrations (alongside control cells with no NPs). Two replicates were used for each condition.

Samples were fixed 1 & 24 hours after NP introduction with 1.5% glutaraldehyde supplemented with 0.1 M cacodylate buffer at 4°C for 1 hour. Once samples were fixed, 1 mL of 1% osmium tetroxide in phosphate buffer was added to each sample for 1 hour followed by 0.5% uranyl acetate for 1 hour. Samples were then slowly dehydrated through a series of alcohol increments from 30-100%, before final dehydration with HMDS. The samples were then stored in a desiccator prior to gold sputter coating.

2.4.2 Transmission Electron Microscopy

Transmission electron microscopy (TEM) was used to observe NP internalisation into cells *via* analysis of a cross section of cells after NP culture. This allows us to verify internalisation and determine the intracellular localisation of the NPs.

Cells were seeded at 1 x 10^5 cells per well on Thermanox coverslips in a 24 well plate for 24 hours prior to NP incubation. Cells were incubated with NPs at desired concentrations alongside control cells containing no NPs (two replicates were

used for each condition). Cell samples were then fixed, stained with 1% osmium tetroxide followed by 0.5% uranyl acetate and dehydrated through a series of alcohol increments from 30-100%, exactly as for SEM processing above. Following dehydration, cells were covered with a propylene oxide: Epon 812 resin araldite mix (1:1) overnight. The samples were then placed in pure resin and cured in an oven at 60°C for 24 hours. Ultrathin sections were cut from the cured block and stained with 2% methanolic uranyl acetate and Reynolds lead citrate before being viewed under a LEOG12AB transmission electron microscope operating at 20−200 kV.

Research Colleague Assistance Mrs. Margaret Mullin, Electron Microscopy Facility, University of Glasgow aided with the processing and imaging of SEM and TEM samples.

2.4.3 Cell Fluorescence Staining

Fluorescent staining was used to visualise F-actin and β-tubulin filaments within cells in order to determine if NP internalisation compromised the cell cytoskeleton structure.

Cells were seeded at 1 x 10^4 onto glass coverslips within a 24 well plate and cultured for 24 hours before being incubated with NPs (two replicates per condition; control cells containing no NPs). The cells were cultured with the NPs for 24, 48 72 hours (unless otherwise stated). At the time points, cells were washed with warm PBS and samples were fixed with 1 mL 4% formaldehyde for 15 minutes at 37°C. The fixative was removed, samples were washed in PBS and a permeabilising buffer was added to permeate the cell membrane (5 minutes at 4^{o}C). The permeabilising buffer was then removed and 1 mL of 1% BSA/PBS solution was added for a further 5 minutes at 37^{o}C. Once removed, rhodamine phalloidin (1:100 in PBS/BSA) and anti-tubulin (1:100 in PBS/BSA) was added to each sample. The samples were then aluminium foil wrapped (to prevent loss of fluorescence) and incubated for 1 hour at 37^{o}C. The solution was removed and the coverslips were washed three times in PBS/0.5% Tween. The relevant secondary biotin conjugated antibody (anti-mouse) was added (1:100 in PBS/BSA; 500 µL per coverslip) and samples were incubated a further hour at 37^{o}C. After remove and washing (PBS/0.5% tween), FITC-streptavidin was added (500 µL per well;

1:100 PBS/BSA) for 30 minutes at 4^{o}C. The cell samples were washed again in PBS/0.5% tween; the coverslips were mounted onto glass slides and finally stained with fluorescent DAPI. A 20x20 mm coverslip was subsequently placed on top and samples were viewed under a fluorescent microscope.

2.5 Statistical Analysis

One-way analysis of variance (ANOVA) was performed using GraphPad version 6.01. The statistical significance of results was measured by calculating the probability of the null hypothesis being true using a predetermined limit (p-value). If the level of confidence was less than 5% (p-value ≤0.05), the null hypothesis could be rejected and the results were considered statistically significant. Mean, standard error and standard deviation was calculated using the statistical analysis tool in Microsoft Office Suite (Excel) for each experiment. Studio R was used exclusively to analyse fluidigm data.

Chapter 3

3. Gold Nanoparticles for Photothermal Therapy

3.1 Introduction

3.1.1 Gold Nanoparticles in Photothermal Therapy

Gold nanoparticles (GNPs) exhibit unique properties, including surface plasmon resonance (SPR), which has been capitalised upon for the potential use of GNPs in photothermal therapy (hyperthermia). As discussed in chapter 1, hyperthermia is known to induce apoptotic cancer cell death and also allows increased efficacy of chemotherapy and radiotherapy treatments (W. Li and Chen 2015). However its use as a cancer treatment is limited due to the overall lack of specificity for tumour tissues, the difficulty in heating tumours to therapeutic temperatures and thermolerance after treatment. GNPs are potential photothermic agents, which can be used to generate heat energy from electron excitation and relaxation (*via* SPR) when a laser of appropriate wavelength is applied.

3.1.2 Gold Nanospheres and Nanoshells

To date, many studies have focused on gold nanoshells (eg. silica particles with a gold coating) (Hirsch et al. 2003; Mayle et al. 2016a; Stern et al. 2007; Vera and Bayazitoglu 2009). This is because gold nanoshells present a tunable SPR, which can be tuned to the near-infrared (NIR) region, thus optimising the potential for achieving tumour tissue penetration (X. Huang and El-Sayed 2010; Mayle et al. 2016b; Prevo et al. 2008; G. Zhang et al. 2012; J. Zhao et al. 2014). However in recent years, advancements in nanoparticle synthesis have allowed for a variety of different GNP shapes and structures to be created. For example gold nanorods, whereby the aspect ratio can be altered to permit NIR benefits. When the shape of a GNP changes from spheres to rods, the SPR band is split into two bands; a strong band in the NIR region (corresponding to the long axis) and a weaker band in the visible spectrum (akin to gold nanospheres) (H. Kim et al. 2016a; Z. Zhang et al. 2013b). The NIR band can be tuned depending on the aspect ratio of the nanorod (ie. the length) thus increasing its heating efficacy at NIR wavelengths.

Photothermal therapy using GNPs can be achieved with pulsed or continuous wave lasers, with SRP absorption in the visible spectrum and thus suitable for near surface cancers (eg. skin). GNP photothermal therapy was first demonstrated *in vitro* and *in vivo*, by Hirsch *et al* (Hirsch et al. 2003). This report employed breast cancer cells incubated with PEGylated gold nanoshells. Cell death, *via* Calcein AM staining, was noted after 4 minutes exposure to a continuous wave NIR light (820 nm, 35 W/cm^2). The corresponding *in vivo* study, where the GNPs were directly injected into a tumour, induced tissue damage and cell shrinkage. The following year they injected the PEGylated nanoshells into the bloodstream, rather than direct injection (mouse tail vein) and observed particles accumulation into the tumour *via* the enhanced permeability and retention effect (D. Patrick O'Neal et al. 2004b).

A detailed study was also carried out in 2003 by Lin and co-workers, using a pulsed laser and gold nanospheres (Pitsillides et al. 2003). They targeted lymphocyte cells incubated with antibody-conjugated GNPs and a nanosecond pulsed laser (565 nm, 20 ns duration). Cell death was recorded with 100 laser pulses, with adjacent cells remaining viable and was attributed to micro-scale bubbles around the GNPs. Laser-induced bubbles were noted in subsequent studies using nanosecond laser pulses *in vitro* with breast and cervical cancer cell lines (Hleb et al. 2008; Zharov et al. 2003). However, the heating efficiency using nanosecond pulsed lasers is low, therefore continuous wave laser is often preferred to induce cell death in a larger area *via* hyperthermia, despite the lengthy time required (minutes as compared to seconds).

Since these reports, an exponential number of studies have been conducted evaluating the use of GNPs for photothermal treatment. The heating profiles of thermal treatments can be measured in real time (J. Park et al. 2015). While the biodistribution, accumulation within the liver and eventual clearance from the host without notably signs of toxicity has showcased GNPs as ideal candidates for clinical applications (Bednarski et al. 2015; Fraga et al. 2014).

3.1.3 Gold Nanorods and Nanoprisms

In order to increase the proficiency of light to heat conversion, researchers have explored a range of GNP sizes (K. Jiang et al. 2013), shapes (Eustis and el-Sayed 2006) and composition (hollow or solid GNPs) (Xie et al. 2013). To this end anisotropic GNPs, such as nanorods, have been extensively explored due to their strong optical properties they exhibit as discussed in section 1.5.2. Gold nanorods display an increased absorption cross-section and reduced light scattering in the NIR domain over traditional gold nanosphere shapes.

As stated earlier, gold nanorods have gained particular attention over gold nanoshells and nanospheres due to their tuneable optical properties that can be tailored by changing the aspect ratio (rod length). Huang's research group clearly demonstrated the capability of gold nanorods for use as both cancer cell imaging and photothermal therapy in the near- infrared region (X. Huang et al. 2006a). This study was the first to show photothermal therapy using gold nanorods *in vitro*, whereby ENT cancer cells incubated with gold nanorods were damaged following exposure to a continuous wave laser (4 minutes; 10W/cm^2). Subsequent studies have demonstrated similar results, with cell death *via* apoptosis (Hironobu et al. 2006; L. Tong and Cheng 2009).

Alternative anisotropic GNPs have also been explored including nanoprisms, as previously discussed (chapter 1.5.2). The optical absorbance potential of nanoprisms is governed by a variety of parameters including length, thickness and the sharpness of the vertices (K. L. Kelly et al. 2003; K. L. Shuford et al. 2005a). The combination of these parameters produce nanoprisms that exhibit high aspect ratios and display stronger electromagnetic field enhancement - providing more distinct plasmon resonance in the near-infrared region in comparison to nanospheres and indeed, nanorods (Han et al. 2016b). The manipulation of gold nanoprism characteristics, ease of synthesis, functionalisation and characterisation has extended gold nanoprism use towards photodynamic therapy and imaging (You et al. 2016). An example of the versatility of gold nanoprisms was shown in a very recent study by Bao and co workers (2016). In this study, the group synthesised antibody functionalised gold nanoprisms for photoacoustic imaging, angiography, and photothermal therapy, allowing for the successful imaging and subsequent photothermal therapy treatment *in situ*, while

corresponding *in vivo* experiments led to a reduction in tumour size and improved survival rates within mice (Chenchen Bao et al. 2016).

3.1.4 Successful GNPs Presentation *In Vitro:* Chapter Objectives

GNPs are evaluated based on their *in vitro* and *in vivo* performance in regards to toxicity. To qualify GNPs for potential biomedical applications, such as for hyperthermic treatments, they must demonstrate success across a variety of parameters including low toxicity, high cellular uptake, low cellular stress and successful intracellular heating. To this end, GNP candidates are typically assessed in cell culture. This chapter evaluates the biocompatibility of gold nanorods and gold nanoprisms and assesses their potential as hyperthermic agents *in vitro*.

3.1.4.1 Cell Lines Employed

Two cancer cell lines were employed in this study; a human bone osteosarcoma cell line (MG63) and a human breast cancer cell line (MCF-7). Both cell types represent cancer lineages from bone (hard tissue) and epithelia (soft tissue), therefore MG63 and MCF-7 cells were used as they offer insight into GNP interactions with different cell/tissue types. In addition, we focused on bone and breast cell lines as it is predicted that one-third of women with breast cancer will develop bone metastases, leading to secondary tumours (Koutsilieris et al. 1999).

3.1.4.2 Cell Culture Models

This chapter also diverges from the majority of the literature in this area by comparing the biocompatibility and photothermal capability of gold nanorods and nanoprisms both in standard monolayer culture and 3D tumour spheroid culture. The use of 3D multicellular spheroids aims to better replicate the *in vivo* tumour conditions, which are lost when culturing cells directly on stiff non-native substrates, such as cell-to-cell adhesion, synthesis and secretion of extracellular matrix proteins and structural cell changes. It is well known that 2D cultures are more sensitive to drug exposure producing data that lacks genuine clinical application. This was observed by Loessner et al, 2010, where they found ovarian cancer cell viability was reduced to 40-60% in 3D cultures after paclitaxel

treatment, however the same treatment in the 2D cell monolayer led to an 80% reduced cell viability (Loessner et al. 2010). It is therefore imperative for research groups to move towards 3D systems as a ubiquitous model especially for the evaluation of cancer therapy. This is particularly important for photothermal therapy, while technical issues of tissue penetration and depth of lasers to stimulate GNP heating can also be evaluated (Dreaden et al. 2012).

3.2 Chapter Aims and Objectives

This chapter aims to evaluate the potential of both gold nanorods and nanoprisms as photothermal agents to induce hyperthermia in both MG63 and MCF-7 cells. Once successfully internalised into cells, the GNPs should be able to trigger cell death *via* SPR upon irradiation with a compatible NIR laser. All observations were carried out both in 2D monolayer and 3D multicellular spheroids in order to produce more clinically relevant data.

These aims were achieved as follows:

- Cells were incubated with a range of different GNP concentrations to determine the optimum dose for biocompatibility in terms of cell metabolic activity, viability and morphology.
- GNP internalisation was determined and quantified.
- Laser irradiation of GNPs localised within cells both in 2D and 3D culture models.

3.3 Materials and Methods

3.3.1 Gold Nanorod and Nanoprism Synthesis, Functionalisation and Characterisation

3.3.1.1 Gold Nanorod and Nanoprism Syntheses and Functionalisation

GNPs in the form of nanorods and nanoprisms were synthesised by our collaborators at the Institute of Nanoscience in the University of Zaragoza, Spain. Our collaborators confirmed their hyperthermic potential within 1 minute of laser exposure at a concentration of 0.1 $mg.mL^{-1}$ which was used as a benchmark for future experiments.

Gold Nanorod Synthesis

Gold nanorods were synthesised by preparing a seed stock solution of 1 M $NaBH_4$ (aq) dissolved in 1 M NaOH (aq), which was subsequently dissolved 1:100 in Milli-Q water. Meanwhile, the surfactant, CTAB (aq) 0.2 M was dissolved to homogeneity in a water bath at 37ºC; 5 mL of 1 mM $HAuCl_4$ (aq) and 5 mL of CTAB were prepared. An aliquot of 460 µL of the prepared $NaBH_4$/NaOH stock solution was then added to this solution to produce gold nanoseeds. The growth solution was immediately prepared by mixing 50 mL of 0.2 M CTAB and 50 mL of 1 mM $HAuCl_4$ solution, followed by the addition of 700 µL 0.1 M AgNO3. Finally, 1 mL 0.5 M hydroquinone was added to complete the growth solution. A 1.6 mL aliquot of the seed solution was added and was incubated for 5 hours at 26ºC in a water bath until reaching an LSPR of 1080 nm. Several centrifugation-washing steps were required after each reaction to clean nanorods from excess, toxic CTAB.

For the PEGylation of nanorods, 37 µL of a 1 $mg.mL^{-1}$ $NaBH_4$ (aq.) solution was mixed with 5 mg of heterobifunctional HS-PEG-COOH (5 kDa) diluted in 1 mL Milli-Q water at a ratio of 1:1 to produce a PEG solution. The previously prepared growth solution meanwhile was centrifuged at 15,000 G, 15 min, 30ºC, and pellets were re-suspended in 100 mL Milli-Q water. An aliquot of 1 mL of the prepared PEG solution was then added to the growth solution and the pH raised by the addition of 100 µL of 1M NaOH. The samples were then incubated for 20 hours at

room temperature, to inhibit CTAB crystallisation. After 20 hours, the PEGylation step was repeated and the sample centrifuged (15,000 G, 15 min, 30ºC) to remove excess PEG and CTAB. The resulting mixture was then sonicated for 15 min at 60ºC and the repeat process of addition of PEG solution and consequently centrifugation was repeated two more times, with the last centrifugation step yielding pellets which were re-suspended in a final volume of 15 mL Milli-Q water. These excessive washing and centrifugation steps were necessary to remove toxic CTAB molecules from the solution.

Gold Nanoprism Synthesis

Gold nanoprisms meanwhile were synthesised using a novel wet-chemical synthetic route to produce nanoprisms functionalised with PEG chains to improve stability as described in previous published literature (B. Pelaz et al. 2012) with improved modifications. Briefly, 220 mL 0.5 mM $Na_2S_2O_3$ (aq) was added to 60 µL 0.1 M KI solution (12.2 µM final concentration). An aliquot of 110 mL of this solution was added slowly to 200 mL 2 mM $HACl_4$(aq). A second addition of 110 mL of KI and $Na_2S_2O_3$ was prepared and an additional 70 mL $Na_2S_2O_3$ was mixed. The solution was left for 1 hour at room temperature to produce gold nanoprisms.

Nanoprisms were stabilised using heterobifunctional SH-PEG-COOH (5 kDa). PEG was added to GNPs at a 1:2 ratio (nanoprisms:PEG) of the total weight of gold used in the synthesis. PEG was diluted in 1 mL Milli-Q and a determined volume of a 10 mL, 0.1 $mg.ml^{-1}$ stock solution of $NaBH_4$ was then added to reach 1:1 molar ratio of PEG:$NaBH_4$. This solution was added to the nanoprism solution and attuned to pH 12 with 2 M NaOH. The solution was sonicated for 1 hour at 60 ºC and centrifuged at 4,400 G for 15 min at room temperature. Pellets were resuspended in Milli-Q water and centrifuged three times at 4,400 G for 9 min at room temperature and aliquoted in 50 mL centrifuge tubes and allowed to rest at room temperature for several weeks.

3.3.1.2 Gold Nanorod and Nanoprism Characterisation using Transmisison Electron Microscopy

A 2 µL aliquot of gold nanoprisms and gold nanorods at 0.1 $mg.ml^{-1}$ in miliQ H_2O was dropped onto a carbon-coated grid and dried in air and observed using a LEOG12AB transmission electron microscope operating at 20−200 kV.

3.3.1.3 Gold Nanorod and Nanoprism UV-Visible Absorbance Spectra

The GNP UV-visible absorbance was analysed by our collaborators in Zaragoza. The measurement protocol has been described (Alfranca et al. 2016). Briefly, GNP solutions were mixed with DMEM to a final volume of 300 µL per sample, at a concentration of 0.02 and 0.1 $mg.ml^{-1}$. Spectra were subsequently produced using a Cary 50 Probe® spectrophotometer from Varian.

3.3.1.4 Gold Nanorod and Nanoprism Heating Capacity

The GNP heating capacity was assessed by our collaborators and was monitored using a temperature probe, placed into the GNP solutions during laser therapy, with the temperature recorded every 5 seconds as described (Alfranca et al. 2016). Briefly, 300 µL per sample of GNPs at a concentration of 0.02 and 0.1 $mg.ml^{-1}$ were heated in a 96 WP using a 1 W, 1064 nm laser beam for 1 minute.

3.3.2 Monolayer Cell Expansion and 3D Tumour Spheroid Culture

MG63 and MCF-7 cells were cultured in T75 flasks with Dulbecco's modified Eagles medium (DMEM) as described in section 2.2. Cells were seeded onto sterilised 13 mm coverslips within a 24 well plate at cell density of 1×10^4 per mL (for 2D monolayer culture) or 1×10^5 per mL (for 3D multicellular spheroid culture). Cells were grown for 24 hours prior to GNP exposure at 0.1 $mg.ml^{-1}$ (unless otherwise stated).

3.3.2.1 Tumour Spheroid Formation via Hanging Drop

A hanging drop 'device' to generate cell spheroids was created in-house using two 6 cm petri dishes and nine 200 µL pipette tips. Briefly, an array of 3x3 dots (using 24 WP format) was drawn on the base of a 6 cm dish and 2 mm holes were drilled into the corresponding dots. The holes were gently expanded to 3.5 mm while a 6 mm drill was used to gently widen the opening of the hole. Nine 200 µL pipette tips were cut with the "head" completely removed and half an inch from the bottom removed to acts as "chambers". The tips are then seated firmly onto the pre-drilled holes to create a suitable platform. This platform can be housed inside another 6

cm petri dish to form the lid and base of the device. Once prepared, the device was appropriately sterilised with 70% ethanol overnight, washed with sterile PBS (1x) and nitrogen dried. Cell concentrations with a maximum volume of 50 µL per chamber were gently pipetted into the chambers with the cell suspension forming a droplet at the bottom of the "chambers"/ pipette tips. The device was left in an incubator (37°C, 5% CO_2) overnight for spheroids to form naturally within the droplet.

3.3.2.2 Viability of 3D Tumour Spheroids Over Time

MG63 and MCF-7 cell viability during 3D spheroid culture was determined using the LIVE/DEAD® Viability/Cytotoxicity kit to verify the culture technique. Cells were expanded in flasks as described in section 2.2. MG63 and MCF-7 cells >90% confluence were trypsinised from flasks, centrifuged, counted and aliquots of cell suspensions at 1 x 10^4, 1 x 10^5 and 1 x 10^6 per 50 µL were prepared (n=5 for each cell density). The 50 µL cell solution was then gently pipetted into the chambers of the hanging drop device. The device was placed into an incubated humidified atmosphere with 5% CO_2 in air at 37°C for 24, 48 and 72 hours. After this point, 5 µL of fresh media was added to each chamber daily to accommodate for evaporation and availability of nutrients.

At allocated time points (24, 48 and 72 hours) the droplets containing the spheroids were gently transferred into a new 24 well plate. This was achieved by first removing the base of the device and aligning the 'chambers' of the device over a fresh 24 well plate. The fresh 24 well plate contained 1 mL of pre-warmed sterile PBS in each well. The device was placed on top of the 24 well plate and the droplets, containing the spheroids were carefully dropped into the PBS by gently flooding the top of each chamber with ~250 µL of warm PBS.

Spheroid viability was determined using the LIVE/DEAD® Viability/Cytotoxicity kit, as in section 2.3.2. Briefly, spheroids were washed gently in warm PBS three times. A media solution containing ethidium homodimer and calcein A/M (1 µL per mL) was then prepared and decanted into each well at 1 mL per spheroid. The well plate was foil wrapped and placed into an incubated humidified atmosphere with 5% CO_2 in air at 37°C for 1 hour. Spheroids were then washed twice in fresh warm media and imaged under an inverted fluorescence microscope as described in section 2.3.2. The excitation/emission wavelengths are 485nm/515 nm for

calcein A/M and 525/590 for EthD-1 and is viewed with FITC and TRITC filters, respectively.

3.3.3 GNP Labelled Monolayer and 3D Tumour Spheroid Biocompatibility

3.3.3.1 Cytotoxicity of GNP Labelled Monolayer and 3D Tumour Spheroids via the MTT Assay

The MTT assay, which measures cell metabolic activity, was used to determine the influence of GNP internalisation in MG63 and MCF-7 cells both in monolayer and 3D tumour spheroids. Control groups contained no GNPs.

Monolayer MTT Assay

MG63 and MCF-7 cells were seeded in 3 separate 96 well plates at $1x10^4$ cells per well and incubated for 24 hours prior to GNP introduction as described in section 2.3.1. Briefly, gold nanorods at concentrations of 0.01, 0.05 and 0.1 $mg.ml^{-1}$ and nanoprisms at 0.1, 0.5 and 1.0 $mg.ml^{-1}$were incubated with cells at 24, 48 and 72 hours (n=5). An aliquot of 10 µL of MTT dye solution was added to each well and the plates were incubated at 37°C for one hour. The media was then removed and 200 µL DMSO was used to solubilise the formazan crystals. The absorbance of each well was read on a microplate reader (Dynatech MR7000 instruments) at 550 nm.

3D Tumour Spheroids MTT Assay

A similar method was conducted for the 3D tumour spheroids. Cells were seeded at $1x10^5$ per well in a 96 well plate, after 24 hours cells were incubated with 0.1 $mg.ml^{-1}$ of either gold nanorods or nanoprisms for 24 hours to allow successful internalisation of GNPs into cells. The cells were then trypsinised and $1x10^5$ cells per spheroid were formed *via* a hanging drop method as described in 3.3.2.1, with the slight modification of spheroids dropped into a 96 well plate. The spheroids were then assayed at 24, 48 and 72 hours.

3.3.3.2 Cell Viability of GNP Labelled Monolayer and Tumour Spheroids

The LIVE/DEAD® Viability/Cytotoxicity kit was used to visualise the number of viable and dead cells within a sample. Monolayers of MG63 and MCF-7 cells were cultured at 1 x 10^4 per well for 24, 48 and 72 hours after 0.1 $mg.ml^{-1}$GNP incubation, as described in section 2.3.2. (n=3)

The cell viability of MG63 and MCF-7 cells labelled with GNPs and cultured in monolayer and 3D tumour spheroids was determined qualitatively using a LIVE/DEAD® Viability/Cytotoxicity. MG63 and MCF-7 cells were seeded at a density of 1 x 10^5 per mL, in a 24 well plate for 24 hours. Both nanorods and nanoprism GNPs were introduced to the samples (0.1 $mg.ml^{-1}$ in growth media; n=3) for a further 24 hours to allow for GNP uptake. After 24 hours, the media was removed and samples were washed twice in HEPES solution. An aliquot of 200 µL of trypsin/versene was added to each sample (5 minutes at 37ºC) until cell detachment, when 800 µL of media was decanted into each sample. Each replicate was pooled together and centrifuged for 4 minutes at 1400 rpm. Once centrifuged, the supernatant was removed and the cell pellet was re-suspended in 500 µL media; cells were counted on a haemocytometer and a cell solution of 1 x 10^5 per 50 µL was prepared. The 50 µL cell solution was was gently pipetted into the chambers of the hanging drop device. The device was then incubated at 37°C for 24 hrs. After 24 hours, spheroids were removed from the device and stained with ethidium homodimer and calcein A/M (1 µL per mL) and imaged as described previously (section 2.3.2) (n=5).

3.3.3.3 Scanning Electron Microscopy Analysis of GNP / Cell Interaction

To observe the interaction at the cell membrane level with the gold nanorods and nanoprisms, SEM was carried out. MG63 and MCF-7 monolayers were seeded at a cell density of 1 x 10^4 per mL onto 13 mm coverslips for 24 hours. GNPs at 0.1 $mg.ml^{-1}$ were then added to each sample, with samples fixed at both 1 and 24 hours after exposure. Samples were then processed for SEM as detailed in section 2.4.1.

3.4 GNP Internalisation into MG63 and MCF-7 Cells

3.4.1 Inductively Coupled Plasma Mass Spectroscopy Analysis of GNP Internalisation

To quantitatively assess the uptake rate of GNPs into MG63 and MCF-7 cells ICP-MS was performed. ICP-MS is a form of mass spectrometry capable of quantifying levels of elemental gold within samples, thus the technique was used to quantify the amount of GNPs internalised into both cell types at various GNP concentrations.

MG63 and MCF-7 cells were seeded in a 96 WP at 1 x 10^4 per well for 24 hours. Gold nanorods at concentrations of 0.3, 0.2, and 0.1 mg.ml^{-1}and gold nanoprisms at 0.02, 0.1 and 0.2 mg.ml^{-1} were added to cells (n=3). Cells containing no GNPs were used as control groups. After 24 hours, cells were washed in 1X PBS to remove extracellular GNPs. An aliquot of 200 µL of RIPA buffer was added to each sample for 10 minutes at room temperature. The buffer was then removed and added to 50 mL centrifuge tubes. Each well was then washed with 100 µL of distilled water and subsequently added to each of the corresponding centrifuge tubes. An aliquot of 1 mL of AquaRegia (3:1 mix of HCL and 70% nitric acid) was added to each tube and heated in a water bath overnight at 70°C. The samples were then made up to 50 mL using distilled water and were prepared for ICP-MS analysis. The converted values for GNP uptake were averaged (n=3) and used for statistical analysis.

3.4.2 Cell Cytoskeleton Staining

The fluorescence staining of β-tubulin and F-actin filaments was completed as described in section 2.4.3. Briefly, MG63 and MCF-7 cells were seeded onto 13 mm sterilised coverslips within a 24 well plate at a cell density of 1 x 10^4 for 24 hours. GNPs (0.1 mg.ml^{-1}) were then added to samples for 24 hours prior to fixation and processing (n=3).

3.4.3 Transmission Electron Microscopy Analysis of GNP Internalisation

To qualitatively assess gold nanorod and nanoprism internalisation by both cell types, TEM was carried out. MG63 and MCF-7 cells were incubated with the GNPs (0.1 $mg.ml^{-1}$) in monolayer, prior to spheroid formation. The spheroids were subsequently fixed after 24 hours and processed for TEM as described in section 2.4.2.

3.4.4 Near Infrared Irradiation of GNP Labelled Monolayer and 3D Tumour Spheroids

A Ventus 1 W unfocused continuous wave 1064 nm laser was used to irradiate GNPs that have been successfully internalised within cells in both monolayer and 3D tumour spheroid culture. A viability stain was then used to visualise any resultant cell death after 1 minute laser irradiation (n=3). Control samples containing no GNPs were also irradiated and used to evaluate any potential effect of laser exposure on cells.

3.4.4.1 Monolayer Culture Study

For monolayer study, cells were cultured in a 24 well plate at a cell density of $1x10^4$ per sample. After 24 hours, cells were incubated with 0.1 $mg.ml^{-1}$ GNPs for 12 hours (to allow for GNP internalisation) and subsequently trypsinised and seeded onto 13 mm coverslips. The cells were cultured on the coverslips for a further 12 hours prior to irradiation. Cell samples were transferred to laser compatible culture chambers and positioned directly beneath the laser beam. Samples were then laser irradiated for 1 minute in triplicate, transferred back into the 24 WP and incubated for ~3 hours at 37°C, at which point cells were stained using the viability kit as described in section 2.3.2.

3.4.4.2 3D Tumour Spheroid Study

Spheroids at $1x10^5$ were prepared after monolayer incubation with GNPs (0.1 mg.ml) and were treated exactly as the monolayer samples above.

3.4.5 Statistics

Statistical analysis was performed in Graphpad using a one-way ANOVA. In all figures * = $p<0.05$, ** = $p< 0.01$, *** = $p<0.001$. Two tailed T-test were performed where mentioned.

3.5 Results

3.5.1 Synthesis, Functionalisation & Characterisation of GNPs

3.5.1.1 GNP Size and Morphology via TEM

Gold nanoprism and nanorod size, morphology, aggregation and purity were determined by TEM (figure 3-1). The images confirmed successful synthesis of both nanorods and nanoprism geometries. The nanoprisms were well dispersed, with varying sizes, with no indication of aggregation (figure 3-1 A,B). The nanoprism morphology indicated diversity not simply in size but also in the sharpness of the tips, which has been previously shown to affect absorbance (M. R. Jones et al. 2009; K. L. Kelly et al. 2003; K. L. Shuford et al. 2005a). Gold nanorods were also well dispersed and approximately 50 x 10 nm in size (average aspect ratio 7.2) (figure 3-1 C,D). Both GNP preparations did, however, present pseudo-spherical polyhedral particles.

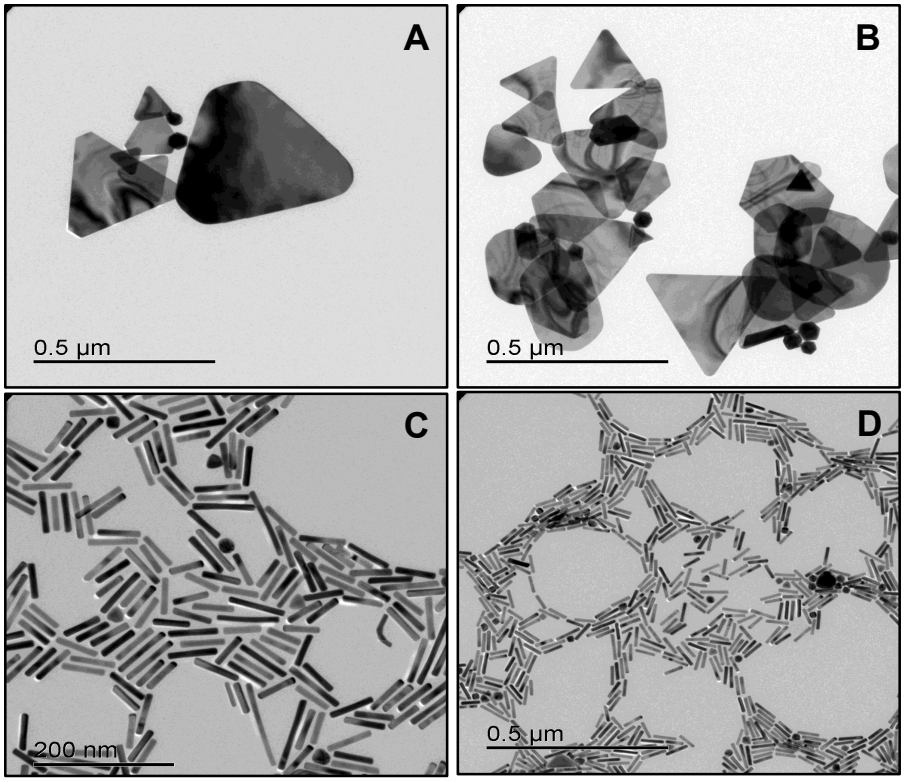

Figure 3-1: TEM images of gold nanoprisms (A,B) and nanorods (C,D), obtained at 20-200kV. Polyhedral by-products were observed in both samples.

3.5.1.2 UV-Visible Spectra of GNP Absorbance

UV-Vis spectroscopy results were performed by our collaborators in Zaragoza (figure 3-2). Both GNP preparations showed increased absorbance at longer wavelengths with peaks ~1064 nm (SPR) and thus heat generation when exposed to NIR wavelengths. While nanorods showed steep absorbance from ~900 nm until ~1064 nm and a subsequent decrease of absorbance at longer wavelengths thereafter, gold nanoprisms show a steady near-linear increase in absorbance from ~630 nm to ~1064 nm with an apparent increase in absorbance at longer wavelengths. Both GNPs also displayed a high absorbance peak at ~530 nm which may be due to a combination of GNPs transversal absorbance and pseudo-spherical polyhedral gold nanoparticles within solutions which were also observed in TEM images above.

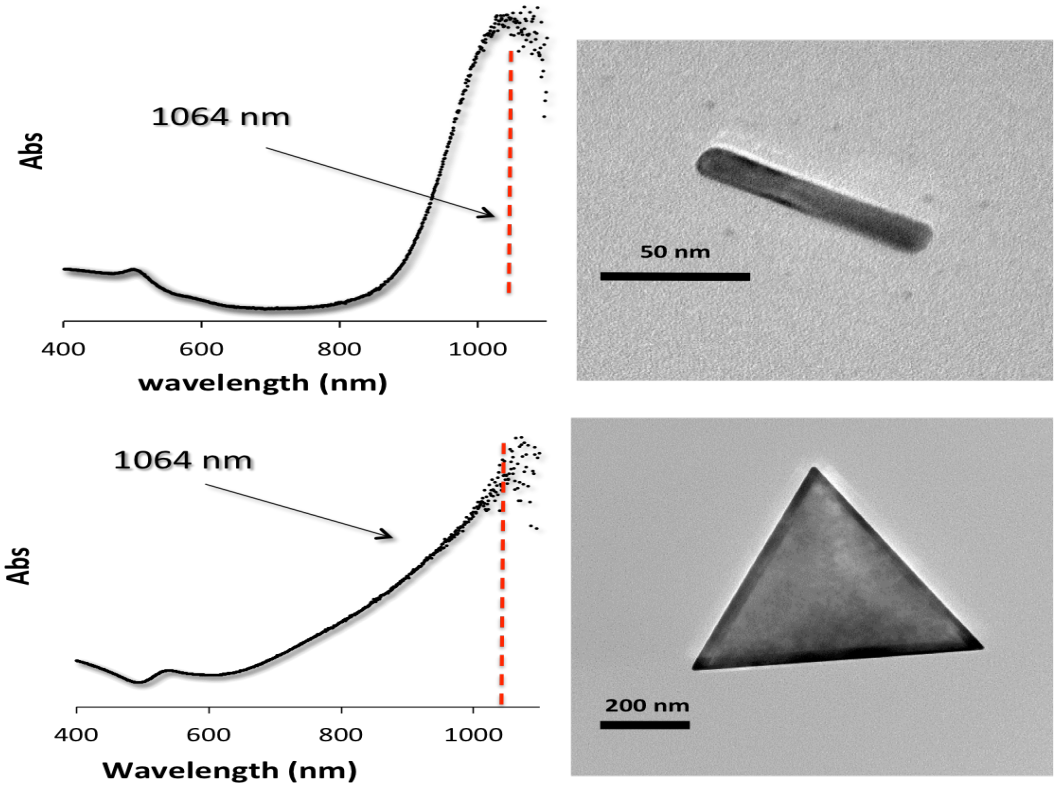

Figure 3-2: The absorbance spectra for both gold nanorods and nanoprisms. Both GNPs present peak absorption values around 1064 nm wavelength (indicated by red dashed line).

3.5.1.3 GNP Heating Capacity in Response to Irradiation

Following verification of the peak absorption at 1064 nm, the heating capacity of both GNPs was investigated following irradiation with a Ventus 1064 nm continuous wave laser. Both gold nanoprisms and nanorods demonstrated impressive heating capability at both 0.02 and 0.1 mg.ml^{-1}, producing hyperthermic profiles within 60 seconds (figure 3-3). Gold nanorods achieved higher temperatures faster than their nanoprism counterparts; nanorods were able to reach hyperthermic profiles at ~30 seconds at 0.1 mg.ml^{-1} while nanoprisms at the same concentration required ~50 seconds. At 60 seconds, 0.1 mg.ml^{-1} concentrations displayed temperatures above hyperthermic profiles, with gold nanorods in particular showing heating above 50°C. Blank samples containing DMEM were used to determine the heating effects of laser exposure alone, within a typical biological solution and a modest elevation of 3°C was noted after 60 seconds.

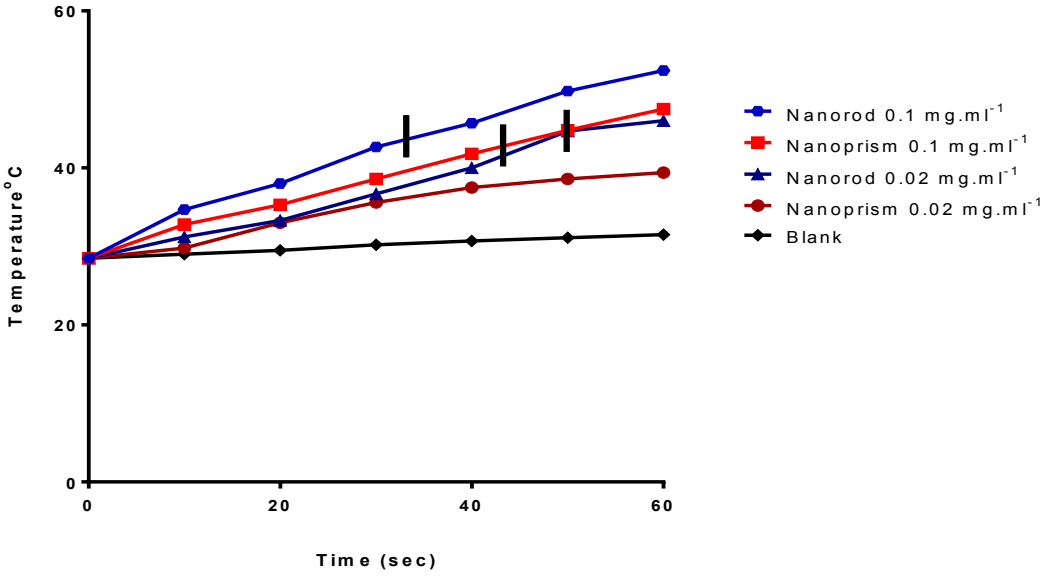

Figure 3-3: The hyperthermic temperature profiles of both gold nanoprisms and nanorods at 0.02 and 0.1 mg.ml^{-1} concentration during 60 seconds of irradiation with a 1064 nm continuous wave 1 W laser.

3.5.2 Monolayer Cell Expansion and 3D Tumour Spheroid Culture

3.5.2.1 Tumour Spheroid Formation via Hanging Drop

MG63 and MCF-7 spheroids were formed *via* an in-house hanging drop device. 50 µL of cell suspension was gently decanted into the nine 200 µL pipette tips, with spheroids forming naturally after ~24 hours incubation.

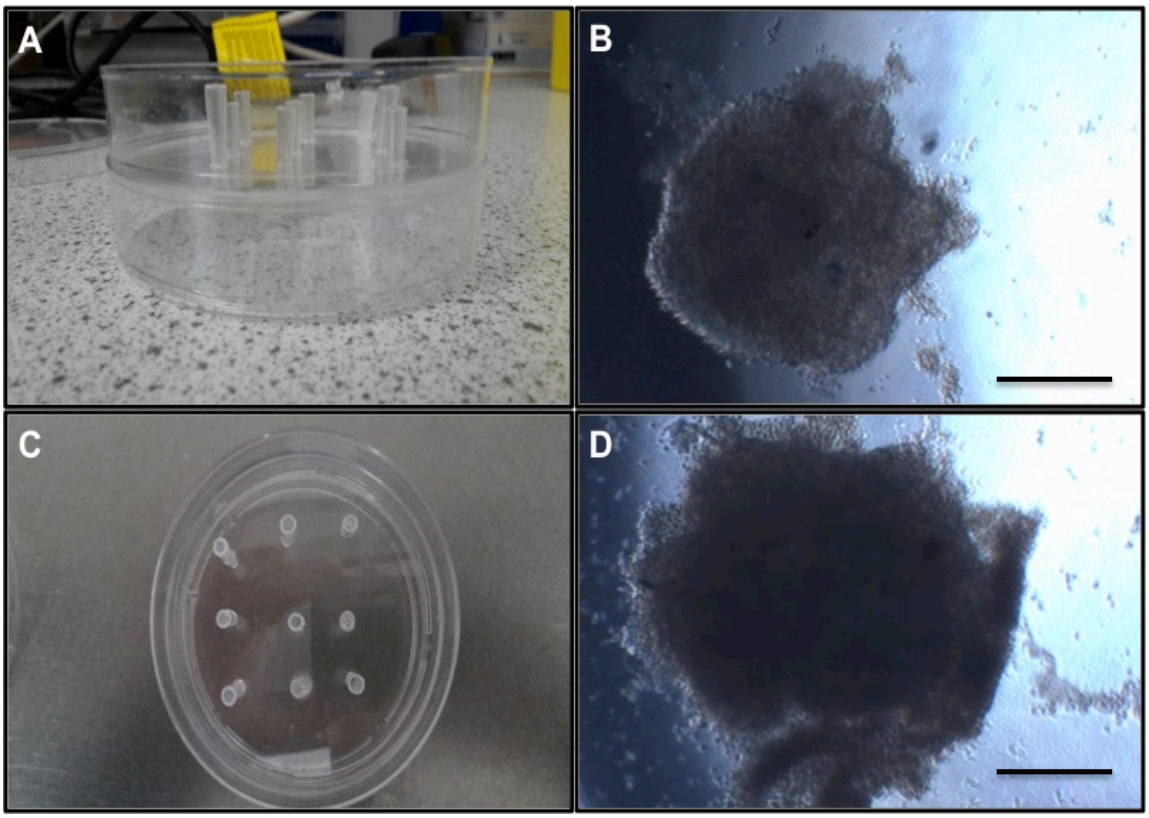

Figure 3-4: In house, hanging drop device (A, C) and formation of MCF-7 cells at a cell density of 1 x10^4 (B) and 1 x 10^5 (D) spheroids. Scale bar depicts 10 µm.

3.5.2.2 3D Tumour Spheroid Viability

Cell viability of 3D tumour spheroids was assessed using the viability staining kit. Figure 3-5 indicates the MG63 spheroids (A and B) and figure 3-6 for MCF-7 spheroids (A and B) at different cell densities when cultured for 24, 48 and 72 hours. Several observations were made; (1) cells were viable across the time points studied; (2) the increased cell density correlated with a larger spheroid

diameter; (3) cells appeared to proliferate over time, with a clear increase in spheroid diameter. Spheroid growth patterns were however inconsistent as indicated by the variability within samples (n=5). It was noted that at lowest, 1 x 10^4 cell density at 24 hours, unified spheroids were not often formed and instead, micro-satellite clusters of cells were observed; this prevented the accurate recording of a single spheroid size per replicate. However, at the same cell density after 48 hours, the maturation of a single spheroid was observed in both cell types. Strikingly, the spheroids displayed very obvious growth in size in modest time frames, which has not been seen in the literature with studies using similar techniques. Due to the technical limitations of using a standard fluorescence microsocope, the focal plane was focussed on the peripheral reigons of the spheroid in order to guage the overal size of the spheroid. Thus, in some of these images, the out of focus plane often coincinded with a lack of observable fluorescence within the centre of the spheroid. This could be remedied using a confocal microscope to appropriately image spheroids, as shown by previous groups (Sirenko et al. 2015; Zanoni et al. 2016).

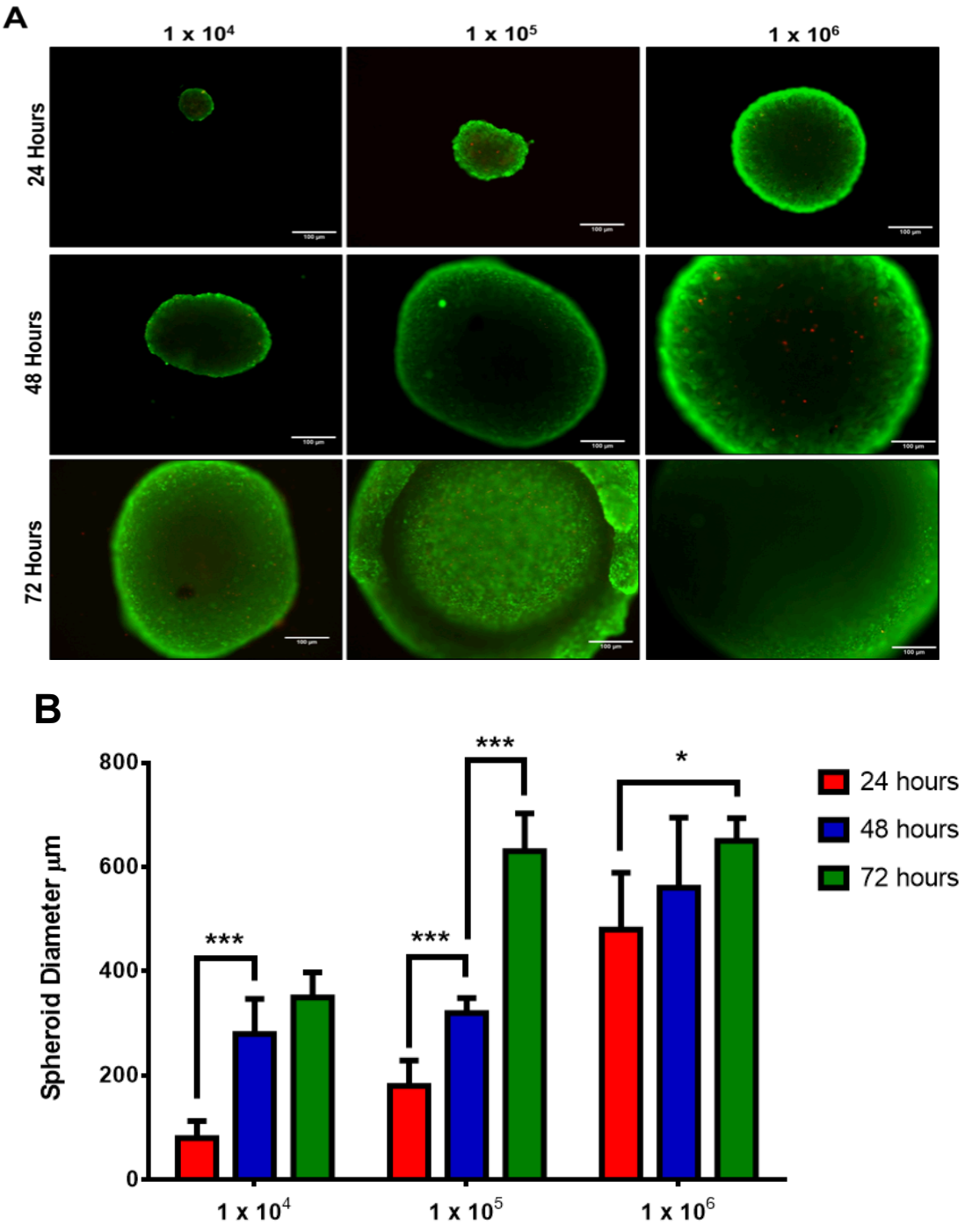

Figure 3-5: Cell viability staining, illustrating the spheroid diameter of MG63 cells and the corresponding graphical representation of spheroids cultured for 24, 48 and 72 hours at a cell densities of 1 x 10^4, 1 x 10^5 and 1 x 10^6. Cells were stained with calcein AM (green) and ethidium homodimer (red) to observe live and dead cells respectively (A). Spheroid diameter measurements were taken; scale bars depict 100 µm (B) Error bars denote standard deviation (n=5). Two tailed T-test was performed * = p<0.05, ** = p< 0.01, *** = p<0.001.

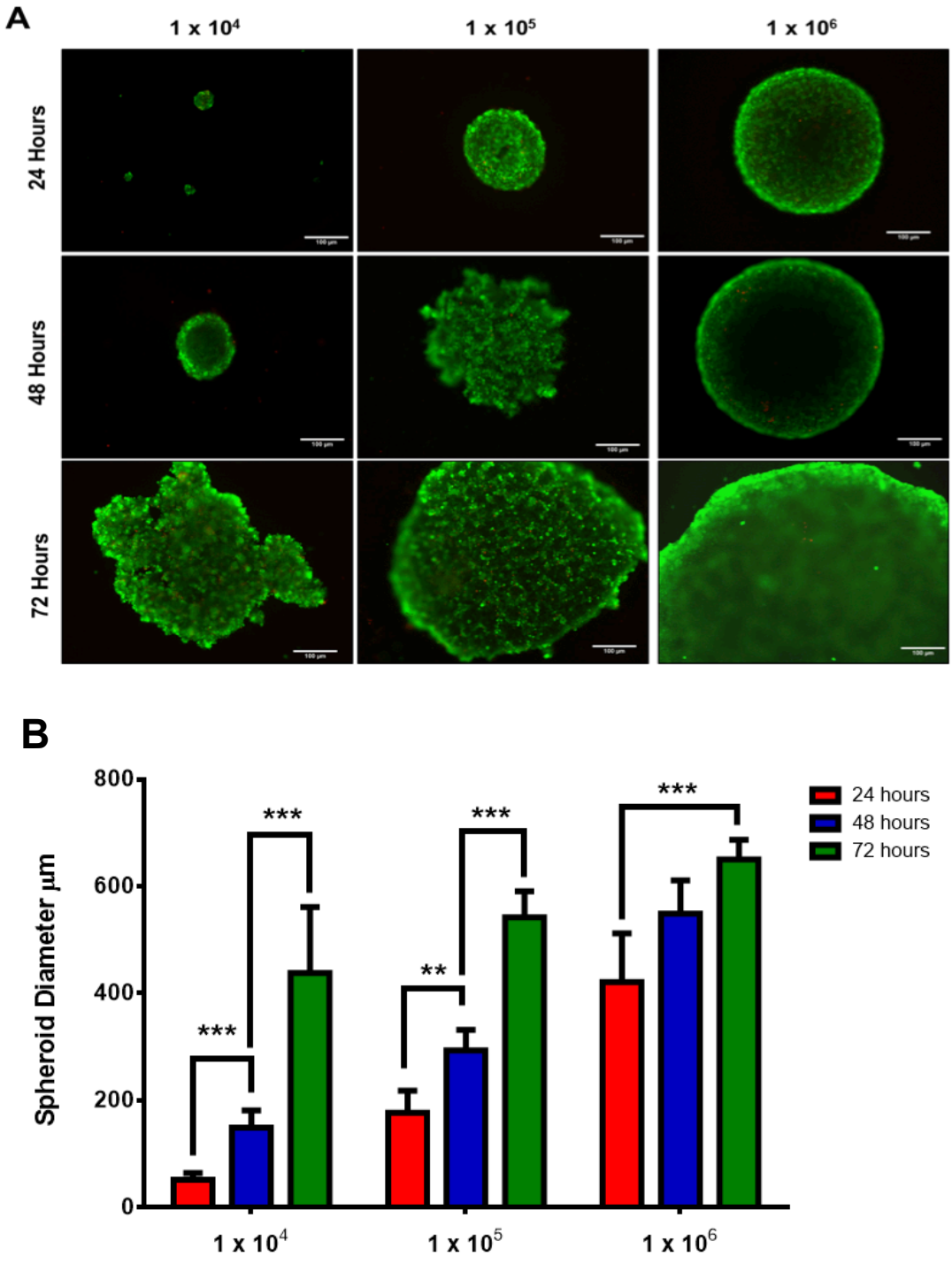

Figure 3-6: Cell viability staining, illustrating the spheroid diameter of MCF-7 cells and the corresponding graphical representation of spheroids cultured for 24, 48 and 72 hours at a cell densities of 1 x 10^4, 1 x 10^5 and 1 x 10^6. Cells were stained with calcein AM (green) and ethidium homodimer (red) to observe live and dead cells respectively (A). Spheroid diameter measurements were taken; scales bar depict = 100 µm (B) Error bars denote standard deviation (n=5). Two tailed T-test was performed * = p<0.05, ** = p< 0.01, *** = p<0.001.

3.5.3 GNP Labelled Monolayer and 3D Tumour Spheroid Biocompatibility

3.5.3.1 GNP Labelled Monolayer and 3D Tumour Spheroid MTT Assay

The debate over the biocompatibility of GNPs utilised in cell culture studies has been discussed extensively within the literature (Chuang et al. 2013; Connor et al. 2005; Naha et al. 2015; H. K. Patra et al. 2007a), however only a modest consensus have suggested GNPs themselves may be inherently toxic (A. M. Alkilany and Murphy 2010; A. M. Alkilany et al. 2012). Therefore an MTT assay was performed to assess the potential toxicity, in terms of cell metabolic activity, of GNPs when cultured with MG63 and MCF-7 cells, both in 2D and 3D spheroid models. The MTT assay was performed on both MG63 and MCF-7 cells in monolayer at 24, 48 and 72 hrs after GNP incubation. Cells were exposed to gold nanoprisms at 0.1, 0.2, 0.5 and 1.0 $mg.ml^{-1}$ and nanorods at 0.01, 0.05, 0.1 and 0.2 $mg.ml^{-1}$. A control group containing no GNPs was used as a benchmark at an assumed 100% metabolic activity.

Monolayer MTT Study

Gold nanoprisms did not appear to show any signs of toxicity, with consistent levels observed at all time points in both cell types, with MCF-7 cells actually indicating an increase in cell metabolic activity (figure 3-8, A). Meanwhile, whilst both MG63 and MCF-7 cells incubated with gold nanorods showed high levels of metabolic activity across the three time points at the lower concentrations, there was a clear drop in cell metabolic activity at the higher concentration at all time points (0.2 $mg.ml^{-1}$; figure 3-7, B and figure 3-8, B). In particular with MCF-7 cells, where cell activity appeared compromised at 24 hours (75%), it did improve with time in culture, rising to 95% at 48 hours and 90% at 72 hours. These results were in agreement with the viability staining, which indicated several dead cells when exposed to gold nanorods.

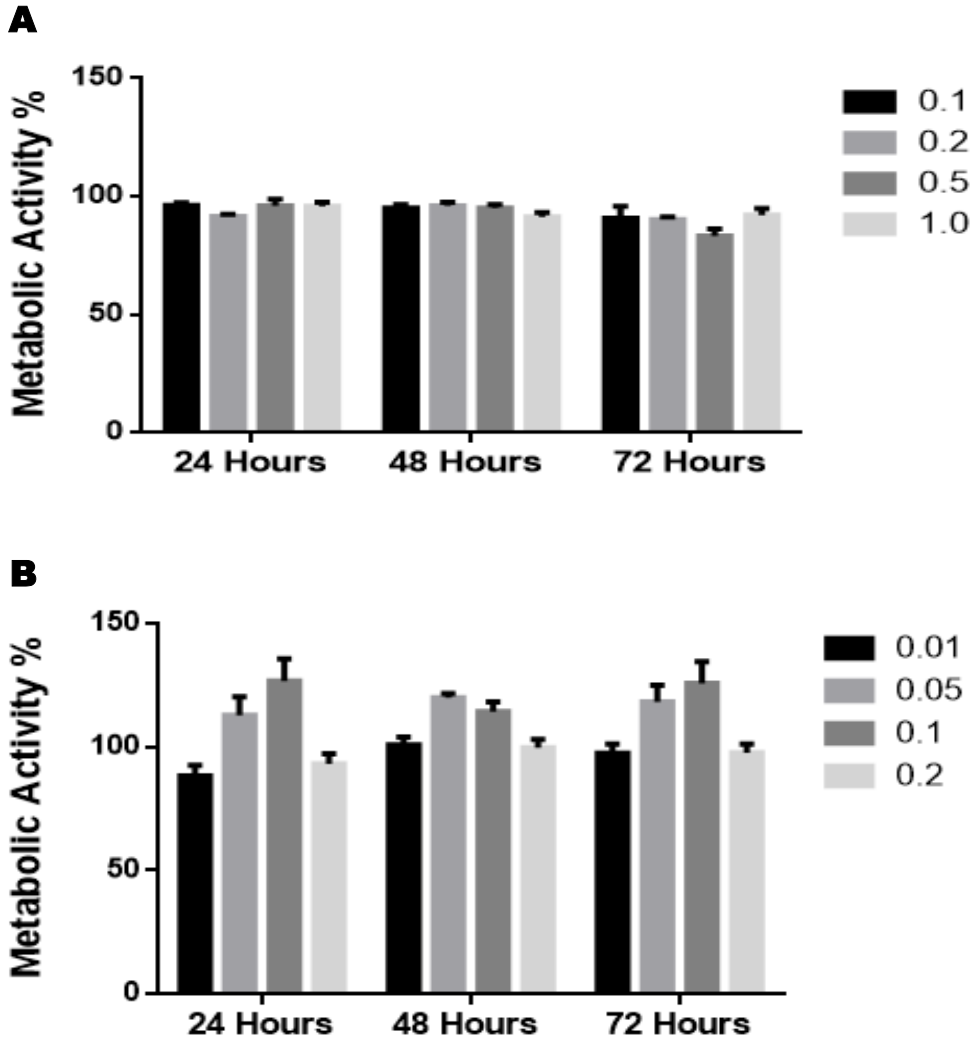

Figure 3-7: MTT assay indicating GNP labelled cell metabolic activity over time in monolayer culture. MG63 cells were treated (A) with gold nanoprisms, and (B) gold nanorods. Values are presented as mean +/- SD (n=5).

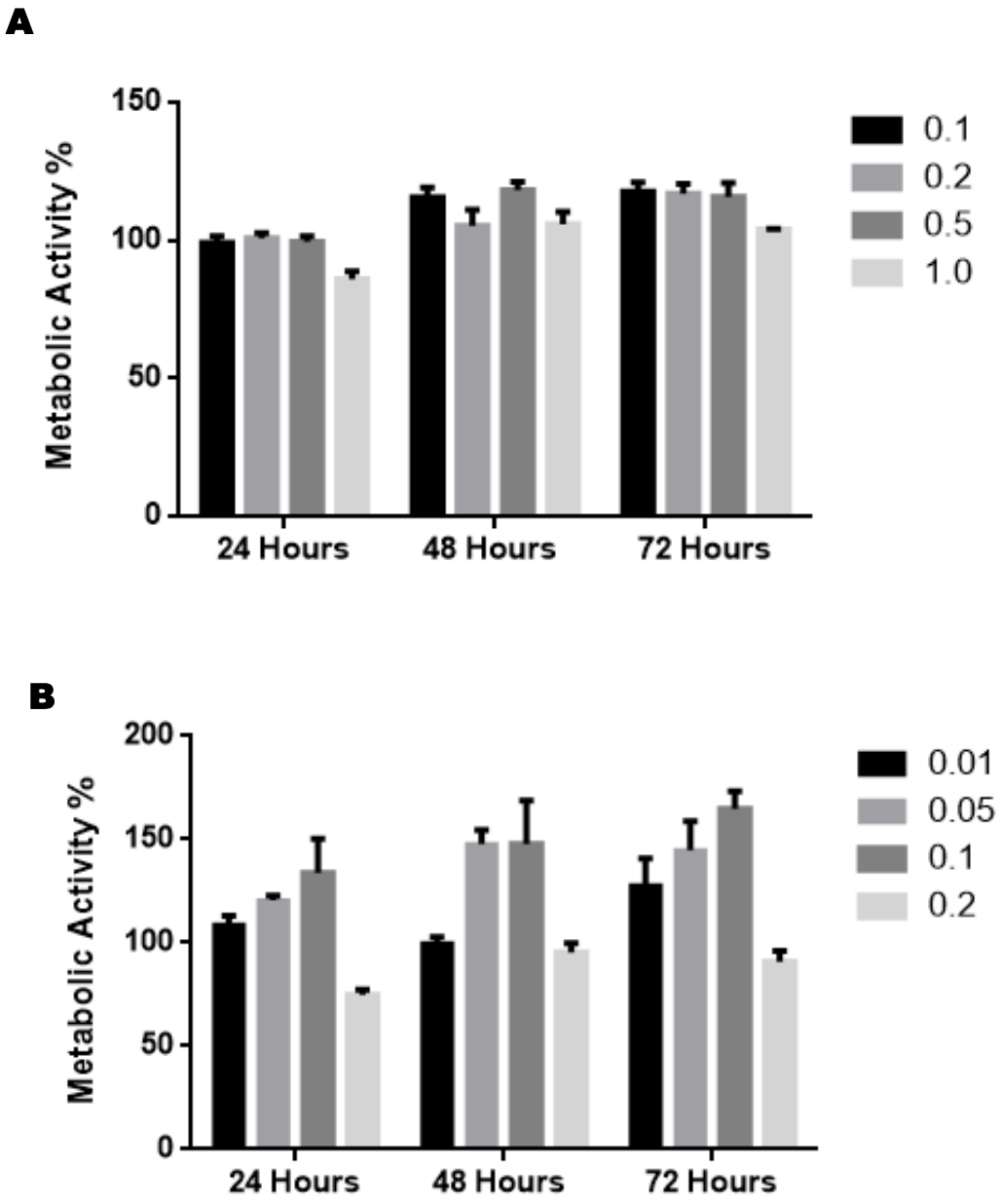

Figure 3-8: MTT assay indicating GNP labelled cell metabolic activity over time in monolayer culture. MCF-7 cells were treated (A) with gold nanoprisms, and (B) gold nanorods. Values are presented as mean +/- SD (n=5).

3D Tumour Spheroid MTT Study

The metabolic activity of GNP labelled spheroids was over 80% in all conditions, with no compromise in spheroid development over 72 hours, demonstrating the biocompatibility of GNPs in 3D systems (figure 3-9). Both cell types showed improved metabolic activity in a near time-dependent manner.

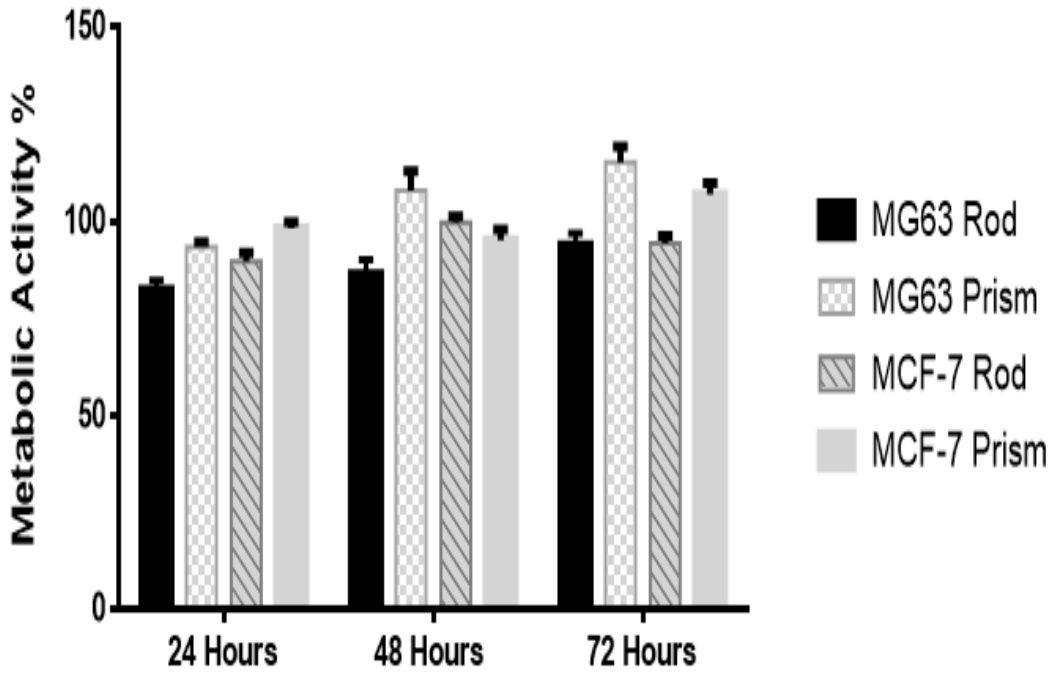

Figure 3-9: MTT assay indicating GNP labelled cell metabolic activity over time in 3D tumour spheroid culture. MG63 and MCF-7 cells were incubated with 0.1 mg.ml^{-1} of gold nanorods and nanoprisms prior to subsequent spheroid formation and culture up to 72 hours. Values are presented as mean +/- SD (n=5).

3.5.4. Viability of GNP Labelled Monolayer and 3D Tumour Spheroids

The cell viability of both MG63 and MCF-7 cells following GNP labelling was determined in monolayer and 3D spheroid culture *via* live/dead staining.

3.5.4.1. Live/Dead assay of MG63 and MCF-7 Monolayers

The fluorescent viability assay was performed to assess the viability of MG63 and MCF-7 monolayer cultured cells incubated with both GNP preparations at 0.1 $mg.ml^{-1}$ for 24, 48 and 72 hours. Both cell types demonstrated a high quantity of viable cells across the time points, similar to control samples (containing no GNPs) (figure 3-10 A, B). In addition, the cell number increased over time in culture, suggesting that the presence of the GNPs did not affect cell proliferation. The gold nanoprisms in particular was coincided by an increase in cell density that was prevalent at all time points. Conversely, the gold nanorods did produce a few dead cells, although the overall cell culture did not appear negatively affected.

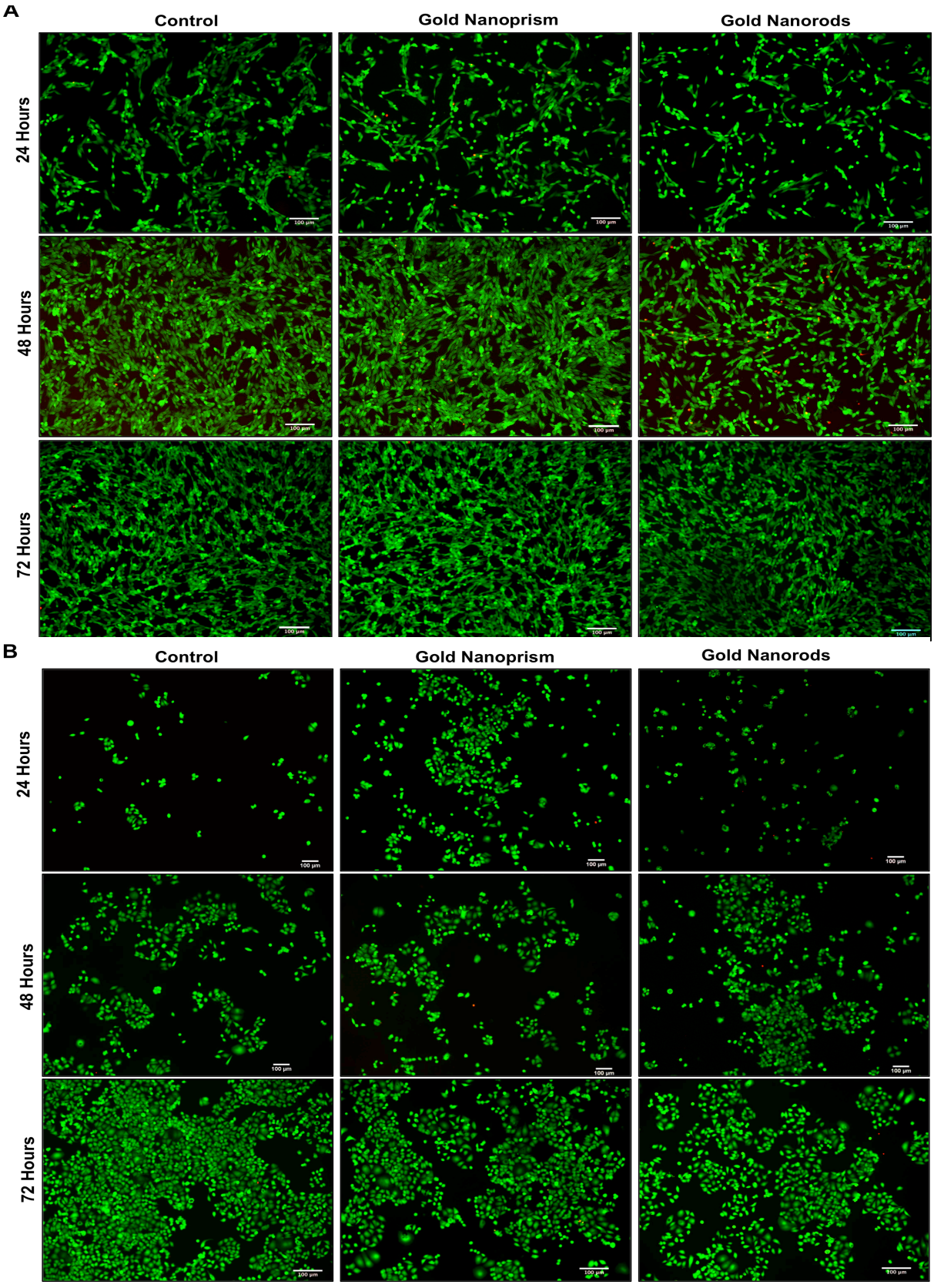

Figure 3-10: Fluorescent viability staining of (A) MG63 cells and (B) MCF-7 cells, incubated with 0.1 mg.ml^{-1} gold nanoprisms or nanorods for 24, 48 and 72 hours. Green fluorescence signals indicate viable cells and red indicates dead (control cells contain no GNPs). Scale bar depicts 100 µm.

3D Tumour Spheroid Viability Study

Figure 3-11 indicates the spheroid viability staining, where cell viability was maintained throughout and successful growth and maturation of spheroids was noted for both cell types in the presence of 0.1 $mg.ml^{-1}$ GNPs.

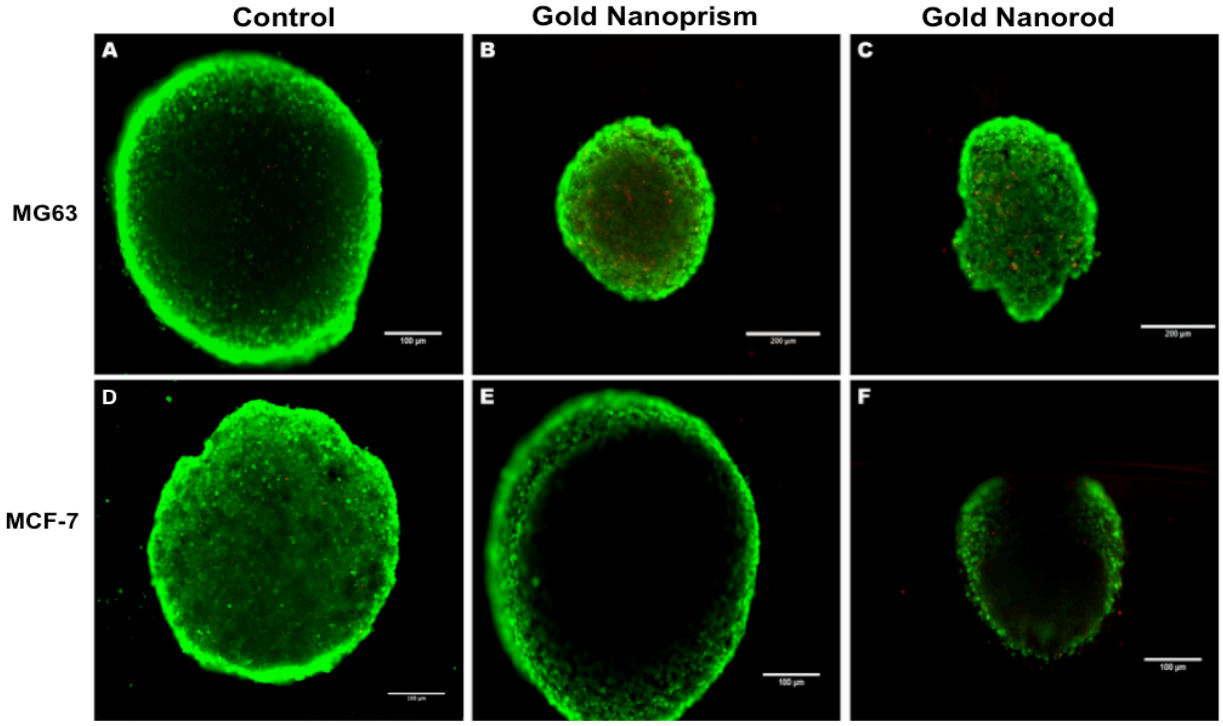

Figure 3-11: Cell viability staining of GNP labelled MG63 and MCF-7 spheroids. ***MG63 spheroids were incubated with (A) no GNPs; (B) gold nanoprisms and (C) gold nanorods, whilst MCF-7 spheroids were incubated with (D) no GNPs; (E) gold nanoprisms and (F) gold nanorods.***

3.5.5. Observation of GNP/Cell Interaction Using SEM

SEM was used to provide a magnified view of the cell morphology after incubation with the GNP preparations. Figure 3-12 and 3-13 show MG63 and MCF-7 cells, respectively. Both figures highlighted an increased number of cytoplasmic extensions in the form of filopodia in the presence of GNPs, while control groups (containing no GNPs) demonstrated a smooth cell surface. GNP deposits were also observed around some of the cells and on the glass coverslip.

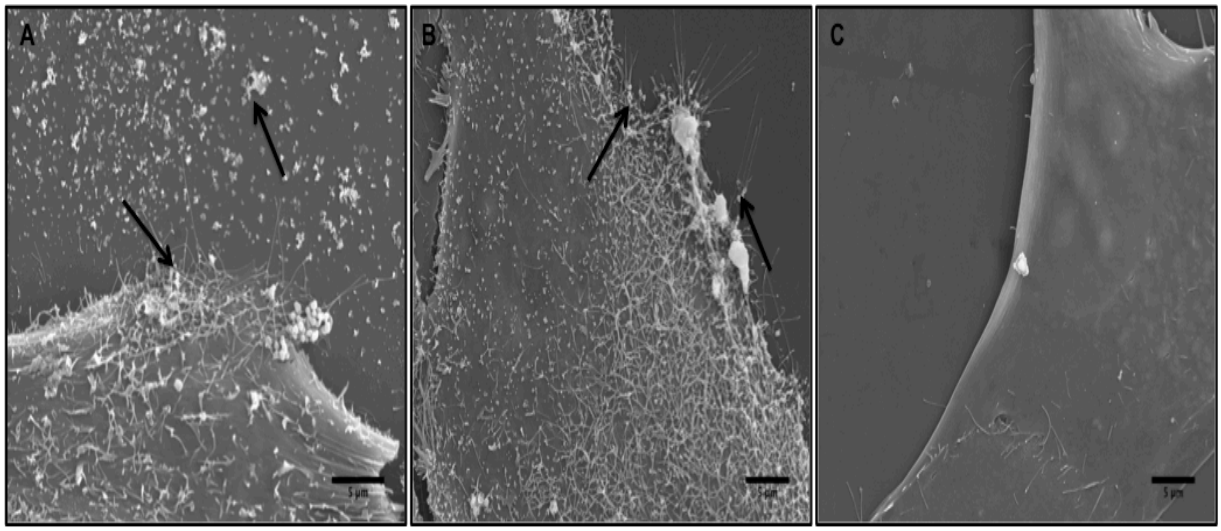

Figure 3-12: SEM images of MG63 cells incubated for 24 hours with (A) gold nanoprisms, and (B) gold nanorod, whilst (C) control cells were not incubated with GNPs. GNP deposits were observed both on the cell membrane and on the coverslip surface (black arrowheads), inducing a large number of filopodia compared to controls. Scale bar depicts 5 µm.

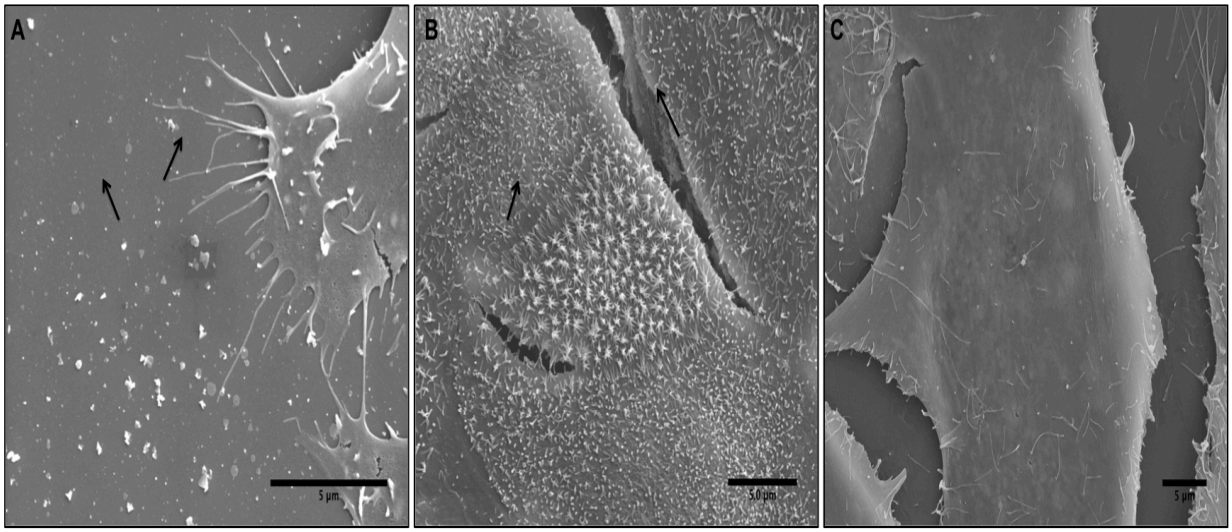

Figure 3-13: SEM images of MCF-7 cells incubated for 24 hours with (A) gold nanoprisms, and (B) gold nanorods, whilst (C) control cells were not incubated with GNPs. GNP deposits were again observed on the cells (black arrowheads), producing more filopodia compared to controls. Scale bar depicts 5 µm.

3.5.6. GNP Internalisation into MG63 and MCF-7 Cells

3.5.6.1 Quantitative Analysis of GNP Internalisation into Cells in Monolayer by Inductively Coupled Mass Spectrometry

ICP-MS is an analytical technique used for the detection of elements in a sample. A quantitative assessment was required to analyse the GNP internalisation after 24 hours to (1) verify cellular internalisation and (2) determine any difference in internalisation due to GNP type (morphology).

Results clearly indicated that the gold nanoprisms were internalised far more efficiently than the nanorods (figure 3-14). The increase in GNP concentration correlated to an increased GNP internalisation for both cell types, but neither GNP types showed any difference in internalisation between the two cell lines. One point to note is that the gold nanoprisms are considerably larger than their nanorod counterparts and thus these results could be slightly misleading as even a low quantity of nanorprism internalisation could translate to a percieved higher internalisation rate compared to nanorods; TEM was therefore conducted to validate these reuslts within 3D multicellular spheroids.

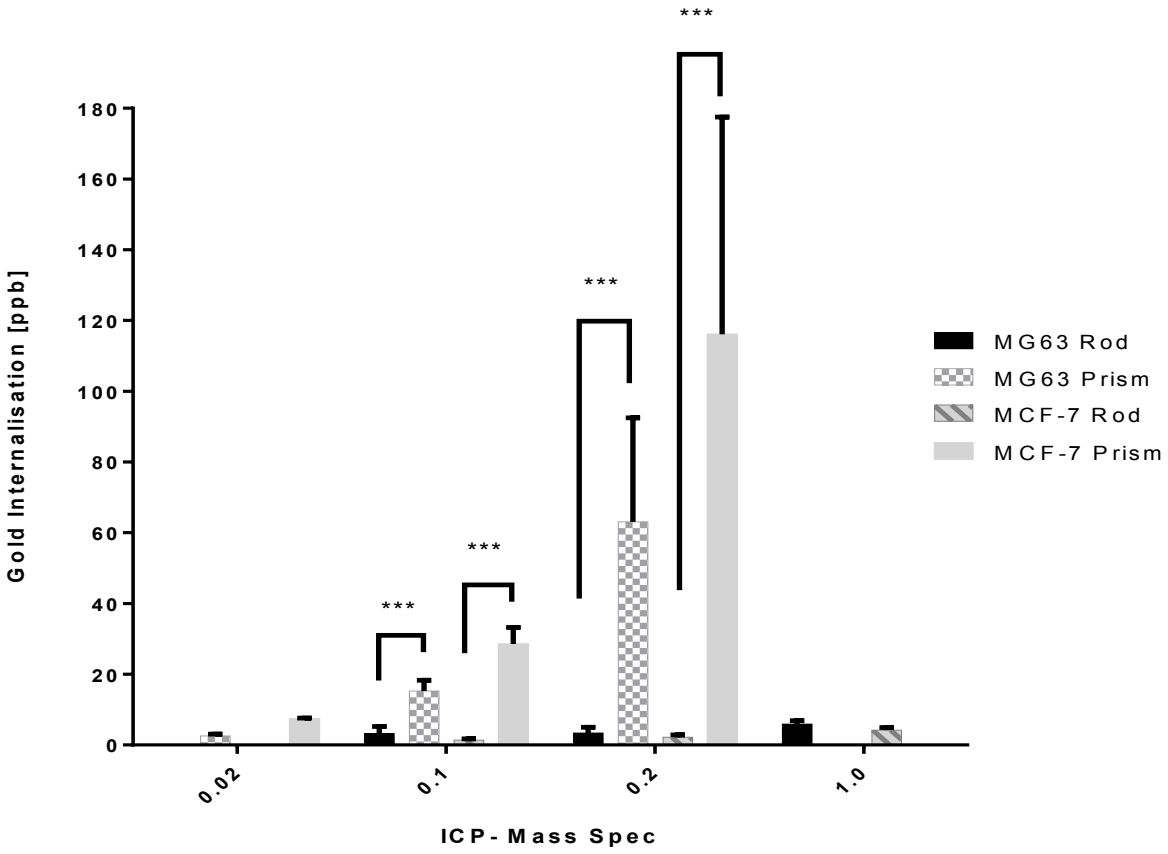

Figure 3-14: ICP-MS analysis of MG63 and MCF-7 monolayer cells treated with various concentrations of GNPs at 24 hours (n=3, error bars denote SD).

3.5.6.2 The Influence of GNP Internalisation on Cell Cytoskeletal Structure

GNP internalisation is thought to be *via* endocytosis, which involves the cell cytoskeleton. The SEM images clearly indicate cell membrane extensions and filopodia in response to GNP incubation and internalisation; therefore components of the cytoskeleton, namely β-tubulin and F-actin microfilaments, were stained and observed. Disruption to the cytoskeleton can lead to inhibition of cell viability, cell proliferation and cell function (Alice Panariti et al. 2012b).

Figure 3-15 illustrates MG63 cytoskeletal staining following cell incubated with gold nanoprisms and gold nanorods at 0.1mg.ml^{-1} after 24 hours (control cells with no GNPs). Control cells are well spread, with distinct microtubules and actin filaments radiating throughout the cells. Conversely, the cells incubated with

nanoprisms exhibit a smaller, more elongated cell morphology, with tightly packed microtubules and filaments. This may reflect the high internalisation noted with ICP-MS and TEM data. The cell morphology of MG63 cells, when incubated with the nanorods was also notably different to control, with a high degree of actin polymerisation, a lack of actin stress fiber formation and ruffling at the cell periphery, most likely due to nanorod endocytosis.

Figure 3-16 is identical, but illustrates MCF-7 cytoskeletal staining. In this case, the cells do not appear to react as strongly as the MG63 cells. Generally, cells incubated with either prisms or rods are comparable with control cells in terms of size and shape, with visible tubulin integrity. F-actin staining suggested some actin remodeling in response to the GNPs but the cells maintained a well spread morphology where microfilaments formed stress fibers heterogeneously throughout the cell. Vacuoles, similar to that seen in MG63 treated gold nanorod samples, were also prevalent, indicating a similar up-take mechanism was adopted by both MG63 and MCF-7 cells, when internalising gold nanorods.

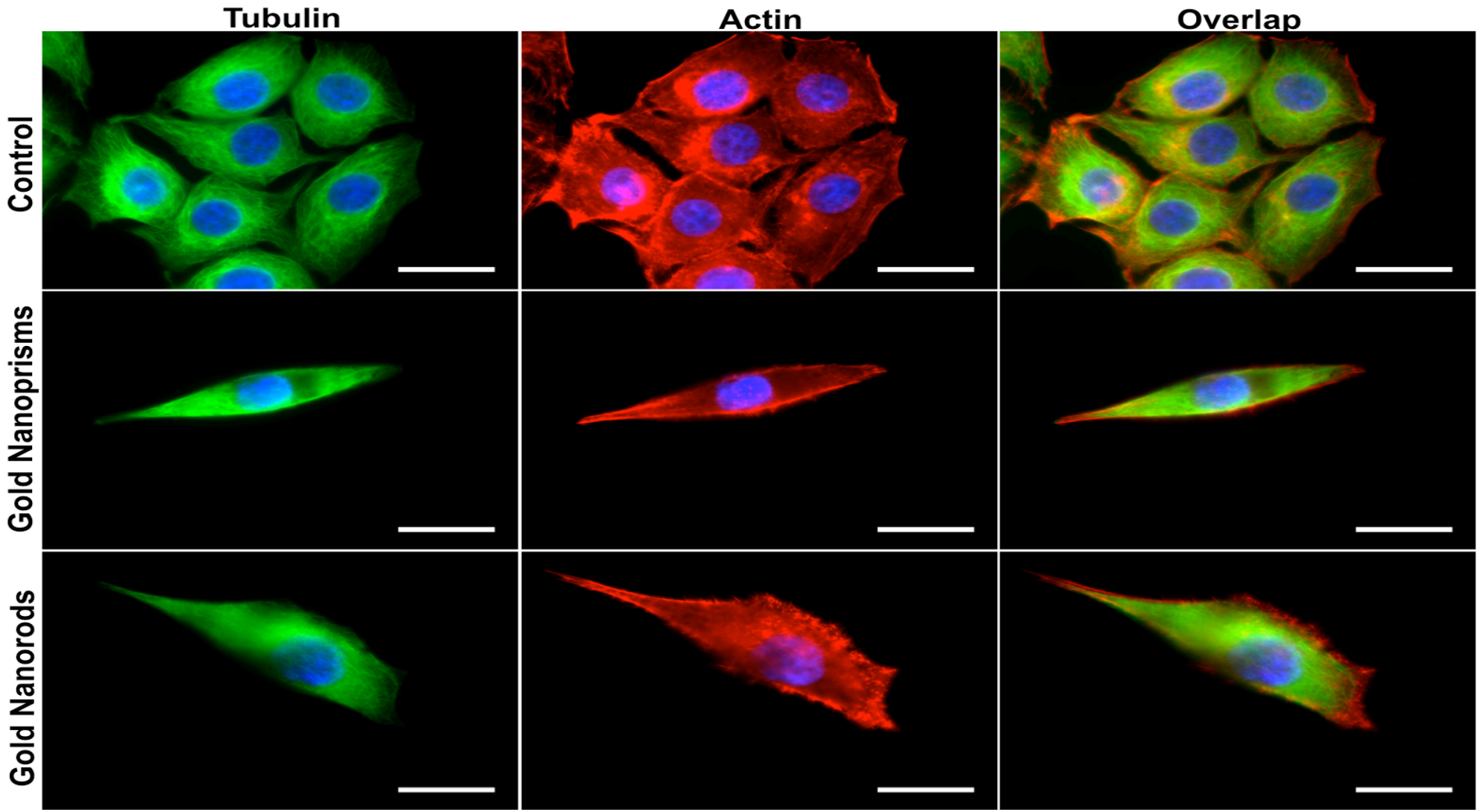

Figure 3-15: Representative fluorescence images of MG63 cells, 24 hours after 0.1 mg.ml-1GNP incubation. Images depict the F-actin cytoskeleton (red), β-tubulin (green) and DAPI-stained nuclei (blue); scale bars: 50 µm.

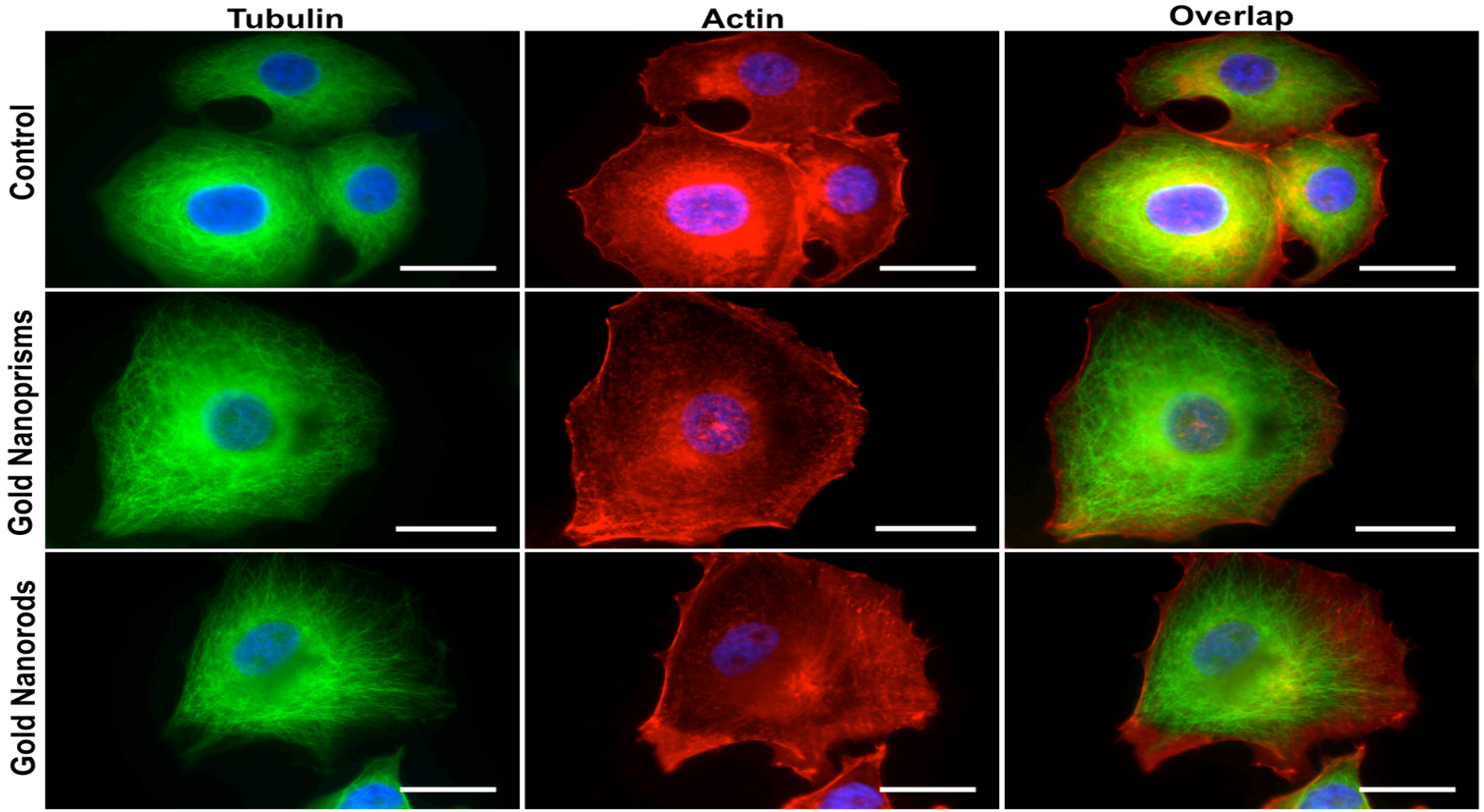

Figure 3-16: Representative fluorescence images of MCF-7 cells, 24 hours after 0.1 mg.ml-1 GNP incubation. Images depict the F-actin cytoskeleton (red), β-tubulin (green) and DAPI-stained nuclei (blue); scale bars: 50 µm.

3.5.6.3 GNP Intracellular Localisation within Spheroid Cultures Observed using TEM

TEM images confirmed the successful internalisation by both cell lines and further indicated the intracellular localisation of both GNP types into endosome-like structures (Huefner et al. 2014) within the 3D tumour spheroids (figure 3-17). The TEM images appeared to support the ICP-MS data with a visible difference between the amount of nanoprisms and nanorods internalised into cells. The nanorods did not appear to be aggregated, however the nanoprisms did seem to aggregate within cell endosomes. No GNPs were observed free within the cytoplasm; suggesting GNP internalisation was *via* a form of endocytosis rather than passive diffusion.

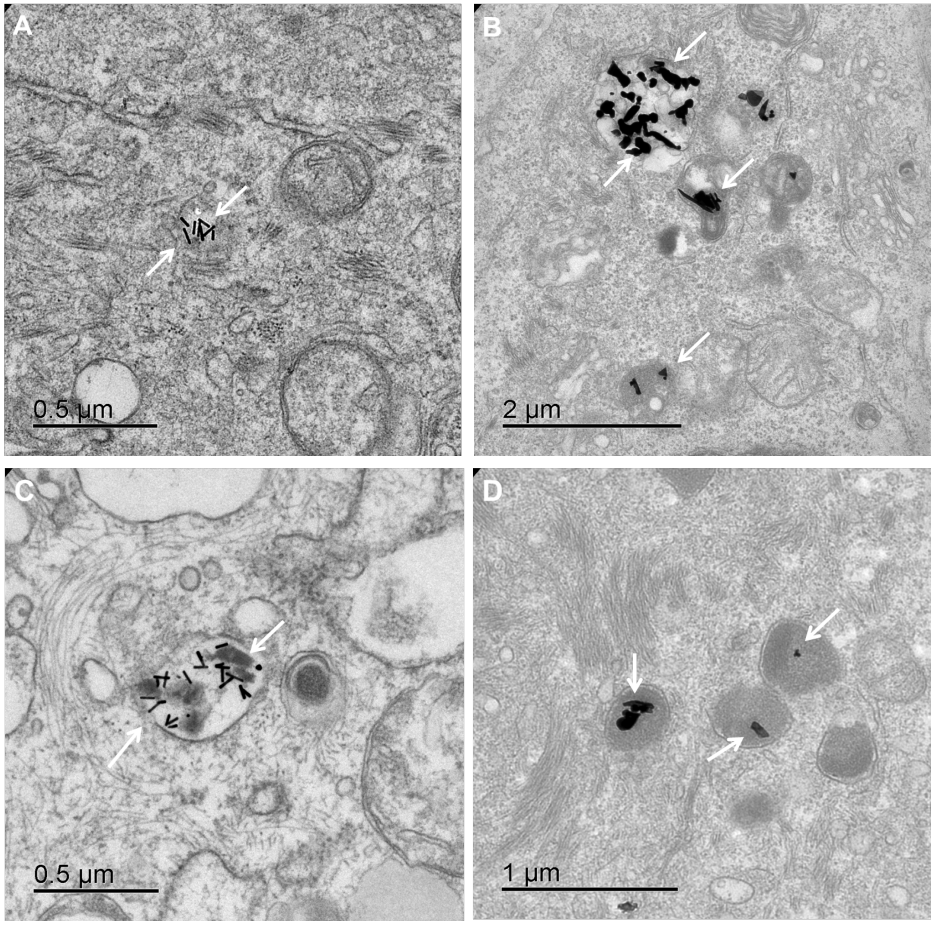

Figure 3-17: TEM images of spheroid cross sections indicate MG63 cells after 24 hours incubation with 0.1 mg.ml nanorods (A) and nanoprisms (B), and MCF-7 cells with nanorods (C) and (D) nanoprisms.

3.5.7 Near Infrared Irradiation of GNP Labelled Monolayer and 3D Tumour Spheroids

Results from 3.5.1.3 (assessment of gold nanoprism and nanorod heating following irradiation) indicated that both types of GNP generated hyperthermic temperature profiles in under 60 seconds. Following confirmation of the biocompatibility of the GNPs and their successful internalisation into both cell lines, this study aimed to irradiate GNP labelled monolayer and 3D spheroid cultures to determine whether the temperatures profiles generated were sufficient to cause cancer cell death.

Monolayer Study

Figure 3-18 illustrates the cell viability staining of both GNP labelled MG63 and MCF-7 cells following irradiation (1064 nm; 1 minute; 1 W). Several observations can be made; (1) both control and GNP labelled cells which were not treated with the NIR laser were viable; (2) control cells treated with the NIR laser were viable and (3) GNP labelled cells treated with the NIR laser were dead. It can therefore be confirmed that the cell death observed was produced from laser energy absorption *via* surface plasmon resonance of GNPs in the area of beam radius (and the immediate periphery) with cells outside this focal point remaining viable. For both cell types, the radius of cell death seems to be larger for gold nanoprisms, which may reflect the increased uptake and concentration of nanoprisms in cells. This could lead to peripheral cells outside the immediate beam focus still absorbing enough laser radiation to lead to cell death, creating a larger “kill zone” than the nanorods.

3D Tumour Spheroid Study

The 3D tumour spheroids mirrored the monolayer results (figure 3-19). Control cells were not affected by laser irradiation, however spheroids incubated with GNPs were clearly affected by laser exposure at focused spots on spheroids. The irradiation of MCF-7 spheroids incubated with gold nanoprisms in particular, showed complete dissection of the spheroid indicating the extremely potent affect of gold nanoprisms, again, perhaps due to their high internalisation.

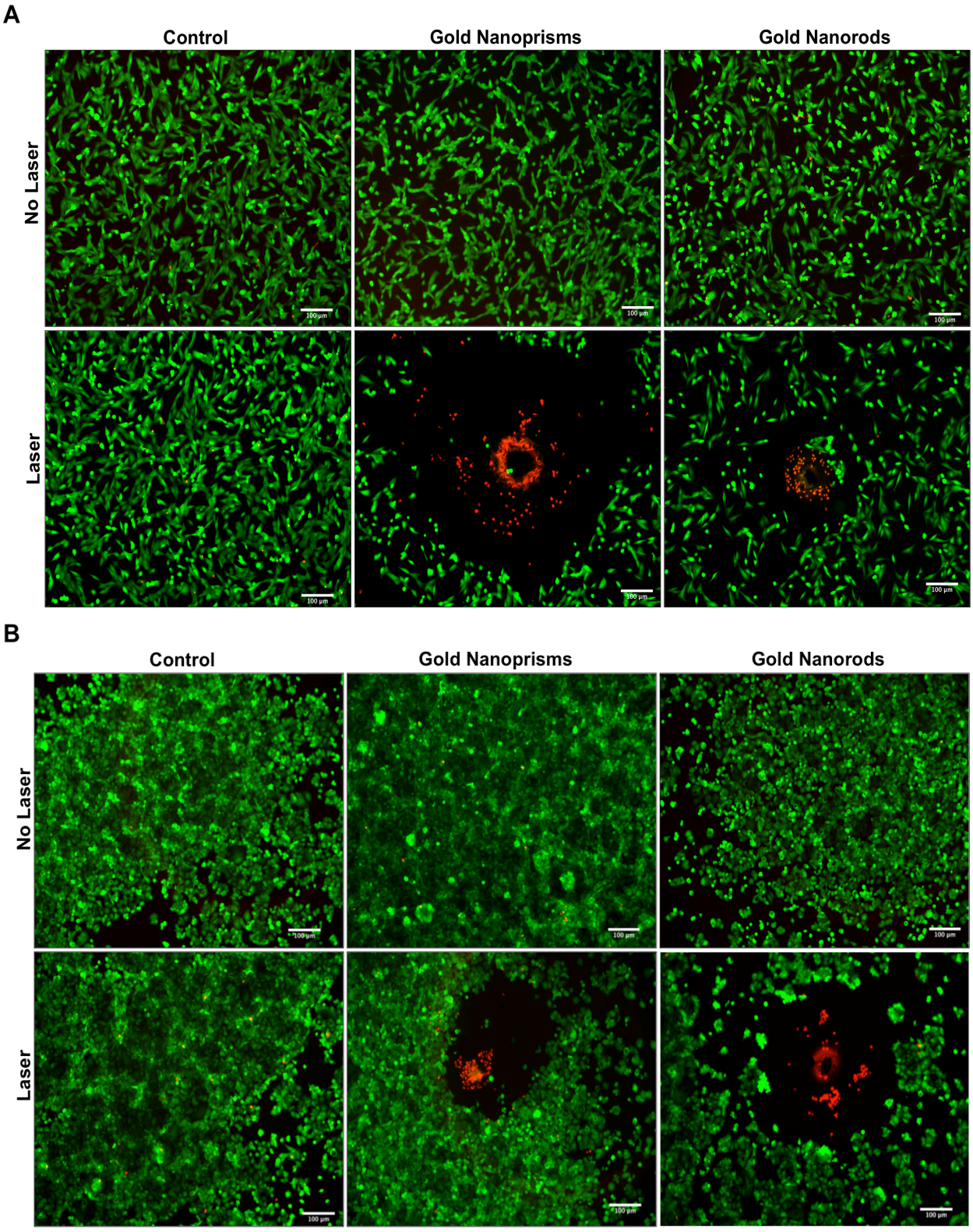

Figure 3-18: Fluorescencent cell viability staining of GNP labelled (A) MG63 cells and (B) MCF-7 monolayer cultures following irradiation with a 1064 nm laser for 1 minute. Control cells contain no GNPs. Green fluorescence indicates viable cells and red indicates dead cells. Scale bar = 100 µm. Three independent biological repeats (n=3).

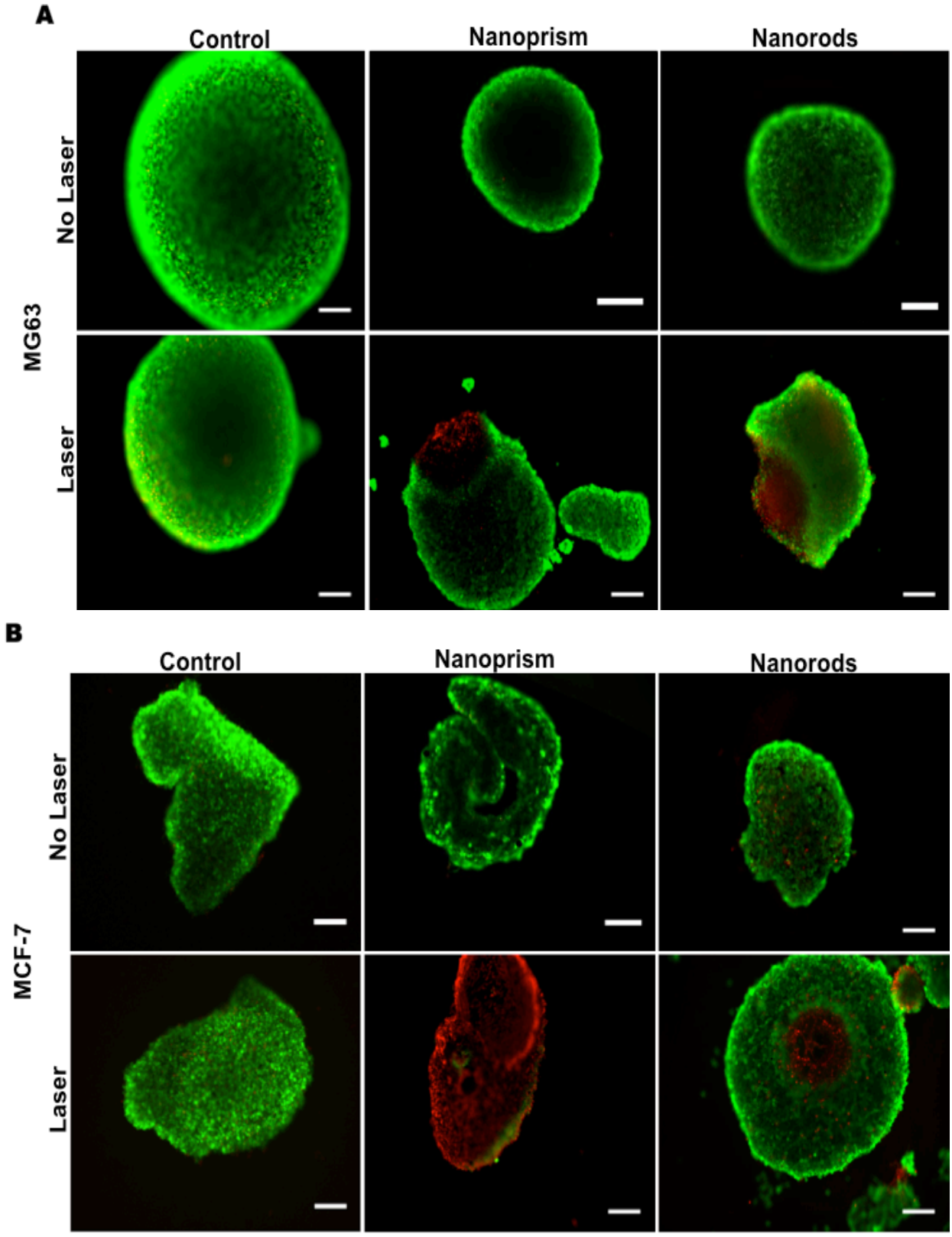

Figure 3-19: Fluorescencent cell viability staining of GNP labelled (A) MG63 cells and (B) MCF-7 3D tumour spheroids following irradiation with a 1064 nm laser for 1 minute. Control cells contain no GNPs. Green fluorescence indicates viable cells and red indicates dead cells. Scale bar = 200 µm. Three independent biological repeats (n=3).

3.6 Discussion

3.6.1 GNP Synthesis: Size and Morphlogy

Both the nanoprisms and nanorods used in this study were successfully synthesised, as observed by TEM. The size range varied depending on the type of particle being synthesised. The gold nanorods produced were controlled and uniform in size and aspect ratio, with rods of ~ 50 x 10 nm in size with an average aspect ratio of 7.2 which have been characterised by our collaborators in a previous study (Alfranca et al. 2016).

However the nanoprisms varied in size, with an average size of around 170 nm edge and 9 nm thickness. The synthesis of triangular nanoprisms tend to yield a small percentage of polyhedral GNPs, while other groups have observed similar tip-truncated nanoprisms or nanodisk by-products (J. E. Millstone et al. 2005; J. E Millstone et al. 2006; Noda and Hayakawa 2016; B. Pelaz et al. 2012). Whilst the images confirmed the succesful synthesis of both geometries, smaller polyhedral GNPs were also observed in both samples. These were identified as a by-product of the synthesis process, which can be extremely difficult to remove (Y. J. Shin et al. 2013). Any by-products are usually removed *via* electrophoresis, centrifugation and decantation however the process is not entirely efficient. However, the contribution of the polyhedral GNP by-products to the overall characteristics of both the gold nanoprisms and nanorods is minimal and did not affect the overall characteristic of the GNP solutions; producing gold nanoprisms with a low size distribution however still remains challenging using conventional wet-chemical synthetic routes with studies now showing lower size distributions using techniques such as biological (green) synthesis (Geng et al. 2016) modified seed-mediated approach (Zhirui Guo et al. 2010b) and plasmon driven synthesis (Brus 2016).

3.6.2 GNP Synthesis: Absorbance and Heating Potential

Complementary UV-visible data provided by our collaborators indicated that the spectra do show both GNPs peak SPR bands finely tuned in the NIR region, at 1064 nm for gold nanorods, corresponding to the longitudinal mode and 1100 nm for gold nanoprisms, corresponding to the in-plane dipolar band (Han et al. 2016a). The fine-tuning of the SPR of these GNPs in the NIR region is integral to their function as biomedical agents (Cai et al. 2008). This is due to the 'biological window' for optical absorption through tissue at NIR regions, that can be capitalised on for non-invasive clinical application (Y. Liu et al. 2015). Interestingly, the presence of the polyhedral GNP by-products may explain the rise in absorbance that can be seen in both samples at ~530 nm (figure 3-2) (Han et al. 2016a) but equally, this increased absorbance at ~530 nm may be in accordance to the transverse mode exhibited by both of these geometries (Jena and Raj 2007; Ye et al. 2016).

The extremely efficient heating potential of both GNPs was observed in just 60 seconds of laser irradiation, even at fairly modest concentrations (figure 3-3). Gold nanorods have been extensively researched and considered to be the most effective photothermal contrast agents, both *in vitro* and *in vivo*, with optimum nanorod sizes explored both theoretically and experimentally by Mackey and co-workers (Mackey et al. 2014). It has been well documented that the surface plasmon resonance absorption characteristics are highly dependent on particle size and shape and in particular for gold nanorods, the maximum wavelength absorbance is directly proportional to the aspect ratio of the nanorods and thus increasing the aspect ratio, increases the maximum wavelength absorbance to the NIR regions (Castellana et al. 2010). The nanorods used in these experiments have an average size of ~50 x 10 nm. Although larger nanorod size are associated with maximum wavelength absorbance in the NIR regions, they are also often associated with an increase in scattering and thus a reduce heating potential. The high aspect ratio of the gold nanorods in this project - which is independent of size, seem to facilitate their excellent heating capacity while their long, thin morphology contribute to their maximum absorbance in the NIR range (P. K. Jain et al. 2006; Near et al. 2013).

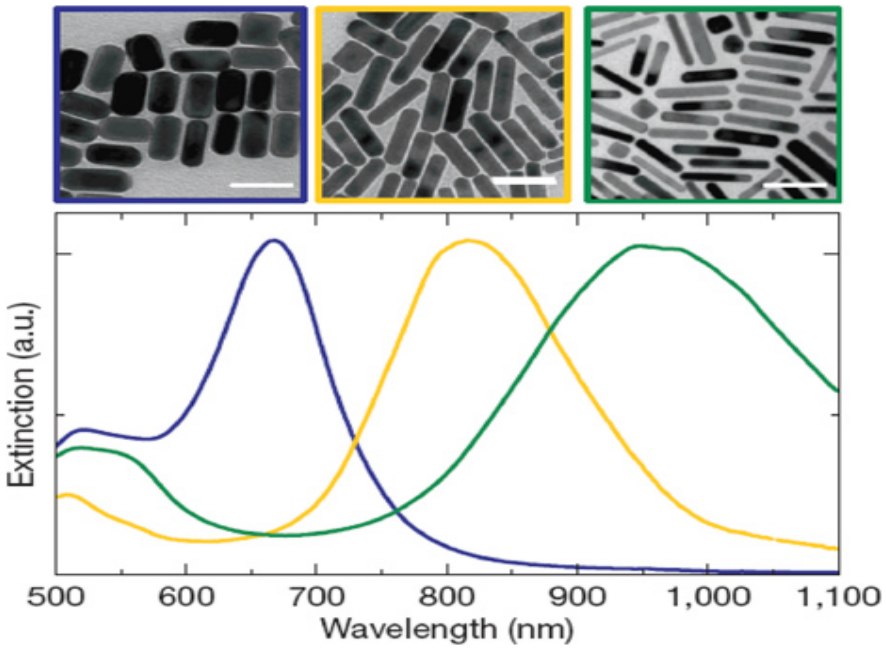

Figure 3-20: Normalised extinction spectra of the gold nanorod solutions. The average sizes of the nanorods are, from left to right, 37 × 19 nm (aspect ratio 2 ± 1), 50 × 12 nm (aspect ratio 4.2 ± 1) and 50 × 8 nm (aspect ratio 6 ± 2) (Junxi et al. 2012).

Gold nanoprisms, owing to their varied optical characteristics, which include triangular structure, high truncations, aspect ratio and three tips, are thought to have stronger electromagnetic field enhancements and provide a more distinct SPR in the NIR compared to their nanorod, nanocube or nanosphere counterparts (Huanjun Chen et al. 2008b; Han et al. 2016a; Xu et al. 2013; You et al. 2016). However, in this study the gold nanorods appeared to display a higher heating efficacy than the gold nanoprisms, presumably due to their higher specific surface area leading to increased NIR absorption (Alfranca et al. 2016).

3.6.3 Cell Lines and 3D Tumour Spheroid Culture

Two cell lines were used in this study; a bone osteosarcoma cell line (MG63) and an epithelial breast cancer cell line (MCF-7). These two cell lines were selected as they represent tumour cells from a ‘hard’ tissue and a ‘soft’ tissue, and so may have intrinsic differences in their behaviour in terms of GNP internalisation and subsequent cellular response to intracellular heating. In addition, on a physiological note, epithelial cancers, in particular breast cancers, suffer from dormancy post metastasis, whereby the cancer cells migrate in the bloodstream

and relocate in the bone marrow (Valastyan and Weinberg 2011; van Zijl et al. 2011). The cancer cells can lie undetected and dormant for many years, suddenly recurring to form secondary bone tumours, which have progressed beyond treatment (Brackstone et al. 2007; Ossowski and Aguirre-Ghiso 2010).

Monolayer cell cultures, typically grown on plastic or glass substrates, are used as *in vitro* models to study tumour cell behaviour and assess anti-cancer therapies. However promising results at this stage are often not translated to animal studies or clinical trials (Edmondson et al. 2014). This is because the extracellular environment, where the tumour cells live, is not reproduced. The use of 3D in vitro models has progressed along with advances in tissue and cell engineering, which provide an opportunity to bridge this gap (Edmondson et al. 2014). To this end, 3D multicellular tumour spheroids have been identified as useful tools, providing a more representative environment, featuring tumour characteristics such as dormancy, hypoxia and anti-apoptotic behaviour, whilst allowing for the strict analysis and control *in vitro* examination allow (Imamura et al. 2015; Weiswald et al. 2015).

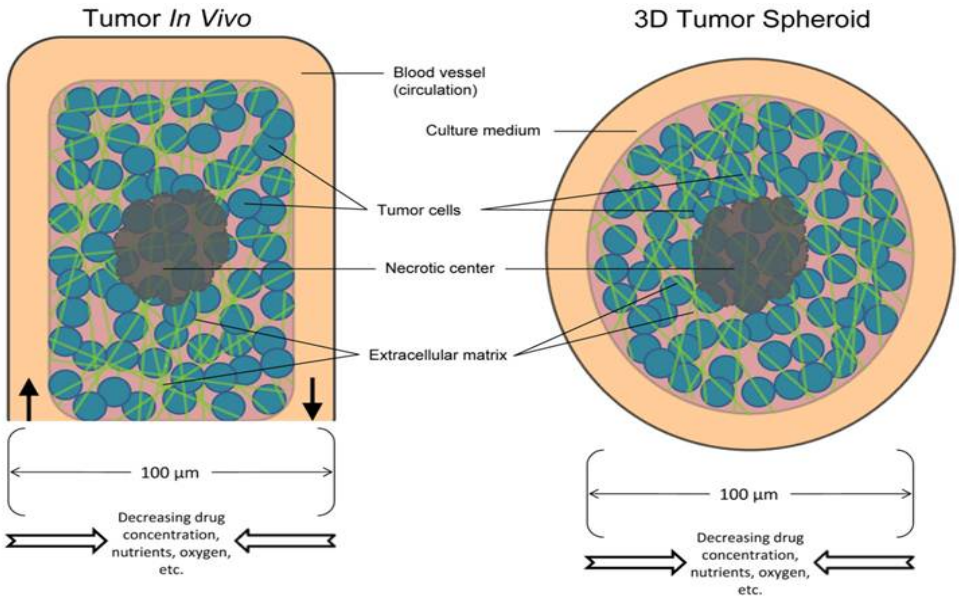

Figure 3-21: A schematic comparison of a typical tumour *in vivo* and an *in vitro* tumour spheroid model (Phung et al. 2011).

Early interest in tumour spheroid models began in the late 1970s, however its recent resurgence has coincided with our increased understanding of cancer cell

resistance to traditional therapies as well as the improved high throughput *in vitro* testing of tumour spheroids (Costa et al. 2016; Grimes et al. 2014). Spheroids often display more *in vivo*-like morphological and functional differentiation than their monolayer counterparts (Hornung et al. 2016), such as the notable diffusion limitation of spheroids, that has been suggested at around 100-150 μm for molecules such as oxygen, nutrients and metabolic waste (Curcio et al. 2007), while larger spheroids (~500 μm) usually display a hypoxic and necrotic core and an outer rim of quiescent cells and a peripheral layer of proliferating cells (R. Z. Lin and Chang 2008). Tumour spheroid models also exhibit similar metabolic and signaling profiles, which are more closely related to *in vivo* conditions, compared to traditional monolayers and of particular interest for researchers is the aforementioned hypoxic environment that has been shown to lead to radiotherapy and chemotherapy resistance (Rey et al. 2016; Samanta et al. 2014). Thus, tumour spheroids help bridge the gap between standard two-dimensional and *in vivo* conditions and can further validate *in vitro* findings to better predict potential outcomes in *in vivo* models.

Multicellular tumour spheroids were successfully produced and matured in this study, in the presence of GNPs, for 24 hours (figure 3-11). Spheroids seeded at a lower initial cell density (1×10^4) often produced smaller 'satellite' aggregates of cells that were dispersed within the hanging drop solution, and therefore, did not readily form single uniform spheroids at the 24 hour time point. Meanwhile, spheroids seeded at the higher cell density (1×10^6) exhibited a number of dead cells within the spheroid structure with variability in the spheroid size (as noted by the higher standard deviations). Whilst characteristics such as a necrotic core would have been desirable, technical issues including the configuration and orientation of large spheroids for laser optics, and the resultant microscopy field of view prevented their use in this study (figure 3-5 and 3-6). Therefore, the middle cell density (1×10^5) was selected for photothermal therapy, due to its reliable production, relatively low variation in spheroid size and practicality; this was used for subsequent experiments.

The presence of GNPs within the MG63 and MCF-7 spheroids did not affect their formation or development over 72 hours. Indeed, at the lower and middle cell densities the spheroids were noted to grow in diameter, suggesting cell

proliferation; the higher density did not appear to promote cell proliferation, with little/no significant change in diameter over time.

3.6.4 GNP Biocompatibility

The metabolic assay considered the 'gold standard' for cytotoxicity is the MTT assay which is a colorimetric assay that measures the enzymatic activity of cellular mitochondria (Carnovale et al. 2016). If cells appropriately metabolise the MTT dye, the cell culture media will change colour, allowing for simple absorbance measurements to be used to quantify cellular activity (Marquis et al. 2009). The MTT assay, however does suffer from minor limitations (S. Wang et al. 2011a), so to supplement the quantitative data, the fluorescent viability staining was performed to visualise samples.

Gold has long been considered to be chemically inert and therefore potentially safe in terms of biomedical applications, with gold-based compounds used in the clinic as anti-inflammatory agents to treat rheumatoid arthritis (Auranofin® and Tauredon®)(A. M. Alkilany and Murphy 2010). Due to the intricacy of nanoparticle toxicity, together with the lack of standardisation of experimental procedures, there is a discrepancy over the biocompatibility of GNPs in biological systems of increasing complexity (cell membrane, cells, tissues, organs and human body) (Fratoddi et al. 2015). The general consensus is that GNPs are well tolerated physiologically, as confirmed in a number of studies with both naked and decorated/functionalised GNPs in various cell lines (Arnida et al. 2010; Connor et al. 2005; J. H. Fan et al. 2009; Orlando et al. 2016). However some studies have also shown a potential toxicity of GNPs, particularly in relation to their size, where smaller GNPs (2-4 nm) can prove toxic (Hung-Jen Yen, 2009). This has been somewhat challenged with Mingfei Yao et al, (2015) who recently demonstrated that increasing particle diameter promoted the depolarisation of mitochondrial membrane potential, an early indicator of apoptosis.

In addition to size, GNP shape has also been identified as being key in cytotoxicity studies, with more sophisticated geometries associated with a higher cytotoxic effect with gold nanorods often cited as a more toxic geometry as compared to nanospheres (Yinan Zhang et al, 2012). For example the *in vitro* cytotoxicity of gold nanorods in a human lung adenocarcinoma cell line was recently published

(Ying Tang, 2015). The study confirmed membrane damage within 4 hours of gold nanorod exposure while ROS production correlated to increased GNP concentration. Gold nanorods of varying aspect ratios were also evaluated for their cytotoxic potential across six different cell lines (Show-Mei Chuang, 2013). All three nanorods tested induced a dose-dependent suppression on cell growth to varying degrees, with ROS induced apopotosis and cell cycle inhibition the main route of GNP cytotoxicity. Bare/non-functionalised GNPs have been shown to lead to cell death in A549 cells (human hepatocellular liver carcinoma) in a dose dependent manner but not in HepG3 (human hepatocellular) and BHK21 (baby hamster kidney) (H. K. Patra et al. 2007a). The study confirmed cell death occurred through Poly ADP-ribose polymerase (PARP) activation. PARP is a protein which can be cleaved and leads to the downstream activation of caspases and cell death (H. K. Patra et al. 2007a) while oxidative stress and increased lactate dehydrogenase leakage was also induced in A549 cells, again in a dose dependent manner (Y. Tang et al. 2015).

Table 3-1: Summary of *in vitro* gold nanoparticle toxicity (A. M. Alkilany and Murphy 2010).

Cell line	NP size (nm)	NP Shape	Nanoparticle surface group	Dose; incubation time	Conclusions	Ref.
COS-1 mammalian cells, red blood cells, E. coli	2	Spheres	Quaternary ammonium, carboxylic acid	0.38–3 μM; 1–24 h	Cationic nanoparticles found to be toxic where anionic not	Goodman et al. 2004
RAW 264.7 mouse macrophage	3.5 ± 0.7	Spheres	Lysine, poly(lysine)	10–100 μM; 24–72h	Nanoparticles are not toxic and not immunogenic	Shukla et al. (2005)
K562 human leukemia	4, 12, 18	Spheres	CTAB, citrate, cysteine, glucose, biotin	0.001–0.25 μM; 72h	All nanoparticles were not toxic	Connor et al. (2005)
MV3 and BLM (Metastatic melanoma)	1.4	Spherical cluster	Triphenylphosphine monosulfonate	Up to 0.4 μM; 72 h	100% cell death at 0.4 μM compared to 10% cell death for cisplatin at same concentration	Tsoli et al. (2005)
HeLa	65 × 11	Rods	CTAB, PEG	0.09–1.45 μM; 24 h	Replacing CTAB with PEG on the surface of nanorods reduced the toxicity	Takahashi et al. (2006)
Human dermal fibroblast	13.1	Spheres	Citrate	0–4 mM; 24–144 h 0–120 nM; 36 h	Nanoparticles decreased cell proliferation rate, adhesion, and motility	Pernodet et al. (2006)
(1) baby hamster kidney cells BHK21 (2) Human liver carcinoma Hep2G (3) Human lung carcinoma cells A549	33	Spheres	CTAB and citrate	A549 and 72 h for both Hep2G and BHK21	Nanoparticles are not toxic to Hep2G and BHK21 but to A549 cell line	Patra et al. (2007)

HeLa 1) Epithelial: HeLa (2) Endothelial: SK-Mel-28 (3) Fibroblasts: L929 (4) Phagocytes: j774A1	18 0.8, 1.2, 1.4, 1.8, 15	Spheres Spheres	Citrate Triphenylphosphine mono and trisulfonate	0.2–2 nM; 3–6 h Up to 5.6 μM; 72 h	Nanoparticles are not toxic and did not change gene-expression patterns (a) 1.4 nm: Most toxic size; (b) 0.8, 1.2, 1.8:4–6 fold toxicity compared to 1.4 nm; (c) 15 nm: completely non toxic; (d) toxicity is not cell line dependent	Pan et al. (2007)
HeLa	40 × 18	Rods	CTAB, PSS, PDADMAC	10–150 μM; 6 h	Polyelectrolyte coating of nanorods are not toxic compared to the CTAB-capped nanorods and no gene expression abnormalities were observed	Hauck et al. (2008)
Dendritic cells from C57BL/6 mice	10	Spheres	Citrate	0.5 mM; 4–48 h	Nanoparticles were not toxic and did not induce dendritic cell activation	Villiers et al. (2009)
HeLa	1.4 and 1.5	Spheres	Triphenylphosphine monosulfonate, GSH	5.6 mM; 48 h	(a) The 1.4 nanoparticles induced necrosis by oxidative stresses where the 15 nm particles were found to be not toxic; (b) GSH-capped nanoparticles were less toxic than TPMS-capped nanoparticles	Pan et al. (2009)
HeLa	3.7	Spheres	PEG	0.08–100 μM; 6–72 h	NPs entered nucleus and did not induce toxicity	Gu et al. (2009)
HT-29 (Human colon carcinoma cells)	65 × 15 nm	Rods	CTAB, PAA, PAH	0.6 nM; 96 h	Nanorods are not toxic, excess CTAB is. Overcoating the CTAB-capped rods with either negatively or positively charged polymers reduces toxicity and affects their uptake	Alkilany et al. (2009)

The GNPs used in this study were functionalised with 5kDa PEG molecules which have been shown in a number of studies to improve the biocompatibility and stability of nanoparticles (T. Gong et al. 2014; Y. C. Park et al. 2014; Tlotleng et al. 2016). However, due to nanorod concerns highlighted above, it was important to evaluate the toxicity of both the nanoprisms and nanorods used in this study with a particular emphasis on the biocompatibility of the nanorods. The MTT assay indicated a slight reduction in cell metabolic activity for both cell lines with the nanorods at the highest concentration (figure 3-7 and 3-8), however, the values noted were not of concern and did not dip below 80% cell activity.

The nanorods are synthesised in the presence of cetyltrimethylammonium bromide (CTAB), a cationic surfactant conventionally used by research groups (including our collaborators) to "grow" gold nanoseeds into nanorods. The surfactant CTAB is typically removed *via* purification or desorption techniques however these processes are often inadequate at removing all CTAB molecules and thus free CTAB molecules can remain within the nanorod solution (A. M. Alkilany and Murphy 2010). The synthesis process of gold nanorods, as described in section 3.3.1.1, detail the exhaustive processes used in order to remove the CTAB molecules from the GNP solutions. CTAB has been argued as the main source of nanorod toxicity. Alkilany and Murphy (2009) validated this claim when they centrifuged GNP solutions, separating and analyzing the supernatant (containing free CTAB molecules), which was found to be cytotoxic (A. M. Alkilany and Murphy 2009). The potent cytotoxic effect of CTAB was also demonstrated well by Connor and co-workers in 2005, whereby using the MTT assay, they evaluated the toxicity of 18 nm GNPs to K562 cells (Connor et al. 2005). The GNP surface was modified with various ligands, including biotin, citrate, and CTAB. Both citrate- and biotin-modified particles were non-toxic when used up to a concentration of 250 mM, whereas CTAB-coated particles indicated toxicity at only 0.05 mM. Once CTAB was cleared from the GNPs, the particle did not exhibit cytotoxic behaviour, highlighting GNPs themselves may not be toxic but rather, their precursors (Connor et al. 2005; N. Khlebtsov and Dykman 2011).

The gold nanoprisms used in this study were synthesised without the use of the surfactant CTAB and thus avoided the potential cytotoxic issues encountered when synthesising the nanorods. In fact, the MTT assay indicated an increase in cell activity in response to the nanoprisms, with consistently high cell viability.

One point to note is that the MTT assay may lead to an overestimation of cell activity. This is due to the technical processing of samples during a typical MTT assay. The GNPs are able to absorb and scatter light in the UV-visible range. The UV-visible spectra (figure 3-2) indicated an increased absorbance at around 530 nm wavelength, while the absorbance wavelength used in by the microplate reader was set at 550 nm and can therefore, theoretically interfere with MTT results (Kong et al. 2011). Diaz et al (2008) assessed a variety of GNPs in media alone over 24, 48 and 72 hours, showing a general increase in absorbance with increased GNP concentration (Diaz et al. 2008), providing false positive results. The higher absorbance of nanorods at around 530 nm may account for the unexpectedly high viability of gold nanorods at the lower concentrations tested, particularly in MCF-7 cells, if they have not been adequately removed from the culture prior to being analysed in the plate reader (figure 3-8). Due to the nature of the MTT assay (the ability of mitochondrial dehydrogenase enzymes present in living cells capable of reducing MTT to purple formazan crystals), samples can display misleading false positive results. This is based on an increased metabolic rate that may occur due the increased cellular activity and energy-consuming processes such as endocytosis, metabolism and exocytosis of the GNPs (van Tonder et al. 2015). This increase in cellular activity thus leads to the increased production of formazan, which can inaccurately be perceived as an increase in cell viability upon absorbance measurements.

3.6.5 GNP Internalisation into the Cell Lines

The SEM and TEM images (figures 3-12, 3-13 and 3-17) confirmed cell-GNP interaction and GNP internalisation. SEM images showed the increased number of cytoplasmic projections in the form of filododia in the presence of GNPs compared with control groups (containing no GNPs). Filopodia are cytoplasmic projections driven by actin polymerisation that extend beyond the leading edge of lamellipodia in migrating cells and are have crucial roles in and cell-cell interaction, migration and sensing (Mattila and Lappalainen 2008; S. Zhang et al. 2015). Hence an increase in filopodia is due to the close proximity of the GNPs to the cells.

TEM imaging of GNP internalisation into MG63 and MCF-7 cells was observed by staining ultrathin cross sections of embedded spheroids (figure 3-17). The images

confirmed the GNP uptake into the cell body, the distribution and compartmentalisation of both GNP types into endosome-like structures (Huefner et al. 2014). This compartmentalisation into endosomes suggests GNP uptake was coordinated by a form of pinocytosis (Huefner et al. 2014), a form of energy-dependent receptor-mediated endocytosis (RME) that is viewed as a dominant internalisation pathway, observed in a number of NP uptake studies (A. Albanese and Chan 2011a; Huefner et al. 2014; S. Jain et al. 2014). Furthermore, as Chithrani and Chan confirmed the influence of clathrin mediated uptake and its subsequent initiation of vesicle fomation in both nanorods and nanosphere internalisation, this suggests that a combination of uptake pathways are activated when cell lines are exposed to NPs (Chithrani and Chan 2007; McMahon and Boucrot 2011).

The TEM images revealed large aggregated populations of gold nanoprisms in both cell types within lysosomes while a visibly lower quantity of nanorods were observed within similar endosome structures with little aggregation. The internalisation of GNPs *via* conventional routes such as receptor-mediated endocytosis follows an established pathway, including the formation of early endosomes, encapsulating GNPs, the maturation of the endosomes and fusion with lysosomes, all occurring in a spatial and temporal order (Huotari and Helenius 2011). The isolation of GNPs within the lysosomal system is believed to protect other important organelles from directly interacting with GNPs, with neither gold nanorods, nor nanoprisms observed in the nucleus, mitochondria, endoplasmic reticulum and Golgi body or free flowing within the cytosol in both cell types (W. Zhang et al. 2013a). It is important to note that GNPs were first introduced to cells whilst in a monolayer configuration (prior to spheroid formation) to allow for maximum GNP uptake however this may not accurately represent the internalisation and indeed the penetration capability of GNPs into spheroids.

The GNP internalisation is dictated by the GNP geometry. This is highlighted in the ICP-MS results, where nanoprisms are internalised into cells far more efficiently than nanorods, in both cell types (figure 3-14). The striking variance between the two GNPs is due to their respective geometries, as NP shapes influences cell internalisation, as recently discussed (N. Ma et al. 2013; S. Salatin et al. 2015a). While relatively few studies have been dedicated to evaluating the uptake kinetics of nanoprisms, the debate over the proficiency of gold nanorods has been

reviewed, with disparity within the literature. For example, within human cervical cancer cells (HeLa cells), nanorods exhibit high internalisation, followed by spheres, cylinders, and cubes (N. Oh and Park 2014). However it was noted in this study that gold nanorod internalisation was prominently decreased with a parallel increase in aspect ratio (N. Oh and Park 2014). The nanorods used in this study have a larger than average aspect ratio and are not functionalised with additional ligands to assist uptake, which may account for their low uptake.

It was also noted that nanorod exocytosis kinetics are faster when compared to spherical GNPs (N. Oh and Park 2014). Zhang and co-workers observed the exocytosis of gold nanorods after just 30 minutes of incubation (W. Zhang et al. 2013a). This may perhaps explain the lower amount of gold nanorods observed in this study, as samples were processed after 24 hours culture with GNPs. Although gold nanorods are capable of being re-internalised into cells, it may be the rate of exocytosis is considerably higher than the rate on endocytosis thus producing a low net concentration of gold nanorods within cells.

3.6.6 The Cytoskeleton Post GNP Internalisation

It has been reported that NPs produce sub-lethal damage to cells that may alter or inhibit cellular function, but are overlooked when assessing gross NP toxicity (Lanone et al. 2009). Therefore, although appearing viable, cells may incur intracellular stress following NP internalisation that is not picked up by assays such as the MTT assay, however such stresses are often indicated by alterations to the cytoskeletal network (Stefaan J. Soenen et al. 2012). Although these modifications to the cytoskeleton framework may simply be due to the internalisation process and subsequent endosomes/lysosome formation, disruption and reorganisation may also be indicative of additional cellular stress (Stefaan J. Soenen et al. 2011).

Cytoskeletal staining was therefore applied to observe any alterations in cytoskeleton arrangement upon GNP internalisation, as reported by previous groups (Mironava et al. 2010; Noël et al. 2016; Tarantola et al. 2011). F-Actin is a filamentous protein that facilitates the formation of microfilaments within the cytoskeleton; these microfilaments are integral for cell mobility and intracellular transport, cell-cell and cell-substrate interactions, and signal transduction (Calero

et al. 2014). Meanwhile, β-tubulin subunits are the major components of microtubules, which have cellular functions similar to those of microfilaments as well as involvement in endosome transport, apoptosis and the separation of chromosomes into daughter cells during interphase (Akhmanova and Steinmetz 2015; Ogden et al. 2014). Potential damage to either of these components would suggest acute toxicity of NPs leading to inhibition of cell cycle, maturation, function, and of course viability.

Our results suggest that, although both F-actin filaments and β-tubulin subunit formation were compromised to various degrees in the presence of GNPs (0.1 $mg.ml^{-1}$) after 24 hours. However, cytoskeletal reorganisation was not at the expense of cell attachment or viability. For MG63 cells exposed to gold nanoprisms the microtubule organising centre, located beside the nucleus, was intact, however disruption to the cytoplasmic microtubule network was noted and accompanied by large intercellular clefts (figure 3-15) (Tarantola et al. 2011). TEM images (figure 3-17) confirmed the accumulation of GNPs enclosed within endosome vesicles. This increase in endosome size and number may actually, sterically hinder and deform the cytoskeletal architecture and thus explain the disruption and lack of dense microtubule networkat the perinuclear region and across the cell body (Alfranca et al. 2016; Estrela-Lopis et al. 2011; Hirak K. Patra et al. 2007b; Stefaan J. Soenen et al. 2012).

Interestingly, actin filaments did not appear as affected within MG63 cells treated with nanoprisms, with a near homogenous distribution of filaments throughout the cell (figure 3-15). Conversely, MG63 cells treated with nanorods appeared to disrupt the microtubule network, again likely due to the formation and trafficking of endosomes (D. Choudhury et al. 2013a). With both nanorods and nanoprisms, a large concentration of actin filaments generating transverse protrusions, from the cell membrane were visible. These filamentous actin protrusions may be an indicator of cell internalisation mechanisms MG63 cells adopted, such as macropinocytosis; (Kuhn et al. 2014) an actin motivated process which is characterised by protrusions at the outer cell membrane, whilst a clathrin-mediated endocytosis is also dependent on actin involvement (Kaksonen et al. 2006). Soenen et al suggested NP-loaded endolysosomal structures located at the perinuclear region and near the microtubule organising centre begin to increase in size and lose their function due to the high influx of NPs into the cell. These large

structures may physically inhibit existing or newly forming cytoskeletal structures (Stefaan J. Soenen et al. 2012).

MCF-7 cells exposed to GNPs were also evaluated in figure 3-16, with samples, containing no GNPs used as controls. The F-actin staining indicated that the majority of MCF-7 cells treated with GNPs did not exhibit an actin ring around the nucleus; a feature found in epithelial cells that featured in MCF-7 control samples although again this did not lead to any notable detrimental effects on the cell with β-tubulin largely remaining unaffected (Tarantola et al. 2011).

3.6.7 Photothermal Treatment of cells

Due to their optical properties, both the gold nanorods and nanoprisms were capable of converting optical energy into thermal energy upon laser irradiation with a 1 W 1064 nm laser for 1 minute, as indicated in figures 3-3, 3-18 and 3-19 (P. M. Tiwari et al. 2015b). This NIR range would allow for maximum tissue depth penetration without causing notable injury to control cells (containing no GNPs) (J. Park et al. 2015), while longer wavelengths are attenuated by biological entities such as hemoglobin, pigments, and water (R. Weissleder 2001a).

Following GNP internalisation, both monolayer and spheroids cell samples were treated with the 1 W 1064 nm laser for up to 1 minutes. All laser treated cells were rapidly killed with both nanorods and nanoprisms, as indicated by fluorescent viability staining. The absorption spectrum of the gold nanorods is dictated by their aspect ratio (length/width), a feature that can be manipulated by researchers to produce highly absorbing or scattering GNPs. By increasing the nanorod aspect ratio, the SPR absorption wavelength maximum of the longitudinal band significantly red-shifts toward the NIR regions. This easily tuneable characteristic has made nanorods a popular photothermal agent for cancer hyperthermia. The nanorods displayed the highest absorption peak in the NIR region that correlates well with laser wavelengths during photothermal irradiation both *in vivo* and *in vitro* (Dickerson et al. 2008; T. S. Hauck et al. 2008a; Qin et al. 2015). Likewise, the gold nanorods used in this study indicated a strong absorbance in the NIR range due to their high aspect ratio of ~7.2, however the nanoprisms appeared to be more efficient at killing the cells, both in 2D and 3D.

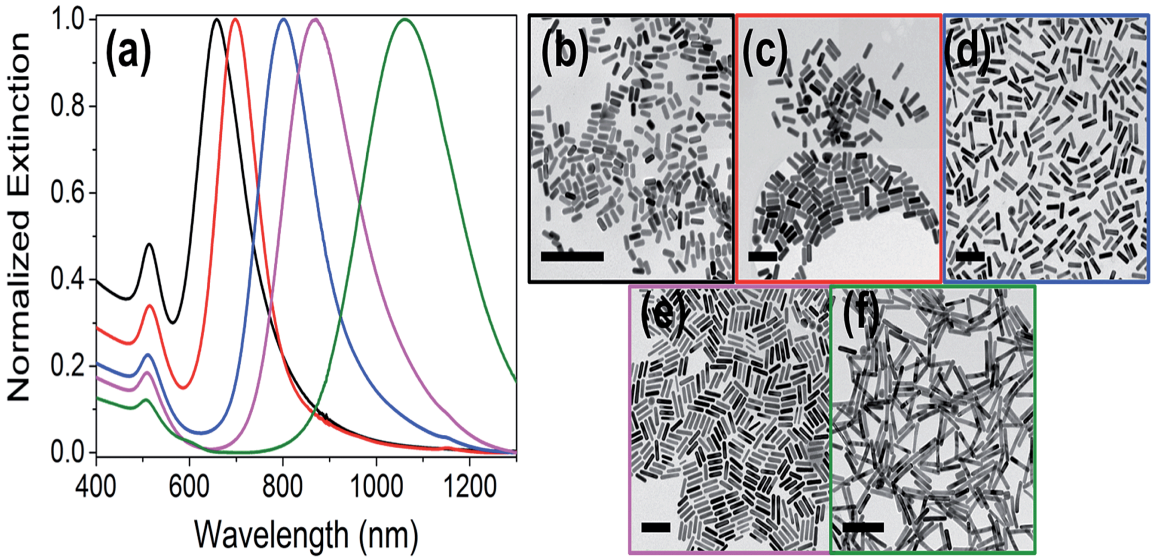

Figure 3-22: (a) Normalised extinction spectra for gold nanorods with increasing aspect ratios showing a shift of wavelength to the right. The black, red, blue, magenta, and green spectra were taken for gold nanorods with aspect ratios 2.4, 2.7, 3.6, 4.4, and 6.1, respectively, with corresponding TEM images in (b) through (f) (Hinman et al. 2016).

The aspect ratio of nanoprisms is based on the thickness of the nanoprism and edge length, however the three tips of the nanoprisms are also crucial characteristics determining its optical properties (E. Hao et al. 2004; Noda and Hayakawa 2016; K. L. Shuford et al. 2005a). The nanoprisms used here displayed excellent cell viability and but also strong heating capability upon laser excitation. The clear perimeter adjacent to the laser's focal point indicates a large circular area with no cells present, and may be understood through the dispersion of heat energy that may also be released through photoacoustic effects. This occurs if the rate of heat absorption is much faster than the relaxation rate. In this instance, GNP surfaces may exceed a hundred degrees, leading to cavitation effects (Lapotko et al. 2006). The formation and collapse of microbubbles releases mechanical shockwaves, which can rupture cell membranes as well as other acoustic associated damage forcing cells away from the laser focal point (Wei et al. 2013). Although laser treatment with both 2D and 3D models were succesful, technical challenges were present with 3D spheroids suspended in media. This included the movement of the spheroid during laser treatment; either through rotation or lateral motion of spheroids during treatment. This created difficulties in isolating the laser bean to specific regions on spheroids, although this was somewhat remedied by gently draining the excess media surrounding spheroid samples prior to treatment in order to restrict their motion.

3.7 Summary

The aim of this chapter was to i) evaluate the biocompatibility of GNPs in both 2D and 3D and ii) assess their effectiveness as photothermal agents upon laser irradiation, leading to cell death

As previously highlighted within this chapter, the debate over the biocompatibility of GNPs is controversial while further investigations into the shape of GNPs, in particular gold nanorods, influencing toxicity has been explored (Qiu et al. 2010; Shuguang Wang et al. 2008). The results in this study demonstrate the low toxicity of both gold nanoprisms and gold nanorods in MG63 and MCF-7 cells both in monolayer and 3D multicellular tumour spheroids, over 24, 48 and 72 hours. The results were particularly encouraging in the case of gold nanorods, which were synthesised in the presence of CTAB, which is believed to be the main culprit of gold nanorod associated toxicity (Wan et al. 2015). Our results also further validates our collaborators removal process of CTAB during nanorod synthesis (Alfranca et al. 2016).

Further investigations into the biocompatibility of the GNPs included the interaction, internalisation, compartmentalisation and quantification of GNPs into cells. Both GNPs successfully internalised within MG63 and MCF-7 cells both in monolayer and spheroids with TEM imaging suggesting GNP entry is predominantly governed by receptor mediated endocytosis and clathrin-mediated endocytosis.

ICP-Mass spectroscopy revealed the large discrepancy between the two geometries, with nanoprisms appearing the more successfully internalised GNP in both cell types, over a range of concentrations. Upon internalisation into cells, GNPs appeared to affect the network of actin and tubulin filaments, although without deleterious consequences and did not appear to greatly impact cell viability. The remodelling of the cytoskeleton may be attributed to the increased quantity and volume of endosomes as a consequence of GNP uptake that can impair cytoskeleton integrity rather than GNPs themselves directly disrupting tubulin and actin formation.

Finally, GNPs were assessed for their photothermal efficiency *via* irradiation, using a 1 W 1064 nm unfocussed laser for 1 minute. Both GNPs displayed proficient heating upon NIR laser exposure as characterised by our collaborators experimentally within a GNP solution. In this project we evaluated photothermal capacity *in vitro* and verified its capability to lead to cell death across a large radius in monolayer. Within multicellular tumour models, the photothermal treatment demonstrated its potential for depth penetration and focus to lead to cell death on isolated regions within the spheroid.

Chapter 4

4 Identifying the Underlying Mechanisms of Photothermal Hyperthermia

4.1 Introduction

4.1.1 Hyperthermia and Cancer Cells

Hyperthermia is the process of raising the temperature, either locally or globally in a patient for medicinal purposes. As previously described in section 1.2. Hyperthermia (42-45°C) can lead to cellular and molecular events that promote cancer cells to undergo apoptosis and also render cancer cells more susceptible to treatments from chemotherapy and radiotherapy. For example, elevating the temperature within the tumour tissue leads to alterations in the vascular permeability, increasing blood flow and tumour oxygenation that can further intensify the cytotoxic effect of radiation or chemotherapy (Beik et al. 2016). Indeed, many clinical studies have confirmed that the use of hyperthermia alongside radiotherapy or chemotherapy significantly improves tumour control and patient survival rates in breast, cervix, bladder, brain, head and neck tumours (Beik et al. 2016).

Generally, there are no intrinsic differences between normal and tumour cell sensitivity upon hyperthermia, however *in vivo* and *in vitro* studies have shown that a selective tumour cell killing effect is achieved at temperatures between 40 and 44°C (Behrouzkia et al. 2016; van der Zee 2002). This has been attributed to the tumour tissue environment, where the disorganised and compact vascular structure of tumourss does not promote heat dissipation, leading to retention of high temperatures for longer periods, subsequently leading to cancer cell apoptosis, while normal vascular architecture facilitates heat dissipation (Hegyi et al. 2013). Cancer cells characteristically survive in a hypoxic environment, with low oxygen, alongside acidic (low pH) conditions, due to insufficient blood perfusion (van der Zee 2002). Interestingly, it has been recently noted that due to their high metabolic demands, constant anabolic and catabolic reactions may also lead to the production of sub-lethal intensities of heat (Hegyi et al. 2013; Keibler et al. 2016). The use of additional hyperthermic treatments could therefore confer additional thermal energy to the cells, which takes them over a toxic threshold,

inducing the cancer cell to commit to apoptosis. The effectiveness of the technique is dependent on exposure time and temperature profiles achieved during treatment while considerations of cell and tissue type may determine these parameters (R. Haghniaz et al. 2015a; Hegyi et al. 2013).

4.1.2 Apoptosis and Necrosis

Apoptosis is integral to homeostatic processes and is involved in various physiological responses during normal development and morphogenesis, while also being activated during cell stress or damage (Nikoletopoulou et al. 2013). The morphological assessments of apoptotic features include; alterations in membrane composition, budding of plasma membrane without loss of integrity, mitochondrial permeability, shrinking of cytoplasm, condensation of nucleus, development of membrane bound vesicles, and fragmentation of cell into smaller bodies (apoptotic bodies) (Elmore 2007).

However at higher temperatures (>47°C) complete thermal ablation of tissue can occur, this frank necrosis is often indiscriminate, effecting both healthy and cancerous cells. Necrosis is an acute and severe response leading to the premature death of cells consequently damaging nearby cells. Major hallmarks of necrosis include loss of membrane integrity, swelling of cytoplasm, mitochondrial disruption and calcification, fragmentation of organelles, and cell lysis leading to the release of intracellular components of the cell into the microenvironment, which is capable of eliciting an inflammatory response, damaging peripheral cells (Y. S. Cho 2014; X. Wang et al. 2014b).

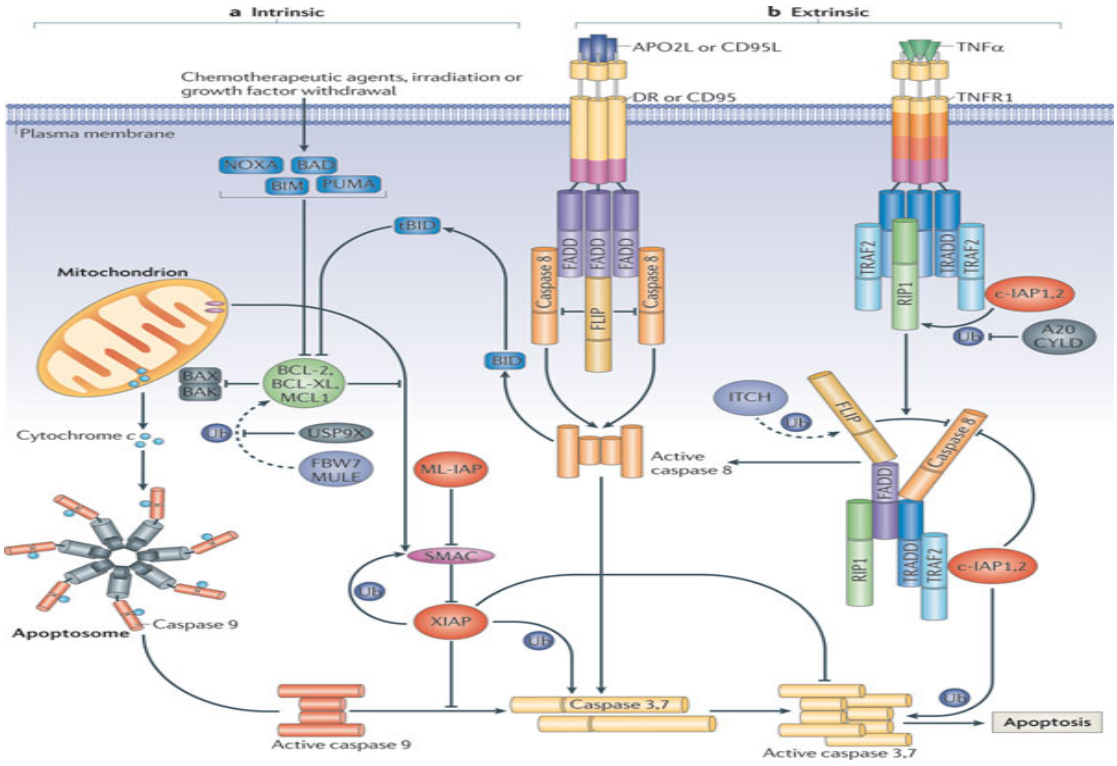

Figure 4-1: Schematic depicting the intrinsic and extrinsic apoptotic pathway, previously described (Vucic et al. 2011).

4.1.3 The Role of Mitochondria and Reactive Oxygen Species (ROS) in Apoptosis

One of the major triggers to stimulate apoptosis is the 'Intrinsic pathway' and the 'Extrinsic pathway' (as shown in figure 4-1). While the major catalyst for the intrinsic pathway is mitochondrial damage and subsequent release of pro-apoptotic proteins, the extrinsic pathway is capable directly activating effector caspases but can also cross talk with the intrinsic pathway leading to mitochondrial disruption, ultimately leading to the formation of the apoptosome and activation of caspases, leading to apoptosis (Yağmur Kiraz et al. 2016b; Winter et al. 2014). Mitochondrial stability is therefore vital for cell viability, with disruption of mitochondria recently been associated with an increase in ROS production (Leadsham et al. 2013; Ricci et al. 2004). The increased concentration of ROS in cells can cause damage to lipids, organelles, membranes and in particular, proteins and nucleic acids, further potentiating apoptosis (Redza-Dutordoir and Averill-Bates 2016). Increased ROS production has also been observed during heat stress with increased ROS concentration associated with increased apoptosis within samples (C.-H. Hou et al. 2014b; Katschinski et al. 2000; Z. Wang et al. 2013c).

4.2 Chapter Aims and Objectives

Chapter 3 assessed the potential use of gold nanorods and gold nanoprisms to induce hyperthermic cell death in bone (MG63) and breast (MCF-7) cancer cell lines. Both nanoparticle types were stable in biological solutions, biocompatible in both monolayer and 3D spheroid cell cultures and exhibited sufficient heating upon irradiation with a NIR laser to lead to cell death. This chapter will focus on assessing the gene and protein expression of key apoptotic candidates to identify the dominant process that occurs during the photothermal cell death induced by gold nanorods and nanoprisms.

At the molecular level, apoptotic cells reveal key molecular players that have been previously discussed in chapter 1 (section 1.2.1), these include pro inflammatory-, initiator- and executioner caspases. Bcl-2 family members are also integral for regulating cell survival or apoptosis. To the best of our knowledge, studies involving nanoparticle-invoked hyperthermia have only screened for very small clusters of apoptotic markers (Espinosa et al. 2016; R. Haghniaz et al. 2015a; L. Mocan et al. 2015a; Shetake et al. 2015; S. Y. Yan et al. 2014; D. Yoo et al. 2013). While other groups determined apoptosis *via* morphological changes such as phospholipid phosphatidylserine (PS) translocation (Y. Oh et al. 2016) and membrane damage (Blanco-Andujar et al. 2016).

This chapter will assess some of the integral molecules that belong to various families (e.g. Bcl-2, Hsps and caspases) that either influence cells to undergo apoptosis or attempt to preserve the viability of cells (in terms of thermotolerance, as described in chapter 1, section 1.3), with a view to identifying the mechanisms of gold nanoparticle induced hyperthermia. Both cells types were assessed in monolayer and 3D tumour spheroid culture. All candidates were evaluated at both the gene and protein level.

Gene expression levels were analysed using a Fluidigm Biomark HD system, which is a fluid dynamic high-throughput real-time automated PCR system that can simultaneously assess up to 96 RNA targets within a dynamic array. Primers were selected based on their association with the intrinsic and extrinsic apoptotic

pathways; this includes members from the Hsp family, caspase family, Bcl-2 family, cathepsins family as well as other notable apoptosis inducing molecules.

Protein expression was measured using a human apoptosis antibody array, which allowed for the targeting of 43 apoptotic targets, including the primary members of the Bcl-2 family, caspase 3 and 8, Hsp -27, -60 and -70.

For both RNA analysis, the cells that have undergone laser treatment were compared to non-laser treated cells. The conditions assessed were:

- MG63 / MCF-7 monolayer; gold nanoprisms; +/- laser treated
- MG63 / MCF-7 monolayer; gold nanorods; +/- laser treated
- MG63 / MCF7 monolayer; no GNPs; +/- laser treated

- MG63 / MCF-7 spheroids; gold nanoprisms; +/- laser treated
- MG63 / MCF-7 spheroids; gold nanorods; +/- laser treated
- MG63 / MCF-7 spheroids; no GNPs; +/- laser treated

For protein analysis, only the monolayer cell samples were analysed, as the protocol uses cell lysates.

Both techniques produced a snap shot of the selected RNA transcripts and selected protein levels after GNP laser treatment in both/either 2D and 3D models in MG63 and MCF-7 cells. Figure 4-2 details the molecules assessed, indicating any overlap where some molecules were assessed by both techniques.

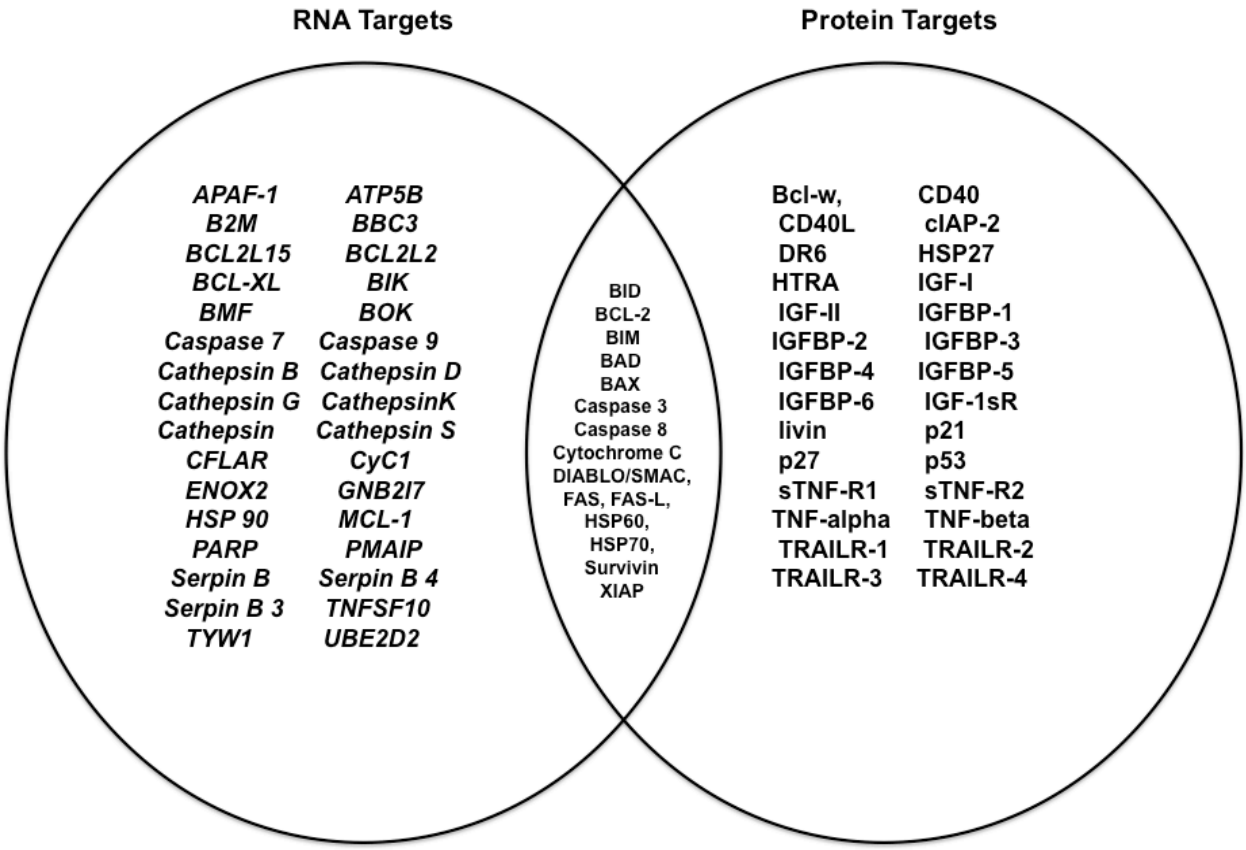

Figure 4-2: Venn diagram representing both the RNA and the protein targets that were assessed as potential apoptotic markers. Protein targets were exclusively investigated in monolayer only.

4.3 Materials and Methods

4.3.1 Laser treatment of Monolayer and 3D Spheroid Culture Models

Both MG63 and MCF-7 cells were seeded at 1 x 10^4 onto 13 mm coverslips and cultured for 24 hours prior to GNP incubation at 0.1 $mg.ml^{-1}$ (section 3.3.2). Meanwhile, MG63 and MCF-7 spheroids were prepared at 1 $x10^5$ cells following incubation with 0.1 $mg.ml^{-1}$ GNP concentration (as section 3.3.2.1). Once prepared, cell samples were subjected to laser treatment, using the Ventus 1 W unfocused continuous wave 1064 nm wavelength laser for 1 minute (as section 3.3.5). Control samples either contained no GNPs or were not subjected to laser treatment (n=3).

4.3.2 RNA Extraction and Isolation

Following laser treatment, samples were further incubated for 3 hours (37ºC, 5% CO_2). Subsequently, the MG63 and MCF-7 monolayers were washed in HEPES, detached with versene/trypsin, resuspended in fresh growth media and centrifuged (3000 x g, 10 minutes) to cell pellets. For spheroid samples, cell spheroids were washed with HEPES saline, centrifuged (1000 x g, 5 minutes). All pellets were re-suspended in 1 mL PBS and prepared for RNA extraction and isolation using PicoPure^{tm} RNA Isolation Kit (thermofisher KIT0202).

Samples were then processed as per the manufacturers instruction. Briefly, the supernatant was gently removed from each sample and re-suspended in 1 ml per sample of suspension media (0.9 mL of 1 x PBS/10%BSA; 0.1 mL of 0.5 M EDTA). Samples were then centrifuged (3000 x g for 5 minutes) and the supernatant removed. Cells were then extracted using 100 µL of extraction buffer (XB) while the cell pellet was gently re-suspended by pipetting; samples were then incubated at 42°C for 30 minutes and centrifuged (3000 x g for 2 minutes). The extracted RNA supernatant was then transferred into a fresh microcentrifuge tube.

Meanwhile, RNA purification columns were pre-conditioned by pipetting 250 µL of condition buffer (CB) on the purification column filter membrane for 5 minutes at room temperature. The purification columns were then placed into corresponding

collection tubes and centrifuged at 16000 x g for 1 minute. Ethanol (10 µL of 70%) was added to the previously extracted RNA solution and the final RNA extract/ethanol mixture was transferred to the pre-conditioned purification column. To bind RNA, the samples were centrifuged for 2 minutes at 100 x g and then immediately centrifuged at 16000 x g for 30 seconds, to remove flowthrough. Subsequently, wash buffer (100 µL) was then added to the purification columns, which were again centrifuged at 8000 x g for 1 minute. Following centrifugation, 100 µL of wash buffer II was then added into the purification column with centrifugation at 8000 x g for 1 minute. Wash buffer II was again added to the purification columns and centrifuged at 16000 x g for 1 minute. After centrifugation, the purification column was transferred to a fresh 0.5 mL microcentrifuge tube. Finally 10 µL of elution buffer was added to each purification column and incubated for 1 minute at room temperature. The columns were then centrifuged at 1000 x g for 1 minute in order to distribute elution buffer in the column and then re-centrifuged at 16000 x g to elute RNA. The isolated RNA was then immediately stored at -80ºC for fluidigm processing.

4.3.3 Fluidigm Analysis

The isolated RNA samples were subjected to reverse transcription using a SuperScript III Reverse Transcriptase (Invitrogen). An aliquot of 11 µL of each sample was added to 1 µL of oligo (dT) and 1 µL dNTPmix, followed by heating at 65ºC for 5 minutes. A solution containing 4 µL 5X First Strand buffer, 1 µL 0.1 M DTT, 1 µL RNaseOUT Recombinant RNase inhibitor, 0.5 µL SuperScript III RT and 0.5 µL water was prepared and added to samples for 5 minutes at 4ºC and then incubated at 50ºC for 30 minutes, and subsequently at 70ºC for 15 minutes to produce cDNA. All 48 primers were pooled together (1 µL) from each primer set pooled and 152 µL of DNA suspension buffer. A fresh solution containing 1.25 µL cDNA from each sample, 2.5 µL 2x TaqMan PreAmp Master Mix, 0.5 µL pooled primer mix and 0.75 µL of water was prepared. Samples were then vortexed, centrifuged and underwent 22 thermal cycles from the following programme.

Table 4-1: Thermal cycles of samples prior to fluidigm analysis

Condition	Hold	22 cycles	Hold	
Temperature	95℃	95℃	60℃	4℃
Time	10minutes	15 seconds	4 minutes	∞

After the cycles were completed a solution comprised of 1.4 µL water, 0.2 µL Exonuclease I reaction Buffer and 0.4 µL Exonuclease were added to each sample buffer being vortexed, centrifuged and incubated at 37ºC for 30 minutes followed by incubation for 15 minutes at 80ºC. Once completed, 18 µL of TE buffer was added to each sample. The Exonuclease I treated sample (2.7 µL) was added to 3 µL of 2x SsoFast EvaGreen Supermix and 0.3 µL of 20x DNA Binding Dye sample loading reagent. Finally, samples were vortexed and centrifuged upon loading onto a 96.96 array chip. Furthermore, 0.3 µL of each individual primer set, as detailed in table 4-2, was added to 3 µL 2X assay loading reagent and 2.7 µL 1x DNA suspension buffer was vortexed and centrifuged before being loaded onto the 96.96 array chip.

Table 4-2: Fluidigm primers designed for human apoptotic targets.

Primer	Sequence
Caspase 3	Forward: 5' TGTGGAAGAACTTAGGCATC 3' (20nt) Reverse: 5' TTTGCTCACACTTTCTCTCA 3' (20nt)
Caspase 7	Forward: 5'-TCTTTTGTGCTGCTTCTTTG-3' (20nt) Reverse: 5'-CCCACTCCTATCTTACTCCA-3' (20nt)
Caspase 8	Forward: 5'- CTGGTCCCTGCTAACATTTG-3' (20nt) Reverse: 5'- CGCATAGTGACGAATGATG-3' (19nt)
Caspase 9	Forward: 5'- CCTGGAGTCTTAGTTGGCT-3' (19nt) Reverse: 5'- TCATATGGGGCCTGAACA-3' (18nt)
Hsp60	Forward: 5'- AGTGGAAATCAGGAGAGGTA-3' (20nt) Reverse: 5'- AGAGGAGGAATGAGAGAAGG-3' (20nt)
Hsp70	Forward: 5'- ATGCCATGTACTTCTCTTGG-3' (20nt)

	Reverse: 5'- ATACAGAACATCTCCCACCT-3' (20nt)
Hsp90	Forward: 5'- CACCACCCCAAATATCTTCT-3' (20nt) Reverse: 5'-'TAGCTCCTCACAGTTATCCA-3'(20nt)

Once completed, a qPCR heat map was created of the CT values:

((CT(target,untreated)-CT(ref, untreated))-(CT(target, treated)-CT(ref,treated))
Samples were normalised to multiple housekeeping genes, representing the increase/decrease in gene expression.

4.3.4 Protein Expression in Monolayer Cell Samples Following Photothermal Therapy using Human Apoptosis Antibody Arrays

Following laser treatment, both MG63 and MCF-7 monolayers were quantitatively assessed for apoptotic markers using the Human Apoptosis Antibody Array Membrane (Abcam, UK) as per the manufacturers protocol. Briefly, samples were laser treated as previously described and incubated for 24 hours to allow for optimal protein expression (Graner et al. 2016; Moussa et al. 2016; A. S. Song et al. 2014; D. Tang et al. 2005; Sihong Wang et al. 2004; K.-L. Yang et al. 2016). Samples were washed twice in cold PBS and lysed with a protease inhibitor cocktail containing 1X lysis buffer and 100X Protease Inhibitor Cocktail Concentrate. Samples were incubated for 30 minutes at 4°C. The total protein lysate was then analysed *via* Thermo Scientific NanoDrop 2000c Spectrophotometer and normalised to 2.5 ug/µL per sample. Samples were transferred to microfuge tubes and centrifuged at 14000 x g for 10 minutes. The supernatant was removed from each lysate and transferred into fresh microfuges. Meanwhile, 2 mL of 1X blocking buffer was added to each membrane at room temperature (RT) for 30 minutes with gentle rocking. After 30 minutes, the blocking buffer was removed from membranes and sample lysates were added to membranes overnight at 4°C with gentle rocking. Sample lysate was aspirated from membranes and washed 3 x 5 minutes with 2 mL wash buffer I at room temperature RT and subsequently washed 2 x 5 minutes with 2 mL of 1X Wash Buffer II at RT. Once thoroughly washed, 1 mL of 1 X Biotin-conjugated Anti

Cytokines was added to each membrane with further incubation at 4°C (gentle rocking). Anti-cytokine reagent was aspirated from membranes and washed with 2 mL wash buffer I at 3 x 5 minutes at RT and 2 mL 2 x 5 minutes with 1X Wash Buffer II at RT per membrane. Membranes were then incubated at room temperature (RT) for 2 hours with 1.5 mL of 1X Streptavidin-HRP. After 2 hours, samples were washed with wash buffer I and II as previously described and incubated overnight at 4°C. A solution containing detection Buffer C and detection Buffer D (250 µL of each buffer *per* membrane) was added to each membrane and plastic film was placed over the membranes. Samples were incubated for 2 minutes at RT. The chemiluminescence of the samples was imaged using myECL Imager (thermofisher). Quantitative comparison of array images was produced *via* densitometry analysis using imageJ software.

Many of these targets increase during apoptosis, and are induced during thermotolerance or change in response to environmental insults leading to dynamic genomic changes. While the majority of these targets have other primary functions within cells, the Bcl-2 family members, caspase members and Hsps are of particular interest as their main function within cells appears instrumental between cell survival and cell death. Other proteins such as cytochrome c, XIAP, livin, p53, SMAC, survivin, TRAILR -1, -2, -3, -4 and XIAP were also evaluated due to their direct/indirect effect on cell survival or death.

4.3.5 Reactive Oxygen Species (ROS) Production Following Photothermal Treatment

Following laser treatment of monolayer cell cultures, the cells were further incubated for 1 hour (37ºC, 5% CO_2) and washed in HEPES saline. MitoSOX Red mitochondrial superoxide indicator (Molecular Probes, Invitrogen, USA) was pre-treated according to manufacturer's instructions and added to samples at 1 mL per sample at 5 µM, final concentration in media. In the same media solution, MitoTracker® Green FM (molecular probes, Invitrogen, USA), at 100nM final concentration, was added. Samples were then incubated for an additional 30 minutes (37ºC, 5% CO_2) prior to washing in PBS and observation using a Axiovert 200m fluorescence microscope (the excitation/emission wavelengths are 510/580 nm for MitoSox Red and 490/516 for MitoTracker® Green). Images were acquired with ImagePro Plus Version 6.01 software (Media Cybernetics) and a sideport

Evolution QEi Monochrome CCD camera (Media Cybernetics). Images were processed using imageJ software (https://imagej.nih.gov). The immunofluorescence images were merged, with the co-localisation of the mitochondria and ROS, producing a representative fluorescence yellow image.

4.4 Results

4.4.1 Apoptotic Marker Analysis *via* Fluidigm

Following laser induced hyperthermia, the gene expression levels of apoptosis targets in MG63 and MCF-7 cells in both monolayer and 3D spheroid cultures were verified by fluidigm analysis. The 42 apoptotic gene markers assessed included members of the caspase family, Hsp family members, Bcl-2 only family members and cathepsin members as indicated in table 4-3

APAF-1, ATP5B, B2M, BAD, BAK, BAX, BBC3, Bcl-2, BCL2L15, BCL2L2, BCL-XL, BID, BIK, BIM, BMF, BOK, Caspase 3, Caspase 7, Caspase 8, Caspase 9, Cathepsin B, Cathepsin D, Cathepsin G, Cathepsin K, Cathepsin L, Cathepsin S, CFLAR, CyC1, Cytochrome C, DIABLO, ENOX2, FAS, FAS-L, GNB2L7, Hsp60, Hsp70, Hsp90, MCL-1, PARP, PMAIP, Serpin B 10, Serpin B 3, Serpin B4, Survivin, TNFSF10, TYW1, UBE2D2, XIAP

Table 4-3: RNA targets for human apoptotic pathways.

Target	Pathway
APAF-1	Predominantly intrinsic pathway but also linked to extrinsic pathway
ATP5B	Housekeeping gene
B2M	Housekeeping gene
BAD	Intrinsic Pathway
BAK	Predominantly intrinsic pathway but also linked to extrinsic pathway
BAX	Predominantly intrinsic pathway but also linked to extrinsic pathway
BBC3/PUMA	Predominantly intrinsic pathway but also linked to extrinsic pathway
Bcl-2	Predominantly intrinsic pathway but also linked to extrinsic pathway
BCL2L15	Predominantly intrinsic pathway but also linked to extrinsic

	pathway
BCL2L2	Intrinsic pathway
BCL-XL	Intrinsic pathway and ROS induced-apoptosis pathway
BID	Extrinsic and intrinsic pathway
BIK	Intrinsic pathway
BIM	Intrinsic pathway
BMF	Intrinsic pathway
BOK	Intrinsic pathway
CASPASE 3	Intrinsic and extrinsic pathway
CASPASE 7	Intrinsic and extrinsic pathway
CASPASE 8	Extrinsic pathway
CASPASE 9	Intrinsic pathway
Cathepsin B	Lysosome-mediated apoptosis
Cathepsin D	Lysosome-mediated apoptosis
Cathepsin G	Lysosome-mediated apoptosis
Cathepsin K	Lysosome-mediated apoptosis
Cathepsin L	Lysosome-mediated apoptosis
Cathepsin S	Lysosome-mediated apoptosis
CFLAR/C-FLIP	Extrinsic pathway
CyC1	Intrinsic pathway
Cytochrome c	Intrinsic pathway
DIABLO/SMAC	Intrinsic pathway
ENOX2	House keeping gene
FAS	Extrinsic pathway
FAS-L	Extrinsic pathway
GNB2L7	House keeping genes
Hsp60	Expressed in response to heat stress
Hsp70	Expressed in response to heat stress
Hsp90	Expressed in response to heat stress
MCL-1	Extrinsic pathway (TRAIL mediated apoptosis)
PARP	Intrinsic, extrinsic pathway and lysosome activation
PMAIP/NOXA	Oxidative stress-triggered p53-mediated apoptosis
Serpin B3	TNF-α induce apoptosis
Serpin B4	TNF-α induce apoptosis

Serpin B 10	TNF-α induce apoptosis
Survivin	Intrinsic pathway
TNFSF10	Extrinsic pathway
TYW1	House keeping gene
UBE2D2	House keeping gene
XIAP	Caspase-dependent pathway and lysosome activation

The following figures depict the screening of apoptotic genes using a 96x96 Fluidigm Biomark HD system. In an attempt to visually plot and compare the considerable differences identified, the average fold change was transformed to $\log_2$ to graphically depict all the results within a modest range. The graphs therefore all show the $\log_2$ gene fold changes based on CT calculations using average values from 6-housekeeping genes and then comparing laser to non laser samples.

4.4.1.1 MG63 and MCF-7 Monolayer Control Cultures (no GNPs)

The fold change in apoptotic genes of MG63 control monolayers containing no GNPs when comparing laser treated to non-laser treated is shown in figure 4-3. There were little/no changes to the majority of apoptotic genes in the presence of laser treatment, indicated by the relatively low fold change expression in the majority of targets. Targets that show >2 fold change will be discussed in further detail and include the pro-apoptotic associated genes such as *BID, BOK, FAS-L, caspase 3, BIM, BIK* but also the anti-apoptotic gene *Bcl-2*. Although these pro-apoptotic markers increased >2 fold, suggesting cellular stress upon laser exposure, these molecular events did not translate to cell death within the culture, as inferred in previous results from viability staining post-laser treatment (chapter 3, section 3.4.7).

The fold change in MFC-7 cells is shown in figure 4-4. Again, minimal fold change expression was detected, indicating that laser treatment did not drive cells towards apoptosis. The increased expression of *cytochrome c*, an early apoptotic indicator did show a 5-fold increase (Chandra et al. 2002), however this did not activate *caspase 9* or further downstream apoptotic markers, resulting in viable cells (chapter 3, section 3.4.7).

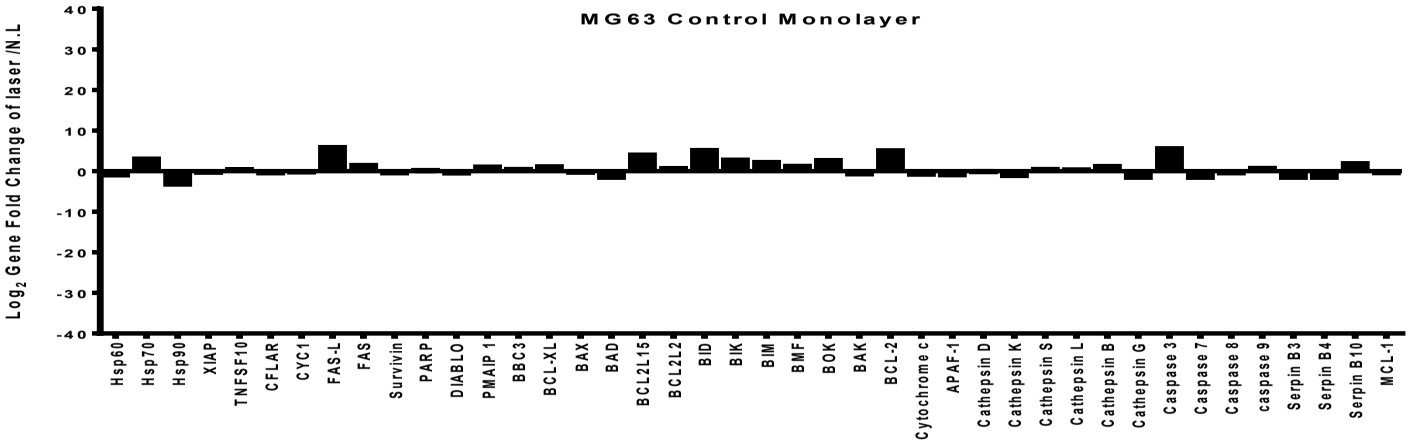

Figure 4-3: Fold change in apoptotic gene expression in monolayer control MG63. Cells contained no GNPs, laser treated samples are normalised against non-laser treated samples (n=3).

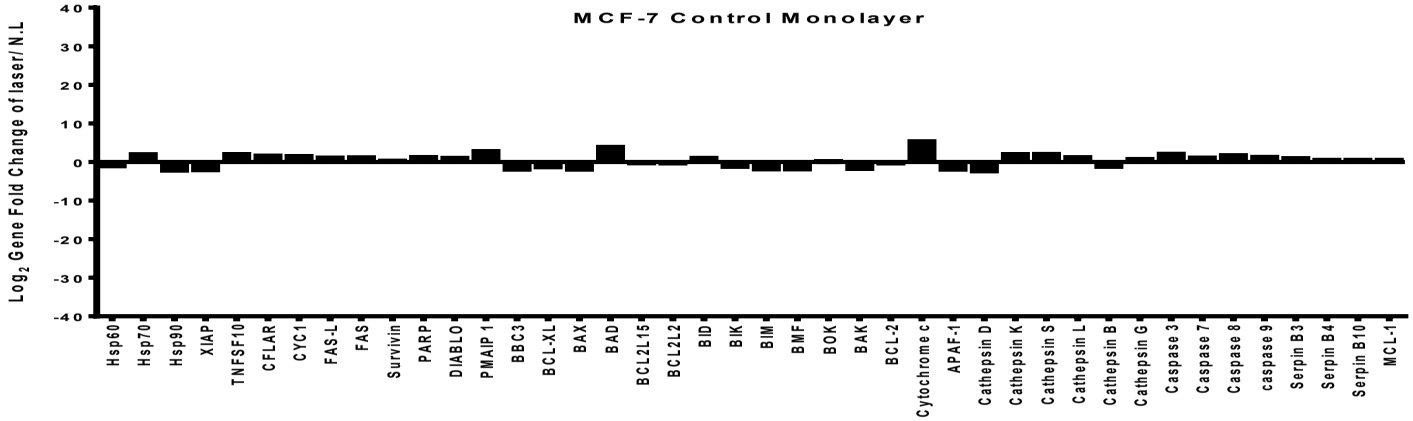

Figure 4-4: Fold change in apoptotic gene expression in monolayer control MCF-7. Cells contained no GNPs, laser treated samples are normalised against non-laser treated samples (n=3).

4.4.1.2 MG63 and MCF-7 Spheroid Control Cultures (no GNPs)

The fold change in apoptotic genes of MG63 control spheroids is shown in figure 4-5. Results indicate a greater fold change expression when compared to the corresponding monolayer results, with >2 fold in the majority of markers. Of these targets, *Hsp90, Cytochrome c, BCL2L15, BID, and caspase 3*, showed >4 fold change expression. This suggests that spheroid cultured MG63 cells induce a larger cellular stress in response to laser exposure than monolayer cells, however it should again be noted that little/no cell death was evident in viability staining (section 3.4.7).

The fold change for MCF-7 cells is shown in figure 4-6. As with its monolayer counterpart, laser exposure did not appear to lead to any notable changes in apoptotic marker expression.

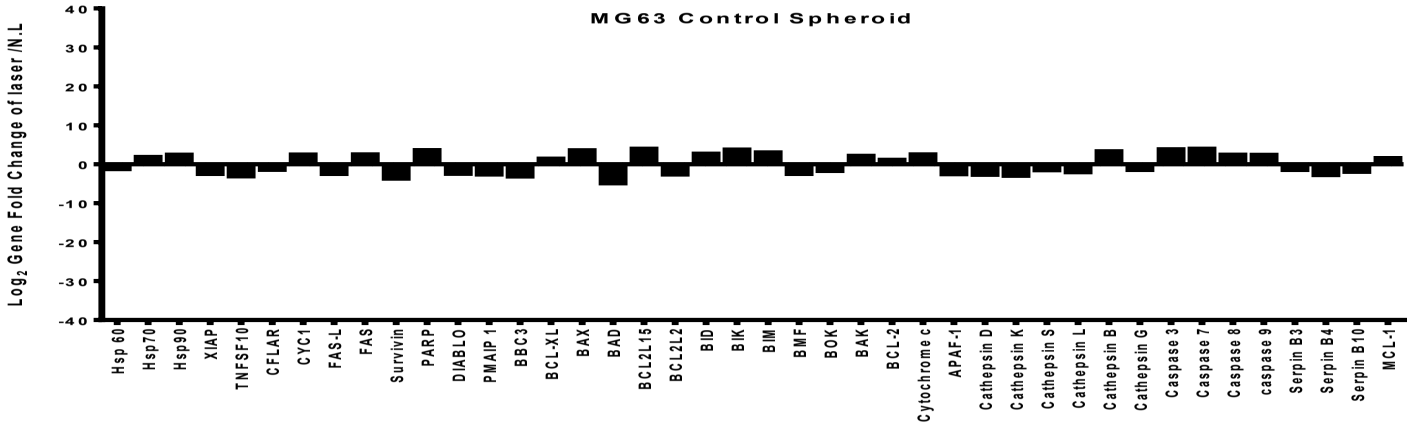

Figure 4-5: Fold change in apoptotic gene expression in control spheroid MG63 cells. Cells contained no GNPs, laser treated samples are normalised against non-laser treated samples (n=3).

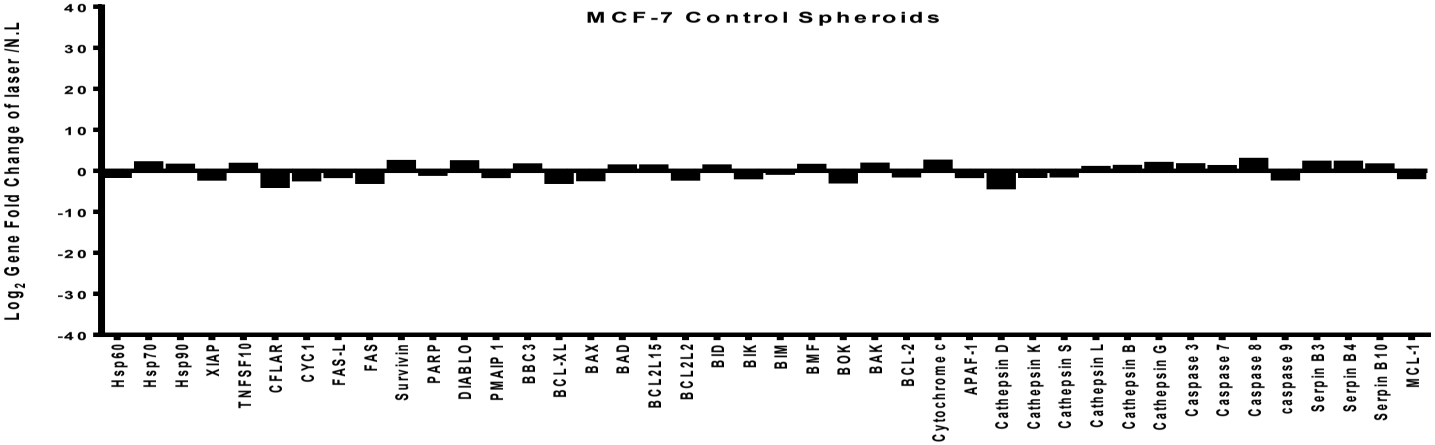

Figure 4-6: Fold change in apoptotic gene expression in control spheroid MCF-7 cells. Cells contained no GNPs, laser treated samples are normalised against non-laser treated samples (n=3).

4.4.1.3 MG63 and MCF-7 Monolayer Cultures Labelled with Gold Nanoprisms

The fold change in apoptotic genes of MG63 monolayers labelled with gold nanoprisms and laser treated is shown in figure 4-7. Large increases were observed in almost all markers, in agreement with the cell death observed following laser treatment in chapter 3 (section 3.4.7). The majority of cell death occurred *via* the intrinsic pathway, with >10 fold change in the expression of markers associated with this pathway, such as, *BID, BAK, BAD, DIABLO/SMAC, BCL-XL*, and *caspase 3, 7 and 9* (Elmore 2007; M. Tiwari et al. 2015a; C. Wang and Youle 2009; Zhou et al. 2011). *Hsp70* and *Hsp90* showed pronounced expression changes, >15 and >20 fold respectively, indicative of hyperthermia induced thermotolerance (Tomoyuki Miyagawa et al. 2014b).

The fold change for MCF-7 cells is shown in figure 4-8. The majority of these markers showed >2 fold increase in expression with a particular increase in *APAF-1, BMF, Hsp70, DIABLO/SMAC, XIAP, caspase 9* and *BID*. *Caspase 8* in particular showed a fold change of >21.

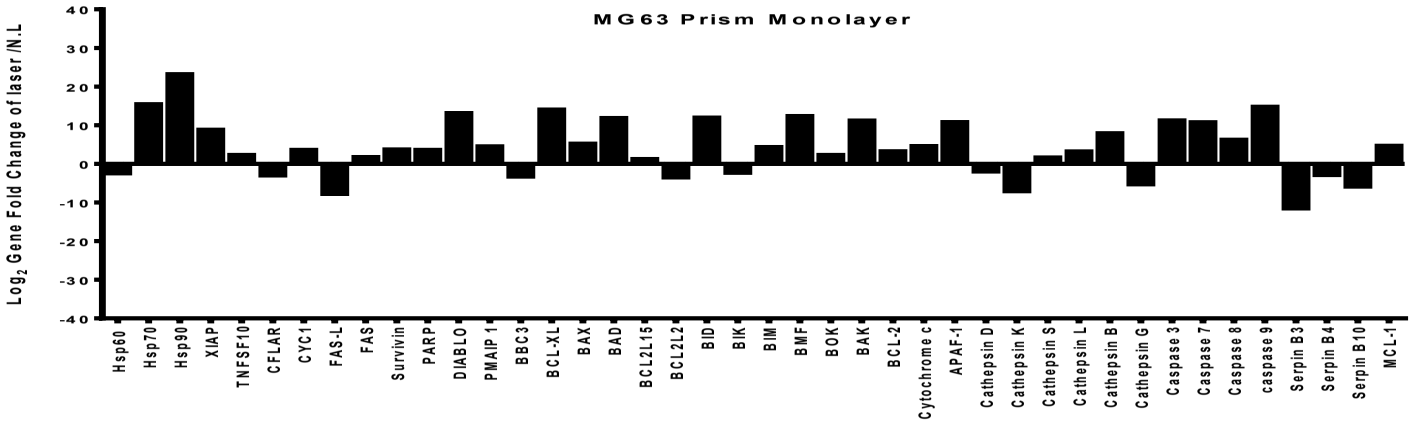

Figure 4-7: Fold change in apoptotic gene expression in monolayer MG63 cells labelled with gold nanoprisms. Laser treated samples are normalised against non-laser treated samples (n=3).

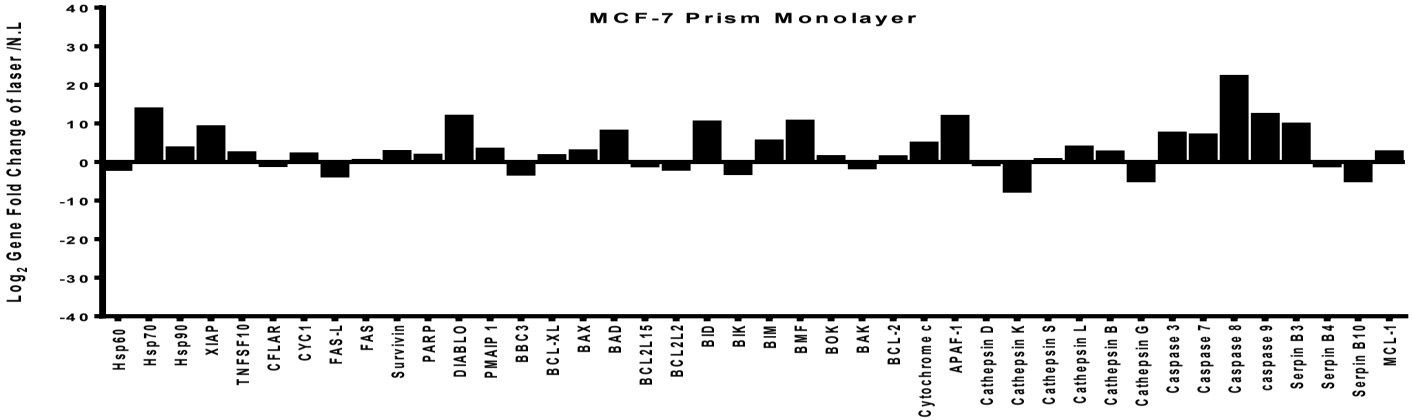

Figure 4-8: Fold change in apoptotic gene expression in monolayer MCF-7 cells labelled with gold nanoprisms. Laser treated samples are normalised against non-laser treated samples (n=3).

4.4.1.4 MG63 and MCF-7 Spheroid Cultures Labelled with Gold Nanoprisms

The fold change in apoptotic genes of MG63 spheroids labelled with gold nanoprisms is shown in figure 4-9. As with the corresponding monolayer cultures (figure 4-7), results showed an increased expression of almost all markers, with a particular increase in *caspase 3, cathepsin S, MCL-1, caspase 8* and *9*, *APAF-1, BAX, BID, cathepsin –B, –K, -S, FAS, SERPIN B3*, *Cytochrome c* and *BAD*. These results support activation of both the intrinsic and extrinsic pathways. *Hsp70* and *Hsp90* were again expressed at high levels to induce thermotolerance and preserve cell viability (Behrouzkia et al. 2016; X. Wang et al. 2014b).

The fold change for MCF-7 spheroid is shown in figure 4-10. Large increases in apoptotic markers were observed; *CFLAR* (also referred to as, C-FLIP), *cytochrome c, caspase 9, Bcl-2, BAK, caspase 8* and *BAX* demonstrated high expression changes (>10 fold change) as well as >20 fold change in *BID*, indicating the intrinsic pathway is predominantly responsible for cells undergoing apoptosis, while the increased expression of *Hsp90* was noted.

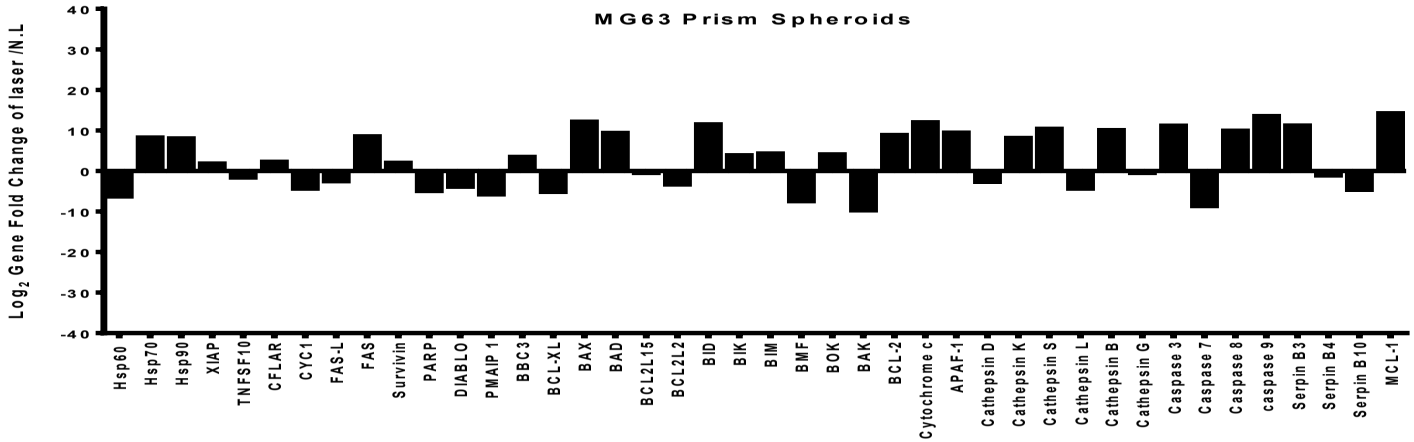

Figure 4-9: Fold change in apoptotic gene expression in spheroid MG63 cells labelled with gold nanoprisms. Laser treated samples are normalised against non-laser treated samples (n=3).

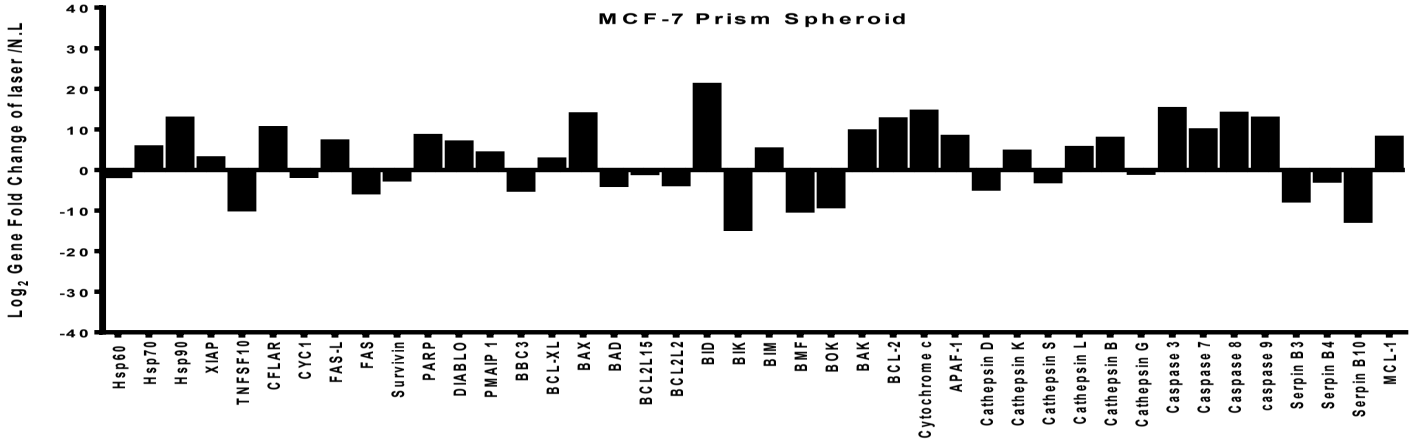

Figure 4-10: Fold change in apoptotic gene expression in spheroid MCF-7 cells labelled with gold nanoprisms. Laser treated samples are normalised against non-laser treated samples (n=3).

4.4.1.5 MG63 and MCF-7 Monolayer Cultures Labelled with Gold Nanorods

The fold change in apoptotic genes of MG63 monolayers labelled with gold nanorods and laser treated is shown in figure 4-11. Changes were noted in most markers. Whilst large fold changes (>10) were observed in markers associated with the intrinsic pathway (*BID, capasase 9, caspase 7, BAK*), increased levels of *SERPINB10, FAS-L and BBC3* also suggested an alternative route of cell death to the more commonly associated hyperthermia-induced apoptosis involving the traditional intrinsic and/or extrinsic pathway.

The fold change for MCF-7 monolayers is shown in figure 4-12. Although a fold change >2 is seen in most markers, the changes themselves appear more subtle than MCF-7 samples incubated with gold nanoprisms, with >10 fold increase observed in *XIAP, Hsp90* and *Hsp70*. However a >5 fold increase was observed in *BMF, CLFAR, Cathepsin K, BIM, Cathepsin S, Cathepsin B, BAK, SERPIN B10, caspase 9*, *cytochrome c, BID and caspase 7*. These results suggest a combination of both the intrinsic and extrinisic (TNF) apoptosis pathways.

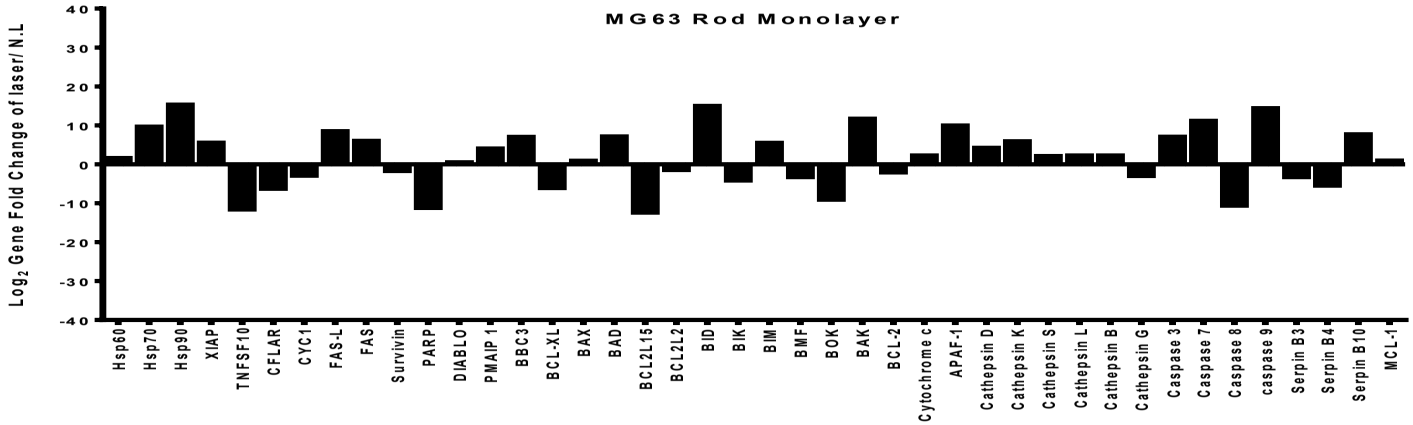

Figure 4-11: Fold change in apoptotic gene expression in monolayer MG63 cells labelled with gold nanorods. Laser treated samples are normalised against non-laser treated samples (n=3).

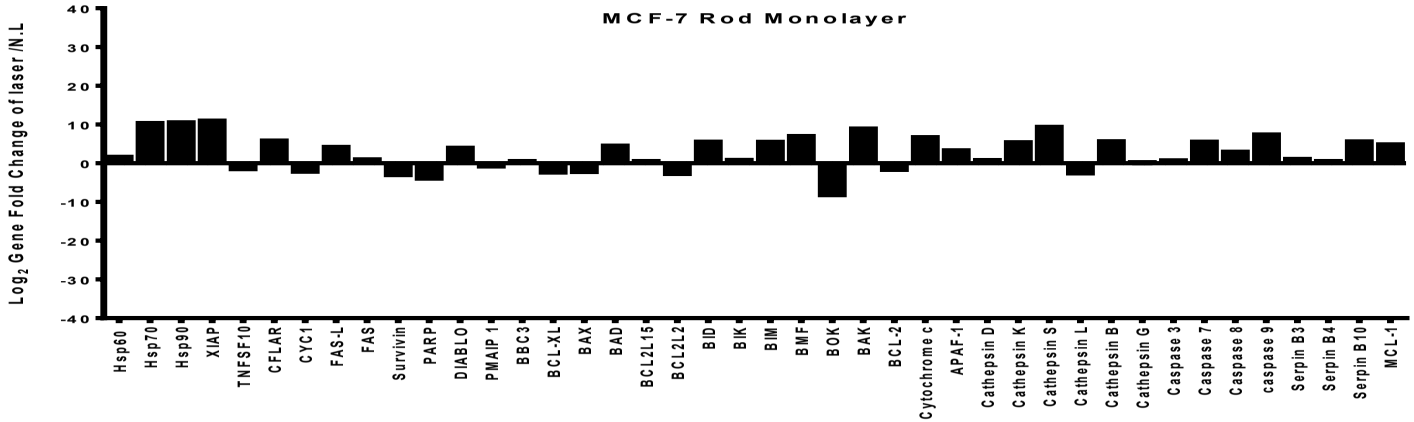

Figure 4-12: Fold change in apoptotic gene expression in monolayer MCF-7 cells labelled with gold nanorods. Laser treated samples are normalised against non-laser treated samples (n=3).

4.4.1.6 MG63 and MCF-7 Spheroid Cultures Labelled with Gold Nanorods

The fold change in apoptotic genes of MG63 spheroids labelled with gold nanorods is shown in figure 4-13. High fold changes (>10) were noted for many apoptotic markers, with *cytochrome c* and *caspase 8* indicating fold changes of >30 and >27, respectively. Again, heat shock proteins were induced, with *Hsp70* and *Hsp90* increased >14 and >18 respectively.

Differences in gene expression levels were noted with MCF-7 cells (figure 4-14) but the pattern was different to MG63 cells. A large increase was observed with many markers showing a fold change of >3. Of these markers, *Bcl-2, PARP, cathepsin S, BIK, caspase 8, BAK*, and *cytochrome c* show fold changes >10.

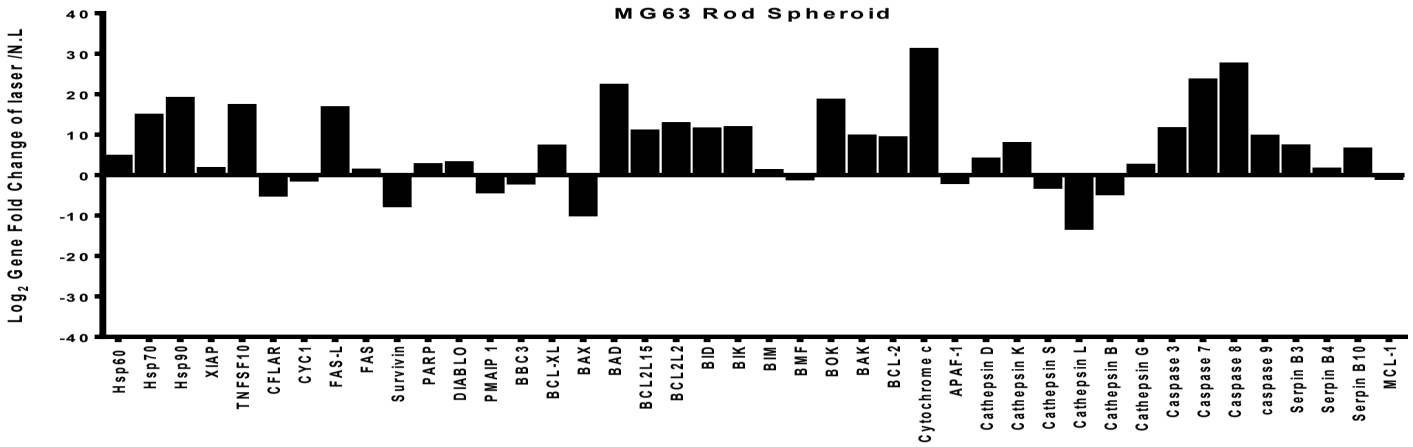

Figure 4-13: Fold change in apoptotic gene expression in spheroid MG63 cells labelled with gold nanorods. Laser treated samples are normalised against non-laser treated samples (n=3).

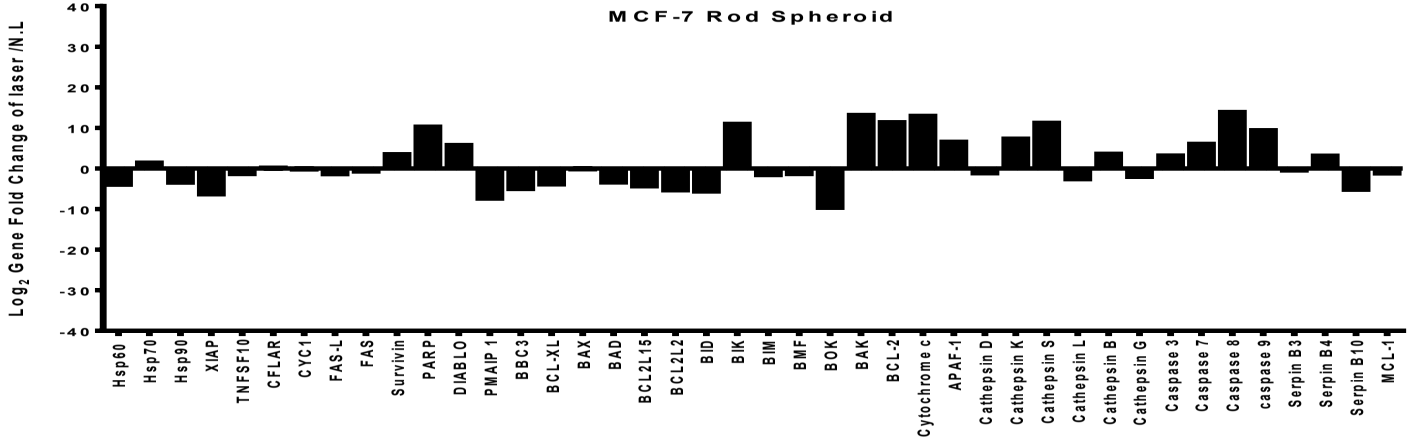

Figure 4-14: Fold change in apoptotic gene expression in spheroid MCF-7 cells labelled with gold nanorods. Laser treated samples are normalised against non-laser treated samples (n=3).

4.4.2 Apoptotic Protein Marker Analysis

Antibody arrays were used to quantify the expression and fold change of 43 apoptotic proteins within monolayer MG63 and MCF-7 cells labelled with gold nanorods or nanoprisms following photothermal laser treatment. Whilst the RNA levels have been identified, mRNA molecules are transient and often shortly after synthesis are degraded, therefore not all mRNAs will be used as templates to generate proteins. For example, in mammalian cells, on average two copies of a given mRNA are synthesised per hour, however cells are capable of producing dozens of copies of the corresponding protein per mRNA per hour and, while the half-life of mRNA is short (2.6–7 hours), proteins exist for longer time periods (46 hours); thus can also impact on the perceived fold change expression of samples (Vogel and Marcotte 2012b). By profiling the expression of genes and proteins from samples it was possible to evaluate the effects of hyperthermia on cells at both the genomic and proteomic level.

Table 4-4: The array contained a membrane substrate enclosing 43 antibodies of known apoptotic markers;

Target	Pathway
Bad	Intrinsic Pathway
Bax	Predominantly intrinsic pathway but also linked to extrinsic pathway
Bcl-2	Predominantly intrinsic pathway but also linked to extrinsic pathway
Bcl-w/bcl2l2	Intrinsic pathway
BID	Extrinsic and intrinsic pathway
BIM	Intrinsic pathway
Caspase3	Intrinsic and extrinsic pathway
Caspase 8	Extrinsic pathway
CD40 (TNFR) family member)	JNK/AP-1 pathway
CD40L	JNK/AP-1 pathway
cIAP-2 (Inhibitor of apoptosis family)	Extrinsic pathway
Cytochrome c	Intrinsic pathway

DR6 (death receptor family)	Intrinsic pathway
Fas	Extrinsic pathway
FasL	Extrinsic pathway
Hsp27	Expressed in response to heat stress
Hsp60	Expressed in response to heat stress
Hsp70	Expressed in response to heat stress
HTRA (member of the serine protease)	Intrinsic pathway
IGF-I (insulin-like growth factor member)	Inhibits apoptosis
IGF-II	Inhibits apoptosis
IGFBP-1 (Insulin-like growth factor-binding protein	Inhibits apoptosis (forms a proapoptotic p53/BAK complex to promote cell survival)
IGFBP-2	Inhibits apoptosis
IGFBP-3	Promotes apoptosis (p53-induced apoptosis)
IGFBP-4	Promotes apoptosis *via* intrinsic pathway
IGFBP-5	Promotes apoptosis (caspase-dependent apoptosis)
IGFBP-6	Promotes apoptosis (p53-induced apoptosis)
IGF-1sR	Blocks apoptosis by inhibiting BAD activation
livin	Blocks apoptosis by inhibiting members of the intrinsic pathway
p21 (The cyclin-dependent kinase inhibitor p21)	Inhibitor of apoptosis
p27	Inhibits apoptosis
p53	Promotes apoptosis
DIABLO/SMAC	Intrinsic pathway
Survivin (member of the inhibitor of apoptosis family)	Inhibits apoptosis
sTNF-R1 (soluble TNF receptors)	Activates extrinsic pathway
sTNF-R2	Promotes extrinsic pathway
TNF-alpha (tumour necrosis factor)	Activates extrinsic pathway
TNF-beta	Activation of the JNK pathway and intrinsic

	pathway
TRAILR-1 (TNF related apoptosis inducing ligand receptor 1)	Activate extrinsic pathway linked to lysosomal apoptosis
TRAILR-2	Activate extrinsic pathway linked to lysosomal apoptosis
TRAILR-3	Inhibits apoptosis via TRAILR-1 and -2 inhibition
TRAILR-4	Inhibits apoptosis via TRAIL inhibition
XIAP	Caspase-dependent pathway

These targets have been shown in a variety of studies to increase in response to cells either undergoing apoptosis or responding to environmental insults leading to dynamic proteomic changes within cells (K. Ahmed et al. 2015a; Hassan et al. 2014; Moulin and Arrigo 2008). While Hsps, caspases and Bcl-2 members have been discussed, proteins such as cytochrome c, XIAP, livin, p53, DIABLO/SMAC, survivin, TRAILR -1, -2, -3, -4 and XIAP will also been evaluated due to their direct/indirect effect on the survival or death of cells. An example of a stained antibody array is shown in figure 4-15, imaged by myECL Imager (ThermoFisher). Differences in protein levels were quantified by comparison of array images produced *via* densitometry analysis using imageJ software.

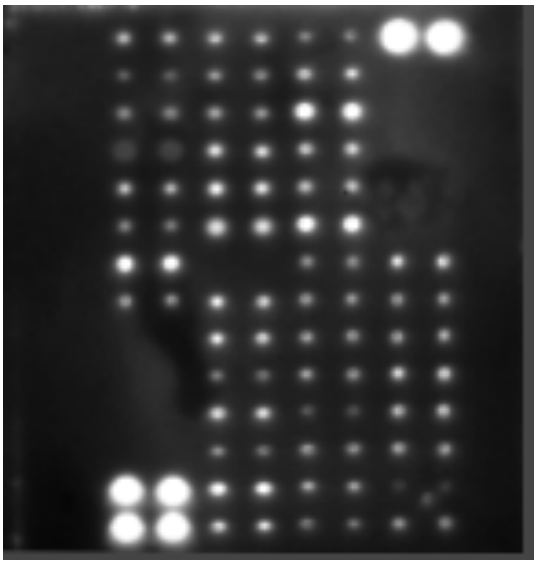

Figure 4-15: Example of a human apoptosis antibody array membrane, targeting 43 apoptotic markers expressed by MCF-7 cells incubated with gold nanoprisms and laser treated. Positive controls are indicated by bright spots, whilst negative controls are blank areas on the membrane.

4.4.2.1 MG63 and MCF-7 Monolayer Control Cultures (no GNPs)

The protein expression of pro-apoptotic and anti-apoptotic markers in control monolayer MG63 cells, that were either exposed to laser treatment or not, is shown in figure 4-16. A basal level of almost all markers was recorded, with an increase in several markers in response to laser treatment, indicating cellular stress, however previous results noted that cell viability was not compromised during laser treatment alone (chapter 3, section 3.4.7).

Similarly, the protein expression of apoptosis markers in control monolayer MCF-7 cells also demonstrated an increase in several markers in response to laser treatment, as shown in figure 4-17. In particular, an increase of ~1.5 fold was observed in Hsp27 and caspase 8, which have been previously demonstrated to interact with each other (Y. Guo et al. 2015). While Hsp60, a potent anti-apoptotic chaperon, showed increased expression. These results do, therefore, confirm that laser irradiation does cause mild stress to cells, but these molecular events do not lead to cell death.

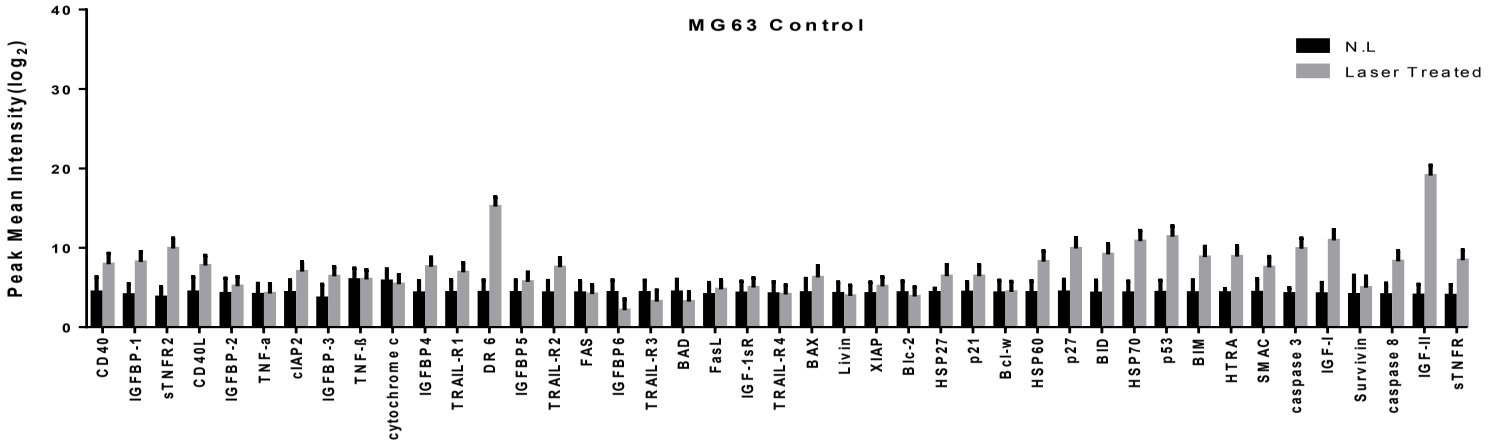

Figure 4-16: Apoptotic protein marker expression in monolayer control MG63 cells, without or with laser treatment. Average peek intensity was transformed to log_2. Data shown is mean ± S.D. (n = 4).

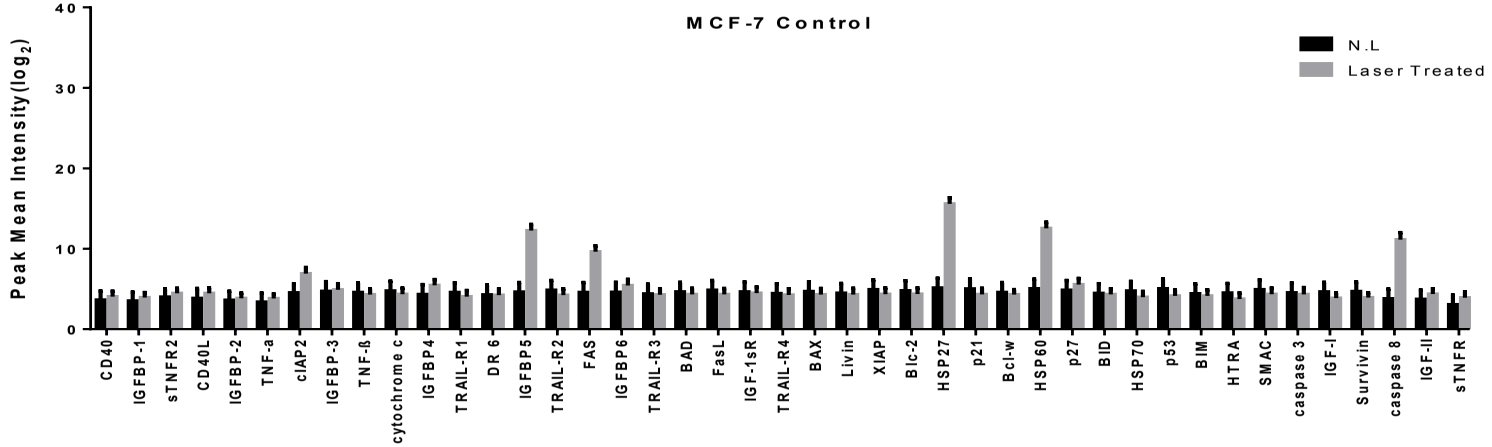

Figure 4-17: Apoptotic protein marker expression in monolayer control MCF-7 cells, without or with laser treatment. Average peek intensity was transformed to log_2. Data shown is mean ± S.D. (n = 4).

4.4.2.2 MG63 and MCF-7 Monolayer Cultures Labelled with Gold Nanoprisms

The protein expression of apoptosis markers in monolayer MG63 cells labelled with gold nanoprisms, and either exposed to the laser or not is shown in figure 4-18. There was a significant increase in all markers for laser treated cells when compared to non-laser treated, demonstrating that the gold nanoprisms facilitate cellular heating and subsequent stimulation of apoptotic markers. The nanoprism labelled cells which were not exposed to the laser (i.e. the darker bars in figure 4-18) exhibited higher values across almost all markers when compared the corresponding non-laser treated cells in figure 4-16, suggesting that the internalisation of the gold nanoprisms causes cellular stress. This was expected, as previous studies have shown an increase in cellular stress markers upon NP internalisation (Xifei Yang et al. 2010). However this internalisation was assessed in chapter 3 and did not compromise cell viability.

The protein expression pattern was similar for the gold nanoprism labelled MCF-7 cells, as shown in figure 4-19. The nanoprism labelled cells exposed to laser treatment consistently showed higher levels of apoptosis markers. Furthermore, the non-irradiated samples again showed higher levels of marker expression than the control MCF-7 cells (figure 4-17), indicating that nanoprism internalisation caused cellular stress.

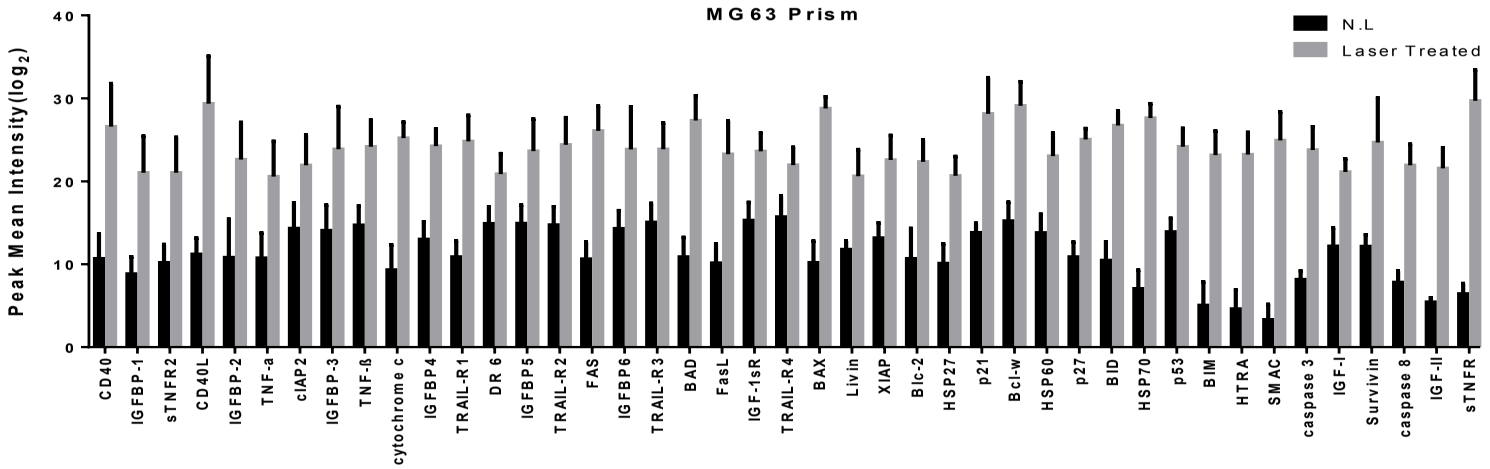

Figure 4-18: Apoptotic protein marker expression in monolayer MG63 cells labelled with gold nanoprisms, without or with laser treatment. Average peek intensity was transformed to log_2. Data shown is mean ± S.D. (n = 4).

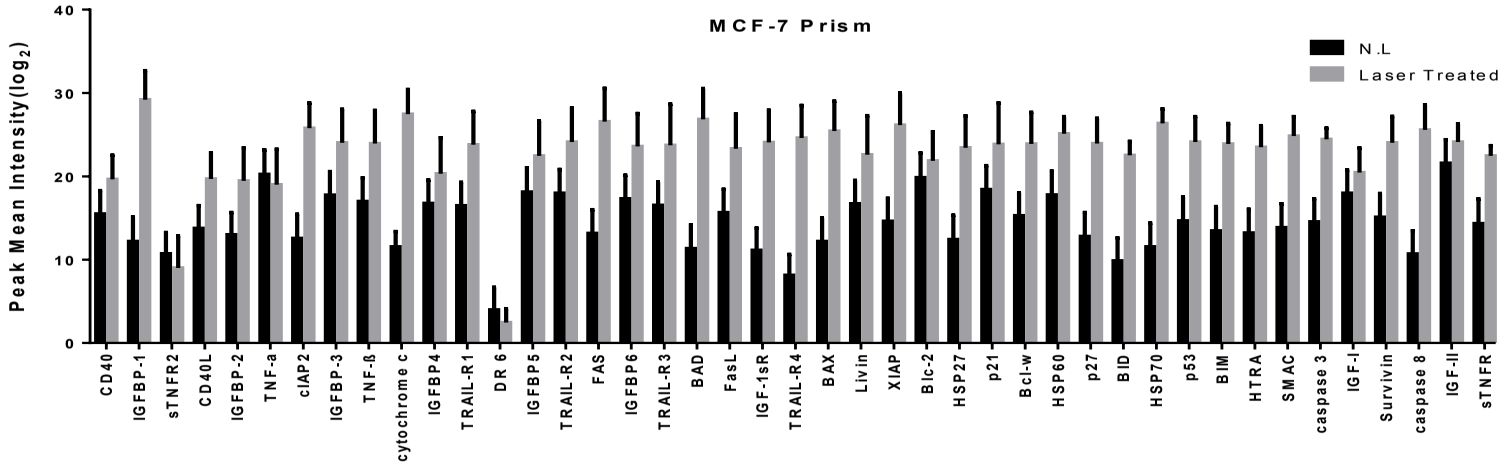

Figure 4-19: Apoptotic protein marker expression in monolayer MCF-7 cells labelled with gold nanoprisms, without or with laser treatment. Average peek intensity was transformed to log_2. Data shown is mean ± S.D. (n = 4).

4.4.2.3 MG63 and MCF-7 Monolayer Cultures Labelled with Gold Nanorods

Figure 4-20 and figure 4-21 shows the protein marker expression in MG63 and MCF-7 monolayer cells labelled with gold nanorods respectively. In both cell types, a large increase in apoptotic markers is noted following laser treatment.

As with the nanoprisms, there was an increase in protein expression for non-irradiated cell samples (when compared to corresponding control monolayers in figure 4-16 and figure 4-17 for MG63 and MCF-7 samples, respectively), however as stated, the internalisation, metabolism and downstream effects of GNPs could lead to minor cellular stress (Petrache Voicu et al. 2015).

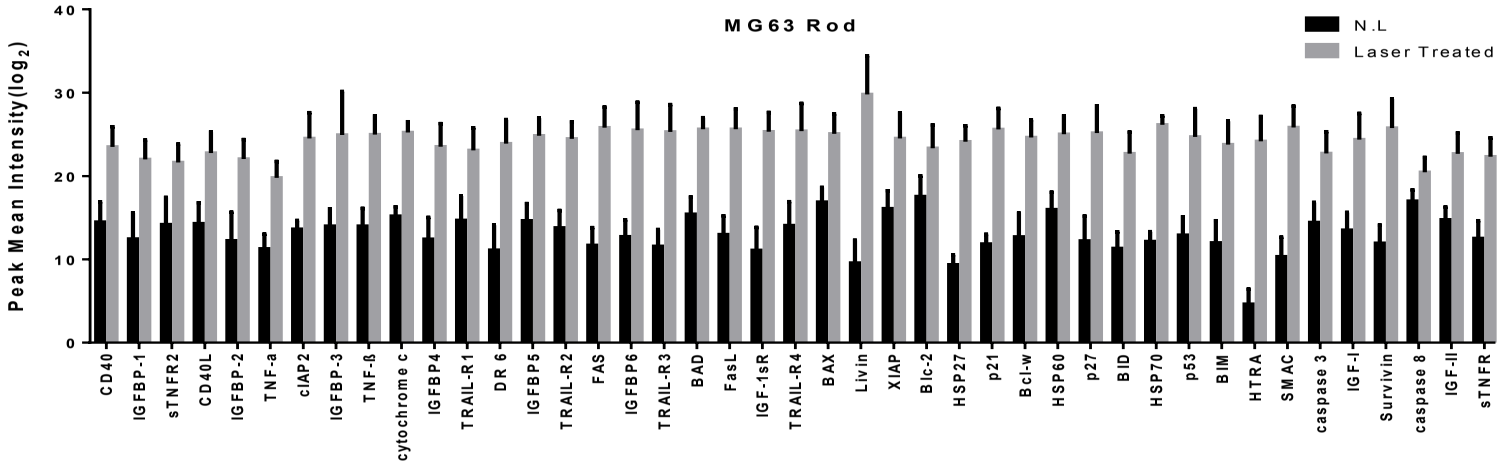

Figure 4-20: Apoptotic protein marker expression in monolayer MG63 cells labelled with gold nanorods, without or with laser treatment. Average peek intensity was transformed to log_2. Data shown is mean ± S.D. (n = 4).

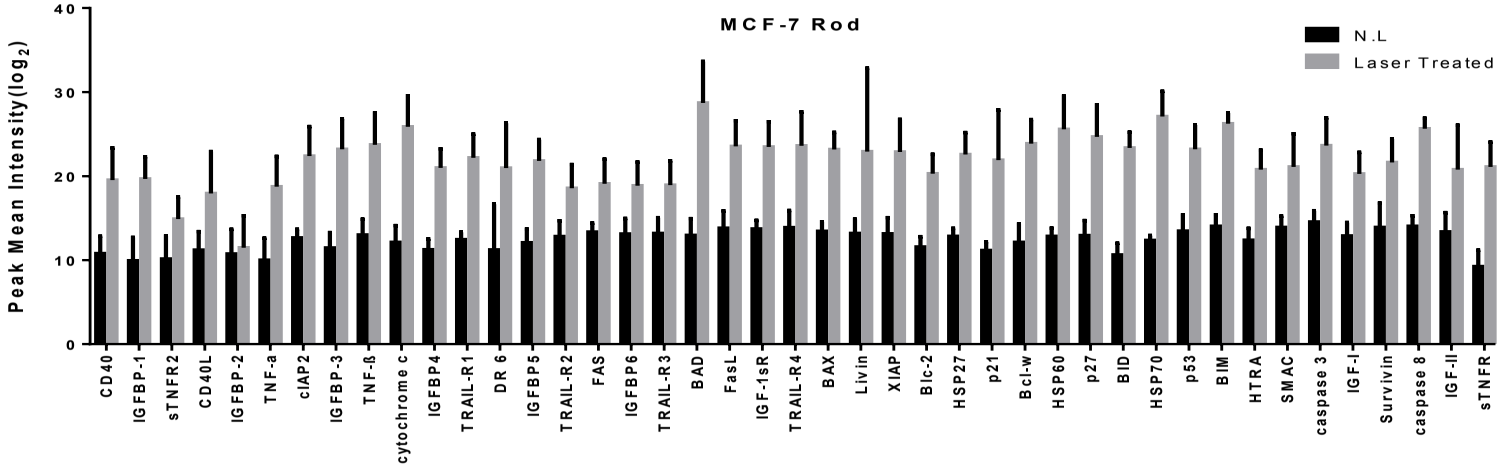

Figure 4-21: Apoptotic protein marker expression in monolayer MCF-7 cells labelled with gold nanorods, without or with laser treatment. Average peek intensity was transformed to log_2. Data shown is mean ± S.D. (n = 4).

4.4.3 Reactive Oxygen Species (ROS) production Following Photothermal Treatment

Results from the previous fluidigm and protein expression analysis appeared to show the importance of ROS generation in stimulating apoptosis within cells *via* the increased expression of cathepsin members as well as p53, XIAP and TRAIL (Aits and Jäättelä 2013; Werneburg et al. 2012). Therefore, a mitochondrial and ROS fluorescence stain was used to visualise the mitochondria and ROS accumulation in MG63 cells, both laser treated and non-laser treated, labelled with gold nanoprisms and nanorods, or controls (containing no GNPs), shown in figure 4-22. The non-laser treated results showed no cellular stress in control cells, with some minor co-localised staining evident in GNP labelled cells (upper panel figure 4-22). However, a mass accumulation of ROS was observed in laser treated GNP labelled cells, as indicated by the overlay of both Mitotracker (green; mitochondria) and MitoSox (red; ROS). The staining confirmed an increase in cellular stress evident following photothermal treatment, which is linked to the mitochondria.

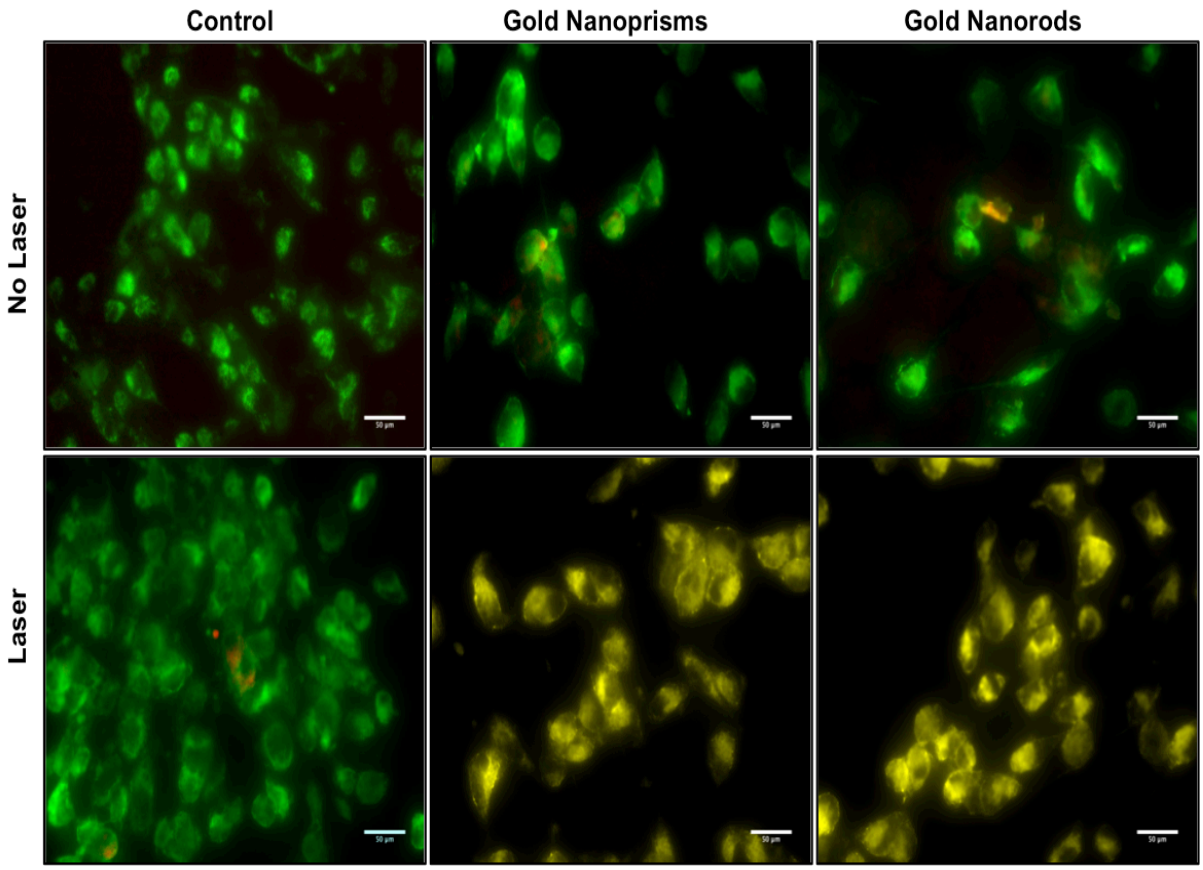

Figure 4-22: Representative immunofluorescence showing MitoTracker staining (green fluorescence) and MitoSox staining (red fluorescence) in MG63 cells in laser treated and non-laser treated samples, labelled with gold nanoprisms, gold nanorods, or controls (containing no GNPs). Co-localisation is indicated by yellow; scale bar represents 50 µm.

4.5 Discussion

Gold nanoparticles (GNPs) are excellent potential candidates for photothermal therapy. In the previous chapter, gold nanoprisms and nanorods were assessed in terms of their biocompatibility in bone and breast cancer cell lines and their ability to generate toxic heat levels in cells following irradiation. The resultant cell death, both in monolayer and 3D tumour spheroid cultures, was verified using a fluorescence viability stain.

In this chapter, I aimed to confirm cell death *via* apoptosis and identify the pathways responsible, by using both gene and protein analysis. Most cancer treatments, including radiotherapy and chemotherapy, involve the activation of apoptosis in cancer cells, *via* the intrinsic and/or extrinsic pathway. It is believed that understanding the molecular events involved in apoptosis activation in response to photothermal therapy will contribute towards the development of a rational approach to combating cancer (S. Fulda and Debatin 2006).

4.5.1 Activation of Apoptosis *via* the Extrinsic and Intrinsic Pathway

Apoptosis is initiated through two main routes involving the plasma membrane by activating death receptors (the extrinsic pathway) or the mitochondria (the intrinsic pathway). The main molecules that have been identified and extensively studied to date are highlighted in figure 4-23. Both pathways converge to induce the activation of caspases as the terminal molecules that effect cell death (although it is noted that caspase-independent apoptosis pathways have been identified).

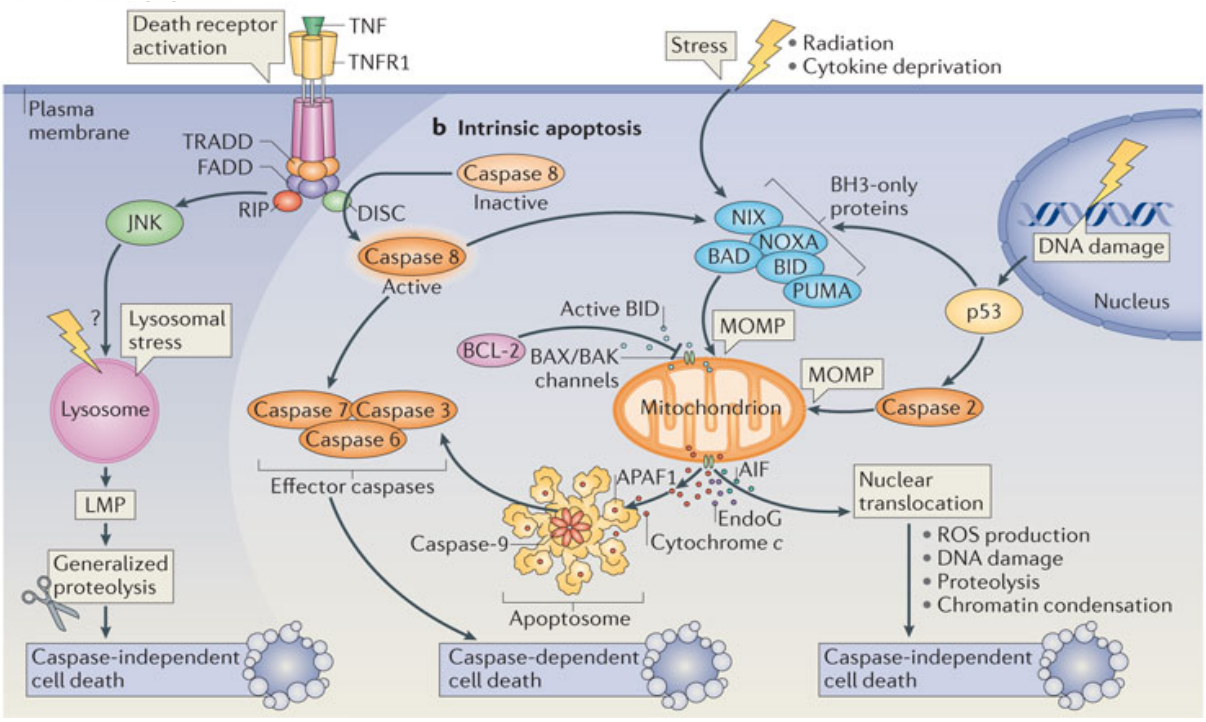

Figure 4-23: Schematic depicting the extrinsic and intrinsic apoptosis pathways with key molecules involved in initiating cell death. Note that the extrinsic pathway utilise membrane-bound death receptors, whilst the intrinsic relies on external stimuli to influence the mitochondria (Mariño et al. 2014).

4.5.1.1 The Intrinsic Pathway

The intrinsic, mitochondrial, pathway is initiated by stress signals such as radiation, hypoxia, free radicals and hyperthermia (Elmore 2007). These stimuli can directly affect the inner mitochondrial membrane, resulting in the mitochondrial permeability transition (MPT) pore, loss of the mitochondrial transmembrane potential and DNA damage. This in turn causes the release of apoptotogenic factors such as cytochrome c, apoptosis inducing factor (AIF) or Smac/DIABLO from the mitochondrial intermembrane space into the cytosol and activation of p53 (Nikoletopoulou et al. 2013). *P53* is a potent tumour suppressor gene and upon activation during DNA damage or intrinsic/extrinsic signalling, acts a transcription factor to activate the transcription of target genes such as *BAX, NOXA* and *PUMA*, all key pro-apoptotic proteins involved in the disruption of the mitochondrial membrane and thus, the intrinsic pathway (Yağmur Kiraz et al. 2016b).

As indicated in figure 4-23, once cytochrome c has been released into the cytosol, it is capable of activating caspase 9 by interacting with the cytoplasmic protein, Apaf-1 and procaspase-9 to form the active multiprotein apoptosome. Activating caspase 9 in turn stimulates effector caspases 3, 6 and 7, resulting in degradation of cellular components and apoptosis (Ilmarinen et al. 2014; K. Sinha et al. 2013). Meanwhile, SMAC/DIABLO, along with HtrA2/Om, also released from the mitochondria are capable of interacting with, and impeding IAPs (inhibitors of apoptosis proteins), including XIAP (X-linked inhibitor of apoptosis protein), c-IAP1 (Apoptosis Inhibitor 1) and c-IAP2 Apoptosis Inhibitor 2) (Du and Elemento 2015; Gustavo Martinez-Ruiz et al. 2008b; Q.-H. Yang and Du 2004).

In addition, activation of BAX/BAK also occurs at the mitochondrial outer membrane (MOM) (Nikoletopoulou et al. 2013). Upon activation, BAK and BAX undergo conformational changes to form homo-oligomers and translocate to the mitochondrial membrane, disrupting mitochondrial potential and the subsequent release of important pro-apoptotic molecules such as cytochrome c and DIABLO/SMAC (Ren et al. 2010). Though the exact mechanism of BAK/BAX initiation is still unknown, it has been proposed that the pro-apoptotic protein, PUMA can activate BAX and BAK-dependent permeabilization of the MOM (Nakano and Vousden 2001). Although Willis et al also observed BAX/BAK activation occurring naturally once BH-3 only proteins inhibit pro-survival proteins such as Bcl-2, Bcl-xL, and Mcl-1 (Willis et al. 2007).

The mitochondrial outer membrane (MOM) permeability is a vital catalyst to activating the intrinsic pathway, with Blc-2 members responsible for regulating its permeability (Gillies and Kuwana 2014). Disruption to the MOM can occur *via* truncated BID (tBID); the conformational change of BID to tBID is actually orchestrated by caspase-2 in response to various stimuli including an increase in ROS concentration (Bonzon et al. 2006; S. Kumar 2009). The activation of tBID leads to the oligomerisation of Bak and/or Bax at the MOM, again leading to the disruption of mitochondrial outer membrane potential and the subsequent release of cytochrome c and SMAC/DIABLO into the cytosol (S. Fulda and Debatin 2006; Kantari and Walczak 2011; Ren et al. 2010). The convergence between the intrinsic and extrinsic pathway is observed in this initiation as BID is also activated by caspase 8, which has been previously shown to be an active member of both the extrinsic and intrinsic pathways (Kantari and Walczak 2011).

4.5.1.2 The Extrinsic Pathway

In apoptosis initiated by death receptor signalling, the extrinsic pathway, mitochondrial damage is not required in most cells as caspase 8 can directly activate downstream caspases (Westphal et al. 2011). The cell surface death receptors, include Fas (CD95/APO1), TRAIL-R (TNF related apoptosis receptor), death receptor 5 (DR5; also known as TNFRSF10B) receptors and TNFα (tumour necrosis factor-α) receptors (Nikoletopoulou et al. 2013). These receptors can be activated by their respective ligands, such as CD95 ligand, TNFα as well as TRAIL (Simone Fulda 2015). Once activated, corresponding receptors begin to activate and the recruitment of adaptor proteins such as adaptor FADD (FAS-associated DEATH domain protein), or in the case of TNFR1 the adaptor TRADD (TNFR1-associated DEATH domain protein), begin to complex with inactive caspase 8, leading to the formation of DISC (death-inducing signaling complex) (Simone Fulda 2015; Vucic et al. 2011). DISC can activate caspase 8, this active caspase 8 is then capable of cleaving BID to tBID, thus leading to the downstream activation of BAX/BAK, and the intrinsic apoptosis pathway, although it can also activate caspase 3 and 7 independently, thus bypassing the intrinsic pathway (Y. Kiraz et al. 2016a).

4.5.1.3 Lysosome-mediated apoptosis

For many years, caspases have been regarded as the chief instigators of apoptotic signaling however fairly recent studies have begun to show the significance of proteases from the endosomal/lysosomal systems (Ivanova et al. 2008). Lysosomes are cytoplasmic membrane-enclosed organelles containing a plethora of hydrolytic enzymes, including proteases such as cathepsin members (cathepsin -B,-D, -L) which are capable of activating pro-apoptotic effectors such as caspase 2, BID, BAX/BAK and can even directly influence the MOMP, prompting the intrinsic pathway (Boya and Kroemer 2008b). For cathepsins (and other hydrolytic enzymes) to escape the lysosome and become active within the cytosol, the lysosome membrane must first be permeabilised, this lysosomal membrane permeabilisation (LMP) can occur *via* various stimuli, including an increase in ROS concentration, upstream protease activation, p53 activation/DNA damage and pro-apoptotic Bcl-2 members (Aits and Jäättelä 2013). LMP has also

been shown to be involved in processes such as necrosis, necrotoposis, autophagy as well as apoptosis (Repnik et al. 2013). It is thought that a quantitative relationship exists between the amounts of LMP within a cell and the pathway of cell death with more moderate stimuli triggering a modest LMP reaction leading towards more of an apoptotic pathway while more rigorous insults leading to an increased LMP response and a complete release of lysosomal contents, favouring a more necrotic pathway (Kroemer and Jaattela 2005; Repnik et al. 2013; B. Turk and Turk 2009).

4.5.2 Changes in Apoptotic Gene Expression

4.5.2.1 Laser Treatment Alone Induces Mild Cell Stress

The results in this chapter indicate that laser treatment of unlabelled cells (i.e. control cells) causes mild cellular stress but does not affect cell viability. The results indicating which genes were increased in both monolayer and 3D cultured cells are summarised in table 4-5.

Table 4-5. A table indicating the genes expressed and the related apoptosis pathway following laser treatment of unlabelled control MG63 (bone) and MCF-7 (breast) cancer cell lines in 2D and 3D culture.

Cell Type	Culture	Increased Genes Expressed	Apoptosis Pathway	Thermotolerance
MG63	monolayer	*BID, BOK, BIK* *FAS-L,* *Caspase 3* (>2 fold change)	Intrinsic Extrinsic	
MCF-7	monolayer	*PMAIP 1* *Cytochrome c* (>2 fold change)	Intrinsic	*Hsp90*
MG63	spheroid	*BAX* *Caspase 7* *PARP* (>5 fold change)	Intrinsic Intrinsic/extrinsic DNA damage, oxidative stress	*Hsp90*
MCF-7	spheroid	*Caspase 8* *Cytochrome c,* *Survivin* (>2 fold change)	Extrinisic pathway Intrinsic pathway	

With MG63 monolayer cells, the main increases noted were in *BOK, BID, FAS-L, Bcl-2* and *caspase 3*. *BOK* is a pro-apoptotic Bcl-2 family member that has been shown to lead to BAX/BAK activation and thus the intrinsic pathway (Echeverry et al. 2013), while the overexpression of BID is also linked to BAX/BAK activation and the subsequent release of pro-apoptotic proteins from mitochondria. The elevated *Bcl-2* expression may have reduced *capsase 9* and thus *caspase 3* activation through inhibition of *cytochrome c* release (Elmore 2007), however *caspase 3* expression was elevated, suggesting involvement of the extrinsic pathway involving *FAS-L* (although subsequent activation of *FAS* and *caspase 8* would be required, which was not shown here). It may therefore appear that *caspase 3* was activated by a novel ROS activated pathway (C.-H. Hou et al. 2014b). The mitochondrial / ROS fluorescent staining in figure 4-22 did indicate

the presence of ROS in some cells while the generation of ROS in cells upon continuous wave laser exposure has been previously confirmed (Mohanty et al. 2006).

Interestingly the breast cancer cell line, MCF-7, whilst also indicating signs of cellular stress, showed very small variations in markers, although a fold change >2 was observed in *Hsp70, PMAIP 1* and >4 fold change in *cytochrome c*. These markers have previously been noted in response to an increase in ROS accumulation within cells, an occurrence that has been linked to NIR exposure (Eno et al. 2013). Oxidative stress within cells can also lead to the downstream release of cytochrome c from mitochondria, which may account for its increase expression (C.-H. Hou et al. 2014b).

When cells were cultured in 3D spheroids, MG63 cells showed a greater level of cell stress as an increase in the majority of apoptotic markers were observed with *BAX, caspase 7, PARP* and *Hsp90* showing >5 fold increase. Caspase 7 can be directly activated by capsase 9 and as our results suggest, this intrinsic activation may be responsible for its increased expression (Brentnall et al. 2013). PARP-1 plays key roles in DNA repair, chromatin modulation, and transcription upon cellular stress and is highly expressed in cells exposed to oxidative stress and thermal pressure (Luo and Kraus 2012). Its unregulated expression suggests laser exposure may increase ROS concentration in cells and possible genetic disruption, although again previous data supports the high viability of MG63 spheroid control samples. Hsp90, as previously described in chapter 1 (section 1.3.1) is an integral member of the heat shock protein family, Hsp90 is involved in cellular homeostasis, transcriptional regulation, chromatin remodeling, and DNA repair (Pennisi et al. 2015). The expression of both Hsp90 and PARP-1 suggest DNA damage *via* increased ROS production. Hsp90 may also be critical in regulating apoptosis by supporting Protein kinase B (PKB) activation, which in turn prevents cytochrome c release, and also by negatively regulating the association of Apaf-1 with caspase 9 (Workman and Powers 2007).

However, MCF-7 spheroids displayed similar results to their monolayer counterparts, although a >2 fold change increase was observed in *caspase 8*, *cytochrome c*, and *survivin*. Survivin is a member of the IAP family and can inhibit apoptosis and promote cell proliferation (S. Cho et al. 2010b). Survivin has

previously been shown to inhibit SMAC/DIABLO while also stabilising XIAP – a protein capable of inhibiting caspase 3,7 and 9 (S. B. Bratton et al. 2002; Y.-F. Lin et al. 2013b; Pavlyukov et al. 2011).

In summary, the bone cancer cell line (MG63) appears to be more susceptible to laser treatment than the breast cancer cells (MCF-7). Furthermore, cells respond more acutely to the laser when cultured as 3D spheroids rather than in monolayer cultures. This may be due to the tighter cell-cell interactions within spheroid culture allowing for a greater number of cells to be activated, or it may point towards an issue in heat dissipation in 3D compared to 2D, which has not been previously observed (Khoei et al. 2004; A. S. Song et al. 2014; Yamamoto et al. 2015). In both cases cellular stress appears to be linked to an increase in ROS within the cells, which is supported by the occasional ROS/mitochondria staining in figure 4-22.

4.5.2.2 Laser Treatment of GNP Labelled Cells Activates Apoptosis

The screening of 42 apoptotic genes has provided a widespread analysis of the molecular events that occur following hyperthermia *via* photothermal laser treatment of samples labelled with GNPs. Fluidigm analysis confirmed cell death occurred *via* apoptosis, in both 2D monolayers and 3D multicellular tumour spheroids when cells were labelled with GNPs and laser treated. The results are summarised in table 4-6 detailing the genes that were increased and the apoptosis pathway they are lined to (table 4-6.). When considering all samples, it appears the predominant pathway to induce apoptosis within cells is the intrinsic (mitochondrial) pathway (Z.-G. Cui et al. 2014e; Pérez-Hernández et al. 2015; J.-f. Zhang et al. 2016). However the high expression of *caspase 8, BID* and *caspase 3* in some samples may suggest that apoptosis occurring *via* the extrinsic pathway (Nagarsekar et al. 2008).

Table 4-6. A table indicating the genes expressed and the related apoptosis pathway following laser treatment of unlabelled MG63 (bone) and MCF-7 (breast) cancer cell lines in 2D and 3D culture containing GNPs. (* = fold change >5, # = fold change >10).

Cell Type	Culture	GNP	Genes Expression	Apoptosis Pathway	Thermo-Tolerance
MG63	monolayer	prisms	*Cathepsin B* Cathepsin S*, Cathepsin D#,* *Survivin* BAD* BAX* PMAIP 1* BAK* BID# caspase 9# caspase 3# Cytochrome C# DIABLO/SMAC# BCL-XL# # caspase 7#* *caspase 8#*	Lysosome Intrinsic Extrinsic	 *Hsp70* *Hsp90*
MG63	monolayer	rods	*BAD*, BAK*, BCL-XL*, BBC3 (PUMA)*, BOK* BID# capsase 3*, APAF-1* BCL2L15# Caspase 9#,* *TNFSF10#, SERPIN B10#, Fas-L# Caspase 8#*	Intrinsic Extrinsic	*Hsp70** *Hsp90#*
MCF-7	monolayer	prisms	*cytochrome c*, caspase 9#, APAF-1#, DIABLO#, caspase 7* caspase 3** *caspase 8 (>21 fold change)*	Intrinsic Extrinsic	*Hsp70#* *Hsp90**

MCF-7	monolayer	Rods	*BMF*, BIM*, BAK*, caspase 9* Cytochrome c* caspase 7** *SERPIN B10*, CFLAR** *Cathepsin B*, Cathepsin K* Cathepsin S**	Intrinsic Necrotoposis Autophagy Lysosome	 *Hsp70*[#] *Hsp90*[#]
MG63	Spheroid	Prism	*BAX*,BAD*,BID*,Cytochrome C*, APAF-1*,Caspase 3* (F.C ~20), *DIABLO** *FAS*BCL-2*,MCL-1*[#]*, SERPIN B3** *Cathepsin K*, Cathepsin S*, Cathepsin B**	Intrinsic Extrinsic Lysosome	 *Hsp70*[#] *Hsp90*[#]
MG63	Spheroid	Rod	*BID*[#] *BIK BAK*, BCL-2*, Cytochrome C* (~30 F.C), *Caspase 3*[#] *Caspase 7*[#] (~23 F.C), *Caspase 8* (~27 F.C), *Caspase 9*, PARP** *SERPIN B3*,SERPIN B10*, MCL-1** *Cathepsin K**	Intrinsic Extrinsic Lysosome	 *Hsp70* (~15 FC) *Hsp90* (~18FC)
MCF-7	Spheroid	Prism	*BAX*[#], *BIM*, BCl-2*[#], *BAK*, APAF-1*, Caspase 3*[#], *Caspase 7* Caspase 9*[#] *BID* (F.C ~21),*Caspase 8*[#]*,MCL-1*,CFLAR*, FAS-l*, PARP**	Intrinsic Extrinsic	 *Hsp70** *Hsp90*[#]
MCF-7	Spheroid	Rods	*Caspase 8*[#]*, PARP*[#] *BCL-2*[#]*, BAK*[#]*, BIK*[#]*, Caspase 7*, Caspase 9*, Cytochrome c*[#] *DIABLO*[#] *Cathepsin K*, Cathepsin S*[#]	Extrinsic Intrinsic lysosome	 *Hsp70*[#] *Hsp90*[#]

Monolayer MG63 Cells: Gold Nanoprisms and Nanorods

MG63 monolayers labelled with gold nanoprisms showed an increased gene expression in the majority of apoptotic markers, with >5 fold change expression measured in *survivin, BAD, BAX, PMAIP 1, BAK* and *cathepsin S*. While a >10 fold change expression was measured in *caspase 8, cathepsin B, caspase 3, BID, caspase 7, caspase 9, DIABLO/SMAC, BCL-XL and Hsp70 and Hsp90*. The majority of these markers indicate the intrinsic apoptotic pathway, as seen by the increased expression of *BID*, *cytochrome c, DIABLO/SMAC and caspase -3, -7* and *-9*, however the expression of *caspase 8* also supports the activation of the extrinsic pathway.

The up regulation of cathepsin has been linked to activating caspase 3 and 7, as well as BID activation (Leist and Jaattela 2001). Cathepsins are proteases which mainly located within lysosomes and capable of protein degradation; they were originally believed to cause degradation during necrotic and autophagic death (V. Turk et al. 2012). Their functions have been extensively explored and shown to promote apoptosis by degrading anti-apoptotic proteins such as Bcl-2, Bcl-xL, Mcl-1 and XIAP, thereby tipping the scale towards apoptosis (V. Turk et al. 2012).

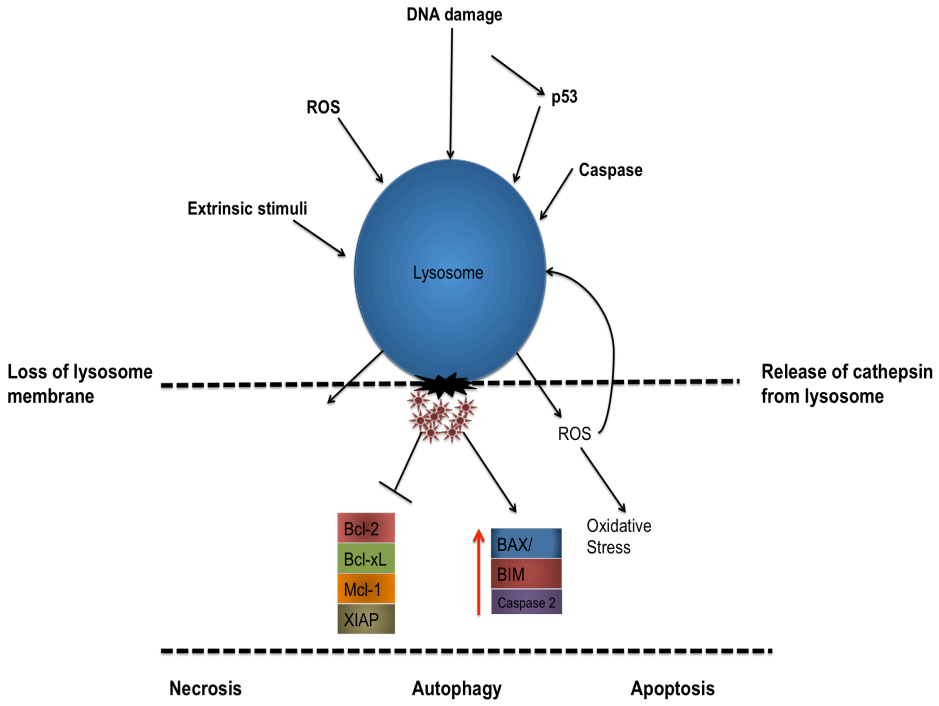

Figure 4-24: Schematic depicting the permeabilization of a lysosome membrane by a variety of external stimuli, DNA damage or *via* intracellular signalling leading to the release of cathepsin from the lysosome and the simultaneous degredation of pro-survival proteins and subsequent activation of pro-apoptotic proteins.

Cathepsin S is a cellular cysteine protease, with the over-expression of this protease, associated with cell survival (K.-L. Chen et al. 2012). However the increased expression is also linked to autophagy - a highly conserved metabolic process that permits the degradation and recycling of cellular constituents, in response to cell stress (Mariño et al. 2014). Cathepsin B is released upon lysosomal disruption and has been shown to degrade Bcl-xL proteins, thus promoting apoptosis and shifting the intracellular events away from necrotic activity (de Castro et al. 2016). Cathepsin D activity is more controversial, and has shown both anti- and pro- apoptotic properties and has unfortunately not been fully characterised, although its activation appears similar to cathepsin B, released into the cytosol upon lysosome disruption (Minarowska et al. 2007). Oxidative stress again appears as a marker, as the increased expression of *PMAIP* (Noxa) was observed in increasing ROS concentrations (Eno et al. 2013). *PMAIP* expression has been shown to elevate in response to increased ROS concentration, in

particular hydrogen peroxide (h_2O_2) (Eno et al. 2013). H_2O_2 has also shown to cause lysosomal membrane permeabilisation, which may explain the increased expression of cathepesin observed.

The increase in NOXA expression is also associated with a decrease in Bcl-2 and Bcl-xl and may explain the more modest expression values seen in Bcl-2 expression (Barkinge et al. 2009). BAD is a pro-apoptotic marker, that contributes to the intrinsic pathway and is integral at lowering the threshold at which tBID and BAX/BAK are instigated and inhibiting Bcl-2 and Bcl-xl, although results show a minor fold change in *Bcl-2, Bcl-xl* expression remains unaffected by its increased expression (Howells et al. 2011). *Survivin*, is a unique inhibitor of apoptosis, that also showed >5 fold change, and although its function has not been entirely characterised, it has been shown that survivin can inhibit caspase 9 activation, although our results do not reflect this (Y. Lin et al. 2016; McKenzie and Grossman 2012). Bcl-xl is an anti-apoptotic protein, found localised in the cytosol, surrounding the outer mitochondrial membrane, although its definitive role still remains controversial, Bcl-xl has been shown to inhibit pro-apoptotic members such as BAX/BAK tBID, BIM and PUMA (Janet H. Zheng et al. 2016; Zhou et al. 2011). These results show a heavy influence of both the intrinsic pathway and ROS induced-apoptosis pathway, which has been explored and supported in isolation by previous groups.

When MG63 monolayers were labelled with gold nanorods a similar large increase (>10 fold) was observed in genes including *BID, Hsp90, caspase 9, SERPIN B10,* and *Fas-L*, whilst *BAD, BAK, BBC3 (PUMA), capsase 3, Hsp70 and APAF-1* targets were also increased (>5 fold). As with the MG63 cells labelled with gold nanoprisms, many genes were linked to the intrinsic pathway, however there were some key genes in this pathway that differed from the MG63 cells labelled with nanoprisms, such as *BBC3* (commonly referred to as *PUMA*). This is a pro-apoptotic complex and has been discussed for its role in directly activating Bax and Bak activation proteins leading the subsequent release of cytochrome c from mitochondria and caspase 3 activation. This in turn leads to the proteolysis of key cellular substrates, including PUMA itself (Ramírez-Labrada et al. 2015).

Monolayer MCF-7 Cells: Gold Nanoprisms and Nanorods

MCF-7 monolayers labelled with gold nanoprisms displayed potent intrinsic markers such as *cytochrome c caspase 9, APAF-1, DIABLO, caspase 7* and *caspase 3*, suggesting hyperthermia contributed to the direct disruption of the outer membrane mitochondrial potential *via* ROS production and/or rupture by the persistent opening of the permeability transition pore due to mitochondrial calcium overload during heat stress (Belhadj Slimen et al. 2014). This would explain the more modest fold change expression of *BAX* and *BAK*, which are the notable proteins that instigate the intrinsic pathway.

With regards to the extrinsic pathway, *caspase 8*, which chiefly coordinates the pathway, demonstrated a large increase (>21 fold change). No notable expression changes were observed in *FAS* or *TNFSF10* gene expression, but the *caspase 8* fold change coincided with increased expression of *BID* and the subsequent release of *cytochrome c*. With regards to thermotolerance, as seen previously, in MG63 monolayers labelled with gold nanoprisms, in hyperthermic conditions, both *Hsp70* (> 10 fold) and *Hsp90* (>5 fold) were expressed.

When MCF-7 cells were labelled with gold nanorods, as with the MG63 cells, the majority of genes were linked with the intrinsic pathway, with a >5 fold change in *BMF, BIM, BAK, caspase 9, cytochrome c* and *caspase 7*. BIM, a pro-apoptotic Bcl-2 family member and is believed to facilitate BAX/BAK activation (Bean et al. 2013; Koenig et al. 2014). Unlike MG63 cells, there were little/no changes in the extrinsic pathway, however interestingly the lysosome pathway was strongly implicated, with large increased noted in *cathepsins -B, -K and -S*. In addition, a >5 fold was noted in *CFLAR* (*c-FLIP*), CFLAR is a protein that can inhibit the extrinsic pathway by blocking the activation of FAS and TRAIL receptors thus preventing the activation of caspase 8, however it has been suggested CFLAR expression may potentiate necrotoposis (Safa 2013; Tsuchiya et al. 2015). The potent expression of *Hsp70* and *Hsp90* (>10 fold change) suggest a high concentration of denatured proteins *via* hyperthermia, while the overexpression of *XIAP* (>10 fold change) is associated with anti-apoptotic features as previously described (Hamacher-Brady and Brady 2015).

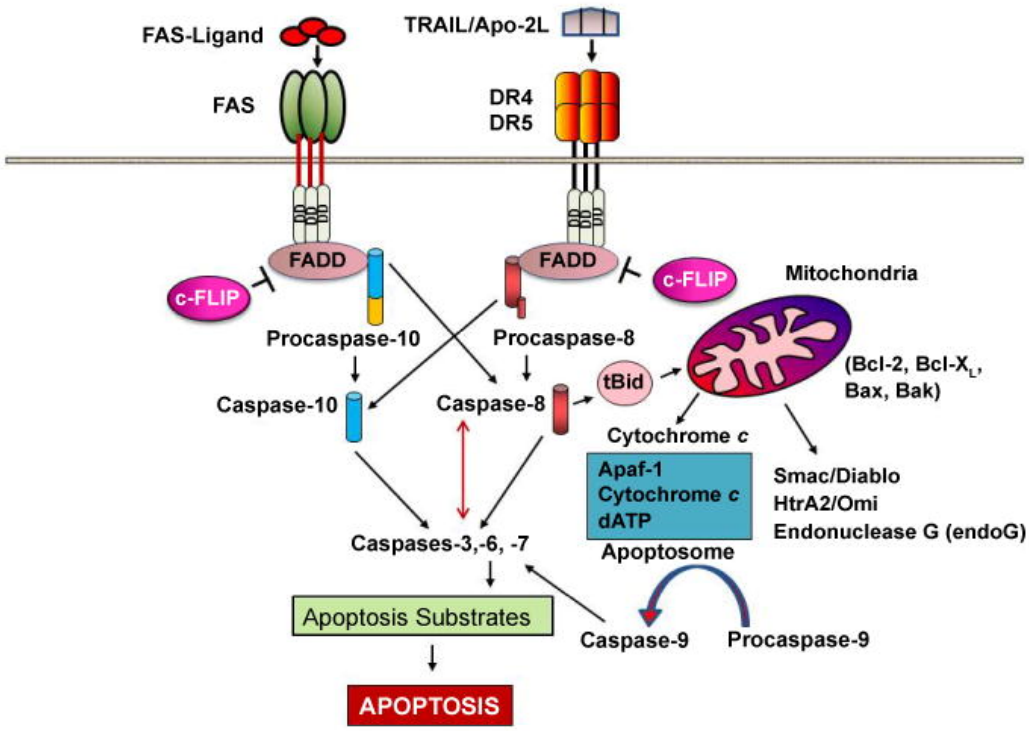

Figure 4-25: Apoptosis signaling pathways and roles of c-FLIP in preventing apoptosis. Interaction of TRAIL with its receptors DR4 and DR5 or binding of Fas ligand to Fas receptor initiates the death receptor (extrinsic) and subsequently mitochondrial apoptosis signaling pathways through FADD-dependent autocatalytic activation of caspases -8 and -10 and Bid cleavage. c-FLIP inhibits caspase-8 and -10 activation, preventing the downstream apoptosis cascade. (Taken from(Safa 2013)).

In summary, when referring to table 4-6 to identify and compare changes in monolayer MG63 and MCF-7 cultures following GNP induced photothermal hyperthermia, similarities and differences are noted between cell types. Both bone and breast cancer cell lines respond strongly to hyperthermic treatment, with large increases noted in apoptotic genes. Gold nanoprisms activate apoptosis mainly through the intrinsic pathway, involving mitochondria, in both cell types. However MG63 cells also engage the lysosomal pathway (figure 4-24). Meanwhile, when apoptosis was activated by gold nanorods, MG63 cells initiated both the intrinsic and extrinsic pathways, whilst MCF-7 cells responded differently, utilising the intrinsic and lysosomal pathways and necrotoposis/autophagy.

3D Spheroid MG63 Cells: Gold Nanoprisms and Nanorods

MG63 spheroids labelled with gold nanoprisms demonstrated a large increase in markers associated with both the intrinsic and extrinsic pathway and the lysosomal pathway. Similar to their corresponding monolayer results, which heavily relied on the intrinsic pathway, a >5/>10 fold change expression was observed in *BAX, BAD, BID, cytochrome c, APF-1* and *caspase 3*. However when MG63 cells were cultured as 3D spheroids and labeled with nanoprisms, several new genes were highly expressed (>5/>10 fold) including *FAS, Bcl-2* and *MCL-1*; all involved in the extrinsic pathway. In addition, spheroid culture further activated apoptosis *via* the lysosomal pathway, with >5 fold changes in *cathepsins -K, -S* and *-B*. Thermotolerance was again noted, with >10 fold change in *Hsp90* and *Hsp70*. Therefore, results suggest that MG63 cells in 3D culture undergo apopotosis *via* the conventional intrinsic and extrinsic pathway, but also *via* more novel caspase-independent pathway orchestrated by cellular oxidative stress.

As the majority of these molecules have been discussed, focus will be drawn to the lesser-known apoptotic markers. *MCL-1* showed ~13.8 fold change expression. Although known as a potent anti-apoptotic Bcl-2 family member, precisely how it functions to promote survival of normal and malignant cells is poorly understood although it has been shown to interact with BAK, tBID, BIM and PUMA (Gelinas and White 2005; Perciavalle et al. 2012; Thomas et al. 2010). In addition, *SERPIN B3* displayed ~12.4 fold change. SERPIN B3 (Squamous Cell Carcinoma Antigen, SCCA1) is a member of the ov-serpins, a serine protease inhibitors family and is an important modulator in apoptosis, serving to protect cells from apoptotic stimuli, such as TNF-α signaling. While its role in inhibiting cytochrome c has been observed (Thomas et al. 2010). Importantly, however, SERPIN B3 protects against oxidative damage caused through the increased intracellular ROS concentration and interestingly, is upregulated under hypoxic conditions, a feature associated with 3D multicellular tumour spheroids (Cannito et al. 2015; Ciscato et al. 2014; Vidalino et al. 2009).

When MG63 spheroids labelled with gold nanorods were laser treated, as with the nanoprism labelled spheroid MG63 cells, apoptosis was activated through a range of pathways, including the intrinsic, extrinsic and lysosomal. Genes involved in the intrinsic pathway were similar to monolayer cultures and nanorod spheroids, they

included a >5 fold change in *BID, BIK, BAK, Bcl-2, BCL2L15, caspases 3, 7 and 9*, with a > 20 fold increase in *BAD*, and a >30 fold increase in *cytochrome c*. Whilst these are similar genes to monolayer samples, the increases in 3D culture are much higher.

The extrinsic pathway was again activated when MG63 cells were laser treated in 3D culture with a >10 fold change in *TNFSF10, FAS-L* and a >27 fold increase in *caspase 8* observed. TNFSF10 (also referred to as tumour- necrosis-factor-related apoptosis-inducing ligand -TRAIL) once activated by appropriate complexes can aggregate, leading to the oligomerisation of TRAIL receptors and the initiation of adapter molecules such as FADD as well as signalling molecules such as caspase 8 to form the death-inducing signalling complex (DISC), eventually leading to the activation of caspase 8 and thus, the extrinsic pathway, as previously described (Ramírez-Labrada et al. 2015). This would validate the greatly increased expression observed in *caspase 8* (>27Fc), while Fas-L (fas ligand), upon binding to FAS receptors, can initiate the same pathway. However as compared to the prism spheroid cultures a >5 fold change was noted in *SERPIN B3*. *Survivin*, a member of the family of inhibitor of apoptosis proteins, capable of inhibiting active caspase 9, also showed > 5 fold increase (Y. Lin et al. 2016; Alain C. Mita et al. 2008b), while thermotolerance was again induced with increases noted in *Hsp90* and *Hsp70*, indicative of hyperthermia-induced apoptosis (Reihaneh Haghniaz et al. 2015b).

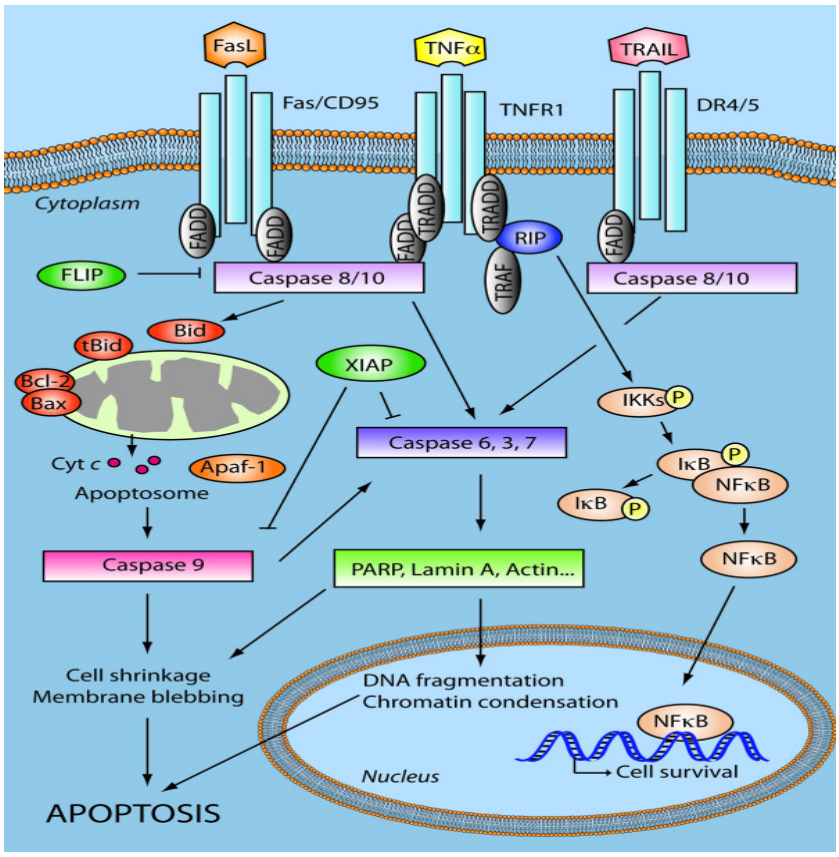

Figure 4-26: Extrinsic Apoptosis Signaling Network. The extrinsic apoptosis pathway is activated upon ligand binding to death receptors (TNFR1, Fas/CD95, DR4/5) leading to the assembly of FADD/TRADD and caspase 8 to form the death-inducing signaling complex (DISC), leading to caspase 8 activation and downstream effects. TNFR1 may promote survival signaling through activation of NFκB (from(Krakstad and Chekenya 2010)).

3D Spheroid MCF-7 Cells: Gold Nanoprisms and Nanorods

Whilst apoptosis was activated mainly *via* the intrinsic pathway in nanoprism monolayer cultures, the 3D MCF-7 spheroids labelled with gold nanoprisms employed both intrinsic and extrinsic pathways. Increases of >5 fold were noted in *BIM, BAK, caspase 7* and >10 fold in *BID, BAX, caspase -3 -8* and *-9, Bcl-2* and *cytochrome c* for the intrinsic pathway. However >5 fold changes were recorded for *PARP, FAS-L*, and *MCL-1* in the extrinsic pathway, suggesting accumulation of ROS concentration and oxidative stress within MCF-7 spheroids (Luanpitpong et al. 2013; Luo and Kraus 2012). The denaturing effect of hyperthermia was again apparent with the increased expression of *Hsp90* and *Hsp70*.

The MCF-7 spheroids labelled with gold nanorods indicated that apoptosis was activated mainly by the intrinsic and lysosome pathways, similar to the corresonding monolayer cultures. Fold changes (>5) in *APAF-1*, *caspase 9*, *cathepsin K, DIABLO/SMAC, caspase 7*, while a > 10 fold change was detected in *cytochrome c*. These results suggest that apoptosis was mainly orchestrated by the intrinsic pathway, owing to the increased expression of *caspase 9* and *APAF-1* expression, although preceding markers (e.g. BAX/BAK) expression was low, which may indicate that hyperthermic treatment with nanorods disrupted the outer membrane potential, independently from these complexes, as has been hypothesised elsewhere (White et al. 2012). The lysosomal pathway was also implicated, up to a lesser extent, with increased expression of *cathepsin -B, -L,* and *-K*, which is released upon lysosomal disruption and has been shown to degrade Bcl-xL proteins and promote apoptosis (de Castro et al. 2016).

In summary, when considering the apoptosis response of 3D spheroid cultures at the gene expression level, both bone and breast cancer spheroid cultures commit to apoptosis following GNP-induced hyperthermia using a combination of pathways. MG63 spheroids differed from their corresponding monlayer culture results by utilising a wider range of pathways and demonstrating higher levels of gene changes, whilst response between prisms and rods in 3D were similar. Meanwhile MCF-7 spheroids also differed from their corresponding monolayer results with the nanoprism results, as this time the extrinsic pathway was also involved, whilst nanorods induced a similar response in monolayer and spheroid.

Apoptotic Gene Expression: Apoptosis Pathways and Thermotolerance

The quantification of various apoptotic gene markers was conducted *via* fluidigm analysis. Overall, these results suggested that laser treatment alone can induce mild cellular stress within samples. Cellular stress was believed to be to due to an increase in ROS accumulation within cells, as indicated by the increase in markers up-regulated in response to ROS such as *PARP-1* (Rodríguez-Vargas et al. 2012), *PMAIP* (Tonino et al. 2011) and *caspase 3* (D. Y. Shin et al. 2009). ROS generation in cells has been directly linked to laser exposure (Mohanty et al. 2006). Mohanty and Gupta studied the effects of a continuous wave 5W laser laser on HeLa cells and observed mitochondrial membrane potential changes, with

the subsequent leakage of electrons from the respiratory chain, resulting in the increased generation of ROS in the cytosol (Mohanty et al. 2006). However, whilst these intracellular events also occurred in our control samples (with no GNPs), they did not translate to cell death, as shown in previous viability staining (section 3.4.7).

As expected, cells labelled with GNPs and laser irradiated displayed a far larger fold change in apoptotic markers, resulting in cell death (viability staining, section 3.4.7) (Lucian Mocan et al. 2015b). The activation of the intrinsic pathway was expected as several previous reports had demonstrated activation of intrinsic pathway markers in response to hyperthermic temperature profiles (C.-H. Hou et al. 2014b; Klostergaard et al. 2006; Tu et al. 2006). In this study, *caspase 3, 9, APAF-1, and BAX/BAK* expression was particularly highlighted. However, the extrinsic pathway was also activated within this study, in particular with the spheroid cultures (Nagarsekar et al. 2008), as demonstrated by the increased expression of *caspase 8, BID, FAS*, and *FAS-L*; indeed, MG63 spheroid samples incubated with gold nanorods resulted in a >25 fold change in *caspase 8*.

The expression of cathepsins was also an interesting observation, which was particularly notable in MG63 monolayers and spheroid cultures when labelled with nanoprisms, and MCF-7 monolayer and spheroid cultures when labelled with nanorods. As previously explained, (figure 4-24) cathepsins are proteases that are located primarily within lysosomes, known as ‘suicide bags’. The loss of the lysosomal integrity, and the subsequent release of cathepsin into the cytosol, has been implicated in various forms of cell death including necrosis (de Castro et al. 2016). Due to their broad spectrum of protein degradation, cathepsin up-regulation can lead to necrotic cell death due to loss of cellular functions, such as energy production and osmotic balance, as well as loss of cell structural integrity. However, cathepsin release has also been associated with caspase-dependent apoptosis *via* BID activation and mitochondrial membrane permeability (de Castro et al. 2016). Cathepsin (B) expression is also a feature during hypoxia, which may likely occur in tumour spheroids, and may therefore explain its dramatic up-regulation in spheroid samples rather than monolayer samples that appear to have elevated basal cathepsin B expression (Wickramasinghe et al. 2005). Nonetheless, the increased expression of cathepsin measured in nanoprism

labelled MG63 monolayers may suggest cell death *via* necrosis or be indicative of the process of autophagy.

Autophagy has been reported in response to hyperthermia, though it has been argued that it's role may be more protective than destructive, by degrading misfolded proteins and preserving protein homeostasis (Dokladny et al. 2015). This has been further validated by previous studies in which Hsp70 inhibitors prevented the activation of autophagy (Budina-Kolomets et al. 2014). The exponential expression of caspase 8 in nanoprism labelled MCF-7 monolayer/spheroid cultures, as well as nanorod labelled MCF-7 spheroids, and nanoprism/nanorod labelled MG63 monolayers was difficult to explain, as the majority of these samples did not show an increased expression in preceding extrinsic factors (Fas, Fas-L, TNFSF10), although isolated studies have shown that the activation of caspase 8 may occur during hypoxia and ROS generation (Byeong Mo Kim and Chung 2007). Caspase 3 has also shown to increase the expression of caspase 8, which then activates BID and the activation of BAX/BAK to further permeate the mitochondrial membrane, thus feeding a positive loop of caspase-depenent apoptosis (Karine Sá Ferreira et al. 2012b). Gonzalvez et al, (2008) also challenged the activation of caspase 8, describing caspase 8 integration into Cardiolipin (CL)-rich domains of the outer mitochondrial membrane results in full activation of caspase 8 which can then directly access and cleave its substrate Bid (Schug and Gottlieb 2009). The quantification of caspase 8 from our samples suggests caspase 8 up-regulation occurs predominantly *via* the caspase 3 positive feedback loop and activation by Cardiolipin at the outer mitochondrial membrane, as well as the conventional extrinsic pathway involving death receptor aggregation and DISC formation (figure 4-23).

With regards to thermotolerance, in all hyperthermic cell cultures both Hsp70 and Hsp90 were upregulated owing to their chaperon functioning upon disruption to protein homeostasis as previously described in section 1.3. While Hsp27 is a potent chaperon, Hsp90 and Hsp70 are primarily investigated during heat shock response (Zunino et al. 2016). Miyagawa and co-workers validated this by demonstrating that the inhibition of Hsp90 and Hsp70 increased the sensitivity of magnetic nanoparticle-mediated hyperthermia in melanoma cells (Tomoyuki Miyagawa et al. 2014b). In a similar set up to our own, Ali et al demonstrated that Hsp70 inhibition produced an increased level of cells undergoing apoptosis and a reduction in MCF-7 cell viability after photothermal treatments using gold nanorods

(Ali et al. 2016). Hsp70 functions in the transportation of precursor proteins into cellular compartments and is vital for protein homeostasis, including protein folding and degradation of unstable proteins (Sanjay Kumar et al. 2016). However, during cellular stress human cells produce high levels of Hsp70, constitutively expressed as Hsp70, mitochondrial Hsp75, and GRP78, which are found in the endoplasmic reticulum and act as molecular chaperones, assisting proper folding/refolding (Sanjay Kumar et al. 2016). While its chaperon activity has been established, Hsp70 has also been shown to participate as an anti-apoptotic protein, capable of inhibiting both strands of the extrinsic and intrinsic pathway. In the intrinsic pathway Hsp70 has been shown to inhibit BAX translocation, inhibiting the formation of the apoptosome (caspase 9, APAF-1, cytochrome c, complex) (Shawn B. Bratton and Salvesen 2010). In the extrinsic pathway, Hsp70 has been shown to inhibit BID activation (to tBID) (Lanneau et al. 2008a). These events are summarised in figure 4-26. Hsp90 has also demonstrated similar inhibitory mechanisms, inhibiting BID and indirectly inhibiting caspase 8, as shown in figure 4-26 (Lanneau et al. 2008a).

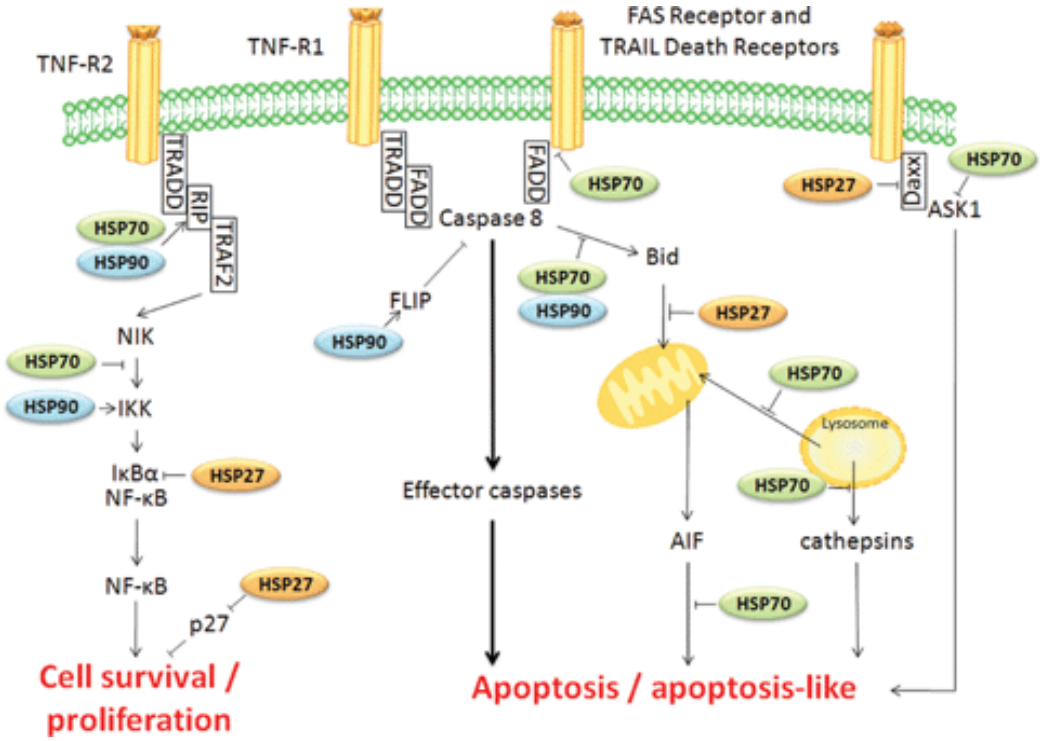

Figure 4-27. Heat shock proteins: essential proteins for apoptosis regulation (Lanneau et al. 2008).

4.5.3 Photothermal Changes in Apoptotic Protein Expression

Following on from the gene expression studies, the expression of 43 protein apoptotic markers were evaluated in bone cell (MG63) and breast cell (MCF-7) monolayer cultures to (i) determine the key molecules involved in apoptosis and (ii) verify the apoptosis pathways highlighted in the gene expression studies. All monolayer cultures were labelled with either gold nanoprisms or nanorods (0.1 $mg.ml^{-1}$) and intracellular protein levels were assessed by cell lysis and antibody arrays.

4.5.3.1 Laser Treatment Alone Induced Cellular Stress Response

The results (figures 4-16 and figure 4-17), of laser treatment on control cell culture (with no GNPs) indicated an increase in several apoptotic markers in the presence of laser treatment alone compared to control groups (no laser treatment), however these peak mean intensity fold changes were small, with a large standard deviation leading to lack of statistical validity, therefore suggesting that the effect of laser treatment may not be as prominent as first assumed.

With regards to MG63 cells, the markers that were increased included proteins involved in the extrinsic pathway (DR6), those involved in both the intrinsic and extrinsic pathway (BID, caspase 3), with apoptosis promoters (p53) and a range of apoptosis inhibitors (p27, IGF-I and in particular IGF-II). Both p27 and p53 have been widely explored for their roles in apoptosis and cell cycle arrest (L. Fan et al. 2014). The tumour suppressor p53 protein has important functions within cells, regulating cell senescence, metabolism, DNA repair and, importantly, cell cycle and apoptosis (J.-P. Kruse and Gu 2009). It is believed that an increased expression of p53 can encourage cell cycle arrest or apoptotic initiation upon cellular stress, however levels of p53 expression can activate p27 and p21 expression (L. Fan et al. 2014). This may explain the proportional increase in p27 expression observed, although only a small increase in expression was detected in p21. This may somewhat be explained as p21 can be activated by, and act as, a substrate for caspase 3 (Chiappara et al.), therefore an increase caspase-3 concentration may reduce p21 levels in cells, this collaboration leads to pro-apoptotic signalling, encouraging cells to undergo apoptosis.

The increase in BID expression has been previously linked to hyperthermia *via* caspase-2 activation (Bonzon et al. 2006). However the increase in BID, caspase-8 and caspase-3 is closely associated with the intrinsic pathway cumulating to apoptosis - although it is noted that this pathway is associated with increased cytochrome c expression, as shown in figure 4-23, which our results do not indicate (K. S. Ferreira et al. 2012a). As previously explained, cytochrome c is released from the mitochondria upon the destabilisation of the mitochondrial membrane potential (figure 4-25). Once released into the cytosol, cytochrome c can trigger the intrinsic apoptotic pathway *via* caspase cascade or amplify extrinsic apoptotic signalling (Kulikov et al. 2012). Interesting, caspase 3 and 8 are also integral players in the extrinsic pathway (Westphal et al. 2011). Caspase 8 activation is believed to activate both caspase 3 and BID activation leading to either apoptosis or stimulating the intrinsic pathway. Caspase 8 activation however is predominantly orchestrated by ligands such as FasL, tumour-necrosis factor α (TNFα), or TNF-related apoptosis inducing ligand (TRAIL) which did not appear to show significant changes (Kulikov et al. 2012).

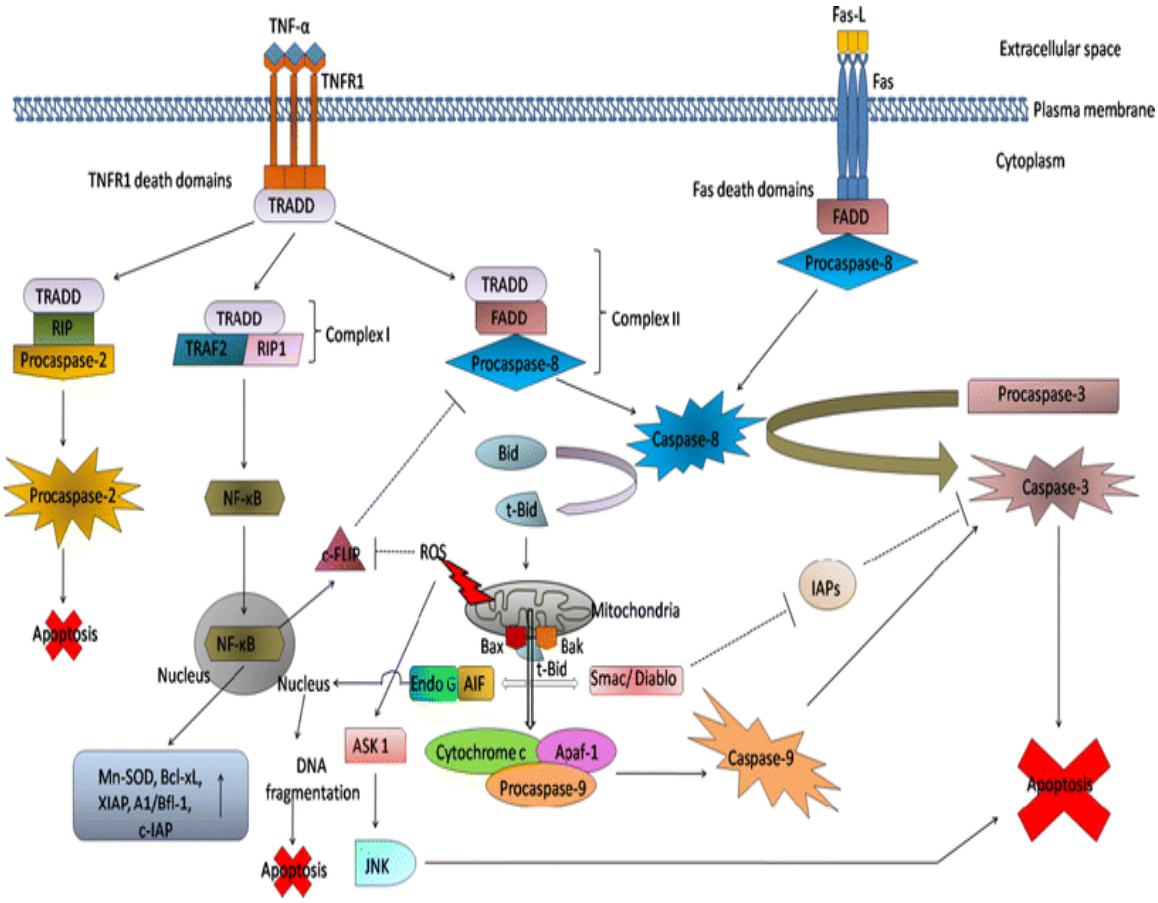

Figure 4-28: Oxidative stress: the mitochondria-dependent and mitochondria-independent pathways of apoptosis, (Sinha et al. 2013). Multiple pathways to apoptosis. The *mitochondrial* (or intrinsic) pathway is induced as a response to cellular stress and results in the activation of the pro-apoptotic BH3-only proteins. BH3-only proteins may *directly* bind and activate Bax and Bak (I, dashed lines), and may also bind to the prosurvival Bcl-2-like proteins to *indirectly* activate Bax and Bak (II). Once activated, Bax and Bak oligomerise to form pores in the mitochondrial outer membrane that release cytochrome *c*. Cytosolic cytochrome *c* leads to caspase activation and subsequent cell death. The *death receptor* (extrinsic) pathway is initiated by death ligands such as FasL, tumour-necrosis factor α (TNFα), or TNF-related apoptosis inducing ligand (TRAIL) binding to cell surface receptors, resulting in the activation of caspase-8. Active caspase-8 can either activate downstream caspases directly (in type I cells) or engage the intrinsic pathway via a cleaved form of the BH3-only protein Bid (tBid) (in type II cells) (Kulikov et al. 2012; Westphal et al. 2011).

One of the most notable fold changes in MG63 laser irradiated control sample was observed in the DR6 protein. DR6, conversely known as TNFRSF21, is a fairly new member of the death receptor family and only in the last few years has been confirmed for over expression to induce apoptosis (Sessler et al. 2013; Zeng et al. 2012). Zeng and co-workers demonstrated the unusual characteristics of DR6 with their results suggesting that DR6 functions independently from the conventional type I and II signal transduction pathways *via* death receptor-mediated death signals, with the inhibition of caspase-8 and knockdown of BID having no effect on DR6-induced apoptosis (Zeng et al. 2012). The authors suggest that DR6-induced apoptosis occurs through a novel, BAX dependent pathway (Zeng et al. 2012). This would suggest that the large increase in DR6 expression could promote cells to commit to apoptosis *via* BAX activation, however the modest increase in BAX expression suggests minimal apoptotic activation within the sample and would support the notion of only a small quantity of cells undergoing apoptosis during laser exposure.

MCF-7 control cells (figure 4-17) displayed fairly innocuous results; only a few markers were increased, FAS (extrinsic pathway), caspase 8, which is involved in both the intrinsic/extrinsic pathway, IGFBP5 which propmots apoptosis (through caspase action) and heat shock proteins (Hsp27 and Hsp60). IGFBP5 (Insulin-like growth factor-binding protein 5) is one of six members of the insulin-like growth factor-binding protein family, which are integral modules of the IGF (insulin-like growth factor) axis (Beattie et al. 2006). Of the six members, IGFBP5 has been heavily researched for its role in cancer progression and cancer development, whilst also being touted as a therapeutic target for human melanoma (Junyun Wang et al. 2015). IGFBP5 overexpression has been recently shown to promote apoptosis and cell cycle arrest (Su et al. 2011), and can induce a caspase-dependent apoptotic pathway in human breast cancer cells *via* activation of caspase 8 (Butt et al. 2005). This was also observed in our results however the intrinsic activation (i.e. of cytochrome c and BID) was not, observed in comparison to the previous study using human breast cancer cells (Butt et al. 2005).

FAS, is a cell-surface receptor, commonly known as Cd95, and is the most well-characterised member of the tumour necrosis factor (TNF) superfamily of receptors (Peter and Krammer 2003). The association of FAS and FASL has demonstrated pro-apoptotic signaling, as highlighted in figure 4-28 (Punsawad et

al. 2015). Thermotolerance was induced following laser treatment, with increases noted in Hsp27 and Hsp60. While the ubiquitous nature of Hsps as 'molecular chaperones' has been highlighted and illustrated in figure 4-27 (Hsp -27, -70 and -90), the mechanism of action for Hsp60 has been poorly characterised. Hsp60 has been recognised for its protective function in cells (Ortega-Ortega et al. 2011), but does provide difficulty in characterising as studies have suggested an additional role in actually promoting apoptosis and subsequent phagocytosis of dying cells (Goh et al. 2011; S. Gupta and Knowlton 2005). Hsp60 is believed to have a protective quality, inhibiting apoptosis in stressed cells. This is further supported by Zhang and co-workers, who demonstrated bacterial GroEL-like Hsp60 protected epithelial cells from UV radiated stress-induced death through activation of ERK and inhibition of caspase 3 (L. Zhang et al. 2004).

Interestingly, unlike MG63 cells, there was no increase in DR6 as an apoptosis-inducing receptor. The may reflect that DR6 is cell-type dependent, as exogenous expression of DR6 was found previously to induce apoptosis in HeLa cells (cervical carcinoma cell line) but not in MCF-7 cells (Kasof et al. 2001).

In summary, while we know that cell viability was not compromised, the results here show that, as with the RNA markers, laser treatment of control cell monolayer culture (ie. no GNPs) did indicate mild cellular stress. As with the RNA gene expression results, the bone cancer cell line (MG63) appeared to respond to laser treatment more that the breast cancer cell line (MCF-7), with a higher number of protein markers increased in response to treatment.

4.5.3.2 Gold Nanoprisms Activate Apoptosis Following Photothermal Treatment

When considering the effect of labelling cells with gold nanoprisms, the first results of note reflects the RNA apoptotic targets; with an immediate cell response of cells when labelled with gold nanoprisms (without laser treatments). An increase in fold change of ~1 to ~1.5 for the majority of apoptotic protein markers was recorded when compared to non-labelled control cells. This increased expression of both pro-apoptotic and anti-apoptotic markers indicated that the internalisation of gold nanoprisms caused cell stress, an observation corresponding to previous MTT results. Of these proteins, cIAP2 (cellular inhibitor of apoptosis proteins 2)

increased around 2 fold in the presence of gold nanoprisms. CIAP2 is one of 8 members of a family of factors called inhibitor of apoptosis (IAP) proteins. This family has been found to play a major role in a multitude of cellular processes, while cIAP2 remains one of the most characterised members (Kocab and Duckett 2016). As their name suggests, IAPs are capable of inhibiting apoptosis in response to both extrinsic (death receptors-mediated) and intrinsic (cell stress-mediated) signalling pathways (Guicciardi et al. 2014). CIAP2 in particular has shown cytoprotective features by inhibiting TNF-α-induced apoptosis (S. Guo et al. 2014). CIAP2 contain unique features such as a conserved RING domain at their C-terminal end, allowing these proteins to mimic E3 ubiquitin ligase, allowing for the ubiquitination and proteasomal degradation of caspases (casapse 3 and 7), TRAF2, and several other partner molecules (K. Wang and Lin 2013). CIAP has been shown to also bind to caspase 9, and XIAP that can additionally stimulate downstream signalling pathways such as the Akt survival cascade and/or NF-κB activation, which can counteract apoptosis (K. Wang and Lin 2013).

When analysing the protein marker increases in nanoprism labelled cells following laser treatment, apoptosis was very clearly activated, with large increases in almost every single marker studied (figure 4-18). Large increases in particular were noted for protein markers linked to the intrinsic pathway (cytochrome c, BAD, BAX, BIM, SMAC), the extrinsic pathway (CIAP2, FAS, caspase 8) and those linked to both (BID, caspase 3), supporting wide scale apoptosis activation. The apoptosis promoter p53 was increased, but inhibitors of apoptosis were also activated, in particular IGFBP-1 and p27, indicating cell protection mechanisms were activated, along with Hsp70. Interestingly, DR6, which was highly expressed in control cells (figure 4-16) following laser treatment, was not particularly affected with nanoprism labelled cells following laser treatment.

A large increase was noted in Hsp70. Hsp70 has been extensively researched as an anti-apoptotic protein, preserving cells against environmental insults, including protecting cells from both chemotherapy, radiotherapy and ROS production whilst also being expressed during cell proliferation and differentiation (Multhoff et al. 2015). Hsp70 has a multitude of functions within the cell, including protein homeostasis *via* protein folding, refolding, and assembly of nascent polypeptides. During cellular stress, Hsp70 is involved in preventing protein aggregation, and assisting the transport of other proteins across membranes (Multhoff et al. 2015).

It has also been noted as a potent inhibitor of apoptosis. Our results also suggests FAS, FAS-L and caspase expression was uninhibited by the elevated Hsp70 expression. This was also a similar trend in BAX expression, whose activation is usually inhibited by Hsp70 expression therefore preventing mitochondrial membrane permeabilization and the release of pro-apoptotic factors such as the aforementioned cytochrome c as well as caspase 3 (Radons 2016; Xiaokui Yang et al. 2012b). However our results suggest these pro-apoptotic markers are unaffected even in the presence of the high Hsp70 expression.

As with MG63 cells, when MCF-7 cells were labelled with gold nanoprisms (non-laser treated), an increase in apoptotic markers was noted (as compared to non-labelled cells), indicating cellular stress. However, as previously stated, this did not influence cell viability. A substantial increase in all apoptotic markers was noted, across a range of apoptosis pathways. The results were very similar to the MG63 protein markers although the difference between laser and non-laser treated were more pronounced. Again, DR6 was not affected, reinforcing the hypothesis of its cell specific role.

The larger noted fold change expressions (compared to non-laser treated cells) were for TRAIL-R4 and BAX proteins. TRAIL-R4 (TNF-related apoptosis-inducing ligand- receptor 4) is a member of the TNF-receptor superfamily, alluded to in figure 4-28. The debate over its role in apoptosis still remains elusive, as TRAIL-R4 does not contain a functional death domain and thus, upon activation *via* TRAIL, does not appear to induce the apoptotic pathway commonly associated with other TRAIL-R members (TRAIL R 1 and 2) (Lalaoui et al. 2011). Instead TRAIL-R4 has been considered an anti-apoptotic complex, with a number of studies showing the expression of TRAIL-R3 or TRAIL-R4 providing resistance to TRAIL-induced apoptosis in tumours (Lalaoui et al. 2011).

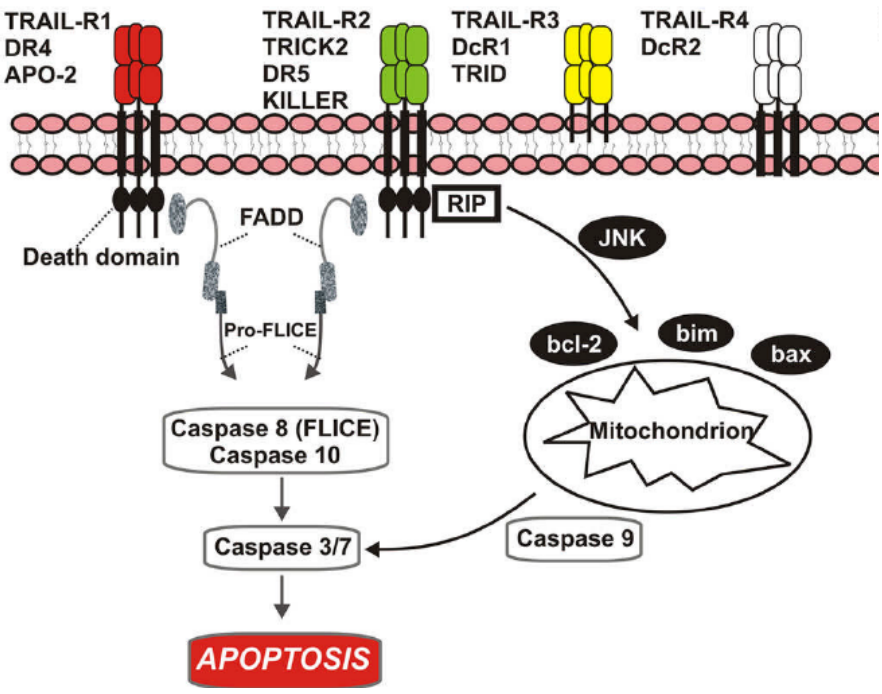

Figure 4-29: Human TRAIL receptors and intracellular signal cascade. TRAIL binds to two death-mediating receptors, TRAIL-R1 and TRAIL-R2, and to two non-death receptors ("decoy receptors"), TRAIL-R3 and TRAIL-R4. TRAIL-mediated apoptosis occurs upon binding of the trimerized ligand to the receptor, which instigates the recruitment of the signaling protein, FADD (Fas-associated death domain) and pro-caspase 8 (pro-FLICE). Activation of pro-caspase 8 leads to the generation of caspase 8 and subsequent activation of caspase 3, which mediates caspase-activated DNase and apoptotic demise of the cell. Moreover, TRAIL signaling may modulate mitochondrial apoptosis routes via induction of JNK and regulation of the bcl-2 family members bcl-2, BIM and BAX (taken from (Aktas et al. 2007)).

TRAIL-R4 expression had been shown to inhibit TRAIL-mediated apoptosis in various tumours, while also binding to the pro-apoptotic complex, TRAIL-R2 (Koschny et al. 2015). Typical TRAIL activation involves the clustering of receptor complexes and the activation of the death-inducing signalling complex (DISC) and the eventual activation of caspase 8 and 3 (Bertsch et al. 2014). The inhibition of this pathway *via* TRAIL-R4 interaction may explain the increased expression of TRAIL-R4, and indeed TRAIL-3, which has also shown pro-apoptotic potential, leading to a modest increase of TRAIL-R1, TRAIL-R2, caspase 8 and caspase 3 expression. (Degli-Esposti et al. 1997) when comparing non-laser treated and laser treated samples.

In summary, gold nanoprisms activated apoptosis following laser treatment, with large increases observed across the intrinsic and extrinsic pathways, as well as instigating cell protective mechanisms and thermotolerance. Whilst the pattern of protein marker expressions were similar for both cell types, the difference between non-laser treated and laser treated nanoprism labelled cells were greater in bone cancer cells (MG63 cells).

4.5.3.3 Gold Nanorods Activate Apoptosis Following Photothermal Treatment

As with the nanoprisms, the internalisation of gold nanorods also initiated cell stress, although again there was no compromise in cell viability. In the untreated nanorod labelled MG63 cells, Hsp27 displayed a near 4-fold increase in expression. The overexpression of Hsp27 has been shown to increase the resistance of cell to various apoptotic stimuli (Takayama et al. 2003). Although, conversely, the overexpression of Hsp27 can actually lead to the increased expression of caspase -3, -8 and -9, as well BIM activation, which were all highly expressed in our results (Y. Guo et al. 2015). Guo and co-workers also noted the pro-apoptotic role of Hsp27 in both the intrinsic and possibly extrinsic pathway *via* TRAIL in pancreatic cancer cells (Y. Guo et al. 2015).

Nanorod labelled MG63 cells that were subsequently laser treated demonstrated increased apoptotic markers, resulting in the cell death observed in chapter 3. The makers were across a range of apoptosis pathways including the intrinsic (cytochrome c, BAD, SMAC), extrinsic (FAS, FASL, TRAILR2) and lysosome (CD40, TNFB) (figure 4.23). In addition, promoters of apoptosis were increased (p53) as well as apoptosis inhibitors (p21, p27, surviving, livin) and indicators of thermotolerance (Hsp -27, -60 and -70).

Livin is a novel member of the inhibitor of apoptosis (IAP) protein family and highly expressed in many types of human malignancies, preserving the cell against apoptotic stress through the inhibition of the caspase signaling cascade, as well as inhibiting the cell death receptor tumour necrosis factor receptor-mediated apoptosis signaling pathway (Zhuang et al. 2015). Livin is believed to function by inhibiting the caspase-3, -7, and -9, as well as promoting SMAC degradation (B. Yan 2011). Our results, however, show SMAC expression was increased compared to controls, suggesting SMAC was not degraded by livin.

SMAC (second mitochondria-derived activator of caspases) is a pro-apoptotic factor, found within mitochondria. Upon mitochondria damage, SMAC, along with cytochrome c, is released from the mitochondria, into the cytosol (figure 4-27). SMAC interacts with apoptosis inhibitor proteins, such as XIAP, cIAP1 and cIAP2, allowing for the release of caspase 3 and 9, causing apoptosis (G. Martinez-Ruiz et al. 2008a).

Survivin is a member of the family of inhibitor of apoptosis proteins and predominantly functions in the regulation of mitosis progression and apoptosis inhibition (Y. Lin et al. 2016). Survivin activity is inhibited by increased expression of SMAC and interesting, p53, another key apoptotic marker that showed increased expression. Although survivin is known to inhibit apoptosis by inhibiting active caspase-9, it showed no inhibition towards caspase-3 and caspase-7 while its functionality seems dependent on association with X-linked IAP (A. C. Mita et al. 2008a).

HTRA (high temperature requirement A) showed a five-fold increase in expression compared to untreated samples. HTRA is a protective protease complex involved in protein quality control pathways and is crucially up-regulated under protein folding stresses, to prevent accumulation and aggregation of misfolded proteins that induce cellular stress and apoptosis (Tennstaedt et al. 2012). This 5-fold increase in HTRA strongly suggests a potent accumulation of unfolded and aggregated, denatured proteins, a hallmark of hyperthermic treatment (Yanting Cui et al. 2014b).

As with the MG63 cells, non-laser treated MCF-7 cells showed an increase in most apoptotic markers following gold nanorod internalisation, inducing mild cell stress. However, following laser treatment, these marker levels were again highly increased, demonstrating cell apoptosis. The protein markers that were highly increased following laser treatment were again across a range of apoptotic pathways, including the intrinsic pathway (cytochrome c, Bcl-2, BAD), the extrinsic pathway (TRAILR1) and proteins linked to both pathways (caspases 3 and 8, BID) as well as lysosome stress (CD40) and cathepsin activation (figure 4.23). Several pro-apoptotic proteins were also highlighted, such as IGFBP-3 (*via* promotion of p53) and IGFBP-4 (*via* involvement in the intrinsic pathway). In addition, numerous

anti-apoptotic proteins were also induced, including p21, p27 and IGFBP-5 (through caspase interactions), as well as thermotolerance (Hsp -27, -60 and -70).

The results from this experiment therefore seem to suggest laser treated MCF-7 cells containing gold nanorods are led to apoptosis *via* the intrinsic, extrinsic and lysosomal pathways. In summary, gold nanorods, as with nanoprisms, strongly activate apoptosis in both cell lines. In particular the JNK pathway was activated with both cell types (only observed in bone – MG63 – cells with the nanoprisms), supporting caspase-independent cell death.

4.5.4 Hyperthermia-Induced Apoptosis *via* Increased ROS Production

The RNA and protein apoptosis marker studies suggest that one of the main triggers of apoptosis may be due to the increase generation and accumulation of intracellular ROS concentration (Bettaieb and Averill-Bates 2008; F. Chen et al. 2008a). Much focus within the hyperthermia literature to date has been hyperthermia leading to protein denaturation, indicated by increased expression Hsp family members (Glory et al. 2014; Kalamida et al. 2015; I. S. Singh and Hasday 2013; Y. Zhang and Calderwood 2011). While our results do support this (both RNA and protein analysis), the strong association of ROS production indicated in the fluorescent staining (figure 4-22) during onset of apoptosis in cells may reflect ROS-induced cellular stress (Kanwal Ahmed et al. 2015b). Hyperthermia has been shown in a number of studies to increase ROS production in various cell lines, including MG63 and MCF-7 cells (Bohara et al. 2015; Z.-G. Cui et al. 2014f; C.-H. Hou et al. 2014b; Q.-L. Zhao et al. 2006). For example, hyperthermia-induced increases in ROS generation were noted by decreasing the expression of superoxide dismutase 1 (SOD-1), a potent antioxidant enzyme at both the mRNA and protein level (El-Orabi et al. 2011). This can lead to the overexpression and accumulation of ROS such as superoxide anion (El-Orabi et al. 2011), which can dismute to form hydrogen peroxide or react with other radicals such as NO to produce potent oxidant species (Q.-L. Zhao et al. 2006).

The increased expression of ROS leads to nonspecific modifications of lipids, proteins, and nucleic acids, resulting in global, cellular dysfunction (Kanwal Ahmed et al. 2015b). ROS accumulation can also lead to mitochondrial damage and the activation of the intrinsic pathway, while also linked to the extrinsic pathway by

directly activating death receptors (TNFα, FASL, and TRAIL) and thus apoptotic induction through ROS-induced receptor clustering (Circu and Aw 2010). ROS accumulation can also stimulate apoptosis through independent signalling which can induce both the intrinsic and extrinsic pathways (Circu and Aw 2010).

Hyperthermia has also been shown to induce endoplasmic reticulum (ER)-triggered apoptosis in numerous cancers; the ER is responsible for protein folding, modification and synthesis as well as lipid synthesis (C.-H. Hou et al. 2014b; Shellman et al. 2008). Cellular stress can be caused *via* heat and oxidative stress, that can disrupt ER homeostasis and thus lead to the accumulation of unfolded or misfolded proteins (C.-H. Hou et al. 2014b). Our results confirm hyperthermia increased ROS concentration, while laser treatment on control cells did yield some ROS accumulation, this is expected to occur as laser irradiation has been demonstrated to disrupt cellular organelles, including the mitochondria, leading to the disruption of ROS homeostasis and thus a small increase of ROS was observed in control samples exposed to laser treatment (Minai et al. 2013).

4.6 General Conclusion

4.6.1 GNP internalisation causes mild cell stress

The results obtained from the apoptotic marker analysis confirmed that the labelling of both MG63 and MCF-7 cells with either gold nanorods or gold nanoprisms elicited mild cellular stress as indicated by the increased expression of apoptotic markers. Although this global increase in apoptotic markers revealed cellular stress, it did not translate to a decrease in cell viability as confirmed in chapter 3 (section 3.4.3).

4.6.2 Laser treatment causes mild cell stress, but no cell death.

Laser treatment alone appeared to cause minor cellular stress in both cell types but again this did lead to a compromise in cell viability (section 3.4.7). The increased expression of Hsp members (Hsp -26, -60, -70) also demonstrated the protective characteristics of Hsps in response to environmental insults such as laser exposure. While previous studies have shown intense laser exposure can induce mitochondrial damage and ROS generation, our moderate laser exposure showed minor ROS production upon laser irradiation (figure 4-22) (M. J. Jou et al. 2002; M.-J. Jou et al. 2004).

4.6.3 Nanoprisms & Nanorods caused cell death by a range of apoptotic pathways

Our results suggest that GNP-assisted photothermal treatment of MG63 and MCF-7 cells, both in monolayer and multicellular tumour spheroids leads to the activation of both the intrinsic and extrinsic pathway as indicated by the increased expression of pro-apoptotic Bcl-2 family members and caspases. As previously alluded to, many groups attempt to confirm apoptosis after photothermal treatment by quantifying a handful of effector caspases such as caspase 3, 6 and 7 (Abadeer and Murphy 2016; Espinosa et al. 2016; L. Mocan et al. 2015a). Although the increase in expression of these markers confirms cell death *via* apoptosis, the actual pathways are often overlooked. In this project, we determined cell death predominantly occurs via the intrinsic and extrinsic pathway,

although we have also observed the more novel and less characterised, lysosomal apoptotic pathway, which was continuously observed in photothermal treated samples and is associated with an increase in ROS generation. This was an important discovery as lysosomal degradation, cathepsin release and ROS generation have also been linked to autophagy, necrotopsis and necrosis (Boya and Kroemer 2008a; Brojatsch et al. 2015; Eskelinen and Saftig 2009; Vandenabeele et al. 2010). While thermotolerance was induced by samples, as indicated by the increased expression of Hsp members, the process appeared unsuccessful at preventing apoptosis as observed in chapter in 3 (section 3.4.7).

4.6.4 Correlation between RNA & protein targets

In this project, we attempted to characterise cell death using a range of apoptotic markers and attempted to quantify their expression at the genomic and proteomic level to better understand the molecular events leading to cell death upon exposure to photothermal treatment. The targets that were quantified at both the genomic and proteomic level are shown in figure 4-2. For RNA expression, the results presented here were transformed (log_2) due to the large disparity between targets and to provide a more symmetrical data and thus any value below 0, although indicating positive fold change is insignificant. The notoriously genome-wide correlation between expression levels of mRNA and protein having ~40% explanatory power across has been shown in numerous studies (Abreu et al. 2009; Koussounadis et al. 2015; Vogel and Marcotte 2012a). Despite this, our results indicate strong correlation between both gene and protein markers in monolayer samples with only BID and Bcl-2 markers showing particularly high disparities between data sets. Both data sets however, are in an agreement that multiple apoptotic pathways appear to be activated simultaneously upon photothermal treatment while a photothermal response (Hsp -60 and -70) was activated, regardless of cellular signalling to undergo apoptosis.

4.6.5 Comparison of monolayer and Spheroid response to photothermal treatment

The results from this project suggests 3D tumour spheroids were more susceptible to photothermal therapy compared to monolayer samples, although a thorough statistical analysis would be required to validate. The susceptibility of spheroids

may be due to the thermodynamic nature of heat. In monolayer, laser exposure occurred in the middle of the sample with heat dissipating across the sample however only those cells in the epicentre of the laser displayed cell death while peripheral cells remained viable, possibly due to hyperthermic temperature profiles not reached as heat dissipated away from the epicentre of the sample. With spheroid samples however, due to laser penetration, the spheroid could be heated not only on the peripheral cells on the outer rim of the spheroid, but those near the core of spheroid (figure 3-18), with heat radiating from near the core of the spheroid, superficially more cells were thus affected by higher temperature profiles, promoting cellular stress and apoptosis.

4.6.6 Influence of cell type on photothermal treatment

The effectiveness of photothermal therapy *via* GNPs was evident in both cell types, with both MG63 and MCF-7 cells displaying apoptotic tendencies however it appears MG63 cells are slightly more susceptible to photothermal treatment although again, a detailed statistical analysis would be required to confirm this observation however it is reasonable that different cell lines, owing to their physiological differences, detoxification pathways, thermotolerance and metabolic output may show slight variations during hyperthermic exposure.

4.6.7 Gold nanoprisms and gold nanorods can successfully instigate apoptosis *via* laser irradiation

Both GNPs successfully triggered apoptotic events upon exposure to laser irradiation in different cell types as well as within monolayer and spheroids. From our apoptotic protein analysis data (section 4.3.2) it appears that gold nanoprisms were particularly effective in both cell types and this may be due to the remarkable internalisation of gold nanoprisms into both cell types in comparison to gold nanorods that demonstrated poor internalisation even at a higher concentration (figure 3-13). This may explain why gold nanorods, although displaying a higher temperature profile than gold nanoprisms (figure 3-3) does not yield a significantly increased apoptotic response within samples.

Chapter 5

5 Magnetic Nanoparticle Induced Hyperthermia

5.1 Introduction

5.1.1 Magnetic Nanoparticles and Hyperthermia

Hyperthermia is not intrinsically cancer-specific, however hyperthermic techniques can capitalise on tumour physiology in order to deliver and concentrate toxic heat levels to cancer cells within a tumour (Kaddi et al. 2013). This is due to the heterogeneous tissue structure and unregulated growth which tumours exhibit, making them more prone to heat stress (Vaupel and Kelleher 2010). Tumours are also distinguishable by their grossly disordered vascular architecture, high interstitial fluid pressure, and hypoxic regions, features that actually diminish the potency of conventional treatment such as chemotherapy and radiotherapy (C. L. Dennis and Ivkov 2013a). Hyperthermia has been seen to address these issues by increasing blood perfusion, oxygenating tumours and facilitating transport of compounds into the tumour (B. F. Jordan and Sonveaux 2012). Magnetic nanoparticles (mNPs) are capable of producing heat when subjected to an alternating magnetic field and as tissue is weakly diamagnetic, it does not attenuate or scatter static or low frequency magnetic fields allowing for the easy transmission of an alternating magnetic field (AMF) through an entire tissue with relative ease and minimal toxicity issues (C. L. Dennis and Ivkov 2013a).

As described in chapter 1, section 1.6, mNPs have demonstrated their potential in various biomedical applications including drug delivery (Unterweger et al. 2014), gene delivery (Majidi et al. 2016), magnetic resonance imaging (G. Wang et al. 2014a) and hyperthermia (Gruttner et al. 2013). The use of mNPs in hyperthermia has seen a dramatic rise in research interest over the last 20 years, as noted with a simple literature search in figure 5-1. There have been a number of successful applications *in vitro* (Liao et al. 2015; Munoz de Escalona et al. 2016; Sabale et al. 2015) and *in vivo* studies (Attaluri et al. 2015; Moros et al. 2015; Radovic et al. 2015). As with GNPs, mNPs are being explored with the view to use in therapy as an adjunct to both radiotherapy and chemotherapy (H. C. Kim et al. 2015; M. Lin et al. 2013a).

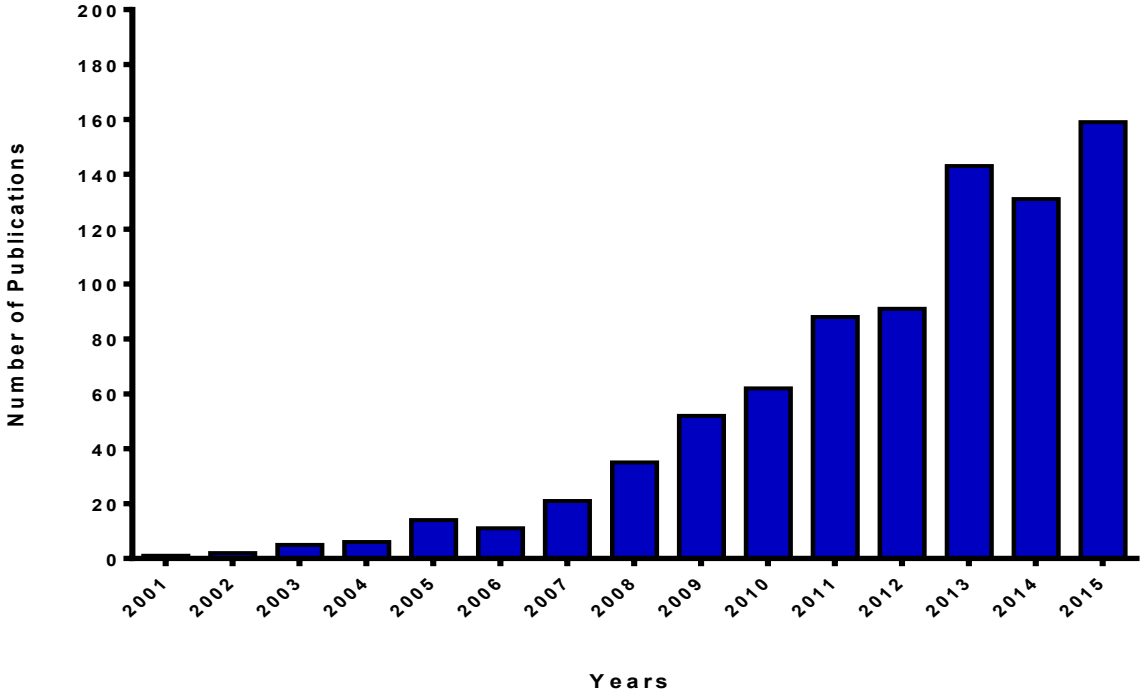

Figure 5-1: Number of publication hits using 'magnetic nanoparticle hyperthermia' search term, from 2001 to 2015 (pubmed).

The multifunctional capability of these particles with regards to hyperthermia have also been highlighted by Yallapu et al (2011), in which superparamagnetic NPs (SPIONs) were used for simultaneous imaging, heating and drug delivery on A2780CP (ovarian), MDA-MB-231 (breast), and PC3 (prostate) cancer cells (Yallapu et al. 2011). Interestingly, iron oxide NPs have recently shown bimodal capacity, being effectively used for magnetic and photothermal treatment, termed 'magnetophotothermal' treatment, both *in vitro* and *in vivo* (Espinosa et al. 2016).

5.1.2 Magnetic Nanoparticle Heat Generation

With regards to hyperthermia, mNPs are assessed for their intrinsic ability to generate heat upon exposure to an alternating magnetic field *via* Neel and Brownian Relaxation mechanisms. As alluded to previously (chapter 1, section 1.6.2), mNP size influences their heating capability, as the superparamagnetic properties iron oxides exhibit is observed at around 1-20 nm. Parmar et al performed a series of experiments to characterise 13 nm and 20 nm SPIONs synthesised from co-precipitation and solvothermal reduction, respectively. Though the 20 nm mNPs displayed a higher magnetisation than their 13 nm

counterpart (due to higher crystallinity and phase purity), the smaller 13 nm mNP produced higher heating capacity when dispersed in a glycerol solution (Parmar et al. 2015). This is directly related to size; the Neel relaxation time is much greater than the Brownian relaxation time with smaller NPs (John Pearce et al. 2013b). Both Neel and Brownian times depend on the size of the particles, however the Brownian time is influenced in a linear fashion with the size of mNP, which means Brownian relaxation forces are the dominant force in heating larger mNPs (Reeves and Weaver 2012). This becomes problematic in more viscous mediums, with Brownian forces becoming severely reduced and only modest Neel relaxation mechanisms contributing to heat production, thus lowering the overall heating potential of larger mNPs. Therefore, the mNPs used in this project have been synthesised at ~11 nm diameter, so as not to be influenced by cellular viscosity (Kuimova et al. 2009).

In this project, a device termed the magnetherm was employed to induce mNPs to generate heat (Nanothermics, Keele, UK). The magnetherm allows the measurement of thermal effects from mNPs by subjecting them to an alternating current magnetic field, of variable strength and frequency. Aside from the mNP size, as described above, other parameters also dictate successful heating, including saturation magnetisation, magnetic susceptibility, magnetic anisotropy, particle distribution, field strength and frequency of the AC field. Whilst NP synthesis allows us to control the NP physical characteristics, the magnetherm allows us to control the magnetic field strength and frequency.

The sample loading chamber in the magnetherm was designed ideally for small animal use, therefore we needed to design and create a cell seeding substrate which could be adapted for use in the device. Cura, an online computer aided design (CAD) software was used to design and 3D print a novel cell seeding chamber which could be used with the magnetherm sample loading chamber, allowing us to carry out hyperthermic experiments.

5.1.3 Magnetic Nanoparticle Biocompatibility

The toxicity of mNPs, in particular SPIONs has been discussed in several reviews and studies and remains controversial (Ghasempour et al. 2015; G. Liu et al. 2013a; S. Naqvi et al. 2010a; Y. C. Park et al. 2014; L. Harivardhan Reddy et al. 2012b). One of the major issues when working with mNP, in particular SPIONs, is the metabolism and subsequent degradation of iron oxide into free iron, which can subsequently lead to the increased generation of ROS, capable of damaging proteins, lipids, polysaccharides and DNA, ultimately leading to cellular apoptosis (N. Singh et al. 2010a).

Previous studies have also shown that following cellular internalisation, mNPs can accumulate in mitochondria, vesicles and lysosomes, suggesting that any observed cytotoxicity is related to inflammatory response and oxidative stress (Hanini et al. 2011; Hussain et al. 2005; Xia et al. 2006). In addition, Soenen and co-workers reported how the intracellular trafficking of various SPIONs across two different cell lines ultimately led to a reduced efficiency of protein expression and disrupted the maturation of actin fibres (S. J. H. Soenen et al. 2010).

In this study, following synthesis and characterisation, mNPs were assessed in terms of their impact on cell metabolic activity, cytoskeleton and viability, as well as their ability to be internalised into cells and subsequently produce heat *via* exposure to an alternating magnetic field.

5.2 Chapter Aims and Objectives

The previous two chapters have focused on the use of gold nanoparticles for photothermal hyperthermia in bone (MG63) and breast (MCF-7) cancer cell lines, this chapter will focus on the use of mNPs as potential hyperthermic agents to induce hyperthermia in bone cancer cells (MG63). The mNPs used in this project were kindly donated by our collaborators in Spain and were characterised prior to use in cell culture, with a zeta-potential (mV) of -40, a core size of ~11 nm and a hydrodynamic size of 100 nm due to the biocompatible coating of dextran. As with any NP platform, following successful synthesis and characterisation, mNPs should be internalised into cells without causing structural damage or invoking cellular stress. Once biocompatibility is established, the mNPs should be able trigger apoptosis *via* hysteresis and Neel and Brownian relaxation mechanisms upon exposure to an alternating magnetic field.

These objectives were achieved as follows:

- Particle biocompatibility was assessed via MTT assay and fluorescent cell viability staining, labelling cells with a range of different mNP concentrations over time in culture.
- Cell – particle interaction was studied using scanning electron microscopy (SEM).
- The mNP internalisation was assessed by transmission electron microscopy (TEM).
- The heating potential of the mNPs was determined using the magnetherm.
- 3D printing software was used to design a cell culture chamber for use in monolayer cell studies using the magnetherm.

5.3 Materials and Methods

5.3.1 Magnetic Nanoparticle Characterisation

MNPs were synthesised and characterised by our collaborators at the Aragón Materials Science Institute, Spain.

5.3.1.1 Cell Metabolic Activity (MTT Assay)

The MTT assay was performed as described in chapter 2, section 2.3.1. Briefly, MG63 cells were seeded at 1 x 10^4 in a 96 well plate for 24 hours to allow attachment prior to mNP introduction. Cells were then incubated with mNPs at concentrations of 0.1 and 1.0 mg.ml^{-1} for 24, 48 and 72 hours (n=5). The 0.1 mg.ml^{-1} concentration in particular was recommended by our collaborators as the lowest concentration that could be utlised for hyperthermic experiments and was used as the standard for future experiments, while the 1.0 mg.ml^{-1} concentation was evaluated for its potential biocompatibility for future cell work. The MTT assay was run at the time points stated, whereby cells were further incubated with MTT for 1 hour before the solution was solubilised with DMSO. The absorbance of each well was read on a microplate reader (Dynatech MR7000 instruments) at 550 nm.

5.3.1.2 Cell Viability

The cell viability assay was carried out as described in chapter 2, section 2.3.2. MG63 cells were seeded at 1 x 10^4 in a 24 well plate for 24 hours before incubation with mNPs at concentrations of 0.1 and 1.0 mg.ml^{-1} for 24, 48 and 72 hours (n=3). The cell viability was assessed by simultaneous incubation with calcein AM and ethidium homodimer for 1 hour followed by washing with fresh warm growth media and immediate imaging.

From the cell viability and cell metabolic activity results; it appeared only 0.1 mg.ml^{-1} mNP concentration would be applicable for future cellular experiements and thus only was the only concentration selected for downstream experiments including cell-NP interaction and *in vitro* hyperthermia experiments.

5.3.1.3 Cell – Nanoparticle Interactions

SEM

The MG63 cells were seeded at 1 x 10^4 in a 24 well plate, left for 24 hours, then incubated with 0.1 mg.ml^{-1} mNPs for 1 hour and 24 hours (n=2) prior to fixation and processing as stated in section 2.4.2.

Fluorescent Cytoskeleton Staining

The MG63 cells were seeded at 1 x 10^4 in a 24 well plate, left for 24 hours, then incubated with 0.1 mg.ml^{-1} mNPs for 24, 48 and 72 hours (n=2) prior to fluorescently stained for F-actin and β-tubulin using the protocol described in section 2.4.3.

Nanoparticle Internalisation *via* TEM

The MG63 cells at seeded at 1 x10^5 in a 24 well plate for 24 hour, then incubated with 0.1 mg.ml^{-1} mNPs for 1 hour and 24 hours (n=2) prior to fixation and processing as stated in section 2.4.3

5.3.2 Magnetic Heating and Magnetherm Studies

5.3.2.1 Heating of mNP Samples via Magnetherm Device

Samples of mNP solutions were assessed for their heating potential using the magnetherm device (nanotherics, UK). Aliquots of 2 mL of various concentrations of mNPs were placed within a universal and located in the sample loading chamber in the magnetherm device, as illustrated in figure 5-2, producing an optimised characterised magnetic field (volt= 27.2, current= 9.3, frequency= 115 kHz). Concentrations ranging from 0.01, 0.1, 1.0, and 5.0 mg.ml^{-1} were utilised to obtain a range of heating potentials. The temperature was measured *via* a thermocouple device and samples were recorded from baseline room temperature. The samples were left in the magnetherm device until a desired temperature profile was met, with a cut-off point of approximately 30 minutes if unsuccessful.

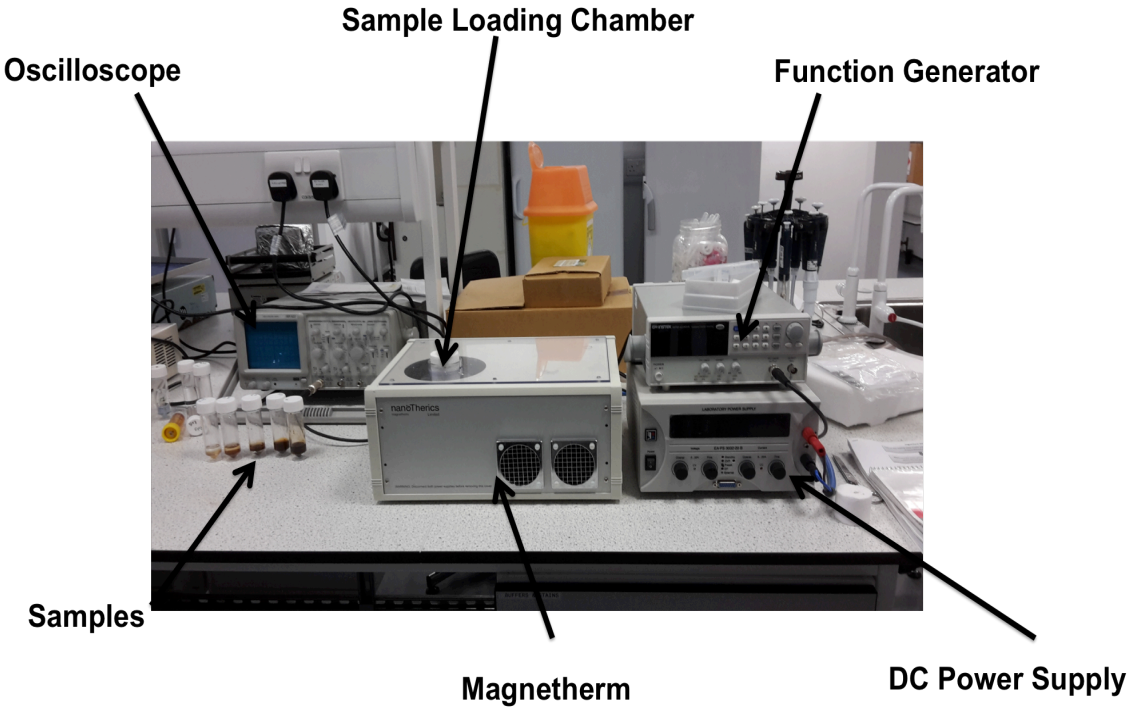

Figure 5-2: A photograph of the magnetherm set-up as used in experiment. The samples were loaded into the sample loading chamber, power applied and magnetic fields generated using the function generator (viewed on the oscilloscope). The magnetic fields were governed by a capacitor / copper coil located within the maghetherm.

5.3.2.2 3D Printing of Culture Chambers for the Magnetherm Experiment

The magnetherm is not presently designed to allow testing of monolayer cell culture samples, with the cylindrical sample loading chamber proving difficult to position petri dishes to allow simultaneous multi-well analysis of treated cell cultures. In order to pursue cell culture work within the magnetherm device and to compare samples, conditions and controls simultaneously, a 3D cell seeding chamber was constructed onto a polycarbonate substrate using acrylonitrile butadiene styrene (ABS). This 3D device was constructed onto a 2 cm^2 polycarbonate platform *via* a 3D printer (Ultimaker^2) to create four identical culture chambers (1.25 X 10^4 cells per chamber). The final dimension of the device was 2 cm^2 with each of the four chambers measuring 9 mm^2, as shown in figure 5.3.

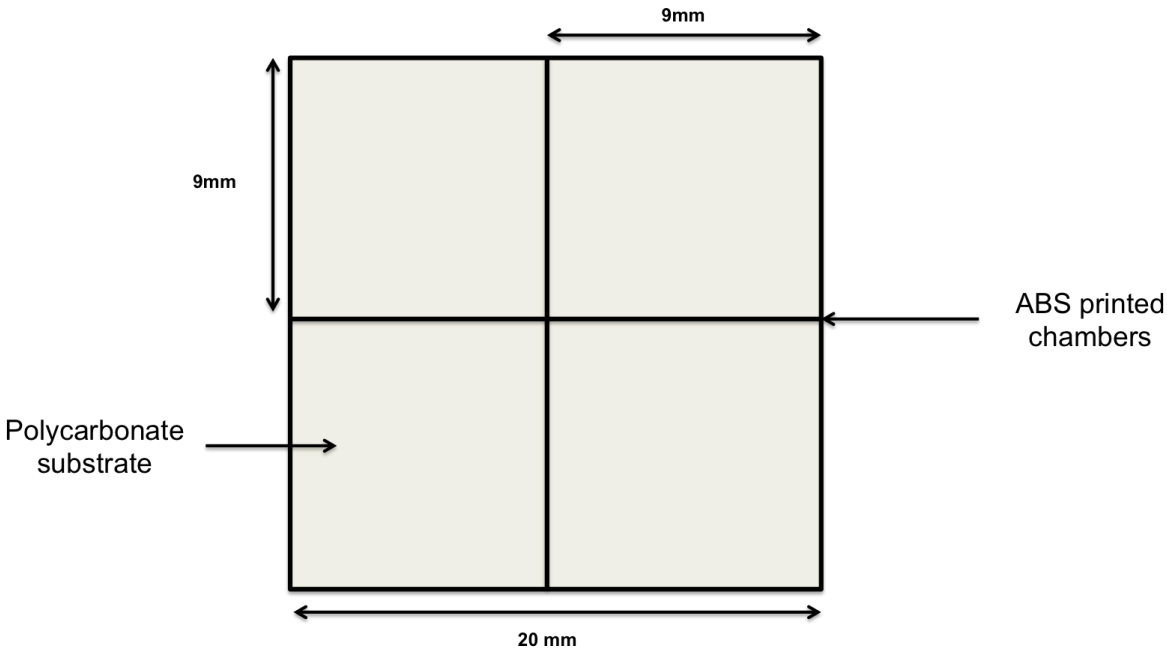

Figure 5-3: Schematic of the 3D printed cell seeding chambers, printed onto a polycarbonate substrate using ABS.

Prior to use with cells, the 3D chambers were initially rinsed with 70% ethanol and 0_2 plasma treated (to ensure hydrophilicity) for 1 minute. The chambers were subsequently sterilised with 70% ethanol and allowed to dry within a laminar flow hood for 30 minutes. The chambers were finally washed thoroughly with HEPES saline and air dried within a laminar flow hood ready for cell culturing

5.3.2.3 In Vitro heating of MG63 Cell via Magnetherm using 3D Printed Culture Chambers

The MG63 cells were seeded at a cell density of 1.25 x 10^4 per 200 µL in each chamber. The device was then carefully housed within a 35 mm petri dish and incubated for 24 hours (5% CO_2; 37°C). After 24 hours, culture media was removed and cells were washed three times in PBS before incubation with mNPs in media, at a final concentration of 0.1 $mg.ml^{-1}$ (200 µL per chamber), and incubated for a further 24 hours (5% CO_2; 37°C). The device was then removed from the incubator and two of the four chambers were washed with PBS and re-suspended with 200 µL of fresh media (this was to evaluate the performance of internalised mNPs only and not simply those within the media) before being placed into the sample loading chamber in the magnetherm. The magnetherm was then

tuned to an optimised magnetic field (volt= 27.2, current= 9.3, frequency= 115 kHz) for 20 minutes. The potential effects from AMF exposure alone was determined by a control sample containing no mNPs.

5.3.2.4 Cell Staining via Coomassie Blue

Following hyperthmic treatment of MG63 cells, the 3D printed chambers were removed from the magnetherm and placed into an incubator (5% CO_2; 37°C) for 3 hours. The media was then removed from each chamber, the cells were fixed in 4% formaldehyde for 15 minutes at 37°C washed in PBS and 200 µL coomassie blue stain was added for 2 minutes. The stain was washed well with PBS and subsequent light microscopy images were then taken on an inverted light microscope.

5.4 Results

5.4.1 Magnetic Size and Morphology *via* TEM

MNP size, morphology and aggregation state were determined by TEM (figure 5-4). The image confirmed successful synthesis of mNPs that were well dispersed and with no indication of aggregation. MNPs displayed a low size distribution between 9 and 15 nm and an average size of 11 nm which has been previously shown to display optimal heating capactiy (Gonzales-Weimuller et al. 2009; Ganeshlenin Kandasamy and Maity 2015b).

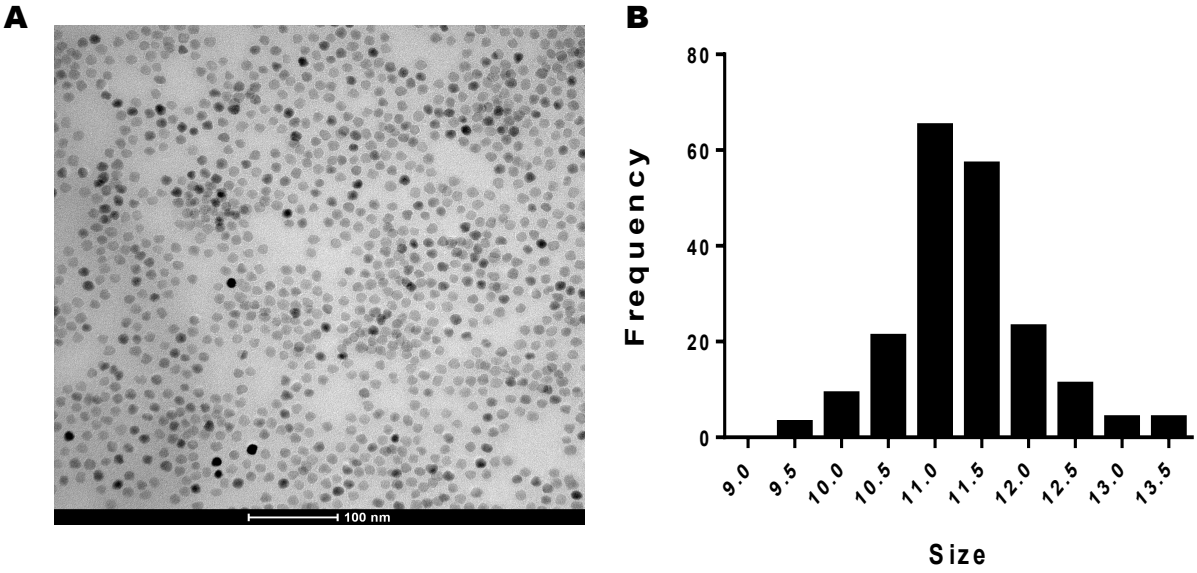

Figure 5-4: TEM of mNPs (A) and size distribution graph (B).

5.4.2 Magnetic Nanoparticle Biocompatibility

5.4.2.1 Cell Metabolic Activity (MTT Assay)

The MTT assay provides an insight into the metabolic activity of cell cultures, providing an indicator of cell health. As may be expected, the metabolic activity was inversely proportional to mNP concentration, concluding that higher mNP concentrations invoked a negative cell response. However the lower 0.1 $mg.ml^{-1}$ mNP concentration did not substantially affect cell metabolic activity, although there was a time dependent effect noted with prolonged mNP exposure (Bellusci et al. 2014).

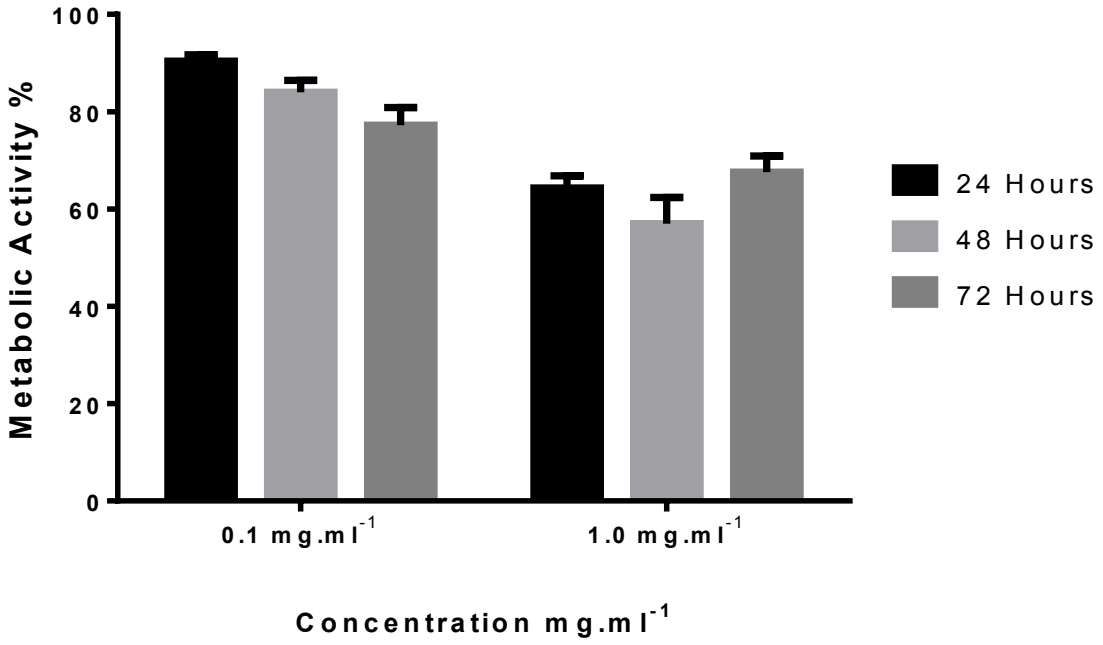

Figure 5-5: Metabolic activity of MG63 cells following incubation with magnetic nanoparticles. MTT analysis of MG63 cells treated with 0.1 and 1.0 mg.ml^{-1} for 24, 48 and 72 hours (n = 5; error bars indicate SD).

5.4.2.2 Cell Viability

While the MTT assay provides a quantitative assessment of the cell metabolic activity, limitations over the use of the assay have been highlighted (Kong et al. 2011; S. Wang et al. 2011a) which could lead to false positive and false negative results. The cell viability fluorescent imaging allows the qualitative assessment of cell sample based on the integrity of cell membranes – a major indicator of apoptosis.

The viability images are shown in figure 5-6 and show correlation with the MTT assay; cells exhibit an initial high viability at 24 hours, as observed by the high number of green (live cells) and low number of red (dead cells), however after prolonged exposure (48 and 72 hours) cell viability depreciates in comparison to control samples (containing no mNPs). In summary, cell viability appears compromised in correlation to the increased NP concentration (Saba Naqvi et al. 2010b).

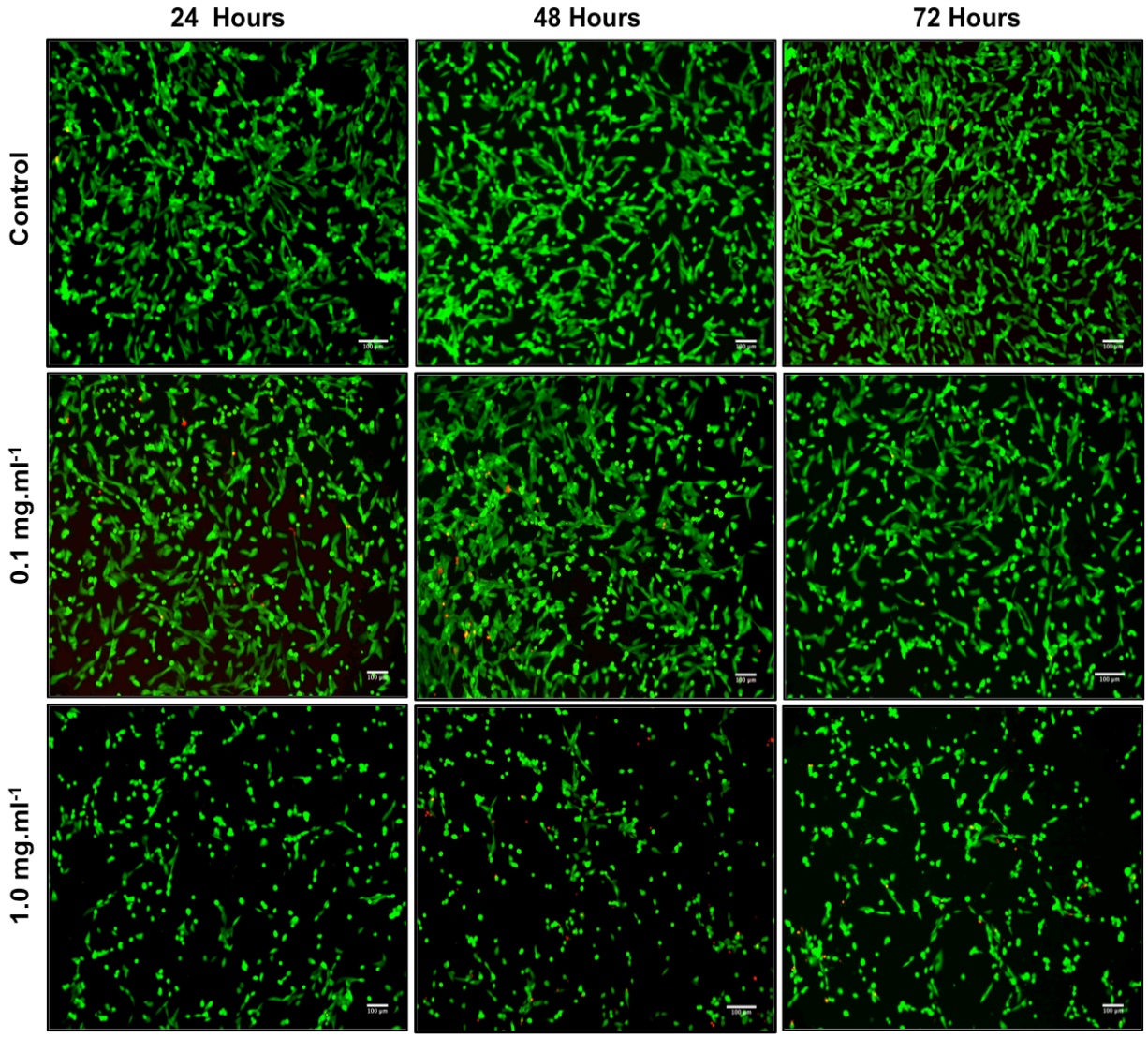

Figure 5-6: MG63 cell viability following incubation with magnetic nanoparticles. Fluorescence images of MG63 cells treated with 0.01, 0.1 and 1.0 mg.ml^{-1} mNPs for 24, 48 and 72 hours. Green and red fluorescence indicates living and dead cells, respectively (controls are cells containing no NPs, n=2). Scale bar = 100 µm.

5.4.2.3 Cell – Nanoparticle Interactions

SEM Imaging

Figure 5-7 shows SEM images of MG63 cells after 1 and 24 hours incubation with mNPs. Corresponding cells containing no mNPs were used as controls. Cells incubated with mNPs displayed an increased expression of filopodia, both as protrusions on the edges of the cell surface, with long protrusions extending from the cell edges as well as notable filopodia protrusions on the cell body (P. Tseng et al. 2012). SEM images also indicated the aggregation of mNPs, both on the cell surface and also on the coverslip, which may have consequences for cell toxicity, internalisation and metabolism (Bae et al. 2011; Stefaan J. Soenen et al. 2011)

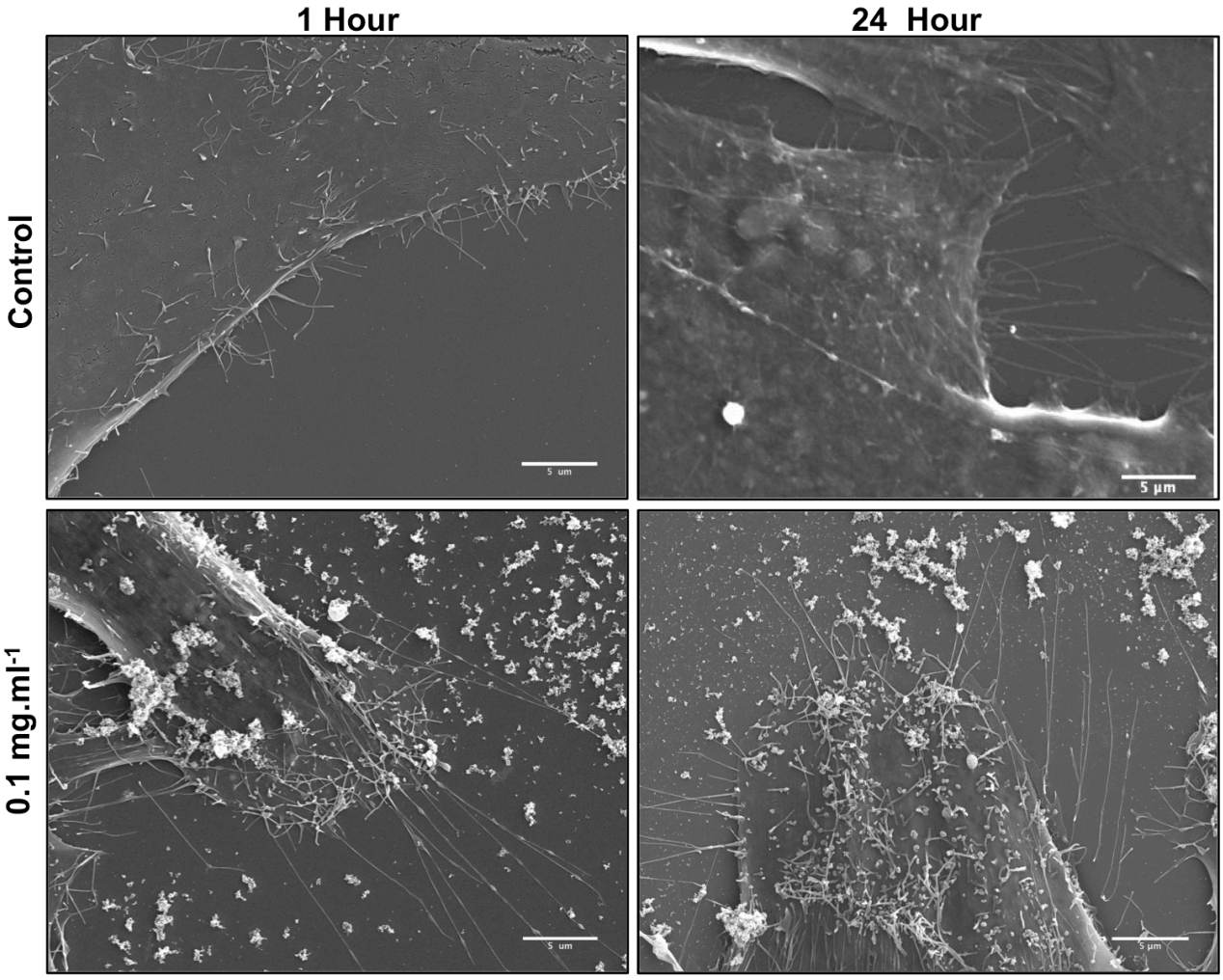

Figure 5-7: SEM image of MG63 cells incubated with 0.1 mg.ml^{-1} mNPs at 1 hour and 24. Subsequent control cells containing no NPs were used for comparison at 1 hour (A) and 24 hours (B). SEM images were taken at 3000 x magnification at 300kV voltage.

Fluorescent Cytoskeleton Imaging

Fluorescence microscopy, as shown in figure 5-8. was performed on MG63 cells incubated with 0.1 mg.ml^{-1} mNPs for 24, 48 and 72 hours to further investigate any adverse interactions with the cell cytoskeleton over time. As time progressed, the mNP treated cells displayed smaller, more condensed cell bodies. The β-tubulin microtubules appeared denser, with less elongation throughout the cell body, whilst F-actin filaments also appeared denser, with punctate areas, which may indicate exocytosis processing (Gasman et al. 2004).

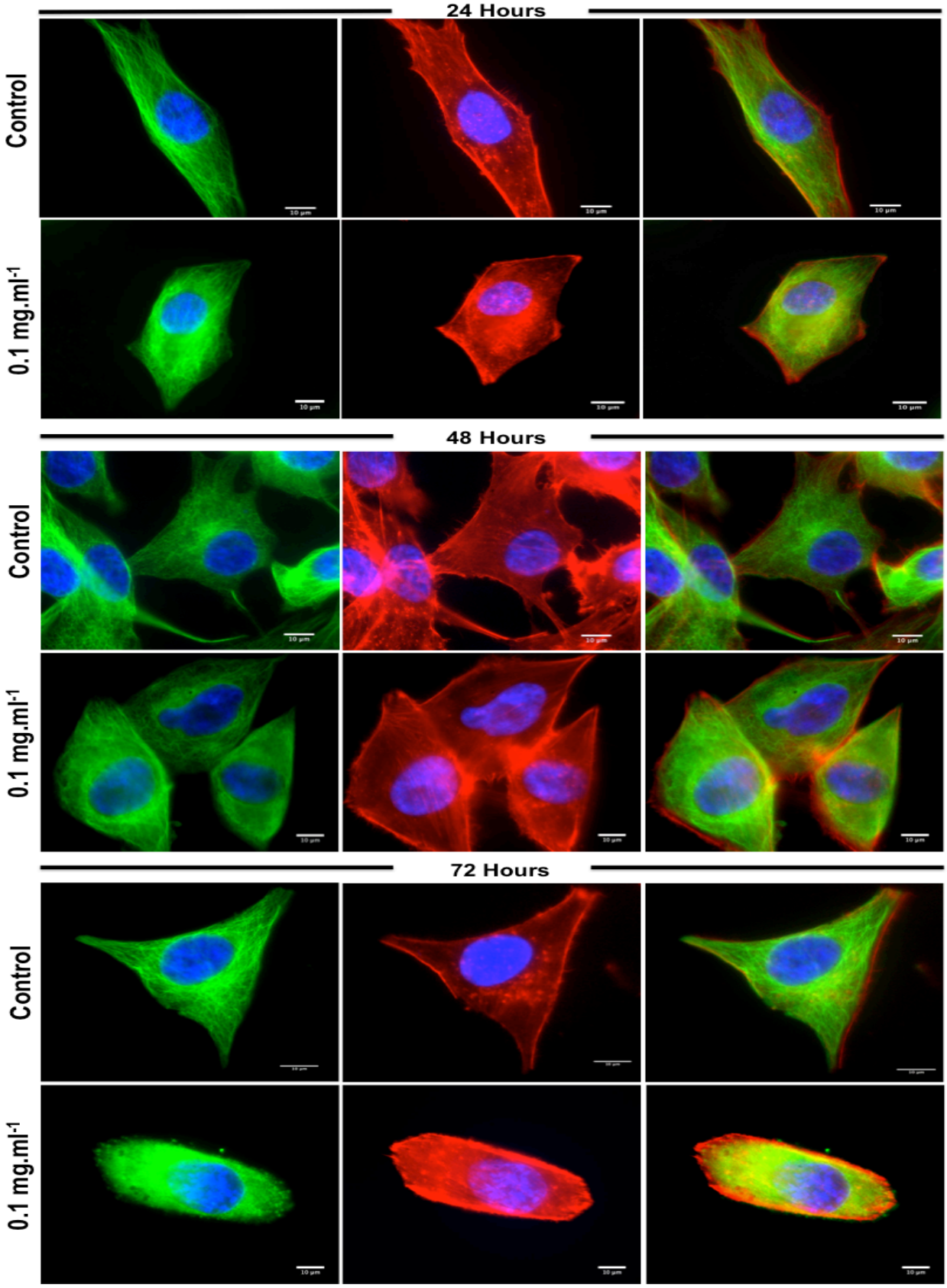

Figure 5-8: Cytoskeletal imaging of MG63 cells following incubation with magnetic nanoparticles. Fluorescent images of MG63 cells incubated with mNPs at 0.1 mg.ml^{-1} for 24, 48 and 72 hours (control cells contained no mNPs). F-actin (red), β-tubulin (green), counterstained with DAPI to visualise the cell nucleus (blue). Scale bar 10 μm.

Particle Internalisation *via* TEM Imaging

TEM images in figure 5-9 confirmed the successful internalisation, distribution and compartmentalisation of mNPs (0.1 mg.ml^{-1}) at 1 and 24 hours, into endosome-like structures. TEM images appeared to show large quantities of mNPs internalised into cells after just 1 hour of mNP incubation (figure 5-9 A,B). Figure 5-9 B in particular appears to show the invagination of the cell membrane around the mNPs, indicative of a form of receptor mediated endocytosis involving invagination and formation of intracellular vesicles (Zhenjia Wang et al. 2011b). No mNPs were observed free within the cytoplasm, suggesting that the NPs entered cells *via* endocytosis rather than passive diffusion. At 24 hours, mNPs were observed densely populated within endosome-like structures Figure 5-9 C,D) however a high concentration of mNPs were also apparent outside the cell, which may indicate slow uptake or exocytosis.

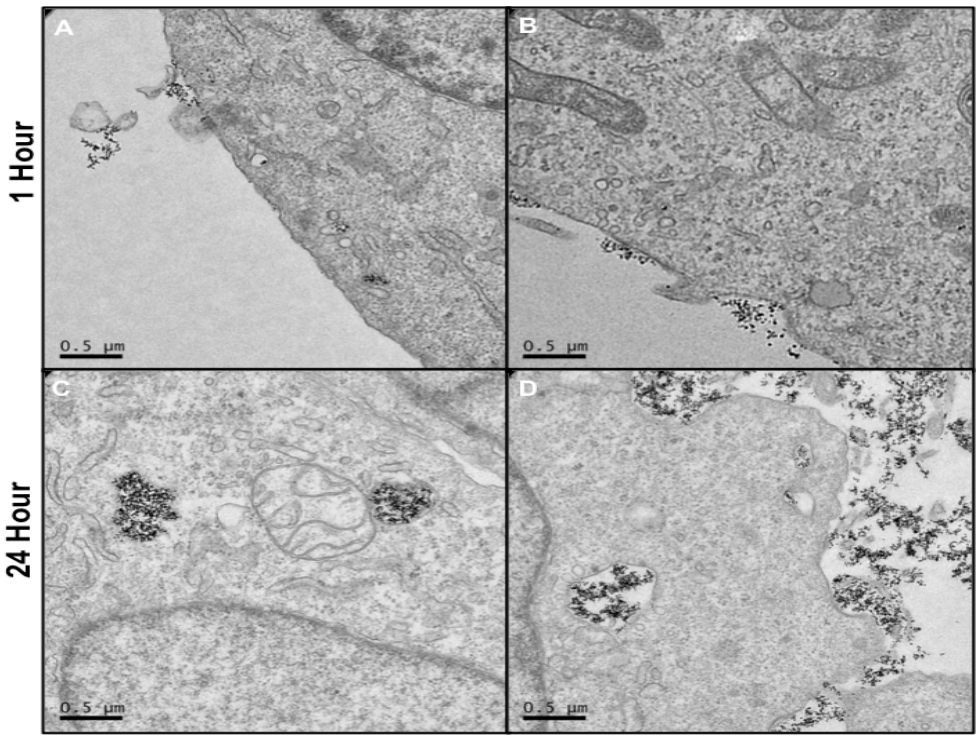

Figure 5-9: The internalisation of magnetic nanoparticles into MG63 cells. TEM images of MG63 cells incubated with 0.1 mg.ml^{-1} mNPs confirming mNP internalisation after just 1 hour with early signs of cell membrane invagination and endocytosis driven uptake (A and B). At 24 hours large concentrations of mNPs were seen grouped and packaged within large endosome like structures however, large concentration of mNPs were also observed outside the cells (C and D). Images were taken at 10000x magnification at 120 kV voltage.

5.4.3 Magnetic Heating and Magnetherm Studies

5.4.3.1 Heating of mNP Samples via Magnetherm Device

Magnetic samples of various concentrations were located in universals and placed into the magnetherm sample loading chamber. Samples were heated for 30 minutes or until hyperthermic profiles were attained (42-45°C) as shown in figure 5-10. The higher concentrations (1.0 and 5 $mg.ml^{-1}$) heated rapidly, reaching the desired temperature profiles in less than 5 minutes. The mid-range concentration (0.1 $mg.ml^{-1}$) achieved the profile in under 20 minutes, however the lowest concentration (0.01 $mg.ml^{-1}$) failed to achieve a hyperthermic temperature profile, with a modest increase of temperature after 30 minutes (~12°C).

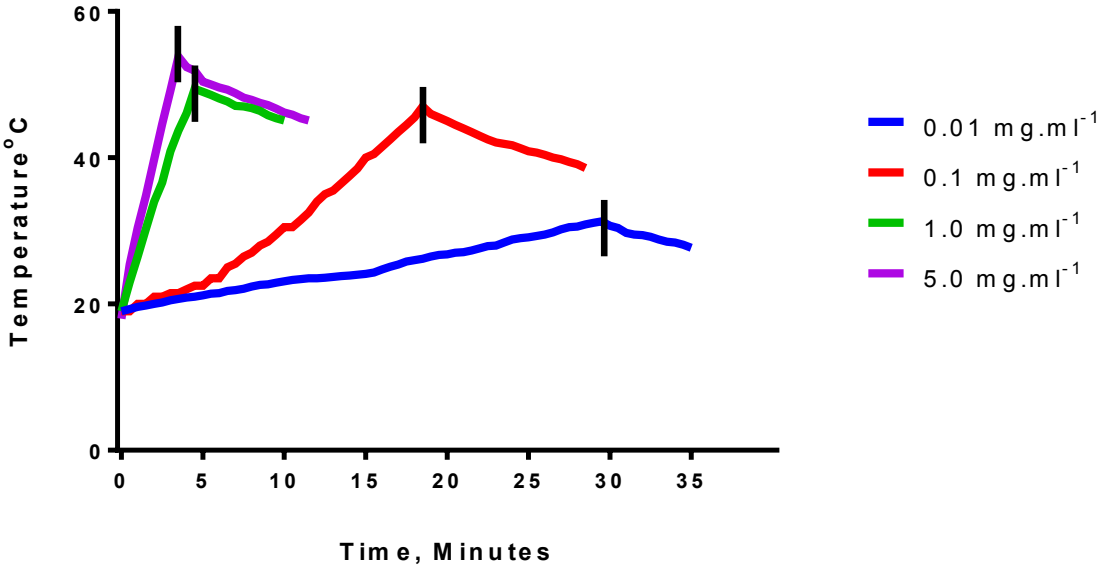

Figure 5-10: Temperature profiles of various concentrations of magnetic nanoparticles stimulated in the magnetherm. The heating potential of 2 mL aliquots of mNPs at concentrations of 0.01, 0.1, 1.0, and 5.0 $mg.ml^{-1}$ within a magnetherm producing a characterized magnetic field (volt= 27.2, current= 9.3, frequency= 115 kHz, nanotherics, UK). The magnetherm device was switched off after 30 minutes or after hyperthermic profiles (42-45°C) were achieved, indicated by the black dash.

5.4.3.2 In Vitro heating of MG63 Cells via Magnetherm using 3D Printed Culture Chambers

Initial hyperthermic experiments were carried out; the MG63 cells were seeded in the 3D printed culture chambers, labelled with 0.1 mg.ml^{-1} mNPs and located with the magnetherm for 30 minutes. Coomassie blue staining was used to assess the cell morphology following treatment, as shown in figure 5-11. Control cells exhibited typical stellate adhered cell morphology, however an immediate alteration in morphology was observed in samples containing mNPs; cells were notably smaller and displayed decreased cell-cell adhesion. At the higher 20 x magnification, the mNP labelled cell bodies appear condensed, with areas of cell debris, suggesting cell death.

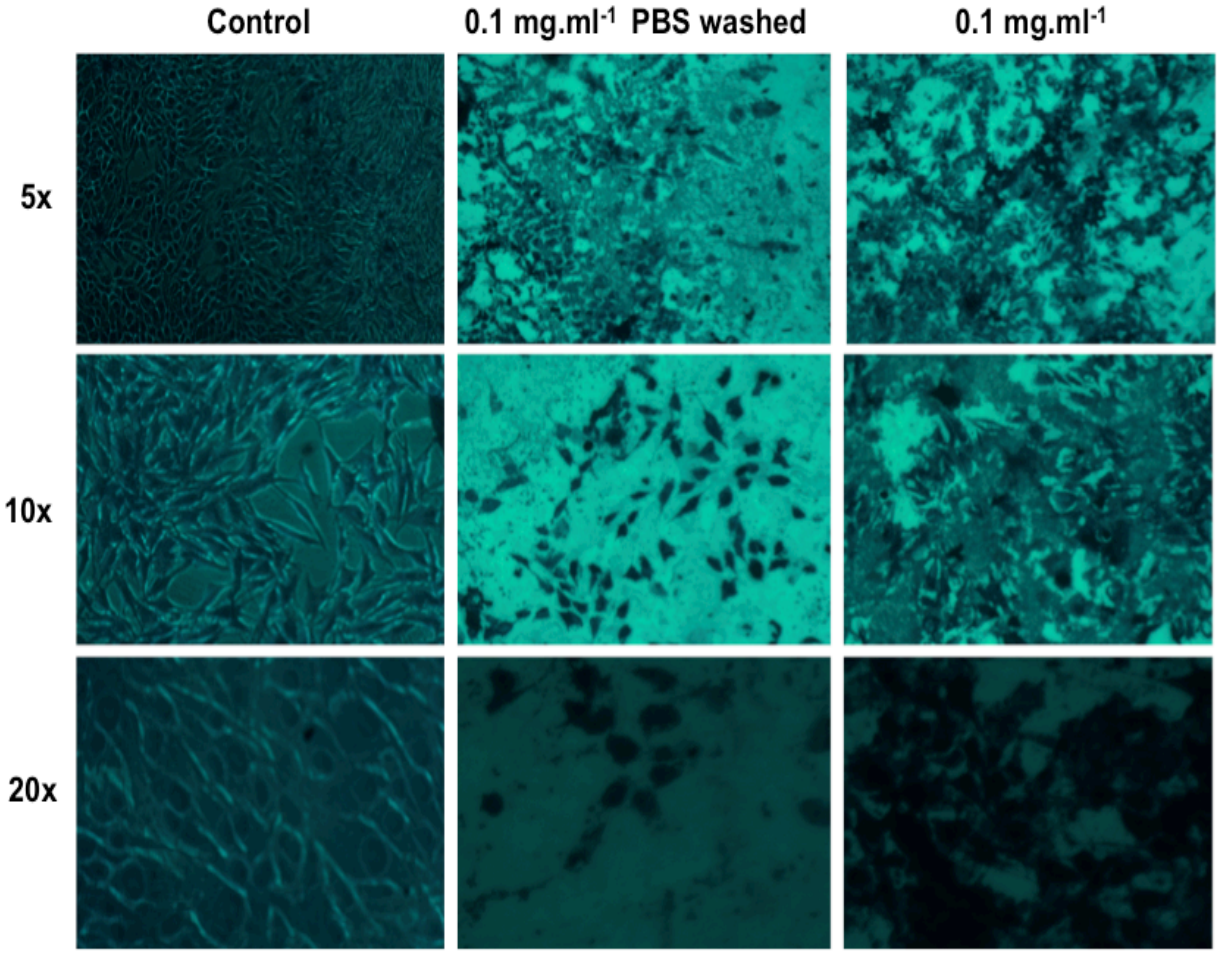

Figure 5-11: Coomassie stain of mNP labeled MG63 cells following hyperthermic treatment within a magnetherm. Cells were labeled with 0.1 mg.ml^{-1} mNPs, +/- PBS washed and located within the magnetherm for 30 minutes, prior to coomassie blue staining.

5.5 Discussion

5.5.1 MNP Synthesis: Size and Morphlogy

MNPs used in this study were successfully synthesised and imaged *via* TEM and a size distribution graph was generated. MNPs synthesised, showed a narrow size distribution predominantly between 9 and 13 nm with an average core size of ~11 nm, a crucial attribute for SPION heating capcity (Gonzales-Weimuller et al. 2009; Ganeshlenin Kandasamy and Maity 2015b). MNPs displayed a consistent sphere morphology and importantly, did not show signs of aggregation, which has been shown to alter NP internalisation rate into cells (Alexandre Albanese and Chan 2011b). Aggregation to mNPs and in particular, SPIONs has also been shown to decrease their heating capacity (SAR), while a further reduction in heating capactiy has been observed for SPIONs in suspensions containing cells, but the origin of this further reduction is still elusive (Jeon et al. 2016).

5.5.2 Magnetic Nanoparticle Biocompatibility

The mNPs used in this study had a magnetic core size of ~ 11 nm, with a hydrodynamic radius of 100 nm following stabilisation with dextran. It is well known that both the size and shape of NPs can influence their biocompatibility and internalisation into cells (Arami et al. 2015; Forest et al. 2017; Neenu Singh et al. 2010b; Vanessa Valdiglesias et al. 2016; Yameen et al. 2014a). Therefore this chapter aimed to characterise the mNPs prior to use as agents for *in vitro* hyperthermia.

There are many methods employed to assess particle toxicity. The MTT assay is a well established technique for *in vitro* cellular toxicity evaluation and is extensively used (Watanabe et al. 2013). The results indicated that lower concentrations were favourable, as cell metabolic activity decreased with an increase in mNP concentration. This is somewhat in agreement with the general consensus of the literature concerning functionalised mNPs (Khot et al. 2013; Y. Liu et al. 2011; Mejias et al. 2013; Mojica Pisciotti et al. 2014). Dextran is a widely used biocompatible coating for many mNPs, including those used for *in vivo* imaging, due to its inert, biocompatible characteristics; indeed many of the FDA approved SPIONs are coated with dextran molecules (L. Harivardhan Reddy et al.

2012b). The difficulty with comparing the toxicological affect of dextran coated SPIONs with those studies in the literature is due, not only by the variance of concentrations used by respective groups, but also the use of different cell lines tested and the physical, chemical and structural characteristics of SPIONs (S. Laurent et al. 2012a).

Recently, the concept of 'nanotoxicity' has evolved as a distinct research area. Nanotoxicity does not only connote cell death in response to nanomaterial exposure, but has broadly extended into identifying other markers associated to cell stress. This includes oxidative stress, genotoxicity, cell cycle disruption and morphological changes, which have all been previously explored in dextran-coated mNPs (Remya et al. 2016; V. Valdiglesias et al. 2015a). A great deal of difficulty therefore exists in forming a cohesive opinion on the toxicity of SPIONs. As well as the various characteristics of NPs that can influence cytotoxicity, it also appears that the response of identical NPs differ among various organs and cell types (Sophie Laurent et al. 2012b). SPIONs in particular appear to demonstrate large variance within cell lines due to various cell types responding differently towards the uptake of SPIONS, and follow different detoxification mechanisms to overcome the toxicity induced by SPIONs (N. Singh et al. 2010a).

The results in this chapter suggest that dextran-coated mNPs over a prolonged period of time (> 24hours) are mildly toxic to bone cancer cells (MG63). The increased cytotoxicity at 1.0 $mg.ml^{-1}$ may be due to an increased accumulation of mNP concentration internalised within cells that can be readily metabolised (Buyukhatipoglu and Clyne 2011). The metabolised free iron can be transported and stored (*via* ferritin proteins), however too much free iron that cannot be continually stored in ferritin and similar proteins may lead to the breakdown of iron oxide into free iron ions within lysosomes (Vanessa Valdiglesias et al. 2015b). This 'free iron' has the capacity to cross mitochondrial membranes, and react with hydrogen peroxide and oxygen produced naturally by mitochondria leading to the formation of highly reactive hydroxyl radicals and ferric ions (Fe3) *via* the Fenton reaction (Malvindi et al. 2014; N. Singh et al. 2010a). ROS have been shown to interfere with and cause DNA damage as well as proteins and lipid peroxidation leading to the eventual induction of apoptosis (N. Singh et al. 2010a). Several studies have also drawn concerns of using iron oxide NPs at high concentrations,

including compromises to the cytoskeleton (as shown in this chapter), mitochondria and DNA (Calero et al. 2014; Sadeghi et al. 2015).

5.5.3 Magnetic Nanoparticle Internalisation

The SEM imaging confirmed the interaction of the mNPs on the cell surface, with resultant increased expression and exension of filopodia (Pauksch et al. 2014). Flopodia have been previously described as 'antennae' or 'tentacles' that are capable of probing their microenvironment, although their function has not been fully characterized, filopodia and are capable of creating 'sticky fingers' along the leading edge promoting cell adhesion, migration and guidance towards chemoattractants (Mattila and Lappalainen 2008). Although the cytoskeleton imaging demonstrated reduced cell size and morphology, both the SEM and TEM images suggest that the mNPs do not alter the general morphology of cells too drastically, or compromise the integrity of plasma membrane or affect cellular aherence which has been noted in previous studies (Berry et al. 2003; Calero et al. 2014; Rivet et al. 2012). SEM images however did demonstrate the aggregation of mNPs, which may influence mNP toxicity and uptake.

The mNPs were clearly internalised as shown in the TEM images. Endocytosis is the major route of NP transport across the membrane and broadly categorised into either phagocytosis or pinocytosis. There are several different mechanisms known to be involved in the uptake of NPs, these include clathrin-dependent endocytosis and clathrin-independent endocytosis, which includes caveolae-mediated endocytosis, micropinocytosis and phagocytosis, as shown in figure 5-12 (Kou et al. 2013). The images taken during this chapter support both endocytosis and pinocytosis, with SEM imaging supporting the former, whilst TEM and condensed/punctate F-actin supporting the latter.

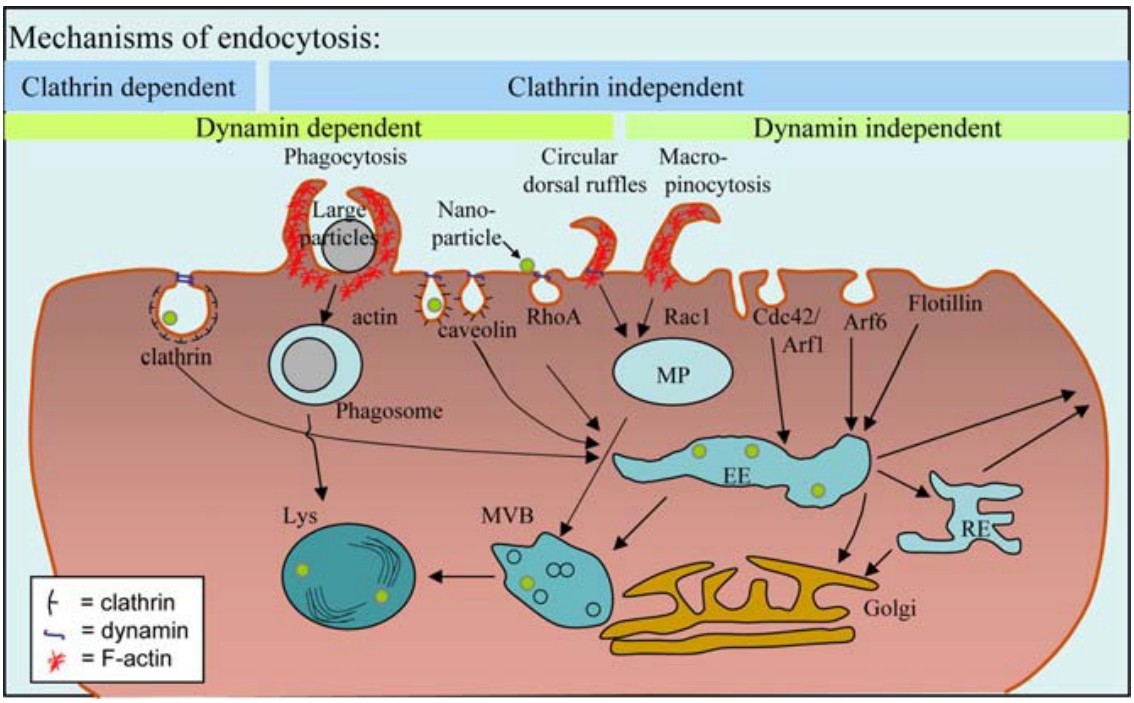

Figure 5-12: Schematic depicting the main routes of nanoparticle internalisation into cells. Nanoparticles (green dots) are taken up by endocytosis and enclosed within early endosomes (EE), which mature to become multivesicular bodies / late endosomes (MVB),which fuse to form lysosomes (Lys). Nanoparticles can also be recycled back to the cell surface through recycling endosomes (RE) (image adapted from 'Cellular Toxicity of Nanoparticles', Seallab wordpress).

These mechanisms of entry are intrinsically dependent on several factors including NP shape, size, surface area, morphology, chemistry and functionalization and could subsequently influence NPs toxicology, exocytosis and metabolism (Kettler et al. 2014; Kou et al. 2013; Sara Salatin et al. 2015b). Although it has been observed that mNP can cause cytotoxic effects without being internalised within cells, most effects are uptake-dependent, with corresponding toxicity dependent on NP fate within the cell (Nel et al. 2009). Thus, an increased uptake of mNPs may lead to a decrease in viability and may account for the decreased metabolic activity observed in higher mNP concentrations.

Invaginations of cell membrane with bound mNPs was observed after 1 hour of mNP incubation, with mNPs contained in large vesicles (Wilhelm and Gazeau 2008). Research groups that have used dextran coated mNPs similar to our own

have also reported mNP uptake *via* an endocytosis pathway. This was confirmed *via* endocytosis inhibition that subsequently blocked mNP uptake into cells, and upon restoration, mNPs were successfully internalised into Hela cells (Wilhelm and Gazeau 2008) and A549 cells (J.-S. Kim et al. 2006). Rofe's group also confirmed final destination of dextran-coated mNPs into lysosomes using lysosome-specific staining which validate our TEM images after 24 hours (figure 5-9. C and D), in which mNPs are clearly observed packaged within vesicles (Rofe and Pryor 2016).

F-Actin is a protein producing linear filaments that facilitates the formation of microfilaments within the cytoskeleton; these microfilaments are integral for cell mobility and intracellular transport, cell-cell and cell-substrate interactions, and signal transduction (Calero et al. 2014). Actin filaments are also involved in cellular processes, including apoptosis and mitosis, through integrin-mediated signaling, as integrins are mechanically linked to the actin cytoskeleton in so-called focal adhesion complexes (FACs) (S. J. H. Soenen et al. 2010). β-tubulin subunits meanwhile, form microtubules, which have fundamental functions similar to that of microfilaments including motility and vesicle transport, however play an essential role in apoptosis and the separation of chromosomes into daughter cells during interphase (Kettler et al. 2014; Mundra et al. 2015; Y. Song and Brady 2015). Potential damage to either of these components would suggest acute toxicity of NPs. The results from previous cell metabolic and cell viability results suggest a time-dependent affect on cell cultures exposed to mNPs, which is in an agreement with the F-actin and β-tubulin staining, where filaments and tubules appear to be compromised with notable morphological changes at 24, 48 and 72 hours. Actin filament disruption has also been shown to increase in a dose dependent manner upon mNP incubation (A. K. Gupta and Gupta 2005). At 72 hours, both F- actin and β-tubulin filaments showed clear alterations, indicating potential long term effects of mNPs on cellular structure and function, although it has been suggested that this reorganisation or remodelling of the cytoskeleton maybe linked to different mechanisms involved in NP internalisation, as shown in figure 5-12, rather than as a direct response to the mNPs (A. K. Gupta and Gupta 2005).

As previously mentioned, the high intracellular concentration of nondegradable and solid nanoparticles, such as mNPs, may provoke the synthesis of large endosomes to compartmentalise internalised mNPs and it may be these

organelles that may actually, sterically hinder and deform the cytoskeletal architecture (Stefaan J. Soenen et al. 2012). The same observation was noted with the MG63 cells exposed to GNPs in chapter 3, with β-tubulin disruption, which further supports that NP internalisation disrupts β-tubulin networks (Diptiman Choudhury et al. 2013b). Regardless of the effects noted with longer term incubation with the mNPs, there was little/no compromise in overall cell viability, as shown in figure 5-6.

5.5.4 Hyperthermia using Magnetic Nanoparticles

SPIONs have been shown to cause hyperthermia both *in vitro* (Reihaneh Haghniaz et al. 2015b) and *in vivo* (C. L. Dennis et al. 2009). To first evaluate the mNP heating potential, samples of various concentrations were assessed as to their heating potential using the magnetherm (figure 5-10). As expected, the heating capacity increased in a dose dependent manner; the mid-range concentration of 0.1 $mg.ml^{-1}$ was selected as the most suitable candidate for cell studies, as this concentration was considered a reasonable threshold between cell tolerance and heating capacity.

In general, mNP-heating capacity is proportional to the applied MF amplitude, with studies showing an increase in field strength corresponding to an increase in mNP-heating capacity (Deatsch and Evans 2014; Mehdaoui et al. 2010). However this approach is not clinically relevant due to the physiological difficulties high frequency magnetic fields may inflict, such as induced local heating in non-magnetic tissue due to induced eddy currents (Deatsch and Evans 2014). Therefore many studies use fairly narrow frequencies between 100 to 150 kHz for medical considerations (André C. Silva et al. 2011b). The characterised MF produced in this chapter for hyperthermic experiments was optimised at 115 kHz and therefore seems towards the upper limit of clinically relevant parameters and the strength was considered the maximum threshold. The mNP diameter/size also plays a role in its heating capacity, with smaller particles often releasing heat predominantly *via* Neel relaxation (< 15 nm), therefore our mNPs are expected to generate heat in this fashion, which is considered ideal as it is not influenced by the viscosity of its environment (Smolkova et al. 2015).

The magnetherm is not ideal for cell culture experiments, and in-house measurements were used to attempt to locate our 3D printed cell chambers in the centre of the applied field, where the force will be strongest, as shown in figure 5-13. If cells are located at the optimal position, the mNP should cluster within the cell upon stimulation, causing maximum cell disruption.

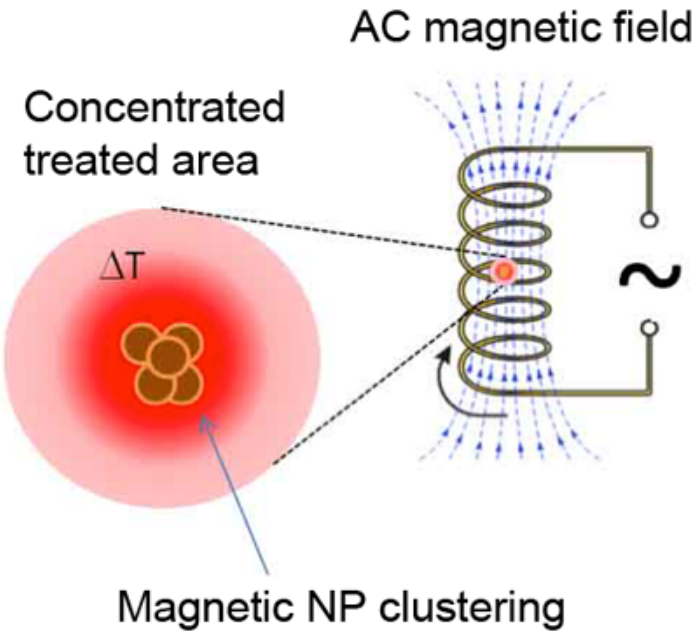

Figure 5-13: Magnetic nanoparticle heating within an alternating magnetic field. Magnetic nanoparticles generate their maximum potential heat, identified as an increase in temperature (ΔT), when located within the centre of an alternating magnetic field (image adapted from Piñeiro-Redondo et al, 2011).

Due to time restraints, only initial gross cell morphology results were obtained. The results suggest MF alone does not contribute to cell death nor does it appear to affect cellular morphology. Cells exposed to mNPs and MF (and thus hyperthermia) showed striking, morphological changes indicative of cell stress such as loss of cell extensions, rounding up morphologies and cell detachment (Reihaneh Haghniaz et al. 2015b). The shrunken morphology and blebbing in cells exposed to hyperthermia may also indicate cells in the latter stages of apoptosis while the loss of the organisation of the cell layer and cell-to-cell contact and a significant decrease in the number of attached cells demonstrate the global effect of hyperthermia on cell monolayers (P. Garcia et al. 2012).

5.6 Conclusion

The aim of this chapter was to evaluate mNPs as potential hyperthermic agents. The ideal candidate must be biocompatible, internalised into cells and able to produce hyperthermic temperature profiles (42-45°C) upon exposure to an external alternating magnetic field (Bañobre-López et al. 2013).

The mNPs used in this study showed great potential when used at 0.1 $mg.ml^{-1}$, demonstrating cell viability, mNP internalisation and hyperthermic temperature profiles in under 20 minutes (M. Gong et al. 2015; S. Naqvi et al. 2010a). (Orynbayeva et al. 2015; Alice Panariti et al. 2012b; M. Yu et al. 2012a). The imaging (SEM, cytoskeleton and TEM) confirmed the interaction and subsequent internalisation of mNPs *via* endocytosis pathways, in particular clathrin-mediated endocytosis and pinocytosis appearing the most dominant processes, with mNPs packaged within lysosome structures within the cell body (no NPs were observed free within the cytoplasm) (Yameen et al. 2014b).

A 3D printed cell culture chamber was designed to adapt our *in vitro* studies to the magnetherm device used and MG63 cells were successfully cultured and exposed to a characterised magnetic field (H. S. Huang and Hainfeld 2013). Subsequent coomassie staining confirmed that exposure to an applied magnetic field (AMF) alone did not affect cells, whilst mNP labelled cells exposed to an AMF showed a considerable decrease in cell attachment, morphology and size, representative of apoptotic/necrotic features. If time had allowed, I had planned a series of experiments to further analyse the effects of the AMF on the MG63 cells; initial cell viability staining would be carried out to confirm cell death, followed by annexin V staining to identify apoptosis. Further TEM imaging could be applied to further identify the mechanism of cell death. As shown in figure 5-14, the application of an AMF is known to result in the release of lysosome contents, therefore TEM analysis post hyperthermic treatment could identify mNP location within cells and verify if any particles were free in the cytoplasm, indicative of lysosomal bursting.

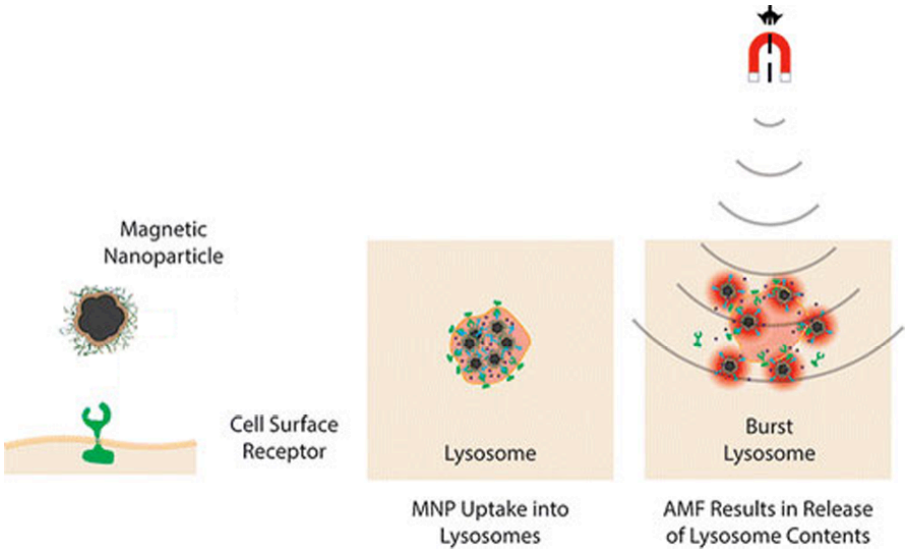

Figure 5-14: Iron oxide nanoparticles induce cell death by release from lysosomes following excitation by an alternating magnetic field (AMF) (image adapted from Domenech et al, 2013).

The vast majority of studies perform hyperthermic experiments at room temperature, however Glover et al recently carried out mNP hyperthermic experiments with a starting temperature of 37°C to mimic *in vivo* like conditions. The temperature was then raised by just 5°C by mNP-induced hyperthermia to 42°C in just 30 seconds. If time permitted, I would be keen to try and replicate this process of culturing cells at a baseline of 37°C before hyperthermic treatment.

5.7 Supplementary Data

During the course of this final chapter, several other magnetic nanoparticles were assessed for their biocompatibility and heating potential *via* the magnetherm, however to date no others qualified for future study. The magnetic field parameters was investigated previously by a postdoctoral researcher to optimise the magnetherm device for hyperthermic experiments however the frequency range and magnetic field strength was curtailed towards more biological and clinically relevant conditions (Deatsch and Evans 2014; A. C. Silva et al. 2011a).

A commercially available SPION formulation were acquired from collaborators in Liquids Research Limited (LRL, UK). These SPIONs had a ~ 13 nm core and a DMSA (dimercaptosuccinic acid) biocompatible layer. They were evaluated in terms of biocompatibility and heating potential using the protocols within this chapter. Although not conventionally used, DMSA is a well-known molecule, considered non-toxicand orally administrated as a chelating agent to remove heavy metals from an organism representing its biocompatibility (M. P. Garcia et al. 2005; Miller 1998). DMSA has also verified its biocompatibility *in vivo* with mouse studies (M. P. Garcia et al. 2005) as well as non-human primates (Monge-Fuentes et al. 2011). Silva et al assessed the biocompatibility and uptake of both magnetic and gold NPs decorated with DMSA on mesenchymal stem cells; both types of NPs showed excellent viability but only mNPs were proficient for magnetic targeting *in vivo* (L. H. Silva et al. 2016). Unfortunately, the compromise between the biocompatibility/toxicity of these particular SPIONs and the concentration required to produce hyperthermic temperature profiles was unattainable, as shown in figures 5-15 and 5-16 respectively. Whilst a mNP concentration of 0.01 $mg.ml^{-1}$ was deemed the most biocompatible for biological experiments (figure 5-15), this concentration only permitted a modest change in temperature was observed that did not reach hyperthermic temperature profiles (figure 5-16). Interestingly, it has been previously reported that dispersed single magnetic nanoparticles were able to increase the temperature of their immediate surroundings within a magnetic field, in an amplitude dependent manner, without increasing the temperature of the bulk solution (Creixell et al. 2011; Krpetić et al. 2010). Perhaps further investigations using these mNPs may identify whether this could occur. Figure 5-17 and 5-18 show the temperature elevation during magnetherm experiements of

both DMSA and PEG coated mNPs at 0.1 $mg.ml^{-1}$ concentration at various characterised frequencies. No strong correlation was observed with an increased frequency on temperature between 100-130 kHz however a frequency of 200kHz showed a notable increase in temperature although this frequency is not considered biologically applicable. A frequency of 115 kHz provided the most biologically appropriate condition as well as consistent and high heating temperature without compromising cell viabilty and was subsequently selected for experiments conducted within this study.

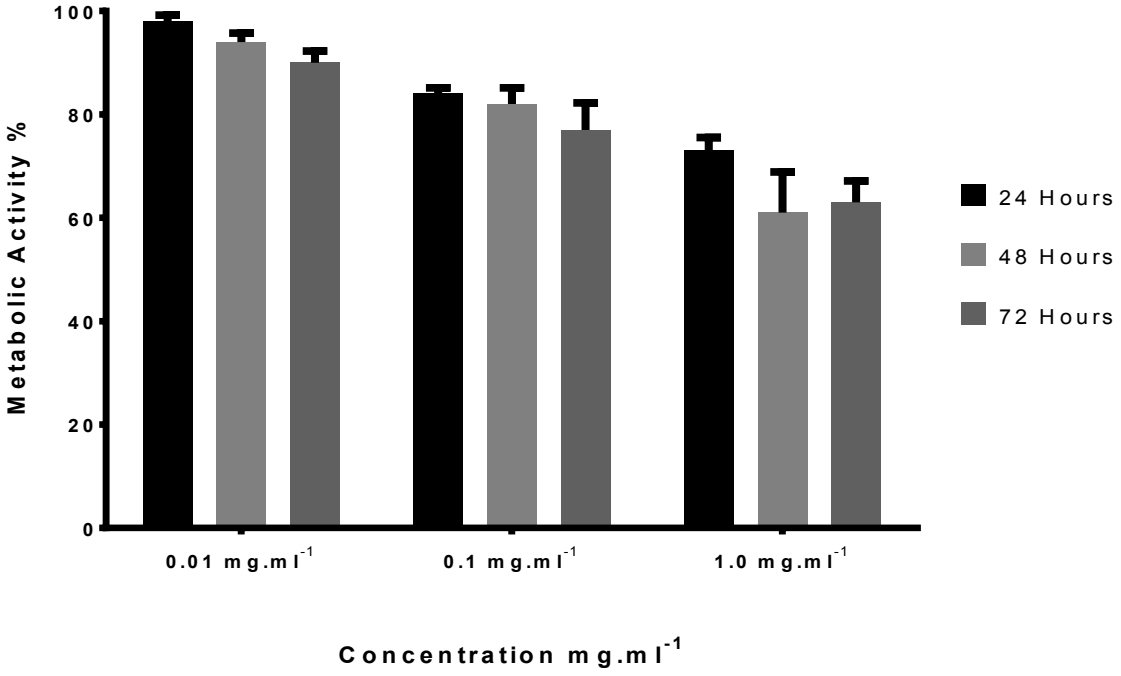

Figure 5-15: Metabolic activity of MG63 cells following incubation with LRL magnetic nanoparticles. MTT analysis of MG63 cells treated with 0.01, 0.1 and 1.0 mg.ml^{-1} mNPs for 24, 48 and 72 hours (n = 5; error bars indicate SD).

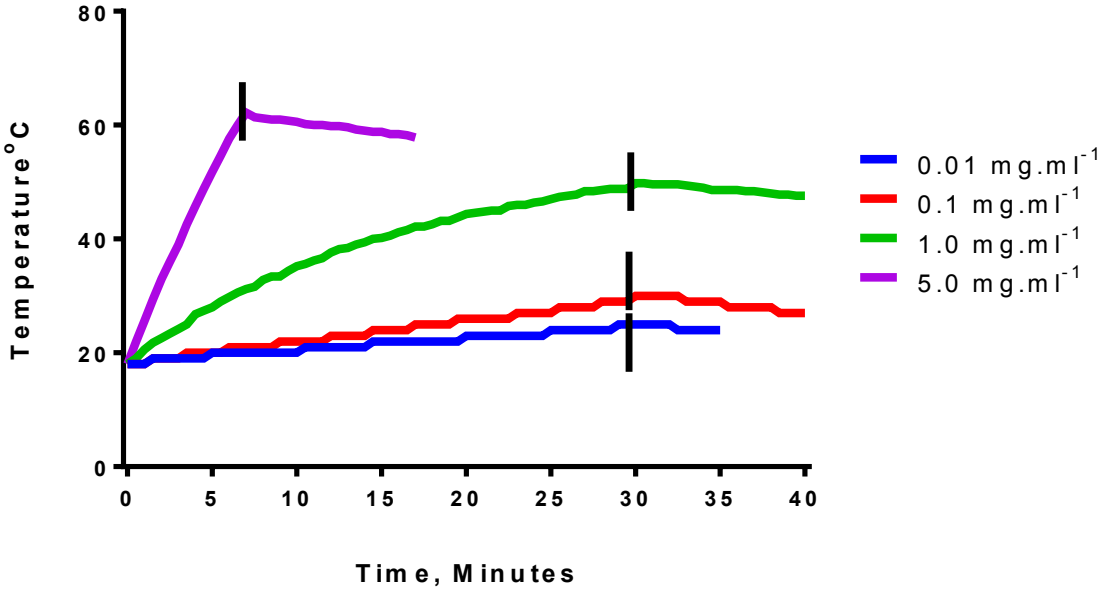

Figure 5-16: Temperature profiles of LRL mNPs stimulated in the magnetherm. Concentration used were 0.01, 0.1, 1.0, and 5.0 mg.ml^{-1}, with a characterised magnetic field (volt= 27.2, current= 9.3, frequency= 115kHz, nanotherics, UK). The magnetherm device was switched off after 30 minutes or once a hyperthermic profile (42-45°C) was achieved, indicated by the black dash.

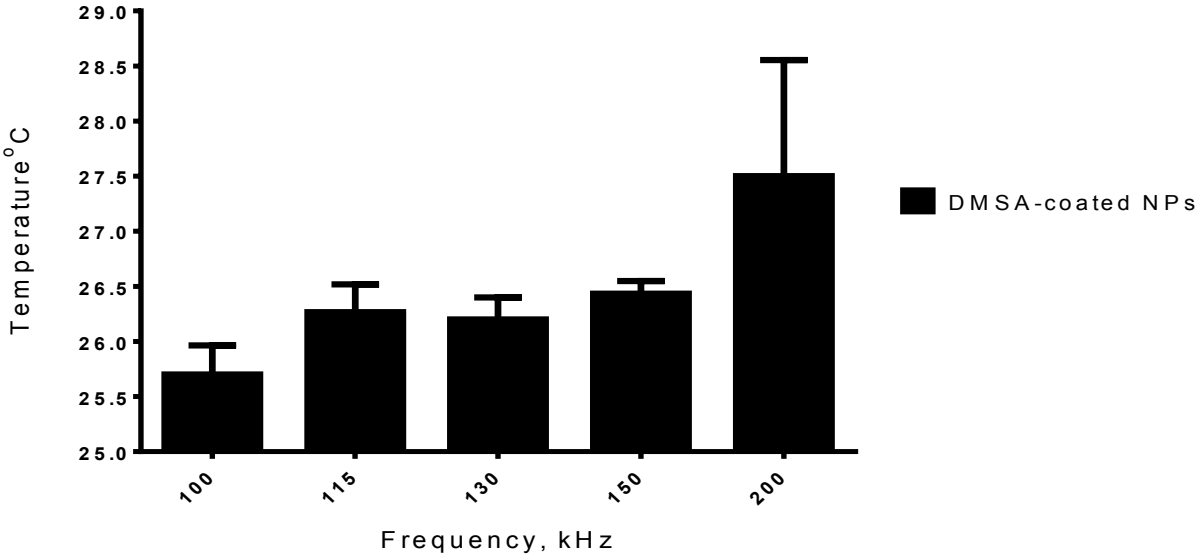

Figure 5-17: Temperature profiles of LRL mNPs at 0.1 mg.ml^{-1} stimulated by the magnetherm device at a range of frequencies. Magnetic field strength was maintained (volt= 27.2, current= 9.3) after 20 minutes.

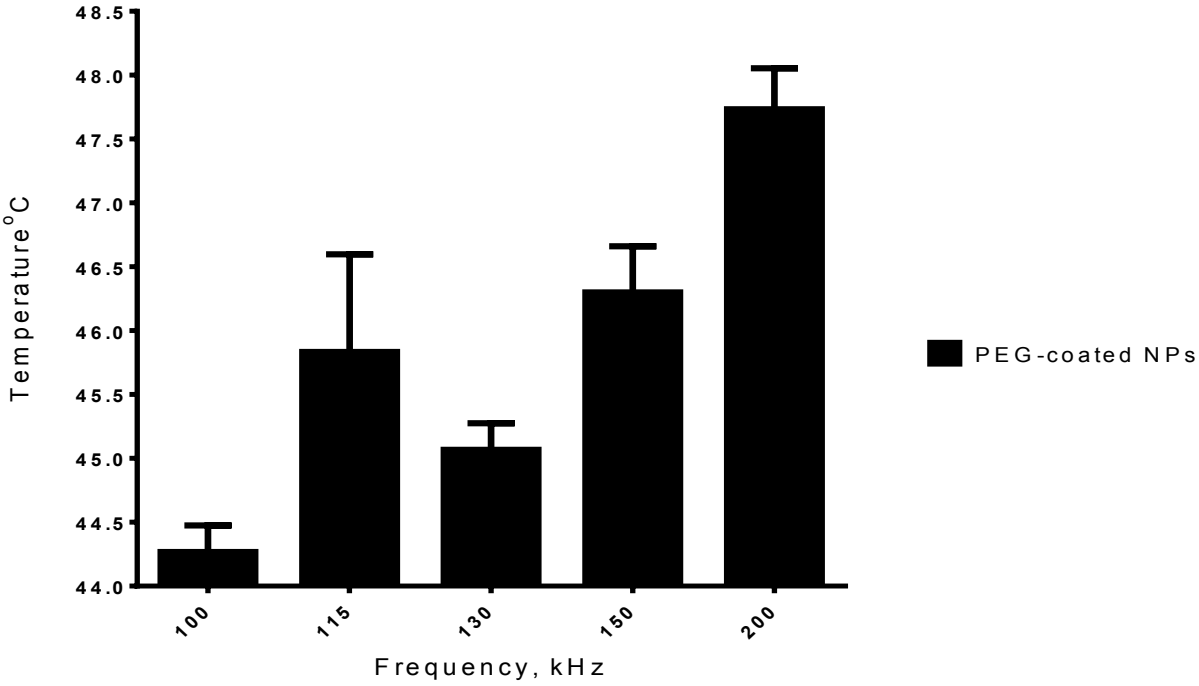

Figure 5-18: Temperature profiles of PEG coated mNPs used throughout this study, at 0.1 mg.ml^{-1} stimulated by the magnetherm device at a range of frequencies. Magnetic field strength was maintained (volt= 27.2, current= 9.3) after 20 minutes.

Chapter 6

6 Final Discussion

6.1 Nanoparticles in Hyperthermic Cancer Treatment

Although nanomedicine is considered a promising field with exciting prospects for the diagnostics and clinical treatment of human disease, important parameters such as the biodistribution, biological interaction and toxicological effects of new nanomaterials must be carefully assessed before actual clinical use (Nikolai Khlebstov et al, 2010; Ruchi Roy et al, 2014). Many nanoparticles (NPs) have the ability to absorb energy (magnetic pulse, laser light, ultrasound etc) and turn it into heat. The use of nanothermal therapy as a viable future option for cancer treatment has been recently discussed (Chatterjee et al. 2011; Krishnan et al. 2010). It is noted that researchers have to focus their attention not only on the NP heating efficacy, but also on parameters such as NP blood half-life, toxicity, organ distribution and renal clearance. To date a number of studies have made the successful leap from *in vitro* to *in vivo* with encouraging results (G. Kandasamy and Maity 2015a; Muldoon et al. 2005). The following discussion sections will detail the key *in vitro* and *in vivo* studies for both gold and magnetic naonparticles that have been carried out to date, including those that have achieved clinical trial status. The ultimate goal of this field of research looks forward towards using gold or magnetic nanoparticles as successful, practical thermal agents in cancer treatment. One consideration when using NPs *in vivo* is the route of administration. For NP intravenous administration - which is the standard to date for accessing tumours, researchers have exploited the phenomenon of the enhanced permeability and retention effect (EPR), which allows the natural 'passive' accumulation of NPs into tumours (Nichols and Bae 2014). This is due to the increased leakiness of tumour blood vessels allowing for NPs to seep into the disorganised vascular architect and accumulate, as shown in figure 6-1 (Nichols and Bae 2014). Accumulation is further amplified through the lack of functional lymphatic drainage in tumours that inhibits the removal of extravasated NPs leading to increased retention times (Baetke et al. 2015). The EPR effect can be further increased through 'active' targeting with nanosystems designed to increase the targeting, uptake and retention of NPs to specifically targeted sites (Cherukuri et al. 2010; Cole et al. 2011b).

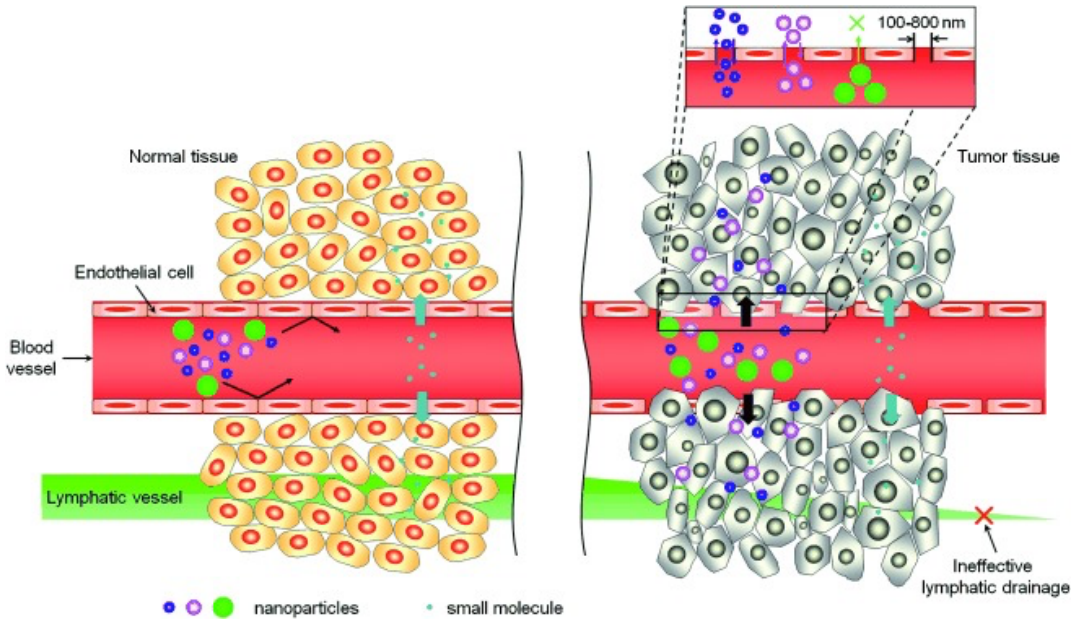

Figure 6-1: Nanoparticle transport to cancerous tissues *via* the enhanced permeability and retention (EPR) effect. Nanoparticles of various sizes accumulate more in cancerous tissues (right) than normal tissues (left) due to disorganised vasculature and impaired lymphatic drainage (Sun et al, 2014).

The interaction, consequences and fate of NPs within a biological system remain complex and it is important for researches to understand the cell-nanoparticle interactions in order to predict potential toxicity issues (Verma and Stellacci 2010). In this regard, a further consideration for NP use *in vivo* is NP interaction with proteins within a biological fluid, such as growth media *in vitro* or blood *in vivo*, which are able to adhere to and essentially coat NPs, thereby influencing the overall NP performance. The type and amount of these proteins that attach onto NPs, termed “protein corona”, could lead to a very different cellular responses as compared to uncoated NPs, by altering the ‘cell vision’ (i.e. how a cell type views a particular NP) (Mahmoudi et al. 2012; Saptarshi et al. 2013). Both the NP protein corona and the cell vision of different cell types could holistically lead to restricted clinical use of NPs and should therefore be considered, or negated, when designing a NP-based platform for bioapplications.

6.2 Gold Nanoparticles as Photothermal Agents

6.2.1 Gold Nanoparticle Biocompatibility *In Vitro*

Bulk gold is well known to be chemically inert and gold-based compounds have been used in clinic, such as anti-inflammatory agents to treat rheumatoid arthritis. The chemical reactivity for nanoscale gold particles, however, is different to bulk gold. The debate over the biocompatibility and potential toxicity of GNPs has been extensively discussed within the literature (Ellen E. Connor, 2005; Pratap C. Naha, 2015; Hirak K. Patra, 2007; Show-Mei Chuang, 2013). However only a modest consensus has suggested that GNPs themselves may be inherently toxic (Ahamed et al. 2016; A. M. Alkilany and Murphy 2010; A. M. Alkilany et al. 2012; Karakoçak et al. 2016). With GNPs being explored as prospective drug delivery agents (Coelho et al. 2015), contrasting agents (Q. Wu et al. 2015), gene delivery agents (Bishop et al. 2015) and, in this case, hyperthermic agents (Hainfeld et al. 2014), the potential short-term and long-term toxicity must be fully realised in order to safely and reliably translate for clinical application.

6.2.1.1 Cytotoxicity is Dictated by Size and Shape: Nanorods and Nanoprisms

GNP toxicity has been directly linked to their size and shape. There have been numerous studies in this regards, table 6-1 summarises some of those studies, indicating the cell culture model used and the size and shape of the GNP. As the table shows, the response is varied.

Table 6-1 Summary of Studies showing GNP toxicty observations (adapted from Clarence S. Yah et al, 2013).

Type exposed organism	Size of GNPs	Route of Exposure	Dose	Surface Coating	Test	Biological Effect	Ref
Male WU Wistar-derived rats	10, 50, 100 and 250 nm	Intravenously	1 mL	Spherical GNPs	Organ index	The GNPs were found in the liver and spleen. 10 nm was presnt in all blood, liver and spleen. GNPs found in the liver and macrophages	[53]
Female mice	2, 40 and 100 nm	Intratracheal	1.4-1.6 mg/kg	Negatively charged monodisperse and spherical GNPs	Organ index (liver)	GNPs found in liver and macrophages	[88]
Mice	13.5 nm	Oral, Intraperitoneal routes and tail vein intravenous injection	137.5-2200 µg/kg	Spherically citrate-coated	Animal survival, weight, heamotology, organ index	High GNP induced decrease in body weight, red blood cells. No effect at low level. Oral admin caused a significant decrease in body weight, spleen index and red blood cells	[14]
BACB/C Mice	3-100 nm	Intraperitoneal	8 mg/k/week	None	Physical and behavioural examination	GNPs of 8, 12, 17, 37 nm induced fatigue, loss of appetite, change of fur colour and weight loss. Most died within 21 days. 3-5 nm did not induce sickness	[68]
Male Wistar rats	20 nm	Tail-vein, intravenous injection	0.2 mL (0.01 mg/kg)	GNPs	Organ index	GNPs accumulated and persisted in the liver and spleen and other organs. Many up and down regulated gene were expressed.	[37]
Male mice C57/BL6	~12.5 nm	Intraperitoneal	40-400 µg/kg/day	Colloids citrate coated GNPs	Animal survival, weight, heamotology morphology and organ index	GNPs were able to cross the vrain barrier and accumulate in neural tissues but no toxicity evident but there was uptake in the spleen, kidney and liver.	[87]

Rat	5 nm	Tail vein intravenous and Intratracheal	570-870 µg/kg	PEG coated GNPs	Organ index	PEG coated GNPs accumulated mostly in liver and spleen	[90]
Male mice	~15 nm	Tail vein intravenous and Intratracheal	150-200 µL	Human serum albumin, GNPs	Organ index	Functionalised GNPs accumulated in the hippocampus, thalamus, hypothalamus and the cerebral cortex	[91]
BALBc/c AnNHsd female mice	~2.5 nm	Subcutaneous injection	200 µL	PEG-TMPC coated	Organ index	100% survial at all the different concentrations of PEG-TMPC and TMPC. Particles present in the organs but TMPC is not suitable for *in vivo* studies	[92]

Smaller GNPs were reported to elicit greater toxicity than larger GNPs, where particles <3 nm were observed to intercalate in DNA (Hung-Jen Yen, 2009). A study by Goodman et al also demonstrated cytotoxicity of cationic 2 nm diameter gold nanospheres (Goodman et al, 2004). However control experiments, assessing the same GNPs with a negatively charged surface, tested in the same cell line with the same dose were not found to be toxic, as the cationic GNPs interacted with the negatively charged cell membrane and caused disruption. Therefore, such studies should always be thorough, to determine the correct parameter influencing toxicity.

The perspective of smaller particle sizes conferring cytotoxicity has been challenged recently by Mingfei Yao et al, who demonstrated that an increase in particle diameter promoted the depolarisation of mitochondrial membrane potential, an early indicator of apoptosis (Yao et al. 2015). Therefore size is not always a clear determinant for cell response.

Synthesised GNPs come in a variety of shapes, including rods, spheres, tubes, wires, cubic, hexagonal triangular and tetrapods. GNP shape is known to influence cytotoxicity, with more sophisticated geometries associated with a higher cytotoxic effect (Carnovale et al. 2016). For example gold nanorods are often cited as a more toxic geometry as compared to nanospheres (Yinan Zhang et al, 2012), nanocages (Y. Wang et al. 2013b) and nanohexapods (Y. Wang et al. 2013b). The *in vitro* cytotoxicity of gold nanorods in a human lung adenocarcinoma cell line was recently published (Ying Tang, 2015). The study confirmed membrane damage within 4 hours of gold nanorod exposure while ROS production correlated to increased GNP concentration. In another study, gold nanorods with three varying aspect ratios were also evaluated for their cytotoxic potential across 6 cell lines (Show-Mei Chuang, 2013). All three nanorods induced a dose-dependent suppression on cell growth to varying degrees, with ROS induced apoptosis and cell cycle inhibition considered the main route of GNP cytotoxicity. Conversely, the nanorods used in this project exhibited low cytotoxicity even at high concentrations and produced similar biocompatible features as their gold nanoprism counterparts.

The associated toxicity of gold nanorods in particular may be due to the synthesis process rather than the actual geometry, as previously highlighted by Alkilany and co-workers (Alaaldin M. Alkilany et al. 2009). As previously highlighted in chapter 3, section 3.5.4, CTAB is a cationic surfactant conventionally used by groups to "grow" gold nanoseeds into nanorods, could indeed be the the primary source of toxicity. CTAB is typically removed *via* purification or desorption techniques, however these processes are often inadequate at removing all CTAB molecules and thus free CTAB molecules can remain within the nanorod solution leading to toxicity (A. M. Alkilany and Murphy 2010). Alkilany and Murphy (2009) validated this claim when they centrifuged GNP solutions and removed and analysed the supernatant (containing free CTAB molecules). They observed the concentration of CTAB in the supernatant was able to cause cytotoxicity and a reduction in cell viability. The study may explain the associated toxicity of gold nanorods and other geometries both *in vitro* and *in vivo* (A. M. Alkilany and Murphy 2010). In addition, gold nanorods synthesized in the presence of CTAB conjugates have been shown to lead to toxicity in both cells and in animals (Akiyama et al. 2009; Wan et al. 2015), with CTAB shown to damage mitochondria and increase the activation of intracellular ROS, inducing cell apoptosis and autophagy (Wan et al. 2015). However, despite its use in the production of the gold nanorods used in this project, our collaborators have taken measures to remove as much CTAB as possible from the gold nanorod solution (chapter 3, section 3.3.1), which may clarify the low toxicity levels observed throughout the project.

6.2.1.2 Variation in Cell Response Between Different Cell Lines

The general outcomes drawn from various studies are unfortunately, inconclusive due to the inherent variations in how the different research groups carry out experiments, including using different cell lines, different NP sizes, different surface coatings, different concentrations/doses and different time points. For example, with regards to cell lines, GNPs have been shown to lead to cell death in A549 cells (human hepatocellular liver carcinoma) in a dose dependent manner, but not in HepG3 (human hepatocellular) or BHK21 (baby hamster kidney) (H. K. Patra et al. 2007a). The study confirmed cell death occurred through Poly ADP-ribose polymerase (PARP) activation, a protein which can be cleaved and leads to the downstream activation of caspases and cell death (H. K. Patra et al. 2007a)

while oxidative stress and increased lactacte dehydrogenase leakage was also induced in A549 cells, again in a dose dependent manner (Ying Tang, 2015).

The results in chapter 3 confirmed the relative inert nature of both gold nanorods and nanoprisms (without heating) in the two cell lines, with no differences noted between MG63 and MCF-7 cells in either monolayer or spheroid culture. This was surprising, given that the gold nanorods that were synthesized in the conventional "see-mediated" method utilizing the CTAB surfactant. Gold nanoprisms were synthesised without the use of CTAB and thus no toxicity was anticipated.
The results in chapter 3 did highlight variation in GNP internalization based on geometry, with nanoprisms being internalized with far greater efficiency than nanorods. The size of GNPS is known to influence both the rate and extent of cellular uptake, with smaller particle sizes proving more efficient (Chithrani et al, 2006). A study by Gao et al adopted a mathematical approach to identify an optimum particle size of 27-30 nm to permit the most efficient internalisation (H. Gao et al. 2005). However, whilst there were no practical experiments to support this claim, the gold nanoprisms used in this project were much larger and quickly internalized by both cell lines.

6.2.1.3 GNP Coating and Cytotoxicity

The biocompatibility of the gold nanoprisms and nanorods may be attributed to their functionalization with 5 kDa PEG chains. The PEGylation of NPs has been shown to improve systemic performance, decreasing inflammatory responses in a PEG dose-dependent manner and increasing endocytosis into lung alveolar endothelial cells (Ibricevic et al. 2013). PEGylated NPs have also been shown to increase cancer cell uptake, reducing nonspecific accumulation and prolonging blood circulation by decreasing the rate of opsonisation and thus RES clearance (Hongwei Chen et al. 2013; J. Liu et al. 2013c).

The PEGylation of NPs has also been demonstrated to increase the accumulation and residence time within tumours while also enhancing the affect of photothermal treatment *in vivo* as compared to bare GNPs, possibly due to the increased uptake and tumour accumulation of PEGylated GNPs (J. Bai et al. 2014a; Huiyu Liu et al. 2013b). The pharmacokinetics of PEGylated GNPs illustrated the passive accumulation of both gold nanoshells and nanorods in tumourss within mice, while

PEG functionalisation preserves GNP stability against agglomeration at physiological conditions during systemic circulation (Constantin et al. 2013; Terentyuk et al. 2013).

One of the major advantages to the use of GNPs over other NPs is their 'active' surface chemistry (Pissuwan et al. 2006). GNPs can be functionalised with ease by a wide range of thiolated molecules with very high affinity (Beatriz Pelaz and del Pino 2012) and can be easily functionalised with various ligands (Constantin et al. 2013), antibodies (Di Pasqua et al. 2009) and proteins (Di Pasqua et al. 2009). Although geometry (Chithrani et al. 2006), size (Freese et al. 2012) and functionalisation (Y. Jiang et al. 2015) can all affect the GNP uptake, it seems the most conventional route is receptor-mediated endocytosis (Dykman and Khlebtsov 2014; N. Oh and Park 2014). Our results support a combination of endocytosis and pinocytosis for nanoprism and nanorod cellular uptake.

The intracellular distribution of GNPs has been previously studied, with consensus supporting storage in vesicles, howvever GNPs are also reported to leave the cell *via* exocytosis. Chithrani and Chan (2007) detailed the elimination of GNPs from cells, which was size dependent, with smaller GNPs removed faster than large GNPs in a practically linear pattern (14, 30, 50, 74, 100 nm), while gold nanorods seem to be removed from cells at a greater rate than spheres. Chan et al group also observed a similar pattern on the uptake rate of sphere and rods, with spheres showing more efficient uptake into cells than rods, with a higher aspect ratio of rods also correlating to a lower uptake rate (Chithrani et al. 2006; Chithrani and Chan 2007; E. C. Cho et al. 2010a).

6.2.2 Gold Nanoparticle biocompatibility in 3D Culture

Traditional *in vitro* studies are performed in 2D, with cells cultured on plastic or glass substrates which provide a lack of relevance to the *in vivo* environment, while the behaviour, intracellular fate and toxicity of NPs in *in vitro* studies often exhibit poor consistency when scaling to *in vivo* models (Joris et al. 2013). Testing NP platforms immediately within animal models does present unique challenges, including ethical issues, while animal models do not correlate to human systems. The economical issues, practicality and feasibility of *in vivo* studies also limit their

use. To bridge the gap between *in vitro* and *in vivo*, with the aim to produce more clinically relevant data, 3D cell culture models are instrumental.

In this project multicellular tumours spheroids were employed alongside corresponding monolayer cell cultures. The standard biocompatibility assessment in chapter 3 did not reveal discriminate differences between the 2D and 3D models, as reported by previous studies that detail 3D models as more resistant to toxicological affects than their 2D counterparts (Jungwoo Lee et al. 2009; H. Tseng et al. 2015; Wills et al. 2016). Recent studies have challenged the hypothesis of 3D cultures being more resistant to toxicity than 2D models, often citing difficulties with colorimetric dye-based cytotoxic assays (such as MTT assays) in 3D cultures (Bonnier et al. 2015). In addition, other groups have observed 3D models as more susceptible to nanotoxicity when compared to 2D models, with different cytotoxic mechanisms occuring in either 2D or 3D culture upon NP exposure (Sambale et al. 2015; Theumer et al. 2015; Miao Yu et al. 2012b).

6.2.3 Gold Nanoparticle Induced Hyperthermia *via* Photothermal Treatment

6.2.3.1 Modest Screening Provides Ambiguous Results

The results from chapters 3 and chapter 4 confirm the that both cell lines labelled with either gold nanoprisms or nanorods and laser treated resulted in hyperthermic temperature profiles, leading to cell death (Raji et al. 2011a). The cell death was apparent in both 2D and 3D cultures, confirming that the laser was capable of penetrating the spheroids, which were approximately 200 μm (Madsen et al. 2015).

Many other groups carried out experiments detailing photothermal treatment on a plethora of monolayer cancer cell cultures using various GNP platforms with success (C.S et al. 2012; Chiu et al. 2015; Gobin et al. 2010; L. Mocan et al. 2015a; Raji et al. 2011b; L. Yang et al. 2015). The majority of studies confirm a decrease in cell viability and increase in apoptosis using standard viability assays and focusing on a single apoptosis pathway (Alfranca et al. 2016; Gobin et al. 2010; Y. Guo et al. 2013; X. Huang et al. 2006b). Unfortunately these studies do

not clearly distinguish if cell death occurred *via* apoptosis or necrosis and of the two, which appeared the more dominant process. There are no studies which have screened both 2D and 3D cultures for a wide range of RNA and protein targets to identify the various pathways activated during cell death, as was carried out during this project.

To somewhat answer these apparent shortcomings, groups have focused on speficic markers, for example evaluating the intracellular events after photothermal treatment by identifying increases in heat shock protein expression (Ali et al. 2016; Leung et al. 2013; L. Yang et al. 2015) and/or apoptosis *via* caspase 3 expression (C.S et al. 2012; Raji et al. 2011a). Although caspase 3 is a good indicator of cell death *via* apoptosis, caspase 3 is actually an effector caspase mediating apoptosis once activated by either the intrinsic, extrinsic pathway, while also playing a role in lysosome degradation, providing ambiguous results (Oberle et al. 2010). To the best of our knowledge only a few groups have attempted to decipher the more intrinsic intracellular events and pathways of apoptosis upon photothermal laser irradiation, including the analysis of Bcl-2 family members and proteins associated with mitochondria (Abadeer and Murphy 2016; Perez-Hernandez et al. 2015; Shiwen Zhang et al. 2014).

6.2.3.2 Identifying the Intracellular Events of Photothermal Treatment

In this project, we attempted to characterise photothermal-induced apoptosis, by screening a variety of apoptotic markers both at the genetic and proteomic level. Experiments were carried out using two cell lines, two GNP types and two cell culture models, with a view to clarifying any differences observed. Although the intrinsic pathway appeared the dominant protagonist for apoptosis, our results also showed a more broad activation of both the extrinsic pathway and cathepsin mediated apoptosis upon photothermal treatment (K. Ahmed et al. 2015a; Shellman et al. 2008). These more novel pathways are orchestrated by cellular oxidative stress as well as autophagy (Shellman et al. 2008). Our results further suggested that hyperthermia-induced apoptosis was activated primarily *via* ROS accumulation as well as protein degradation and activation of pro-apoptotic markers.

6.2.4 Gold Nanoparticle Hyperthermia *In Vivo* and the Clinic

The *in vivo* performance and associated toxicities of GNPs has been discussed (Nikolai Khlebtsov, 2010; Carrie A. Simpson et al, 2015; Xiao-Dong Zhang, 2011; Nikhat J Siddiqi, 2012; Mayara Klimuk Uchiyama, 2012). GNPs have been seen to accumulate at different rates within different tumour models, where the accumulation of GNPs was 5 times higher in breast cancer tumours compared to fibrosarcoma tumours, suggesting tumour type is influential on GNP accumulation (Dam et al. 2015). Interestingly, this group also noted discrepancies in the GNP half-life in males and females, although no hypothesis was put forward. Aside from tumour accumulation, GNPs also accumulate in the spleen and liver (Black et al, 2013). The particle shape appears to be a factor in determining the half-blood life and clearance of NPs, with nanospheres retained for longer in circulation as compared to disks, rods and cages (Black et al, 2013). As with toxicity studies, comparisons are often difficult due to variation in experimental design, including the administration route, passive/active targeting, concentration, exposure time as well as individual particle features (shape, size charge etc). However, in summary most groups showed no significant permanent toxicity associated damage when using *in vivo* animal models (Sung Gu Han et al, 2015; Samuel A. Jensen, 2009), even up to 120 days after exposure (Goel et al, 2009).

The use of GNPs for the thermal tumour therapy was first documented in mice in 2003 by Hirsch et al (Hirsch et al. 2003). Histological samples confirmed the irreversible tissue damage of irradiated tumourss containing gold nanoshells.

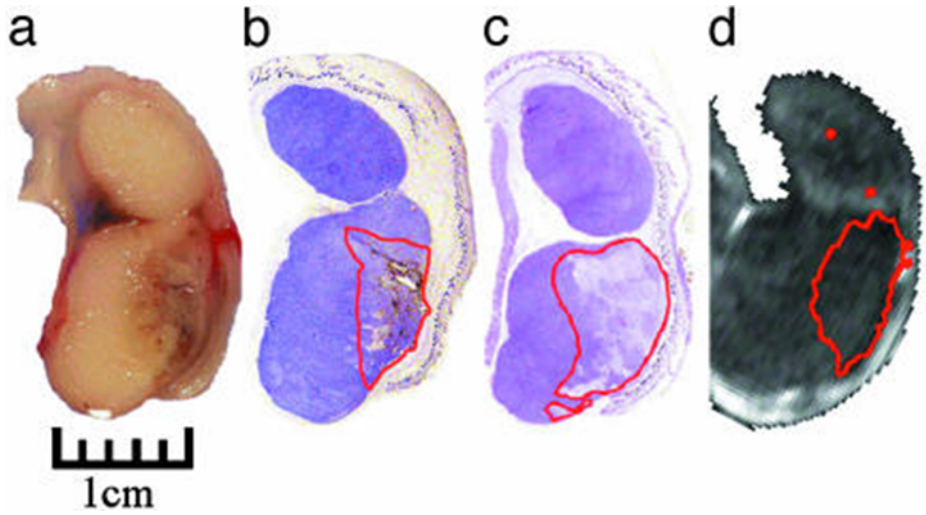

Figure 6-2: Effects of GNP photothermal treatment. *a*) Gross pathology after *in vivo* treatment with nanoshells and NIR laser reveal hemorrhaging and loss of tissue birefringence beneath the apical tissue surface. (*b*) Silver staining of a tissue section reveals the region of localized nanoshells (outlined in red). (*c*) Hematoxylin/eosin staining within the same plane clearly shows tissue damage within the area occupied by nanoshells. (*d*) Likewise, MRTI calculations reveal an area of irreversible thermal damage of similar dimension to *a, b*, and *c*. (taken (Hirsch et al. 2003)).

Since this report, many other *in vivo* animal studies have been conducted with promising results (Bogdanov et al. 2015; Dickerson et al. 2008; Melancon et al. 2008; D. P. O'Neal et al. 2004a; Rengan et al. 2015). Systemic studies focused on GNP biodistribution, has shown that smaller GNPs result in a more widespread distribution in both rat (De Jong et al. 2008) and mouse organs (Hillyer and Albrecht 2001) *via* intravenous injection and oral intake, respectively. A comprehensive systemic review by Mohan Singh et al in 2015 detailed the use of GNP thermal therapy solely for gastrointestinal cancers with eleven studies that were conducted using rodents and demonstrated excellent therapeutic outcomes. However, in another animal trial, more severe effects have been reported by Chen and co workers, where GNPs within a size range (8-37 nm) led to various side-effects including fatigue, loss of appetite, change of fur colour, and weight loss, while more stark characteristics such as crooked spines and loss of lung structural integrity were also noted (Y.-S. Chen et al. 2009). While Zhang and co-workers(2011) demonstrated an increase in alanine transaminase and aspartate transaminase levels, clinical markers signifying liver damage upon the introduction of PEGylated GNPs at 10 nm and 60 nm, within mice (Xiao-Dong Zhang, 2011).

Despite this, GNP thermotherapy has shown more promising potential in a number of studies including treatment for prostate cancer (Terentyuk et al. 2013), pancreatic cancer (C. R. Patra et al. 2010) and breast cancer (Jihyoun Lee et al. 2014b).

The success of *in vitro* and *in vivo* studies has lead to clinical trials. In 2011, a Phase I clinical trial confirmed GNP biocompatibility while a predicted yet controlled fever occurred in patients due to immune activation and inflammation (Elsabahy and Wooley 2013; Libutti et al. 2010). The study not only showed how the use of PEGylated 27 nm colloidal gold nanospheres, even at previously believed toxic concentrations, can be tolerated by the body, but also demonstrated the efficacy of targeting systems to traffic GNPs to tumour tissue (Libutti SK, 2010).

Currently, only one GNP photothermal treatment system has progressed to clinical trials produced by Nanospectra Biosciences, Inc., founded in 2002. The company focuses on commercialising photothermal therapeutics for the destruction of solid tumours (Abadeer and Murphy 2016). While a US Food and Drug Administration (FDA) approved AuroLase® pilot study using silica-gold nanoshells (AuroShells) has been completed, for the photothermal treatment of patients with primary and metastatic lung tumours. AuroLase Therapy involves the use 150 nm PEGylated gold nanoshells. The nanoshells are injected intravenously, while the PEGylation allows GNPs to circulate in the blood long enough to accumulate in tumours *via* the EPR effect (Abadeer and Murphy 2016). As NIR laser penetration is ~10 cm, deep seated tumours may not be adequately treated and therefore fibre optic NIR lasers will be inserted into the body to alleviate this fundamental issue (Abadeer and Murphy 2016; Ralph Weissleder 2001b). The use of a fibre optic NIR laser has been proved effective by Schwartz and co-workers (2009) who successfully utilised photothermal therapy in a venereal tumour in a canine brain model (Schwartz et al. 2009). A second AuroLase® pilot study has also been completed using AuroShells for the treatment of neck and head tumours. Although both studies have been completed, the results have not yet been publicised (Pedro Pedrosa, 2015). A schematic of the GNP core is shown in figure 6-3.

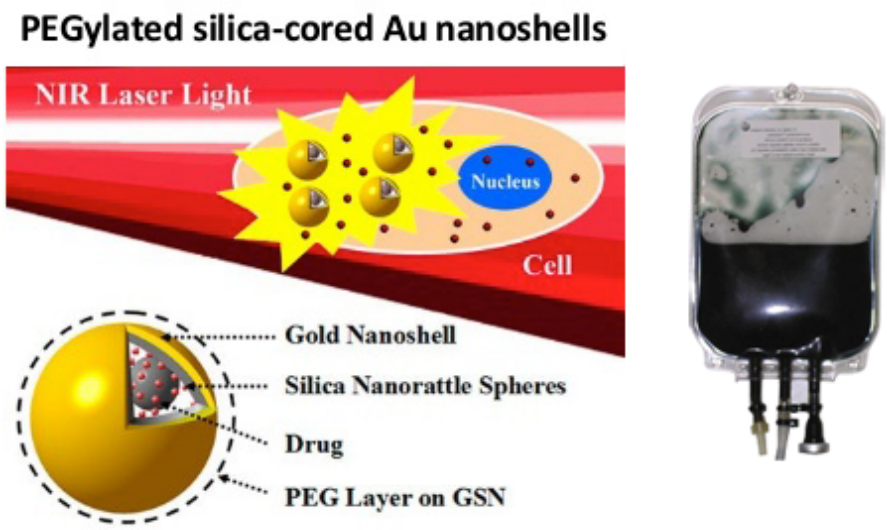

Figure 6-3: The AuroShell GNPs currently being used in the AuroLase clinical trial program. While information is limited; the image on the left shows the particle and its mode of action, whilst the image on the right illustrated an IV bag of AuroShells. (Image adapted from Nanospectra Biosciences;http://nanospectra.com/our-technology/products/aurolase-therapy).

6.2.5 GNPs as an Adjunct to Established Cancer Therapies

While GNP photothermal therapy has been highlighted as a viable, alternative therapy for cancer treatment, GNPs have also recently been investigated as an adjunct to established cancer therapies (J. Lee et al. 2014a; Lucian Mocan et al. 2016). For example, photothermal heating has been synergistically used to reduce the amount of radiation dose required during radiotherapy (James F. Hainfeld, 2014) and for the dual modality of targeted chemotherapeutic delivery and hyperthermia to cells (Hussaina Banu, 2015). Jaesook Park et al, (2015) showed the effectiveness and range of uses of hollow GNPs for triple combination therapy and CT imaging, with the hollow core housing chemotherapeutic payloads. The GNPs also featured a high x-ray absorption capability, which increased the effect of radiotherapy while its own heating capability contributed to hyperthermic profiles. The combination of hyperthermia, radiotherapy and chemotherapy dramatically delayed tumour growth (by a factor of 4.3) and reduced tumour weight (6.8-fold) compared to control tumourss, while the ability of GNPs as contrast agents for CT scans were in accordance with previous literature (Ahn et al. 2013). This extensive study highlights the huge potential of GNPs as contrasting agents and as nanoscale heaters.

6.3 Magnetic Nanoparticles as Hyperthermia Agents

6.3.1 Magnetic Nanoparticle Biocompatibility

As with GNPs, the toxicity of mNPs, in particular SPIONs, have been well documented in several comprehensive reviews (Sophie Laurent et al. 2012b; G. Liu et al. 2013a; Mahmoudi et al. 2011; L. H. Reddy et al. 2012a). The importance of a biocompatible coating surrounding mNPs has been well established, with Miao Yu et al demonstrating the potentially cytotoxic nature of bare SPIONs, while SPIONs coated with PEG or dextran showed little toxicity in both 2D and 3D models (Miao Yu et al. 2012b). Morteza Mahmoudi's group further confirmed the uptake and cytotoxicity at both the cellular and molecular level with thirteen cell lines exposed to the same SPION at various concentrations (Mahmoudi et al. 2012). Not only did the study demonstrate that the toxicity levels of different cell types to SPION exposure varied, it also probed the potential detoxification pathways different cell types use to remove ROS and remain viable.

A number of studies have demonstrated, DNA damage (Mahmoudi et al. 2011), oxidative stress (Ivask et al. 2015; U. A. Reddy et al. 2015), mitochondrial damage (Unfried et al. 2009) and protein denaturation (Vanessa Valdiglesias et al. 2015b) of cells in the presence of mNPs. These toxicity issues are believed to occur upon internalisation of SPIONs, where iron oxide can be metabolised by heme oxygenease-1 to form haemoglobin and hence maintain iron cell homeostasis (Kumar and Faruq, 2011). However the increase concentration of iron within the body can lead to the production of free radicals that can lead to oxidative stress and eventual death of cells (Santhosh and Ulrih 2013).

Despite these potential pitfalls, the FDA and the European Medicines Agency (EMA) have both approved the medical use of selected iron oxide nanoparticles, which have been applied to human clinical trials for the treatment of brain cancer, glioblastoma (Bayazitoglu et al. 2013; Tombacz et al. 2015). For future medical applications, mNPs must show efficacy in biocompatibility and long-term stability i*n vivo* for use in thermotherapy treatment of cancer cells (Gobbo et al. 2015; C. S. Kumar and Mohammad 2011).

Our short study, in chapter 5, confirmed the low toxicity of dextran-coated mNPs, even at a relatively high concentration (0.1 $mg.ml^{-1}$), which was required for adequate hyperthemic temperature profiles (42-45°C) (Toraya-Brown and Fiering 2014). Successful cellular uptake into monolayer MG63 cells was observed, most likely due to the biocompatible dextran, which has been shown to increase mNP internalisation and also reduce mNP toxicity compared to bare and PEG coated mNPs (Miao Yu et al. 2012b). Dextran coated mNPs also boast an advantage in biological systems where they have been shown to prolong blood duration time allowing access to macrophages located in tissues such as lymph nodes, kidney, brain (Easo and Mohanan 2013).

6.3.2 Magnetic Hyperthermia *In Vivo* and the Clinic

The mNPs used in this project were able to generate heat upon exposure to an external alternating magnetic field (volt= 27.2, current= 9.3, frequency= 115 kHz) within 20 minutes, leading to a decrease in cell viability and change in cellular morphology indicative of apoptosis (P. Garcia et al. 2012). Although further analysis is certainly required, the experiments confirmed substantial cell death upon elevated temperature exposure, while cells exposed to AMF alone did not appear to show signs of cellular stress or apoptosis (Beik et al. 2016).

In 2011, Alsayed A.M. Elsherbini's group used mNPs to induce hyperthermia in mice implanted with subcutaneous Ehrlich carcinomas. Although the experiment was not entirely successful at destroying the entire carcinoma, it did demonstrate the dual modality capability of mNPs as both nanoscale heaters for hyperthermia and contrast agents for MRI (Elsherbini et al. 2011; Yallapu et al. 2011). Other *in vivo* studies of magnetic nanoparticles have shown more encouraging results with regards tumour destruction in animal models (Balivada et al. 2010; Espinosa et al. 2016; Hayashi et al. 2013; Ingrid Hilger 2013; J. H. Lee et al. 2011). Studies include systems that use magnetic targeting, by locating a permanent magnet over the tumour to increase SPION concentration in cancer cells, thereby diluting the concentration of SPIONs found in the spleen, liver and tissue (Min et al. 2010; Prijic et al. 2010).

Other groups are taking this forward by designing mNPs which can actively target tumour cells by incorporating targeting systems onto the mNP surface, for example ligands that bind to overexpressed receptors on tumour cells such as transferrin receptor 1 (TfR1) (K. Fan et al. 2012). MNPs have also been functionalised with Galactose-Carrying Polymers (M. K. Yoo et al. 2007), folic acid (Q. L. Jiang et al. 2014), PEG modified, cross-linked starch (Cole et al. 2011a) and homing peptides (A. M. Kruse et al. 2014) to increase their proximity to target cells. The competency of active targeting was demonstrated in SPIONs functionalised with anti-human epidermal growth factor receptor-2 aptamers, with hyperthermia induced at a 90-fold lower concentration than untargeted SPIONs (Kaur et al. 2016). Although a valuable component, active targeting systems *via* ligands, antibodies and peptides are influenced by the complex relationship of mNP shape, size, ligand density, surface hydrophobicity and are compromised with issues of non-specific binding which can influence their overall *in vivo* performance (Bertrand et al. 2014).

One of the first clinical trials using mNP based hyperthermia was conducted in 1991. In this clinical trial, mNP-mediated hyperthermia was performed in 23 brain tumour patients, while the results were still preliminary, an overall response of ~35% was recorded response rate was the ratio of responded cases to the total treated cases) (Kobayashi et al. 1991). A more recent brain tumour clinical trial was performed in 2006, in which patients with glioblastoma multiforme were treated with a combination of magnetic hyperthermia and radiotherapy. This showed promising results with no apparent toxicity, while the exposure of an external AMF was tolerated by the majority of patients with only minor side effects reported (Maier-Hauff et al. 2007). In 2001, Jordan and co-workers developed an alternating magnetic field heating (MFH) device that was made available for medical experiments and developed the world's first MFH (R) 300F-type magnetic induction hyperthermia instrument available for clinical treatment (A. Jordan et al. 2001). To date, clinical trials of mNP hyperthermia have been conducted for prostate cancer (Manfred Johannsen et al. 2007), recurrences of different tumour entities and deep regions of the human body (Gneveckow et al. 2004; Sreenivasa et al. 2003; Thiesen and Jordan 2008; Wust et al. 2006). In no cases were several side effects reported whilst the effectiveness of mNP based hyperthermia proved a feasable alternate therapy prospect for both deep seated and superficial tumours.

6.3.3 Magnetic nanoparticles as an Adjunct to Established Cancer Therapies

More recent and larger scale phase 3 clinical trials have been conducted on 341 patients enrolled in either chemotherapy alone or chemotherapy and hyperthermia *via* mNP heating. Results showed the combinational impact of regional hyperthermia and chemotherapy as an effective future treatment strategy (Rolf D. Issels et al. 2010). Similarly, the combinational approach of radiotherapy and mNP hyperthermia was recently carried out in clinical trials, with the combined effect of hyperthermia and a reduced radiation dose leading to a safe and effective therapy for recurrent glioblastoma, increasing overall survival rates (Maier-Hauff et al. 2011).

6.4 Conclusion

The research involved in this PhD project primarily set out to identify whether gold nanoparticles, in the form of nanoprisms and nanorods, and magnetic nanoparticles could be used as nanoscale heaters in cancer cell cultures to induce toxic heat levels. If successful, I then aimed to further investigate the molecular mechanisms behind the cell death (apoptosis), to establish the types of intracellular pathways involved. If we can understand the process and pathways involved, this can help future nanoparticle design. The first part of the project, chapter 3, characterised gold nanoprisms and nanorods in terms of their biocompatibitly and cellular uptake. This was studied (i) in two cell lines, bone and breast cancer, to determine if tissue origin would influence nanoparticle performance, and (ii) in 2D and 3D cultures, to verify monolayer results were translated to the 3D environment. Both types of GNP proved to be highly biocompatible and rapidly internalised, with minimal disruption to cell morphology or structure. The GNPs demonstrated excellent heating profiles when excited with a 1 W continuous wave laser; 1 minute laser irradiation of labelled cells caused rapid cell death, in both 2D and 3D, demonstrating the potential depth of laser penetration at fairly modest laser intensity and duration.

Following gold nanoparticle characterization and successful photothermal treatment, chapter 4 focused on assessing apoptotic markers at both the genomic and proteomic level with particular emphasis on large families such caspases, Hsps, bcl-2 and cathepsins, while influential molecular markers such as cytochrome C, DIABLO/SMAC, survivin, livin and TRAILR -1, -2, -3 and -4 were also evaluated. This analysis revealed a unique insight into the mechanisms of cell death attributed by elevated temperature profiles (42-45°), which to the best of our knowledge have not been explored in this depth previously. Our results, although conforming to the majority of the literature of hyperthermia-induce apoptosis *via* the intrinsic pathway, also revealed the importance of both the extrinsic pathway and in particular autophagy, orchestrated by members of the cathepsin family. These results indicate that apoptosis can occur *via* more novel or less characterised pathways upon heat stress, while the main instigators of cell death upon hyperthermia exposure may be due to the generation and accumulation of ROS and endoplasmic stress.

The final chapter focused on the use of magnetic nanoparticles as hyperthermia agents. Several types of mNP were trialled during this section of work, however only one particle type was successful in balancing biocompatibility with the generation of hyperthermic temperature profiles. I employed a magnetherm device during this chapter, whereby 3D printed cell culture chambers were designed to be compatible with the device. Although these results were preliminary, the mNP labelled cells did appear to demonstrate a reduction in cell attachment and change in morphology akin to induction of apoptosis following exposure to an an external AMF, while cells exposed to the external AMF alone, did not appear affected.

The NPs used in this project displayed various potential as viable future hyperthermic agents. The extensively studied GNPs used in this study displayed incredibly high heating potential within one minute at low concentrations (0.1 $mg.ml^{-1}$). Although displaying excellent biocompatiblity and low toxicity at this concentration, the GNPs may be used at even lower concentrations (to futher decrease toxicity issues) while still reaching hyperthermic profiles albeit at an increase laser exposure time that would still be applicable for clinical application. Of the two GNP types, our data suggests that although nanorods show higher heating potential, the nanoprism; due to their enhanced biocompatibility and internalisation, may actually produce stronger photothermal effects upon laser treatment. When compared to mNPs, GNPs not only displayed lower toxicity and improved biocompatbility, they demonstrated stronger hyperthermic compatiblity at the same concentration within a minute of laser treatment as opposed to the 20 minutes required during mNP heating *via* an external alternating magnetic field. The limiting factor for photothermal treatment would be the required laser exposure and depth penetration accessible within patients. This can present complications or slightly more invasive treatments in the case of deep seated tumours where a laser light source would be directed into the patient in such cases. In comparion, mNP heating involves magnetic fields that can easily penetrate the body and thus capable of stimulating mNPs located deep within the patients body and possibly in several sites without the need for any invasive procedures and thus maybe more desirable in a clinical application. However, of the two NP types used in this study, it appears GNPs are the stronger candidates for future application and put forward for future research.

6.5 Recommendation for future work

One of the main focuses of the project was to attempt to better understand the elusive molecular events that occur upon hyperthermic exposure in cells, both in 2D and 3D. While this was successful in terms of GNPs and has opened up further potential for future studies, particular areas of interest are described and summarised below.

- Establishing cell death following mNP-mediated hyperthermia and evaluating the molecular events responsible (at the gene and protein level).

- Investigating the effects of ROS generation (individual species) and RE stress upon hyperthermia exposure.

- Further evaluating more novel cell stress/cell death pathways such as autophagy, necotoposis and necrosis after hyperthermia exposure.

- Analysing cell death to quantify and discriminate between apoptosis and necrosis after photothermal and magnetic treatment, optimising laser power/duration to ensure safe treatment.

- The functionalisation of the GNPs with chemotherapeutic payloads may be an attractive possibility for synergistic effect of drug payloads and hyperthermia; this could be assessed by standard monolayer and 3D testing platforms as used here.

- Moving the GNP from successful current 3D *in vitro* studies to an *in vivo* small animal model to confirm the therapeutic effect of photothermal therapy.

References:

Abadeer, Nardine S. and Murphy, Catherine J. (2016), 'Recent Progress in Cancer Thermal Therapy Using Gold Nanoparticles', *The Journal of Physical Chemistry C,* 120 (9), 4691-716.

Abreu, Raquel de Sousa, et al. (2009), 'Global signatures of protein and mRNA expression levels', *Molecular bioSystems,* 5 (12), 1512-26.

Adachi, H., et al. (2009), 'Heat shock proteins in neurodegenerative diseases: pathogenic roles and therapeutic implications', *Int J Hyperthermia,* 25 (8), 647-54.

Adams, J. M. and Cory, S. (2007), 'Bcl-2-regulated apoptosis: mechanism and therapeutic potential', *Curr Opin Immunol,* 19 (5), 488-96.

Ahamed, Maqusood, et al. (2016), 'Cytotoxic response of platinum-coated gold nanorods in human breast cancer cells at very low exposure levels', *Environmental Toxicology,* 31 (11), 1344-56.

Ahmed, K. and Zaidi, S. F. (2013), 'Treating cancer with heat: hyperthermia as promising strategy to enhance apoptosis', *J Pak Med Assoc,* 63 (4), 504-8.

Ahmed, K., Tabuchi, Y., and Kondo, T. (2015a), 'Hyperthermia: an effective strategy to induce apoptosis in cancer cells', *Apoptosis,* 20 (11), 1411-9.

Ahmed, Kanwal, Tabuchi, Yoshiaki, and Kondo, Takashi (2015b), 'Hyperthermia: an effective strategy to induce apoptosis in cancer cells', *Apoptosis,* 20 (11), 1411-19.

Ahmed, M. and Douek, M. (2013), 'The role of magnetic nanoparticles in the localization and treatment of breast cancer', *Biomed Res Int,* 2013, 281230.

Ahmed, M., Pan, D. W., and Davis, M. E. (2015c), 'Lack of in vivo antibody dependent cellular cytotoxicity with antibody containing gold nanoparticles', *Bioconjug Chem,* 26 (5), 812-6.

Ahn, S., Jung, S. Y., and Lee, S. J. (2013), 'Gold nanoparticle contrast agents in advanced X-ray imaging technologies', *Molecules,* 18 (5), 5858-90.

Aits, Sonja and Jäättelä, Marja (2013), 'Lysosomal cell death at a glance', *Journal of Cell Science,* 126 (9), 1905.

Åkerfelt, Malin, Morimoto, Richard I., and Sistonen, Lea (2010), 'Heat shock factors: integrators of cell stress, development and lifespan', *Nature Reviews. Molecular Cell Biology,* 11 (8), 545-55.

Akhmanova, A. and Steinmetz, M. O. (2015), 'Control of microtubule organization and dynamics: two ends in the limelight', *Nat Rev Mol Cell Biol,* 16 (12), 711-26.

Akiyama, Yasuyuki, et al. (2009), 'The effects of PEG grafting level and injection dose on gold nanorod biodistribution in the tumor-bearing mice', *Journal of Controlled Release,* 139 (1), 81-84.

Aktas, O., Schulze-Topphoff, U., and Zipp, F. (2007), 'The role of TRAIL/TRAIL receptors in central nervous system pathology', *Front Biosci,* 12, 2912-21.

Albanese, A. and Chan, W. C. (2011a), 'Effect of gold nanoparticle aggregation on cell uptake and toxicity', *ACS Nano,* 5 (7), 5478-89.

Albanese, Alexandre and Chan, Warren C. W. (2011b), 'Effect of Gold Nanoparticle Aggregation on Cell Uptake and Toxicity', *ACS Nano,* 5 (7), 5478-89.

Alex, S. and Tiwari, A. (2015), 'Functionalized Gold Nanoparticles: Synthesis, Properties and Applications--A Review', *J Nanosci Nanotechnol,* 15 (3), 1869-94.

Alfranca, G., et al. (2016), 'Gold nanoprism-nanorod face off: comparing the heating efficiency, cellular internalization and thermoablation capacity', *Nanomedicine (Lond),* 11 (22), 2903-16.

Ali, Moustafa R. K., et al. (2016), 'Targeting heat shock protein 70 using gold nanorods enhances cancer cell apoptosis in low dose plasmonic photothermal therapy', *Biomaterials,* 102, 1-8.

Alkilany, A. M. and Murphy, C. J. (2009), 'Gold nanoparticles with a polymerizable surfactant bilayer: synthesis, polymerization, and stability evaluation', *Langmuir,* 25 (24), 13874-9.

Alkilany, A. M., et al. (2010), 'Toxicity and cellular uptake of gold nanoparticles: what we have learned so far?', *J Nanopart Res,* 12 (7), 2313-33.

Alkilany, A. M., et al. (2012), 'Gold nanorods: their potential for photothermal therapeutics and drug delivery, tempered by the complexity of their biological interactions', *Adv Drug Deliv Rev,* 64 (2), 190-9.

Alkilany, Alaaldin M., et al. (2009), 'Cellular Uptake and Cytotoxicity of Gold Nanorods: Molecular Origin of Cytotoxicity and Surface Effects', *Small,* 5 (6), 701-08.

Andocs, G., et al. (2016), 'Comparison of biological effects of modulated electro-hyperthermia and conventional heat treatment in human lymphoma U937 cells', *Cell Death Discovery,* 2, 16039.

Andreae, Michael H. and Andreae, Doerthe A. (2012), 'Local anaesthetics and regional anaesthesia for preventing chronic pain after surgery', *The Cochrane database of systematic reviews,* 10, CD007105-CD05.

Anselmo, A. C. and Mitragotri, S. (2015), 'A Review of Clinical Translation of Inorganic Nanoparticles', *AAPS J,* 17 (5), 1041-54.

Arami, Hamed, et al. (2015), 'In vivo delivery, pharmacokinetics, biodistribution and toxicity of iron oxide nanoparticles', *Chemical Society Reviews,* 44 (23), 8576-607.

Arnida, Malugin, A., and Ghandehari, H. (2010), 'Cellular uptake and toxicity of gold nanoparticles in prostate cancer cells: a comparative study of rods and spheres', *J Appl Toxicol,* 30 (3), 212-7.

Attaluri, A., et al. (2015), 'Magnetic nanoparticle hyperthermia enhances radiation therapy: A study in mouse models of human prostate cancer', *Int J Hyperthermia,* 31 (4), 359-74.

Avvakumova, Svetlana, et al. (2014), 'Gold nanoparticles decorated by clustered multivalent cone-glycocalixarenes actively improve the targeting efficiency toward cancer cells', *Chemical Communications,* 50 (75), 11029-32.

Bae, Ji-Eun, et al. (2011), 'The effect of static magnetic fields on the aggregation and cytotoxicity of magnetic nanoparticles', *Biomaterials,* 32 (35), 9401-14.

Baetke, S. C., Lammers, T., and Kiessling, F. (2015), 'Applications of nanoparticles for diagnosis and therapy of cancer', *Br J Radiol,* 88 (1054), 20150207.

Bai, J., Liu, Y., and Jiang, X. (2014a), 'Multifunctional PEG-GO/CuS nanocomposites for near-infrared chemo-photothermal therapy', *Biomaterials,* 35 (22), 5805-13.

Bai, Y. Y., et al. (2014b), 'Non-invasively evaluating therapeutic response of nanorod-mediated photothermal therapy on tumor angiogenesis', *J Biomed Nanotechnol,* 10 (11), 3351-60.

Balivada, S., et al. (2010), 'A/C magnetic hyperthermia of melanoma mediated by iron(0)/iron oxide core/shell magnetic nanoparticles: a mouse study', *BMC Cancer,* 10, 119.

Banobre-Lopez, M., Teijeiro, A., and Rivas, J. (2013), 'Magnetic nanoparticle-based hyperthermia for cancer treatment', *Rep Pract Oncol Radiother,* 18 (6), 397-400.

Bañobre-López, Manuel, Teijeiro, Antonio, and Rivas, Jose (2013), 'Magnetic nanoparticle-based hyperthermia for cancer treatment', *Reports of Practical Oncology & Radiotherapy,* 18 (6), 397-400.

Bao, C., et al. (2013), 'Gold nanoprisms as optoacoustic signal nanoamplifiers for in vivo bioimaging of gastrointestinal cancers', *Small,* 9 (1), 68-74.
Bao, Chenchen, et al. (2016), 'Gold nanoprisms as a hybrid in vivo cancer theranostic platform for in situ photoacoustic imaging, angiography, and localized hyperthermia', *Nano Research,* 9 (4), 1043-56.
Barbosa-Sampaio, H. C., et al. (2015), 'Reduced nuclear protein 1 expression improves insulin sensitivity and protects against diet-induced glucose intolerance through up-regulation of heat shock protein 70', *Biochim Biophys Acta,* 1852 (5), 962-9.
Barkinge, John L., et al. (2009), 'The p53-induced Siva-1 plays a significant role in cisplatin-mediated apoptosis', *Journal of Carcinogenesis,* 8, 2.
Baskar, R., et al. (2012), 'Cancer and radiation therapy: current advances and future directions', *Int J Med Sci,* 9 (3), 193-9.
Bastus, Neus G., et al. (2007), 'Gold nanoparticles for selective and remote heating of β-amyloid protein aggregates', *Materials Science and Engineering: C,* 27 (5-8), 1236-40.
Batulan, Z., et al. (2016), 'Extracellular Release and Signaling by Heat Shock Protein 27: Role in Modifying Vascular Inflammation', *Front Immunol,* 7, 285.
Bayazitoglu, Yildiz, Kheradmand, Shiva, and Tullius, Toni K. (2013), 'An overview of nanoparticle assisted laser therapy', *International Journal of Heat and Mass Transfer,* 67, 469-86.
Bean, Gregory R., et al. (2013), 'PUMA and BIM Are Required for Oncogene Inactivation–Induced Apoptosis', *Science signaling,* 6 (268), ra20-ra20.
Beattie, James, et al. (2006), 'Insulin-like growth factor-binding protein-5 (IGFBP-5): a critical member of the IGF axis', *Biochemical Journal,* 395 (Pt 1), 1-19.
Bechtold, D. A. and Brown, I. R. (2000), 'Heat shock proteins Hsp27 and Hsp32 localize to synaptic sites in the rat cerebellum following hyperthermia', *Brain Res Mol Brain Res,* 75 (2), 309-20.
Beckham, J. T., et al. (2004), 'Assessment of cellular response to thermal laser injury through bioluminescence imaging of heat shock protein 70', *Photochem Photobiol,* 79 (1), 76-85.
Bednarski, M., et al. (2015), 'The influence of the route of administration of gold nanoparticles on their tissue distribution and basic biochemical parameters: In vivo studies', *Pharmacol Rep,* 67 (3), 405-9.
Begg, A. C., Stewart, F. A., and Vens, C. (2011), 'Strategies to improve radiotherapy with targeted drugs', *Nat Rev Cancer,* 11 (4), 239-53.
Behrouzkia, Zhaleh, et al. (2016), 'Hyperthermia: How Can It Be Used?', *Oman Medical Journal,* 31 (2), 89-97.
Beik, J., et al. (2016), 'Nanotechnology in hyperthermia cancer therapy: From fundamental principles to advanced applications', *J Control Release,* 235, 205-21.
Belhadj Slimen, Imen, et al. (2014), 'Reactive oxygen species, heat stress and oxidative-induced mitochondrial damage. A review', *International Journal of Hyperthermia,* 30 (7), 513-23.
Bellusci, Mariangela, et al. (2014), 'Biodistribution and acute toxicity of a nanofluid containing manganese iron oxide nanoparticles produced by a mechanochemical process', *International Journal of Nanomedicine,* 9, 1919-29.
Berry, Catherine C. (2005), 'Possible exploitation of magnetic nanoparticle?cell interaction for biomedical applications', *Journal of Materials Chemistry,* 15 (5), 543.

Berry, Catherine C. (2009), 'Progress in functionalization of magnetic nanoparticles for applications in biomedicine', *Journal of Physics D: Applied Physics,* 42 (22), 224003.

Berry, Catherine C., et al. (2003), 'Dextran and albumin derivatised iron oxide nanoparticles: influence on fibroblasts in vitro', *Biomaterials,* 24 (25), 4551-57.

Bertrand, Nicolas, et al. (2014), 'Cancer Nanotechnology: The impact of passive and active targeting in the era of modern cancer biology()', *Advanced drug delivery reviews,* 66, 2-25.

Bertsch, U., et al. (2014), 'Compartmentalization of TNF-related apoptosis-inducing ligand (TRAIL) death receptor functions: emerging role of nuclear TRAIL-R2', *Cell Death Dis,* 5, e1390.

Bettaieb, Ahmed and Averill-Bates, Diana A. (2008), 'Thermotolerance induced at a fever temperature of 40 °C protects cells against hyperthermia-induced apoptosis mediated by death receptor signalling', *Biochemistry and Cell Biology,* 86 (6), 521-38.

Bishop, Corey J., Tzeng, Stephany Y., and Green, Jordan J. (2015), 'Degradable Polymer-Coated Gold Nanoparticles for Co-Delivery of DNA and siRNA', *Acta biomaterialia,* 11, 393-403.

Blanco-Andujar, C., et al. (2016), 'Real-time tracking of delayed-onset cellular apoptosis induced by intracellular magnetic hyperthermia', *Nanomedicine (Lond),* 11 (2), 121-36.

Bobrovnikova-Marjon, E. and Hurov, J. B. (2014), 'Targeting metabolic changes in cancer: novel therapeutic approaches', *Annu Rev Med,* 65, 157-70.

Boehm, A. K., et al. (2003), 'Transcription Factor and Polymerase Recruitment, Modification, and Movement on dhsp70 In Vivo in the Minutes following Heat Shock', *Molecular and Cellular Biology,* 23 (21), 7628-37.

Bogdanov, Alexei A., et al. (2015), 'Gold nanoparticles stabilized with MPEG-grafted poly-l-lysine: in vitro and in vivo evaluation of a potential theranostic agent', *Bioconjugate chemistry,* 26 (1), 39-50.

Bohara, Raghvendra A., et al. (2015), 'Correction: Cancer cell extinction through a magnetic fluid hyperthermia treatment produced by superparamagnetic Co-Zn ferrite nanoparticles', *RSC Advances,* 5 (127), 104612-12.

Boisseau, Patrick and Loubaton, Bertrand (2011), 'Nanomedicine, nanotechnology in medicine', *Comptes Rendus Physique,* 12 (7), 620-36.

Bonnier, F., et al. (2015), 'Cell viability assessment using the Alamar blue assay: A comparison of 2D and 3D cell culture models', *Toxicology in Vitro,* 29 (1), 124-31.

Bonzon, C., et al. (2006), 'Caspase-2-induced apoptosis requires bid cleavage: a physiological role for bid in heat shock-induced death', *Mol Biol Cell,* 17 (5), 2150-7.

Boya, P. and Kroemer, G. (2008a), 'Lysosomal membrane permeabilization in cell death', *Oncogene,* 27 (50), 6434-51.

Boya, P. and Kroemer, G. (2008b), 'Lysosomal membrane permeabilization in cell death', *Oncogene,* 27 (50), 6434-51.

Bozaykut, P., Ozer, N. K., and Karademir, B. (2014), 'Regulation of protein turnover by heat shock proteins', *Free Radic Biol Med,* 77, 195-209.

Brackstone, Muriel, Townson, Jason L., and Chambers, Ann F. (2007), 'Tumour dormancy in breast cancer: an update', *Breast Cancer Research,* 9 (3), 208-08.

Bratton, S. B., et al. (2002), 'XIAP inhibition of caspase-3 preserves its association with the Apaf-1 apoptosome and prevents CD95- and Bax-induced apoptosis', *Cell Death Differ,* 9 (9), 881-92.

Bratton, Shawn B. and Salvesen, Guy S. (2010), 'Regulation of the Apaf-1–caspase-9 apoptosome', *Journal of Cell Science,* 123 (19), 3209.
Brentnall, Matthew, et al. (2013), 'Caspase-9, caspase-3 and caspase-7 have distinct roles during intrinsic apoptosis', *BMC Cell Biology,* 14, 32-32.
Brojatsch, Jürgen, et al. (2015), 'Distinct cathepsins control necrotic cell death mediated by pyroptosis inducers and lysosome-destabilizing agents', *Cell Cycle,* 14 (7), 964-72.
Broustas, Constantinos G. and Lieberman, Howard B. (2014), 'DNA Damage Response Genes and the Development of Cancer Metastasis', *Radiation research,* 181 (2), 111-30.
Brown, Ashley N., et al. (2012), 'Nanoparticles Functionalized with Ampicillin Destroy Multiple-Antibiotic-Resistant Isolates of Pseudomonas aeruginosa and Enterobacter aerogenes and Methicillin-Resistant Staphylococcus aureus', *Applied and Environmental Microbiology,* 78 (8), 2768-74.
Brown, J. Martin (2007), 'Tumor Hypoxia in Cancer Therapy', *Methods in Enzymology* (Volume 435: Academic Press), 295-321.
Bruey, J. M., et al. (2000), 'Hsp27 negatively regulates cell death by interacting with cytochrome c', *Nat Cell Biol,* 2 (9), 645-52.
Brus, Louis (2016), 'Plasmon-driven chemical synthesis: Growing gold nanoprisms with light', *Nat Mater,* 15 (8), 824-25.
Budina-Kolomets, A., et al. (2014), 'Comparison of the activity of three different HSP70 inhibitors on apoptosis, cell cycle arrest, autophagy inhibition, and HSP90 inhibition', *Cancer Biol Ther,* 15 (2), 194-9.
Burke, A. R., et al. (2012), 'The resistance of breast cancer stem cells to conventional hyperthermia and their sensitivity to nanoparticle-mediated photothermal therapy', *Biomaterials,* 33 (10), 2961-70.
Butt, A. J., et al. (2005), 'Enhancement of tumor necrosis factor-alpha-induced growth inhibition by insulin-like growth factor-binding protein-5 (IGFBP-5), but not IGFBP-3 in human breast cancer cells', *Endocrinology,* 146 (7), 3113-22.
Buyukhatipoglu, Kivilcim and Clyne, Alisa Morss (2011), 'Superparamagnetic iron oxide nanoparticles change endothelial cell morphology and mechanics via reactive oxygen species formation', *Journal of Biomedical Materials Research Part A,* 96A (1), 186-95.
C.S, Rejiya, et al. (2012), 'Laser immunotherapy with gold nanorods causes selective killing of tumour cells', *Pharmacological Research,* 65 (2), 261-69.
Cai, W., et al. (2008), 'Applications of gold nanoparticles in cancer nanotechnology', *Nanotechnol Sci Appl,* 2008 (1).
Calero, M., et al. (2014), 'Efficient and safe internalization of magnetic iron oxide nanoparticles: two fundamental requirements for biomedical applications', *Nanomedicine,* 10 (4), 733-43.
Cannito, Stefania, et al. (2015), 'Hypoxia up-regulates SERPINB3 through HIF-2α in human liver cancer cells', *Oncotarget,* 6 (4), 2206-21.
Carnovale, Catherine, et al. (2016), 'Size, shape and surface chemistry of nano-gold dictate its cellular interactions, uptake and toxicity', *Progress in Materials Science,* 83, 152-90.
Carr, A. C., Vissers, M. C., and Cook, J. S. (2014), 'The effect of intravenous vitamin C on cancer- and chemotherapy-related fatigue and quality of life', *Front Oncol,* 4, 283.
Castellana, Edward T., et al. (2010), 'Longitudinal Surface Plasmon Resonance Based Gold Nanorod Biosensors for Mass Spectrometry', *Langmuir,* 26 (8), 6066-70.

Catherine, C. Berry and Adam, S. G. Curtis (2003), 'Functionalisation of magnetic nanoparticles for applications in biomedicine', *Journal of Physics D: Applied Physics,* 36 (13), R198.
Chandra, D., Liu, J. W., and Tang, D. G. (2002), 'Early mitochondrial activation and cytochrome c up-regulation during apoptosis', *J Biol Chem,* 277 (52), 50842-54.
Chang, Esther H., et al. (2015), 'Nanomedicine: Past, present and future – A global perspective', *Biochemical and Biophysical Research Communications,* 468 (3), 511-17.
Charlton, J. R., et al. (2016), 'Biocompatibility of ferritin-based nanoparticles as targeted MRI contrast agents', *Nanomedicine,* 12 (6), 1735-45.
Chatterjee, D. K., Diagaradjane, P., and Krishnan, S. (2011), 'Nanoparticle-mediated hyperthermia in cancer therapy', *Ther Deliv,* 2 (8), 1001-14.
Chaudhari, K. R., et al. (2012), 'Opsonization, biodistribution, cellular uptake and apoptosis study of PEGylated PBCA nanoparticle as potential drug delivery carrier', *Pharm Res,* 29 (1), 53-68.
Chen, F., et al. (2008a), 'Hyperthermia in combination with oxidative stress induces autophagic cell death in HT-29 colon cancer cells', *Cell Biol Int,* 32 (7), 715-23.
Chen, Hongwei, et al. (2013), ''Living' PEGylation on gold nanoparticles to optimize cancer cell uptake by controlling targeting ligand and charge densities', *Nanotechnology,* 24 (35), 10.1088/0957-4484/24/35/355101.
Chen, Huanjun, et al. (2008b), 'Shape- and Size-Dependent Refractive Index Sensitivity of Gold Nanoparticles', *Langmuir,* 24 (10), 5233-37.
Chen, Kuo-Li, et al. (2012), 'Targeting cathepsin S induces tumor cell autophagy via the EGFR–ERK signaling pathway', *Cancer Letters,* 317 (1), 89-98.
Chen, Yu-Shiun, et al. (2009), 'Assessment of the In Vivo Toxicity of Gold Nanoparticles', *Nanoscale Research Letters,* 4 (8), 858-64.
Cheng, C. J., et al. (2015), 'A holistic approach to targeting disease with polymeric nanoparticles', *Nat Rev Drug Discov,* 14 (4), 239-47.
Cherukuri, P., Glazer, E. S., and Curley, S. A. (2010), 'Targeted hyperthermia using metal nanoparticles', *Adv Drug Deliv Rev,* 62 (3), 339-45.
Chiappara, G., et al. 'Altered expression of p21, activated caspase-3, and PCNA in bronchiolar epithelium of smokers with and without chronic obstructive pulmonary disease', (1521-0499 (Electronic)).
Chicheł, Adam, et al. (2007), 'Hyperthermia – description of a method and a review of clinical applications', *Reports of Practical Oncology & Radiotherapy,* 12 (5), 267-75.
Chithrani, B. D. and Chan, W. C. (2007), 'Elucidating the mechanism of cellular uptake and removal of protein-coated gold nanoparticles of different sizes and shapes', *Nano Lett,* 7 (6), 1542-50.
Chithrani, B. D., Ghazani, A. A., and Chan, W. C. (2006), 'Determining the size and shape dependence of gold nanoparticle uptake into mammalian cells', *Nano Lett,* 6 (4), 662-8.
Chiu, Wei-Jane, et al. (2015), 'Monitoring Cluster Ions Derived from Aptamer-Modified Gold Nanofilms under Laser Desorption/Ionization for the Detection of Circulating Tumor Cells', *ACS Applied Materials & Interfaces,* 7 (16), 8622-30.
Cho, E. C., et al. (2010a), 'The effects of size, shape, and surface functional group of gold nanostructures on their adsorption and internalization by cells', *Small,* 6 (4), 517-22.
Cho, Seok, et al. (2010b), 'Epigenetic methylation and expression of caspase 8 and survivin in hepatocellular carcinoma', *Pathology International,* 60 (3), 203-11.

Cho, Y. S. (2014), 'Perspectives on the therapeutic modulation of an alternative cell death, programmed necrosis (review)', *Int J Mol Med,* 33 (6), 1401-6.
Choi, Jihye, et al. (2011), 'Gold Nanostructures as Photothermal Therapy Agent for Cancer', *Anti-Cancer Agents in Medicinal Chemistry,* 11 (10), 953-64.
Choudhury, D., et al. (2013a), 'Unprecedented inhibition of tubulin polymerization directed by gold nanoparticles inducing cell cycle arrest and apoptosis', *Nanoscale,* 5 (10), 4476-89.
Choudhury, Diptiman, et al. (2013b), 'Unprecedented inhibition of tubulin polymerization directed by gold nanoparticles inducing cell cycle arrest and apoptosis', *Nanoscale,* 5 (10), 4476-89.
Chuang, S. M., et al. (2013), 'Extensive evaluations of the cytotoxic effects of gold nanoparticles', *Biochim Biophys Acta,* 1830 (10), 4960-73.
Chun, J. N., et al. (2010), 'Cytosolic Hsp60 is involved in the NF-kappaB-dependent survival of cancer cells via IKK regulation', *PLoS One,* 5 (3), e9422.
Circu, Magdalena L. and Aw, Tak Yee (2010), 'REACTIVE OXYGEN SPECIES, CELLULAR REDOX SYSTEMS AND APOPTOSIS', *Free radical biology & medicine,* 48 (6), 749-62.
Ciscato, Francesco, et al. (2014), 'SERPINB3 protects from oxidative damage by chemotherapeutics through inhibition of mitochondrial respiratory complex I', *Oncotarget,* 5 (9), 2418-27.
Clerico, E. M., et al. (2015), 'How hsp70 molecular machines interact with their substrates to mediate diverse physiological functions', *J Mol Biol,* 427 (7), 1575-88.
Coelho, Silvia C., et al. (2015), 'Structural characterization of functionalized gold nanoparticles for drug delivery in cancer therapy: a NMR based approach', *Physical Chemistry Chemical Physics,* 17 (29), 18971-79.
Cole, A. J., Yang, V. C., and David, A. E. (2011a), 'Cancer theranostics: the rise of targeted magnetic nanoparticles', *Trends Biotechnol,* 29 (7), 323-32.
Cole, A. J., et al. (2011b), 'Polyethylene glycol modified, cross-linked starch-coated iron oxide nanoparticles for enhanced magnetic tumor targeting', *Biomaterials,* 32 (8), 2183-93.
Colombo, R., et al. (2011), 'Long-term outcomes of a randomized controlled trial comparing thermochemotherapy with mitomycin-C alone as adjuvant treatment for non-muscle-invasive bladder cancer (NMIBC)', *BJU Int,* 107 (6), 912-8.
Connor, E. E., et al. (2005), 'Gold nanoparticles are taken up by human cells but do not cause acute cytotoxicity', *Small,* 1 (3), 325-7.
Constantin, Ungureanu, et al. (2013), 'The 'nanobig rod' class of gold nanorods: optimized dimensions for improved in vivo therapeutic and imaging efficacy', *Nanotechnology,* 24 (21), 215102.
Costa, Elisabete C., et al. (2016), '3D tumor spheroids: an overview on the tools and techniques used for their analysis', *Biotechnology Advances,* 34 (8), 1427-41.
Creixell, Mar, et al. (2011), 'EGFR-Targeted Magnetic Nanoparticle Heaters Kill Cancer Cells without a Perceptible Temperature Rise', *ACS Nano,* 5 (9), 7124-29.
Cui, Y., et al. (2014a), 'Effect of heat stress and recovery on viability, oxidative damage, and heat shock protein expression in hepatic cells of grass carp (Ctenopharyngodon idellus)', *Fish Physiol Biochem,* 40 (3), 721-9.
Cui, Yanting, et al. (2013), 'The effect of hyperthermia on cell viability, oxidative damage, and heat shock protein expression in hepatic cells of grass carp (Ctenopharyngodon idellus)', *Journal of Thermal Biology,* 38 (6), 355-61.

Cui, Yanting, et al. (2014b), 'Effect of heat stress and recovery on viability, oxidative damage, and heat shock protein expression in hepatic cells of grass carp (Ctenopharyngodon idellus)', *Fish Physiology and Biochemistry,* 40 (3), 721-29.
Cui, Z. G., et al. (2014c), 'Molecular mechanisms of hyperthermia-induced apoptosis enhanced by docosahexaenoic acid: implication for cancer therapy', *Chem Biol Interact,* 215, 46-53.
Cui, Z. G., et al. (2014d), 'Molecular mechanisms of hyperthermia-induced apoptosis enhanced by withaferin A', *Eur J Pharmacol,* 723, 99-107.
Cui, Zheng-Guo, et al. (2014e), 'Molecular mechanisms of hyperthermia-induced apoptosis enhanced by docosahexaenoic acid: Implication for cancer therapy', *Chemico-Biological Interactions,* 215, 46-53.
Cui, Zheng-Guo, et al. (2014f), 'Molecular mechanisms of hyperthermia-induced apoptosis enhanced by withaferin A', *European Journal of Pharmacology,* 723, 99-107.
Curcio, E., et al. (2007), 'Mass transfer and metabolic reactions in hepatocyte spheroids cultured in rotating wall gas-permeable membrane system', *Biomaterials,* 28 (36), 5487-97.
Curry, T., et al. (2014), 'Multifunctional theranostic gold nanoparticles for targeted CT imaging and photothermal therapy', *Contrast Media Mol Imaging,* 9 (1), 53-61.
Dam, D. H., et al. (2015), 'Biodistribution and in vivo toxicity of aptamer-loaded gold nanostars', *Nanomedicine,* 11 (3), 671-9.
Dangi, S. S., et al. (2015), 'Expression of HSPs: an adaptive mechanism during long-term heat stress in goats (Capra hircus)', *Int J Biometeorol,* 59 (8), 1095-106.
Datta, N. R., et al. (2015), 'Local hyperthermia combined with radiotherapy and-/or chemotherapy: Recent advances and promises for the future', *Cancer Treatment Reviews,* 41 (9), 742-53.
de Castro, M. A., Bunt, G., and Wouters, F. S. (2016), 'Cathepsin B launches an apoptotic exit effort upon cell death-associated disruption of lysosomes', *Cell Death Discov,* 2, 16012.
De Jong, Wim H., et al. (2008), 'Particle size-dependent organ distribution of gold nanoparticles after intravenous administration', *Biomaterials,* 29 (12), 1912-19.
De Maio, A. (2014), 'Extracellular Hsp70: export and function', *Curr Protein Pept Sci,* 15 (3), 225-31.
Deatsch, Alison E. and Evans, Benjamin A. (2014), 'Heating efficiency in magnetic nanoparticle hyperthermia', *Journal of Magnetism and Magnetic Materials,* 354, 163-72.
Degli-Esposti, Mariapia A., et al. (1997), 'Cloning and Characterization of TRAIL-R3, a Novel Member of the Emerging TRAIL Receptor Family', *The Journal of Experimental Medicine,* 186 (7), 1165-70.
DeNardo, G. L. and DeNardo, S. J. (2008), 'Update: Turning the heat on cancer', *Cancer Biother Radiopharm,* 23 (6), 671-80.
Dennis, C. L. and Ivkov, R. (2013a), 'Physics of heat generation using magnetic nanoparticles for hyperthermia', *Int J Hyperthermia,* 29 (8), 715-29.
Dennis, C. L., et al. (2009), 'Nearly complete regression of tumors via collective behavior of magnetic nanoparticles in hyperthermia', *Nanotechnology,* 20 (39), 395103.
Dennis, Cindi L. and Ivkov, Robert (2013b), 'Physics of heat generation using magnetic nanoparticles for hyperthermia', *International Journal of Hyperthermia,* 29 (8), 715-29.
Di Pasqua, Anthony J., et al. (2009), 'Preparation of antibody-conjugated gold nanoparticles', *Materials Letters,* 63 (21), 1876-79.

Diaz, B., et al. (2008), 'Assessing methods for blood cell cytotoxic responses to inorganic nanoparticles and nanoparticle aggregates', *Small,* 4 (11), 2025-34.
Dickerson, E. B., et al. (2008), 'Gold nanorod assisted near-infrared plasmonic photothermal therapy (PPTT) of squamous cell carcinoma in mice', *Cancer Lett,* 269 (1), 57-66.
Doane, T. L. and Burda, C. (2012), 'The unique role of nanoparticles in nanomedicine: imaging, drug delivery and therapy', *Chem Soc Rev,* 41 (7), 2885-911.
Dobrovolskaia, M. A., Shurin, M., and Shvedova, A. A. (2016), 'Current understanding of interactions between nanoparticles and the immune system', *Toxicol Appl Pharmacol,* 299, 78-89.
Dokladny, Karol, Myers, Orrin B., and Moseley, Pope L. (2015), 'Heat shock response and autophagy—cooperation and control', *Autophagy,* 11 (2), 200-13.
Dreaden, E. C., et al. (2012), 'Size matters: gold nanoparticles in targeted cancer drug delivery', *Ther Deliv,* 3 (4), 457-78.
Dreaden, E. C., et al. (2011), 'Beating cancer in multiple ways using nanogold', *Chem Soc Rev,* 40 (7), 3391-404.
Du, W. and Elemento, O. (2015), 'Cancer systems biology: embracing complexity to develop better anticancer therapeutic strategies', *Oncogene,* 34 (25), 3215-25.
Duncan, E. J., et al. (2015), 'The role of HSP70 and its co-chaperones in protein misfolding, aggregation and disease', *Subcell Biochem,* 78, 243-73.
Duskey, J. T. and Rice, K. G. (2014), 'Nanoparticle ligand presentation for targeting solid tumors', *AAPS PharmSciTech,* 15 (5), 1345-54.
Dykman, L. A. and Khlebtsov, N. G. (2011), 'Gold Nanoparticles in Biology and Medicine: Recent Advances and Prospects', *Acta Naturae,* 3 (2), 34-55.
Dykman, L. A. and Khlebtsov, N. G. (2014), 'Uptake of engineered gold nanoparticles into mammalian cells', *Chem Rev,* 114 (2), 1258-88.
Easo, Sheeja Liza and Mohanan, P. V. (2013), 'Dextran stabilized iron oxide nanoparticles: Synthesis, characterization and in vitro studies', *Carbohydrate Polymers,* 92 (1), 726-32.
Echeverry, N., et al. (2013), 'Intracellular localization of the BCL-2 family member BOK and functional implications', *Cell Death and Differentiation,* 20 (6), 785-99.
Edmondson, Rasheena, et al. (2014), 'Three-Dimensional Cell Culture Systems and Their Applications in Drug Discovery and Cell-Based Biosensors', *Assay and Drug Development Technologies,* 12 (4), 207-18.
El-Orabi, Naglaa F., et al. (2011), 'Heat-induced inhibition of superoxide dismutase and accumulation of reactive oxygen species leads to HT-22 neuronal cell death', *Journal of Thermal Biology,* 36 (1), 49-56.
El-Sayed, I. H., Huang, X., and El-Sayed, M. A. (2006), 'Selective laser photo-thermal therapy of epithelial carcinoma using anti-EGFR antibody conjugated gold nanoparticles', *Cancer Lett,* 239 (1), 129-35.
El-Sayed, Ivan H., Huang, Xiaohua, and El-Sayed, Mostafa A. (2005), 'Surface Plasmon Resonance Scattering and Absorption of anti-EGFR Antibody Conjugated Gold Nanoparticles in Cancer Diagnostics: Applications in Oral Cancer', *Nano Letters,* 5 (5), 829-34.
Elmore, S. (2007), 'Apoptosis: a review of programmed cell death', *Toxicol Pathol,* 35 (4), 495-516.
Elsabahy, Mahmoud and Wooley, Karen L. (2013), 'Cytokines as biomarkers of nanoparticle immunotoxicity', *Chemical Society reviews,* 42 (12), 5552-76.
Elsherbini, A. A., et al. (2011), 'Magnetic nanoparticle-induced hyperthermia treatment under magnetic resonance imaging', *Magn Reson Imaging,* 29 (2), 272-80.

Eng, J. W., et al. (2014), 'Housing temperature influences the pattern of heat shock protein induction in mice following mild whole body hyperthermia', *Int J Hyperthermia,* 30 (8), 540-6.
Eno, Colins O., et al. (2013), 'Noxa couples lysosomal membrane permeabilization and apoptosis during oxidative stress', *Free radical biology & medicine,* 65, 10.1016/j.freeradbiomed.2013.05.051.
Ernsting, Mark J., et al. (2013), 'Factors Controlling the Pharmacokinetics, Biodistribution and Intratumoral Penetration of Nanoparticles', *Journal of controlled release : official journal of the Controlled Release Society,* 172 (3), 782-94.
Eskelinen, Eeva-Liisa and Saftig, Paul (2009), 'Autophagy: A lysosomal degradation pathway with a central role in health and disease', *Biochimica et Biophysica Acta (BBA) - Molecular Cell Research,* 1793 (4), 664-73.
Espinosa, A., et al. (2016), 'Duality of Iron Oxide Nanoparticles in Cancer Therapy: Amplification of Heating Efficiency by Magnetic Hyperthermia and Photothermal Bimodal Treatment', *ACS Nano,* 10 (2), 2436-46.
Estrela-Lopis, I., et al. (2011), 'Nanoparticle uptake and their co-localization with cell compartments – a confocal Raman microscopy study at single cell level', *Journal of Physics: Conference Series,* 304 (1), 012017.
Eustis, S. and el-Sayed, M. A. (2006), 'Why gold nanoparticles are more precious than pretty gold: noble metal surface plasmon resonance and its enhancement of the radiative and nonradiative properties of nanocrystals of different shapes', *Chem Soc Rev,* 35 (3), 209-17.
Evans, C. G., Chang, L., and Gestwicki, J. E. (2010), 'Heat shock protein 70 (hsp70) as an emerging drug target', *J Med Chem,* 53 (12), 4585-602.
Fan, J. H., et al. (2009), 'Biocompatibility Study of Gold Nanoparticles to Human Cells', in Chwee Teck Lim and James C. H. Goh (eds.), *13th International Conference on Biomedical Engineering: ICBME 2008 3–6 December 2008 Singapore* (Berlin, Heidelberg: Springer Berlin Heidelberg), 870-73.
Fan, K., et al. (2012), 'Magnetoferritin nanoparticles for targeting and visualizing tumour tissues', *Nat Nanotechnol,* 7 (7), 459-64.
Fan, L., et al. (2014), 'Silymarin induces cell cycle arrest and apoptosis in ovarian cancer cells', *Eur J Pharmacol,* 743, 79-88.
Ferreira, K. S., et al. (2012a), 'Caspase-3 feeds back on caspase-8, Bid and XIAP in type I Fas signaling in primary mouse hepatocytes', *Apoptosis,* 17 (5), 503-15.
Ferreira, Karine Sá, et al. (2012b), 'Caspase-3 feeds back on caspase-8, Bid and XIAP in type I Fas signaling in primary mouse hepatocytes', *Apoptosis,* 17 (5), 503-15.
Forest, Valérie, et al. (2017), 'Impact of cerium oxide nanoparticles shape on their in vitro cellular toxicity', *Toxicology in Vitro,* 38, 136-41.
Fraga, S., et al. (2014), 'Short- and long-term distribution and toxicity of gold nanoparticles in the rat after a single-dose intravenous administration', *Nanomedicine,* 10 (8), 1757-66.
Fratoddi, Ilaria, et al. (2015), 'The puzzle of toxicity of gold nanoparticles. The case-study of HeLa cells', *Toxicology Research,* 4 (4), 796-800.
Freese, Christian, et al. (2012), 'Size- and Coating-Dependent Uptake of Polymer-Coated Gold Nanoparticles in Primary Human Dermal Microvascular Endothelial Cells', *Biomacromolecules,* 13 (5), 1533-43.
Fulda, S. and Debatin, K. M. (2006), 'Extrinsic versus intrinsic apoptosis pathways in anticancer chemotherapy', *Oncogene,* 25 (34), 4798-811.
Fulda, Simone (2015), 'Targeting extrinsic apoptosis in cancer: Challenges and opportunities', *Seminars in Cell & Developmental Biology,* 39, 20-25.

Gao, Huajian, Shi, Wendong, and Freund, Lambert B. (2005), 'Mechanics of receptor-mediated endocytosis', *Proceedings of the National Academy of Sciences of the United States of America,* 102 (27), 9469-74.

Gao, W. and Zhang, L. (2015), 'Coating nanoparticles with cell membranes for targeted drug delivery', *J Drug Target,* 23 (7-8), 619-26.

Garcia, Mônica Pereira, et al. (2005), 'Morphological analysis of mouse lungs after treatment with magnetite-based magnetic fluid stabilized with DMSA', *Journal of Magnetism and Magnetic Materials,* 293 (1), 277-82.

Garcia, Pereira, Cavalheiro, José Roberto Tinoco, and Fernandes, Maria Helena (2012), 'Acute and Long-Term Effects of Hyperthermia in B16-F10 Melanoma Cells', *PLoS ONE,* 7 (4), e35489.

Gasman, Stéphane, et al. (2004), 'Regulated Exocytosis in Neuroendocrine Cells: A Role for Subplasmalemmal Cdc42/N-WASP-induced Actin Filaments', *Molecular Biology of the Cell,* 15 (2), 520-31.

Geiger, T. R. and Peeper, D. S. (2009), 'Metastasis mechanisms', *Biochim Biophys Acta,* 1796 (2), 293-308.

Gelinas, C. and White, E. (2005), 'BH3-only proteins in control: specificity regulates MCL-1 and BAK-mediated apoptosis', *Genes Dev,* 19 (11), 1263-8.

Geng, Xi, et al. (2016), 'Seed-mediated biomineralizaton toward the high yield production of gold nanoprisms', *Chemical Communications,* 52 (63), 9829-32.

Ghasempour, S., et al. (2015), 'Investigating the cytotoxicity of iron oxide nanoparticles in in vivo and in vitro studies', *Exp Toxicol Pathol*.

Gilcrest (1957), '<Selective Inductive Heating of Lymph Nodes R. K. Gilcrest,.pdf>'.

Gillies, Laura A. and Kuwana, Tomomi (2014), 'Apoptosis Regulation at the Mitochondrial Outer Membrane', *Journal of Cellular Biochemistry,* 115 (4), 632-40.

Giustini, A. J., et al. (2010), 'Magnetic Nanoparticle Hyperthermia in Cancer Treatment', *Nano Life,* 1 (1n02).

Glazer, Evan S. and Curley, Steven A. (2011), 'The Ongoing History of Thermal Therapy for Cancer', *Surgical oncology clinics of North America,* 20 (2), 229-35.

Glory, A., Bettaieb, A., and Averill-Bates, D. A. (2014), 'Mild thermotolerance induced at 40 degrees C protects cells against hyperthermia-induced pro-apoptotic changes in Bcl-2 family proteins', *Int J Hyperthermia,* 30 (7), 502-12.

Gnerlich, Jennifer, et al. (2007), 'Surgical Removal of the Primary Tumor Increases Overall Survival in Patients With Metastatic Breast Cancer: Analysis of the 1988–2003 SEER Data', *Annals of Surgical Oncology,* 14 (8), 2187-94.

Gneveckow, U., et al. (2004), 'Description and characterization of the novel hyperthermia- and thermoablation-system MFH 300F for clinical magnetic fluid hyperthermia', *Med Phys,* 31 (6), 1444-51.

Gobbo, O. L., et al. (2015), 'Magnetic Nanoparticles in Cancer Theranostics', *Theranostics,* 5 (11), 1249-63.

Gobin, André M., et al. (2010), 'Near Infrared Resonant Gold / Gold Sulfide Nanoparticles as a Photothermal Cancer Therapeutic Agent', *Small (Weinheim an der Bergstrasse, Germany),* 6 (6), 745-52.

Goh, Yaw Chong, et al. (2011), 'Heat-shock protein 60 translocates to the surface of apoptotic cells and differentiated megakaryocytes and stimulates phagocytosis', *Cellular and Molecular Life Sciences,* 68 (9), 1581-92.

Gong, Mingfu, et al. (2015), 'Superparamagnetic core/shell GoldMag nanoparticles: size-, concentration- and time-dependent cellular nanotoxicity on human umbilical vein endothelial cells and the suitable conditions for magnetic resonance imaging', *Journal of Nanobiotechnology,* 13, 24.

Gong, T., et al. (2014), 'In vitro toxicity and bioimaging studies of gold nanorods formulations coated with biofunctional thiol-PEG molecules and Pluronic block copolymers', *Beilstein J Nanotechnol,* 5, 546-53.

Gonzales-Weimuller, Marcela, Zeisberger, Matthias, and Krishnan, Kannan M. (2009), 'Size-dependant heating rates of iron oxide nanoparticles for magnetic fluid hyperthermia', *Journal of magnetism and magnetic materials,* 321 (13), 1947-50.

Graner, Arin N., et al. (2016), 'HSP90 inhibitors in the context of heat shock and the unfolded protein response: effects on a primary canine pulmonary adenocarcinoma cell line', *International Journal of Hyperthermia*, 1-50.

Grimes, D. R., et al. (2014), 'A method for estimating the oxygen consumption rate in multicellular tumour spheroids', *J R Soc Interface,* 11 (92), 20131124.

Gruttner, C., et al. (2013), 'Synthesis and functionalisation of magnetic nanoparticles for hyperthermia applications', *Int J Hyperthermia,* 29 (8), 777-89.

Guardia, Pablo, et al. (2012), 'Water-Soluble Iron Oxide Nanocubes with High Values of Specific Absorption Rate for Cancer Cell Hyperthermia Treatment', *ACS Nano,* 6 (4), 3080-91.

Guicciardi, M. E., et al. (2014), 'Cellular inhibitor of apoptosis (cIAP)-mediated ubiquitination of phosphofurin acidic cluster sorting protein 2 (PACS-2) negatively regulates tumor necrosis factor-related apoptosis-inducing ligand (TRAIL) cytotoxicity', *PLoS One,* 9 (3), e92124.

Gunnar, Glöckl, et al. (2006), 'The effect of field parameters, nanoparticle properties and immobilization on the specific heating power in magnetic particle hyperthermia', *Journal of Physics: Condensed Matter,* 18 (38), S2935.

Guo, Shuzhen, et al. (2014), 'Role of A20 in cIAP-2 Protection against Tumor Necrosis Factor α (TNF-α)-Mediated Apoptosis in Endothelial Cells', *International Journal of Molecular Sciences,* 15 (3), 3816-33.

Guo, Yang, et al. (2015), 'Overexpression of heat shock protein 27 (HSP27) increases gemcitabine sensitivity in pancreatic cancer cells through S-phase arrest and apoptosis', *Journal of Cellular and Molecular Medicine,* 19 (2), 340-50.

Guo, Yang, et al. (2013), 'Photothermal ablation of pancreatic cancer cells with hybrid iron-oxide core gold-shell nanoparticles', *International Journal of Nanomedicine,* 8, 3437-46.

Guo, Z., et al. (2010a), 'Achieving high-purity colloidal gold nanoprisms and their application as biosensing platforms', *J Colloid Interface Sci,* 348 (1), 29-36.

Guo, Zhirui, et al. (2010b), 'Achieving high-purity colloidal gold nanoprisms and their application as biosensing platforms', *Journal of Colloid and Interface Science,* 348 (1), 29-36.

Gupta, Ajay Kumar and Gupta, Mona (2005), 'Cytotoxicity suppression and cellular uptake enhancement of surface modified magnetic nanoparticles', *Biomaterials,* 26 (13), 1565-73.

Gupta, S. and Knowlton, A. A. (2005), 'HSP60, Bax, apoptosis and the heart', *J Cell Mol Med,* 9 (1), 51-8.

Haghniaz, R., Umrani, R. D., and Paknikar, K. M. (2015a), 'Temperature-dependent and time-dependent effects of hyperthermia mediated by dextran-coated La0.7Sr0.3MnO3: in vitro studies', *Int J Nanomedicine,* 10, 1609-23.

Haghniaz, Reihaneh, Umrani, Rinku D., and Paknikar, Kishore M. (2015b), 'Temperature-dependent and time-dependent effects of hyperthermia mediated by dextran-coated La(0.7)Sr(0.3)MnO(3): in vitro studies', *International Journal of Nanomedicine,* 10, 1609-23.

Hainfeld, James F., et al. (2014), 'Gold Nanoparticle Hyperthermia Reduces Radiotherapy Dose', *Nanomedicine : nanotechnology, biology, and medicine,* 10 (8), 1609-17.

Hamacher-Brady, Anne and Brady, Nathan Ryan (2015), 'Bax/Bak-dependent, Drp1-independent Targeting of X-linked Inhibitor of Apoptosis Protein (XIAP) into Inner Mitochondrial Compartments Counteracts Smac/DIABLO-dependent Effector Caspase Activation', *The Journal of Biological Chemistry,* 290 (36), 22005-18.

Han, J., et al. (2016a), 'Correction: Glucose-functionalized Au nanoprisms for optoacoustic imaging and near-infrared photothermal therapy', *Nanoscale,* 8 (3), 1704.

Han, J., et al. (2016b), 'Glucose-functionalized Au nanoprisms for optoacoustic imaging and near-infrared photothermal therapy', *Nanoscale,* 8 (1), 492-9.

Hanahan, D. and Weinberg, R. A. (2000), 'The hallmarks of cancer', *Cell,* 100 (1), 57-70.

Hanini, Amel, et al. (2011), 'Evaluation of iron oxide nanoparticle biocompatibility', *International Journal of Nanomedicine,* 6, 787-94.

Hao, Encai, et al. (2004), 'Synthesis and Optical Properties of "Branched" Gold Nanocrystals', *Nano Letters,* 4 (2), 327-30.

Hao, Rui, et al. (2013), 'Developing Fe3O4 nanoparticles into an efficient multimodality imaging and therapeutic probe', *Nanoscale,* 5 (23), 11954-63.

Hassan, Mohamed, et al. (2014), 'Apoptosis and Molecular Targeting Therapy in Cancer', *BioMed Research International,* 2014, 150845.

Hauck, T. S., Ghazani, A. A., and Chan, W. C. (2008a), 'Assessing the effect of surface chemistry on gold nanorod uptake, toxicity, and gene expression in mammalian cells', *Small,* 4 (1), 153-9.

Hauck, Tanya S., et al. (2008b), 'Enhancing the Toxicity of Cancer Chemotherapeutics with Gold Nanorod Hyperthermia', *Advanced Materials,* 20 (20), 3832-38.

Hayashi, K., et al. (2013), 'Superparamagnetic nanoparticle clusters for cancer theranostics combining magnetic resonance imaging and hyperthermia treatment', *Theranostics,* 3 (6), 366-76.

Hegyi, G., Szigeti, G. P., and Szasz, A. (2013), 'Hyperthermia versus Oncothermia: Cellular Effects in Complementary Cancer Therapy', *Evid Based Complement Alternat Med,* 2013, 672873.

Hervault, A. and Thanh, N. T. (2014), 'Magnetic nanoparticle-based therapeutic agents for thermo-chemotherapy treatment of cancer', *Nanoscale,* 6 (20), 11553-73.

Hildebrandt, B., et al. (2002), 'The cellular and molecular basis of hyperthermia', *Crit Rev Oncol Hematol,* 43 (1), 33-56.

Hilger, I., et al. (2002), 'Thermal ablation of tumors using magnetic nanoparticles: an in vivo feasibility study', *Invest Radiol,* 37 (10), 580-6.

Hilger, Ingrid (2013), 'In vivo applications of magnetic nanoparticle hyperthermia', *International Journal of Hyperthermia,* 29 (8), 828-34.

Hillyer, J. F. and Albrecht, R. M. (2001), 'Gastrointestinal persorption and tissue distribution of differently sized colloidal gold nanoparticles', *J Pharm Sci,* 90 (12), 1927-36.

Hinman, J. G., et al. (2016), 'Seed mediated growth of gold nanorods: towards nanorod matryoshkas', *Faraday Discuss,* 191, 9-33.

Hironobu, Takahashi, et al. (2006), 'Photothermal reshaping of gold nanorods prevents further cell death', *Nanotechnology,* 17 (17), 4431.

Hirsch, L. R., et al. (2003), 'Nanoshell-mediated near-infrared thermal therapy of tumors under magnetic resonance guidance', *Proc Natl Acad Sci U S A,* 100 (23), 13549-54.

Hleb, E. Y., et al. (2008), 'LANTCET: elimination of solid tumor cells with photothermal bubbles generated around clusters of gold nanoparticles', *Nanomedicine (Lond),* 3 (5), 647-67.
Hornung, Annkathrin, et al. (2016), 'Toxicity of Mitoxantrone-loaded Superparamagnetic Iron Oxide Nanoparticles in a HT-29 Tumour Spheroid Model', *Anticancer Research,* 36 (6), 3093-101.
Horowitz, Michal and Robinson, Sharon D. M. (2007), 'Heat shock proteins and the heat shock response during hyperthermia and its modulation by altered physiological conditions', 162, 433-46.
Horsman, M. R. and Overgaard, J. (2007), 'Hyperthermia: a potent enhancer of radiotherapy', *Clin Oncol (R Coll Radiol),* 19 (6), 418-26.
Hou, C. H., et al. (2014a), 'Hyperthermia induces apoptosis through endoplasmic reticulum and reactive oxygen species in human osteosarcoma cells', *Int J Mol Sci,* 15 (10), 17380-95.
Hou, Chun-Han, et al. (2014b), 'Hyperthermia Induces Apoptosis through Endoplasmic Reticulum and Reactive Oxygen Species in Human Osteosarcoma Cells', *International Journal of Molecular Sciences,* 15 (10), 17380-95.
Howells, Christopher C., et al. (2011), 'The Bcl-2-associated death promoter (BAD) lowers the threshold at which the Bcl-2-interacting domain death agonist (BID) triggers mitochondria disintegration', *Journal of Theoretical Biology,* 271 (1), 114-23.
Hua, Yi, et al. (2015), 'Shape-Dependent Nonlinear Optical Properties of Anisotropic Gold Nanoparticles', *The Journal of Physical Chemistry Letters,* 6 (24), 4904-08.
Huang, Hui S. and Hainfeld, James F. (2013), 'Intravenous magnetic nanoparticle cancer hyperthermia', *International Journal of Nanomedicine,* 8, 2521-32.
Huang, S. H., et al. (1999), 'Effects of hyperthermia on the cytoskeleton and focal adhesion proteins in a human thyroid carcinoma cell line', *J Cell Biochem,* 75 (2), 327-37.
Huang, X., et al. (2006a), 'Cancer cell imaging and photothermal therapy in the near-infrared region by using gold nanorods', *J Am Chem Soc,* 128 (6), 2115-20.
Huang, X., et al. (2008), 'Plasmonic photothermal therapy (PPTT) using gold nanoparticles', *Lasers Med Sci,* 23 (3), 217-28.
Huang, Xiaohua and El-Sayed, Mostafa A. (2010), 'Gold nanoparticles: Optical properties and implementations in cancer diagnosis and photothermal therapy', *Journal of Advanced Research,* 1 (1), 13-28.
Huang, Xiaohua and El-Sayed, Mostafa A (2011), 'Plasmonic photo-thermal therapy (PPTT)', *Alexandria Journal of Medicine,* 47 (1), 1-9.
Huang, Xiaohua, et al. (2006b), 'Cancer Cell Imaging and Photothermal Therapy in the Near-Infrared Region by Using Gold Nanorods', *Journal of the American Chemical Society,* 128 (6), 2115-20.
Huefner, A., et al. (2014), 'Gold nanoparticles explore cells: cellular uptake and their use as intracellular probes', *Methods,* 68 (2), 354-63.
Huotari, Jatta and Helenius, Ari (2011), 'Endosome maturation', *The EMBO Journal,* 30 (17), 3481-500.
Hussain, S. M., et al. (2005), 'In vitro toxicity of nanoparticles in BRL 3A rat liver cells', *Toxicol In Vitro,* 19 (7), 975-83.
Hyndman, I. J. (2016), 'Review: the Contribution of both Nature and Nurture to Carcinogenesis and Progression in Solid Tumours', *Cancer Microenviron,* 9 (1), 63-9.
Ibricevic, Aida, et al. (2013), 'PEGylation of cationic, shell-crosslinked-knedel-like nanoparticles modulates inflammation and enhances cellular uptake in the lung', *Nanomedicine : nanotechnology, biology, and medicine,* 9 (7), 912-22.

Ilmarinen, Pinja, Moilanen, Eeva, and Kankaanranta, Hannu (2014), 'Mitochondria in the Center of Human Eosinophil Apoptosis and Survival', *International Journal of Molecular Sciences,* 15 (3), 3952-69.

Imamura, Y., et al. (2015), 'Comparison of 2D- and 3D-culture models as drug-testing platforms in breast cancer', *Oncol Rep,* 33 (4), 1837-43.

Inturi, S., et al. (2015), 'Modulatory Role of Surface Coating of Superparamagnetic Iron Oxide Nanoworms in Complement Opsonization and Leukocyte Uptake', *ACS Nano,* 9 (11), 10758-68.

Issa, B., et al. (2013a), 'Magnetic nanoparticles: surface effects and properties related to biomedicine applications', *Int J Mol Sci,* 14 (11), 21266-305.

Issa, Bashar, et al. (2013b), 'Magnetic Nanoparticles: Surface Effects and Properties Related to Biomedicine Applications', *International Journal of Molecular Sciences,* 14 (11), 21266-305.

Issels, R. D. (2008), 'Hyperthermia adds to chemotherapy', *Eur J Cancer,* 44 (17), 2546-54.

Issels, Rolf D., et al. (2010), 'Neo-adjuvant chemotherapy alone or with regional hyperthermia for localised high-risk soft-tissue sarcoma: a randomised phase 3 multicentre study', *The lancet oncology,* 11 (6), 561-70.

Ivanova, Saka, et al. (2008), 'Chapter Nine Lysosomes in Apoptosis', *Methods in Enzymology* (Volume 442: Academic Press), 183-99.

Ivask, A., et al. (2015), 'Toxicity of 11 Metal Oxide Nanoparticles to Three Mammalian Cell Types In Vitro', *Curr Top Med Chem,* 15 (18), 1914-29.

Jain, Prashant K., et al. (2006), 'Calculated Absorption and Scattering Properties of Gold Nanoparticles of Different Size, Shape, and Composition: Applications in Biological Imaging and Biomedicine', *The Journal of Physical Chemistry B,* 110 (14), 7238-48.

Jain, S., et al. (2014), 'Gold nanoparticle cellular uptake, toxicity and radiosensitisation in hypoxic conditions', *Radiother Oncol,* 110 (2), 342-7.

Jego, G., et al. (2013), 'Targeting heat shock proteins in cancer', *Cancer Lett,* 332 (2), 275-85.

Jena, Bikash Kumar and Raj, C. Retna (2007), 'Shape-Controlled Synthesis of Gold Nanoprism and Nanoperiwinkles with Pronounced Electrocatalytic Activity', *The Journal of Physical Chemistry C,* 111 (42), 15146-53.

Jeon, Seongho, et al. (2016), 'Quantifying intra- and extracellular aggregation of iron oxide nanoparticles and its influence on specific absorption rate', *Nanoscale,* 8 (35), 16053-64.

Jiang, Ke, Smith, David A., and Pinchuk, Anatoliy (2013), 'Size-Dependent Photothermal Conversion Efficiencies of Plasmonically Heated Gold Nanoparticles', *The Journal of Physical Chemistry C,* 117 (51), 27073-80.

Jiang, Q. L., et al. (2014), 'Folic acid-conjugated Fe3O4 magnetic nanoparticles for hyperthermia and MRI in vitro and in vivo', *Applied Surface Science,* 307, 224-33.

Jiang, Ying, et al. (2015), 'The Interplay of Size and Surface Functionality on the Cellular Uptake of Sub-10 nm Gold Nanoparticles', *ACS Nano,* 9 (10), 9986-93.

Jihye, Choi, et al. (2011), 'Gold Nanostructures as Photothermal Therapy Agent for Cancer', *Anti-Cancer Agents in Medicinal Chemistry,* 11 (10), 953-64.

Johannsen, M., et al. (2005), 'Clinical hyperthermia of prostate cancer using magnetic nanoparticles: presentation of a new interstitial technique', *Int J Hyperthermia,* 21 (7), 637-47.

Johannsen, Manfred, et al. (2007), 'Thermotherapy of Prostate Cancer Using Magnetic Nanoparticles: Feasibility, Imaging, and Three-Dimensional Temperature Distribution', *European Urology,* 52 (6), 1653-62.

Jokerst, Jesse V., et al. (2011), 'Nanoparticle PEGylation for imaging and therapy', *Nanomedicine (London, England),* 6 (4), 715-28.
Jolesch, A., et al. (2012), 'Hsp70, a messenger from hyperthermia for the immune system', *Eur J Cell Biol,* 91 (1), 48-52.
Jolly, C. and Morimoto, R. I. (2000), 'Role of the heat shock response and molecular chaperones in oncogenesis and cell death', *J Natl Cancer Inst,* 92 (19), 1564-72.
Jones, Daniel J., Bunn, Frances, and Bell-Syer, Sophie V. (2014), 'Prophylactic antibiotics to prevent surgical site infection after breast cancer surgery', *Cochrane Database of Systematic Reviews,* (3).
Jones, E. L., et al. (2005), 'Randomized trial of hyperthermia and radiation for superficial tumors', *J Clin Oncol,* 23 (13), 3079-85.
Jones, Matthew R., et al. (2009), 'Plasmonically Controlled Nucleic Acid Dehybridization with Gold Nanoprisms', *Chemphyschem : a European journal of chemical physics and physical chemistry,* 10 (0), 1461-65.
Jordan, Andreas, et al. (2001), 'Presentation of a new magnetic field therapy system for the treatment of human solid tumors with magnetic fluid hyperthermia', *Journal of Magnetism and Magnetic Materials,* 225 (1–2), 118-26.
Jordan, Bénédicte F. and Sonveaux, Pierre (2012), 'Targeting Tumor Perfusion and Oxygenation to Improve the Outcome of Anticancer Therapy', *Frontiers in Pharmacology,* 3, 94.
Joris, Freya, et al. (2013), 'Assessing nanoparticle toxicity in cell-based assays: influence of cell culture parameters and optimized models for bridging the in vitro-in vivo gap', *Chemical Society Reviews,* 42 (21), 8339-59.
Jou, M. J., et al. (2002), 'Critical role of mitochondrial reactive oxygen species formation in visible laser irradiation-induced apoptosis in rat brain astrocytes (RBA-1)', *J Biomed Sci,* 9 (6 Pt 1), 507-16.
Jou, Mei-Jie, et al. (2004), 'Mitochondrial Reactive Oxygen Species Generation and Calcium Increase Induced by Visible Light in Astrocytes', *Annals of the New York Academy of Sciences,* 1011 (1), 45-56.
Junxi, Zhang, Lide, Zhang, and Wei, Xu (2012), 'Surface plasmon polaritons: physics and applications', *Journal of Physics D: Applied Physics,* 45 (11), 113001.
Kaddi, Chanchala D., Phan, John H., and Wang, May D. (2013), 'Computational nanomedicine: modeling of nanoparticle-mediated hyperthermal cancer therapy', *Nanomedicine (London, England),* 8 (8), 1323-33.
Kaksonen, M., Toret, C. P., and Drubin, D. G. (2006), 'Harnessing actin dynamics for clathrin-mediated endocytosis', *Nat Rev Mol Cell Biol,* 7 (6), 404-14.
Kalamida, D., et al. (2015), 'Fever-range hyperthermia vs. hypothermia effect on cancer cell viability, proliferation and HSP90 expression', *PLoS One,* 10 (1), e0116021.
Kalmar, B. and Greensmith, L. (2009), 'Induction of heat shock proteins for protection against oxidative stress', *Adv Drug Deliv Rev,* 61 (4), 310-8.
Kampinga, H. H. and Dikomey, E. (2001), 'Hyperthermic radiosensitization: mode of action and clinical relevance', *Int J Radiat Biol,* 77 (4), 399-408.
Kandasamy, G. and Maity, D. (2015a), 'Recent advances in superparamagnetic iron oxide nanoparticles (SPIONs) for in vitro and in vivo cancer nanotheranostics', *Int J Pharm,* 496 (2), 191-218.
Kandasamy, Ganeshlenin and Maity, Dipak (2015b), 'Recent advances in superparamagnetic iron oxide nanoparticles (SPIONs) for in vitro and in vivo cancer nanotheranostics', *International Journal of Pharmaceutics,* 496 (2), 191-218.

Kantari, Chahrazade and Walczak, Henning (2011), 'Caspase-8 and Bid: Caught in the act between death receptors and mitochondria', *Biochimica et Biophysica Acta (BBA) - Molecular Cell Research,* 1813 (4), 558-63.

Karagoz, G. E. and Rudiger, S. G. (2015), 'Hsp90 interaction with clients', *Trends Biochem Sci,* 40 (2), 117-25.

Karakoçak, Bedia Begüm, et al. (2016), 'Biocompatibility of gold nanoparticles in retinal pigment epithelial cell line', *Toxicology in Vitro,* 37, 61-69.

Kasof, G. M., et al. (2001), 'Tumor necrosis factor-alpha induces the expression of DR6, a member of the TNF receptor family, through activation of NF-kappaB', *Oncogene,* 20 (55), 7965-75.

Katschinski, Dörthe M., et al. (2000), 'Pivotal Role of Reactive Oxygen Species as Intracellular Mediators of Hyperthermia-induced Apoptosis', *Journal of Biological Chemistry,* 275 (28), 21094-98.

Kaur, P., et al. (2016), 'Hyperthermia using nanoparticles - Promises and pitfalls', *Int J Hyperthermia,* 32 (1), 76-88.

Keibler, M. A., et al. (2016), 'Metabolic requirements for cancer cell proliferation', *Cancer Metab,* 4, 16.

Kelly, K. J., Baird, N. R., and Greene, A. L. (2001), 'Induction of stress response proteins and experimental renal ischemia/reperfusion', *Kidney Int,* 59 (5), 1798-802.

Kelly, K. Lance, et al. (2003), 'The Optical Properties of Metal Nanoparticles: The Influence of Size, Shape, and Dielectric Environment', *The Journal of Physical Chemistry B,* 107 (3), 668-77.

Kerr, J. F., Wyllie, A. H., and Currie, A. R. (1972), 'Apoptosis: a basic biological phenomenon with wide-ranging implications in tissue kinetics', *Br J Cancer,* 26 (4), 239-57.

Kettler, Katja, et al. (2014), 'Cellular uptake of nanoparticles as determined by particle properties, experimental conditions, and cell type', *Environmental Toxicology and Chemistry,* 33 (3), 481-92.

Khadka, Daulat B. and Cho, Won-Jea (2013), 'Topoisomerase inhibitors as anticancer agents: a patent update', *Expert Opinion on Therapeutic Patents,* 23 (8), 1033-56.

Khan, M. S., Vishakante, G. D., and Siddaramaiah, H. (2013), 'Gold nanoparticles: a paradigm shift in biomedical applications', *Adv Colloid Interface Sci,* 199-200, 44-58.

Khlebtsov, Boris N., et al. (2012), 'Plasmonic Nanopowders for Photothermal Therapy of Tumors', *Langmuir,* 28 (24), 8994-9002.

Khlebtsov, N. and Dykman, L. (2011), 'Biodistribution and toxicity of engineered gold nanoparticles: a review of in vitro and in vivo studies', *Chem Soc Rev,* 40 (3), 1647-71.

Khlebtsov, Nikolai G. and Dykman, Lev A. (2010), 'Optical properties and biomedical applications of plasmonic nanoparticles', *Journal of Quantitative Spectroscopy and Radiative Transfer,* 111 (1), 1-35.

Khoei, Samideh, et al. (2004), 'The role of heat shock protein 70 in the thermoresistance of prostate cancer cell line spheroids', *FEBS Letters,* 561 (1-3), 144-48.

Khot, V. M., et al. (2013), 'Induction heating studies of dextran coated MgFe2O4 nanoparticles for magnetic hyperthermia', *Dalton Transactions,* 42 (4), 1249-58.

Kikusato, M. and Toyomizu, M. (2013), 'Crucial role of membrane potential in heat stress-induced overproduction of reactive oxygen species in avian skeletal muscle mitochondria', *PLoS One,* 8 (5), e64412.

Kim, B. M., et al. (2014), 'Heavy metals induce oxidative stress and trigger oxidative stress-mediated heat shock protein (hsp) modulation in the intertidal copepod Tigriopus japonicus', *Comp Biochem Physiol C Toxicol Pharmacol,* 166, 65-74.

Kim, Byeong Mo and Chung, Hai Won (2007), 'Hypoxia/reoxygenation induces apoptosis through a ROS-mediated caspase-8/Bid/Bax pathway in human lymphocytes', *Biochemical and Biophysical Research Communications,* 363 (3), 745-50.

Kim, H. C., et al. (2015), 'Magnetic nanoparticle-conjugated polymeric micelles for combined hyperthermia and chemotherapy', *Nanoscale,* 7 (39), 16470-80.

Kim, Heejung, et al. (2016a), 'Near-infrared light-responsive nanomaterials for cancer theranostics', *Wiley Interdisciplinary Reviews: Nanomedicine and Nanobiotechnology,* 8 (1), 23-45.

Kim, Jun-Sung, et al. (2006), 'Cellular uptake of magnetic nanoparticle is mediated through energy-dependent endocytosis in A549 cells', *Journal of Veterinary Science,* 7 (4), 321-26.

Kim, K. S., et al. (2016b), 'Stimuli-responsive magnetic nanoparticles for tumor-targeted bimodal imaging and photodynamic/hyperthermia combination therapy', *Nanoscale,* 8 (22), 11625-34.

Kiraz, Y., et al. (2016a), 'Major apoptotic mechanisms and genes involved in apoptosis', *Tumour Biol,* 37 (7), 8471-86.

Kiraz, Yağmur, et al. (2016b), 'Major apoptotic mechanisms and genes involved in apoptosis', *Tumor Biology,* 37 (7), 8471-86.

Klostergaard, J., et al. (2006), 'Hyperthermia engages the intrinsic apoptotic pathway by enhancing upstream caspase activation to overcome apoptotic resistance in MCF-7 breast adenocarcinoma cells', *Journal of Cellular Biochemistry,* 98 (2), 356-69.

Klute, Kelsey, et al. (2014), 'Microtubule inhibitor-based antibody–drug conjugates for cancer therapy', *OncoTargets and therapy,* 7, 2227-36.

Kobayashi, Tastuya, et al. (1991), 'Interstitial hyperthermia of malignant brain tumors by implant heating system: Clinical experience', *Journal of Neuro-Oncology,* 10 (2), 153-63.

Kocab, Andrew J. and Duckett, Colin S. (2016), 'Inhibitor of apoptosis proteins as intracellular signaling intermediates', *FEBS Journal,* 283 (2), 221-31.

Kodiha, M., et al. (2014), 'Gold nanoparticles induce nuclear damage in breast cancer cells, which is further amplified by hyperthermia', *Cell Mol Life Sci,* 71 (21), 4259-73.

Koenig, M. N., et al. (2014), 'Pro-apoptotic BIM is an essential initiator of physiological endothelial cell death independent of regulation by FOXO3', *Cell Death and Differentiation,* 21 (11), 1687-95.

Kolhatkar, A. G., et al. (2013a), 'Tuning the magnetic properties of nanoparticles', *Int J Mol Sci,* 14 (8), 15977-6009.

Kolhatkar, Arati G., et al. (2013b), 'Tuning the Magnetic Properties of Nanoparticles', *International Journal of Molecular Sciences,* 14 (8), 15977-6009.

Kong, B., et al. (2011), 'Experimental considerations on the cytotoxicity of nanoparticles', *Nanomedicine (Lond),* 6 (5), 929-41.

Koschny, Ronald, et al. (2015), 'WHO grade related expression of TRAIL-receptors and apoptosis regulators in meningioma', *Pathology - Research and Practice,* 211 (2), 109-16.

Kou, Longfa, et al. (2013), 'The endocytosis and intracellular fate of nanomedicines: Implication for rational design', *Asian Journal of Pharmaceutical Sciences,* 8 (1), 1-10.

Koussounadis, Antonis, et al. (2015), 'Relationship between differentially expressed mRNA and mRNA-protein correlations in a xenograft model system', *Scientific Reports,* 5, 10775.
Koutsilieris, M., et al. (1999), 'Chemotherapy cytotoxicity of human MCF-7 and MDA-MB 231 breast cancer cells is altered by osteoblast-derived growth factors', *Molecular Medicine,* 5 (2), 86-97.
Krakstad, Camilla and Chekenya, Martha (2010), 'Survival signalling and apoptosis resistance in glioblastomas: opportunities for targeted therapeutics', *Molecular Cancer,* 9, 135-35.
Krishnan, Sunil, Diagaradjane, Parmeswaran, and Cho, Sang Hyun (2010), 'Nanoparticle-mediated thermal therapy: Evolving strategies for prostate cancer therapy', *International Journal of Hyperthermia,* 26 (8), 775-89.
Kroemer, Guido and Jaattela, Marja (2005), 'Lysosomes and autophagy in cell death control', *Nat Rev Cancer,* 5 (11), 886-97.
Krpetic, Z., et al. (2010), 'Inflicting controlled nonthermal damage to subcellular structures by laser-activated gold nanoparticles', *Nano Lett,* 10 (11), 4549-54.
Krpetić, Željka, et al. (2010), 'Inflicting Controlled Nonthermal Damage to Subcellular Structures by Laser-Activated Gold Nanoparticles', *Nano Letters,* 10 (11), 4549-54.
Kruse, A. M., et al. (2014), 'Synthesis and characterization of CREKA-conjugated iron oxide nanoparticles for hyperthermia applications', *Acta Biomater,* 10 (6), 2622-9.
Kruse, Jan-Philipp and Gu, Wei (2009), 'Modes of p53 Regulation', *Cell,* 137 (4), 609-22.
Kuhn, D. A., et al. (2014), 'Different endocytotic uptake mechanisms for nanoparticles in epithelial cells and macrophages', *Beilstein J Nanotechnol,* 5, 1625-36.
Kuimova, Marina K., et al. (2009), 'Imaging intracellular viscosity of a single cell during photoinduced cell death', *Nat Chem,* 1 (1), 69-73.
Kulikov, A. V., et al. (2012), 'Cytochrome c: the Achilles' heel in apoptosis', *Cell Mol Life Sci,* 69 (11), 1787-97.
Kumar, C. S. and Mohammad, F. (2011), 'Magnetic nanomaterials for hyperthermia-based therapy and controlled drug delivery', *Adv Drug Deliv Rev,* 63 (9), 789-808.
Kumar, S. (2009), 'Caspase 2 in apoptosis, the DNA damage response and tumour suppression: enigma no more?', *Nat Rev Cancer,* 9 (12), 897-903.
Kumar, S., Aaron, J., and Sokolov, K. (2008), 'Directional conjugation of antibodies to nanoparticles for synthesis of multiplexed optical contrast agents with both delivery and targeting moieties', *Nat Protoc,* 3 (2), 314-20.
Kumar, Sanjay, et al. (2016), 'Targeting Hsp70: A possible therapy for cancer', *Cancer Letters,* 374 (1), 156-66.
Lakhani, P. M., et al. (2015), 'An overview of synthetic strategies and current applications of gold nanorods in cancer treatment', *Nanotechnology,* 26 (43), 432001.
Lalaoui, Najoua, et al. (2011), 'TRAIL-R4 Promotes Tumor Growth and Resistance to Apoptosis in Cervical Carcinoma HeLa Cells through AKT', *PLoS ONE,* 6 (5), e19679.
Langer, R. and Weissleder, R. (2015), 'Nanotechnology', *JAMA,* 313 (2), 135-6.
Lanneau, D., et al. (2008a), 'Heat shock proteins: essential proteins for apoptosis regulation', *Journal of Cellular and Molecular Medicine,* 12 (3), 743-61.
Lanneau, D., et al. (2008b), 'Heat shock proteins: essential proteins for apoptosis regulation', *J Cell Mol Med,* 12 (3), 743-61.

Lanone, S., et al. (2009), 'Comparative toxicity of 24 manufactured nanoparticles in human alveolar epithelial and macrophage cell lines', *Part Fibre Toxicol,* 6, 14.
Lapotko, D. O., Lukianova, E., and Oraevsky, A. A. (2006), 'Selective laser nano-thermolysis of human leukemia cells with microbubbles generated around clusters of gold nanoparticles', *Lasers Surg Med,* 38 (6), 631-42.
Lauber, K., et al. (2015), 'Targeting the heat shock response in combination with radiotherapy: Sensitizing cancer cells to irradiation-induced cell death and heating up their immunogenicity', *Cancer Lett,* 368 (2), 209-29.
Laurent, S., et al. (2011), 'Magnetic fluid hyperthermia: focus on superparamagnetic iron oxide nanoparticles', *Adv Colloid Interface Sci,* 166 (1-2), 8-23.
Laurent, S., et al. (2012a), 'Crucial ignored parameters on nanotoxicology: the importance of toxicity assay modifications and "cell vision"', *PLoS One,* 7 (1), e29997.
Laurent, Sophie, et al. (2012b), 'Crucial Ignored Parameters on Nanotoxicology: The Importance of Toxicity Assay Modifications and “Cell Vision”', *PLoS ONE,* 7 (1), e29997.
Leadsham, Jane E, et al. (2013), 'Loss of Cytochrome c Oxidase Promotes RAS-Dependent ROS Production from the ER Resident NADPH Oxidase, Yno1p, in Yeast', *Cell Metabolism,* 18 (2), 279-86.
Lee, J., et al. (2014a), 'Gold nanoparticles in breast cancer treatment: promise and potential pitfalls', *Cancer Lett,* 347 (1), 46-53.
Lee, J. H., et al. (2011), 'Exchange-coupled magnetic nanoparticles for efficient heat induction', *Nat Nanotechnol,* 6 (7), 418-22.
Lee, Jihyoun, et al. (2014b), 'Gold nanoparticles in breast cancer treatment: Promise and potential pitfalls', *Cancer letters,* 347 (1), 46-53.
Lee, Jungwoo, et al. (2009), 'In vitro Toxicity Testing of Nanoparticles in 3D Cell Culture', *Small,* 5 (10), 1213-21.
Leist, M. and Jaattela, M. (2001), 'Triggering of apoptosis by cathepsins', *Cell Death Differ,* 8 (4), 324-6.
Leung, P. Jennifer, et al. (2013), 'Investigation of Sub-100 nm Gold Nanoparticles for Laser-Induced Thermotherapy of Cancer', *Nanomaterials,* 3 (1).
Li, J. L., et al. (2009), 'In vitro cancer cell imaging and therapy using transferrin-conjugated gold nanoparticles', *Cancer Lett,* 274 (2), 319-26.
Li, L., et al. (2014), 'A novel two-step mild hyperthermia for advanced liposomal chemotherapy', *J Control Release,* 174, 202-8.
Li, Shyh-Dar and Huang, Leaf (2008), 'Pharmacokinetics and Biodistribution of Nanoparticles', *Molecular Pharmaceutics,* 5 (4), 496-504.
Li, W. and Chen, X. (2015), 'Gold nanoparticles for photoacoustic imaging', *Nanomedicine (Lond),* 10 (2), 299-320.
Liao, S. H., et al. (2015), 'Functionalized magnetic iron oxide/alginate core-shell nanoparticles for targeting hyperthermia', *Int J Nanomedicine,* 10, 3315-27.
Libutti, S. K., et al. (2010), 'Phase I and pharmacokinetic studies of CYT-6091, a novel PEGylated colloidal gold-rhTNF nanomedicine', *Clin Cancer Res,* 16 (24), 6139-49.
Lin, Guimei, Zhang, Hong, and Huang, Leaf (2015), 'Smart Polymeric Nanoparticles for Cancer Gene Delivery', *Molecular Pharmaceutics,* 12 (2), 314-21.
Lin, M., et al. (2013a), 'The anti-hepatoma effect of nanosized Mn-Zn ferrite magnetic fluid hyperthermia associated with radiation in vitro and in vivo', *Nanotechnology,* 24 (25), 255101.
Lin, R. Z. and Chang, H. Y. (2008), 'Recent advances in three-dimensional multicellular spheroid culture for biomedical research', *Biotechnol J,* 3 (9-10), 1172-84.

Lin, Yazhou, et al. (2016), 'Survivin is expressed in degenerated nucleus pulposus cells and is involved in proliferation and the prevention of apoptosis in vitro', *Molecular Medicine Reports,* 13 (1), 1026-32.
Lin, Yuan-Feng, et al. (2013b), 'Targeting the XIAP/caspase-7 complex selectively kills caspase-3–deficient malignancies', *The Journal of Clinical Investigation,* 123 (9), 3861-75.
Link, S. and El-Sayed, M. A. (2003), 'Optical properties and ultrafast dynamics of metallic nanocrystals', *Annu Rev Phys Chem,* 54, 331-66.
Liu, Gang, et al. (2013a), 'Applications and Potential Toxicity of Magnetic Iron Oxide Nanoparticles', *Small,* 9 (9-10), 1533-45.
Liu, H., et al. (2012), 'Size dependent cellular uptake, in vivo fate and light-heat conversion efficiency of gold nanoshells on silica nanorattles', *Nanoscale,* 4 (11), 3523-9.
Liu, Huiyu, et al. (2013b), 'Impact of PEGylation on the biological effects and light heat conversion efficiency of gold nanoshells on silica nanorattles', *Biomaterials,* 34 (28), 6967-75.
Liu, Jinbin, et al. (2013c), 'PEGylation and Zwitterionization: Pros and Cons in Renal Clearance and Tumor Targeting of Near-IR-Emitting Gold Nanoparticles', *Angewandte Chemie (International ed. in English),* 52 (48), 12572-76.
Liu, Y., et al. (2011), 'Effects of DMSA-coated Fe3O4 magnetic nanoparticles on global gene expression of mouse macrophage RAW264.7 cells', *Toxicol Lett,* 205 (2), 130-9.
Liu, Y., et al. (2015), 'A Plasmonic Gold Nanostar Theranostic Probe for In Vivo Tumor Imaging and Photothermal Therapy', *Theranostics,* 5 (9), 946-60.
Loessner, Daniela, et al. (2010), 'Bioengineered 3D platform to explore cell–ECM interactions and drug resistance of epithelial ovarian cancer cells', *Biomaterials,* 31 (32), 8494-506.
Look, J., et al. (2015), 'Ligand-Modified Human Serum Albumin Nanoparticles for Enhanced Gene Delivery', *Mol Pharm,* 12 (9), 3202-13.
Love, J Christopher, et al. (2005), 'Self-assembled monolayers of thiolates on metals as a form of nanotechnology', *Chemical reviews,* 105 (4), 1103-70.
Luanpitpong, Sudjit, et al. (2013), 'Regulation of apoptosis by Bcl-2 cysteine oxidation in human lung epithelial cells', *Molecular Biology of the Cell,* 24 (6), 858-69.
Lubbe, A. S., et al. (1996), 'Clinical experiences with magnetic drug targeting: a phase I study with 4'-epidoxorubicin in 14 patients with advanced solid tumors', *Cancer Res,* 56 (20), 4686-93.
Luchetti, F., et al. (2002), 'Actin involvement in apoptotic chromatin changes of hemopoietic cells undergoing hyperthermia', *Apoptosis,* 7 (2), 143-52.
Luo, Xin and Kraus, W. Lee (2012), 'On PAR with PARP: cellular stress signaling through poly(ADP-ribose) and PARP-1', *Genes & Development,* 26 (5), 417-32.
Ma, N., et al. (2013), 'Influence of nanoparticle shape, size, and surface functionalization on cellular uptake', *J Nanosci Nanotechnol,* 13 (10), 6485-98.
Ma, Xingqun, et al. (2015), 'PEGylated gold nanoprisms for photothermal therapy at low laser power density', *RSC Adv.,* 5 (99), 81682-88.
Mackey, M. A., et al. (2014), 'The most effective gold nanorod size for plasmonic photothermal therapy: theory and in vitro experiments', *J Phys Chem B,* 118 (5), 1319-26.
Madersbacher, S., et al. (1998), 'Regulation of heat shock protein 27 expression of prostatic cells in response to heat treatment', *Prostate,* 37 (3), 174-81.
Madsen, Steen J., et al. (2015), 'Nanoparticle-loaded macrophage-mediated photothermal therapy: potential for glioma treatment', *Lasers in medical science,* 30 (4), 1357-65.

Maeda, Hiroshi, Nakamura, Hideaki, and Fang, Jun (2013), 'The EPR effect for macromolecular drug delivery to solid tumors: Improvement of tumor uptake, lowering of systemic toxicity, and distinct tumor imaging in vivo', *Advanced Drug Delivery Reviews,* 65 (1), 71-79.

Mahmoudi, M., et al. (2011), 'Superparamagnetic iron oxide nanoparticles (SPIONs): development, surface modification and applications in chemotherapy', *Adv Drug Deliv Rev,* 63 (1-2), 24-46.

Mahmoudi, M., et al. (2012), 'Cell "vision": complementary factor of protein corona in nanotoxicology', *Nanoscale,* 4 (17), 5461-8.

Maier-Hauff, Klaus, et al. (2011), 'Efficacy and safety of intratumoral thermotherapy using magnetic iron-oxide nanoparticles combined with external beam radiotherapy on patients with recurrent glioblastoma multiforme', *Journal of Neuro-Oncology,* 103 (2), 317-24.

Maier-Hauff, Klaus, et al. (2007), 'Intracranial Thermotherapy using Magnetic Nanoparticles Combined with External Beam Radiotherapy: Results of a Feasibility Study on Patients with Glioblastoma Multiforme', *Journal of Neuro-Oncology,* 81 (1), 53-60.

Majidi, S., et al. (2016), 'Magnetic nanoparticles: Applications in gene delivery and gene therapy', *Artif Cells Nanomed Biotechnol,* 44 (4), 1186-93.

Mallory, M., et al. (2015), 'Therapeutic hyperthermia: The old, the new, and the upcoming', *Crit Rev Oncol Hematol*.

Malvindi, Maria Ada, et al. (2014), 'Toxicity Assessment of Silica Coated Iron Oxide Nanoparticles and Biocompatibility Improvement by Surface Engineering', *PLoS ONE,* 9 (1), e85835.

Mamiya, H. and Jeyadevan, B. (2011), 'Hyperthermic effects of dissipative structures of magnetic nanoparticles in large alternating magnetic fields', *Sci Rep,* 1, 157.

Manjari, R., et al. (2015), 'HSP70 as a marker of heat and humidity stress in Tarai buffalo', *Trop Anim Health Prod,* 47 (1), 111-6.

Mari, M., et al. (2009), 'Mitochondrial glutathione, a key survival antioxidant', *Antioxid Redox Signal,* 11 (11), 2685-700.

Mariño, Guillermo, et al. (2014), 'Self-consumption: the interplay of autophagy and apoptosis', *Nature reviews. Molecular cell biology,* 15 (2), 81-94.

Marquez, C. M., et al. (1994), 'HSP 70 synthesis in clinical hyperthermia patients: preliminary results of a new technique', *Int J Radiat Oncol Biol Phys,* 28 (2), 425-30.

Marquis, Bryce J., et al. (2009), 'Analytical methods to assess nanoparticle toxicity', *Analyst,* 134 (3), 425-39.

Martinez-Ruiz, G., et al. (2008a), 'Role of Smac/DIABLO in cancer progression', *J Exp Clin Cancer Res,* 27, 48.

Martinez-Ruiz, Gustavo, et al. (2008b), 'Role of Smac/DIABLO in cancer progression', *Journal of Experimental & Clinical Cancer Research : CR,* 27 (1), 48-48.

Masoudi-Nejad, A., et al. (2015), 'Cancer systems biology and modeling: microscopic scale and multiscale approaches', *Semin Cancer Biol,* 30, 60-9.

Mattila, P. K. and Lappalainen, P. (2008), 'Filopodia: molecular architecture and cellular functions', *Nat Rev Mol Cell Biol,* 9 (6), 446-54.

Mayer, M. P. (2013), 'Hsp70 chaperone dynamics and molecular mechanism', *Trends Biochem Sci,* 38 (10), 507-14.

Mayle, K. M., et al. (2016a), 'Polypeptide-Based Gold Nanoshells for Photothermal Therapy', *J Lab Autom*.

Mayle, K. M., et al. (2016b), 'Engineering A11 Minibody-Conjugated, Polypeptide-Based Gold Nanoshells for Prostate Stem Cell Antigen (PSCA)-Targeted Photothermal Therapy', *J Lab Autom*.

McIlwain, D. R., Berger, T., and Mak, T. W. (2013a), 'Caspase functions in cell death and disease', *Cold Spring Harb Perspect Biol,* 5 (4), a008656.
McIlwain, David R., Berger, Thorsten, and Mak, Tak W. (2013b), 'Caspase Functions in Cell Death and Disease', *Cold Spring Harbor Perspectives in Biology,* 5 (4), a008656.
McKenzie, Jodi A. and Grossman, Douglas (2012), 'Role of the Apoptotic and Mitotic Regulator Survivin in Melanoma', *Anticancer Research,* 32 (2), 397-404.
McMahon, H. T. and Boucrot, E. (2011), 'Molecular mechanism and physiological functions of clathrin-mediated endocytosis', *Nat Rev Mol Cell Biol,* 12 (8), 517-33.
Mehdaoui, B., et al. (2010), 'Large specific absorption rates in the magnetic hyperthermia properties of metallic iron nanocubes', *Journal of Magnetism and Magnetic Materials,* 322 (19), L49-L52.
Mejias, R., et al. (2013), 'Long term biotransformation and toxicity of dimercaptosuccinic acid-coated magnetic nanoparticles support their use in biomedical applications', *J Control Release,* 171 (2), 225-33.
Melancon, M. P., et al. (2008), 'In vitro and in vivo targeting of hollow gold nanoshells directed at epidermal growth factor receptor for photothermal ablation therapy', *Mol Cancer Ther,* 7 (6), 1730-9.
Mieszawska, A. J., et al. (2013), 'Multifunctional gold nanoparticles for diagnosis and therapy of disease', *Mol Pharm,* 10 (3), 831-47.
Miller, A. L. (1998), 'Dimercaptosuccinic acid (DMSA), a non-toxic, water-soluble treatment for heavy metal toxicity', *Altern Med Rev,* 3 (3), 199-207.
Millstone, J. E, Métraux, G. S, and Mirkin, C. A (2006), 'Controlling the Edge Length of Gold Nanoprisms via a Seed-Mediated Approach', *Advanced Functional Materials,* 16 (9), 1209-14.
Millstone, J. E., et al. (2005), 'Observation of a quadrupole plasmon mode for a colloidal solution of gold nanoprisms', *J Am Chem Soc,* 127 (15), 5312-3.
Min, K. A., et al. (2010), 'Transcellular Transport of Heparin-coated Magnetic Iron Oxide Nanoparticles (Hep-MION) Under the Influence of an Applied Magnetic Field', *Pharmaceutics,* 2 (2), 119-35.
Minai, L., Yeheskely-Hayon, D., and Yelin, D. (2013), 'High levels of reactive oxygen species in gold nanoparticle-targeted cancer cells following femtosecond pulse irradiation', *Sci Rep,* 3, 2146.
Minarowska, A., et al. (2007), 'Regulatory role of cathepsin D in apoptosis', *Folia Histochem Cytobiol,* 45 (3), 159-63.
Minniti, Giuseppe, Goldsmith, Christy, and Brada, Michael (2012), 'Chapter 16 - Radiotherapy', in François Boller Michael J. Aminoff and F. Swaab Dick (eds.), *Handbook of Clinical Neurology* (Volume 104: Elsevier), 215-28.
Miron, K., et al. (2015), 'Oncogenes create a unique landscape of fragile sites', *Nat Commun,* 6, 7094.
Mironava, T., et al. (2010), 'Gold nanoparticles cellular toxicity and recovery: effect of size, concentration and exposure time', *Nanotoxicology,* 4 (1), 120-37.
Misra, R., Acharya, S., and Sahoo, S. K. (2010), 'Cancer nanotechnology: application of nanotechnology in cancer therapy', *Drug Discov Today,* 15 (19-20), 842-50.
Mita, A. C., et al. (2008a), 'Survivin: key regulator of mitosis and apoptosis and novel target for cancer therapeutics', *Clin Cancer Res,* 14 (16), 5000-5.
Mita, Alain C., et al. (2008b), 'Survivin: Key Regulator of Mitosis and Apoptosis and Novel Target for Cancer Therapeutics', *Clinical Cancer Research,* 14 (16), 5000.
Miyagawa, T., et al. (2014a), 'Inhibition of Hsp90 and 70 sensitizes melanoma cells to hyperthermia using ferromagnetic particles with a low Curie temperature', *Int J Clin Oncol,* 19 (4), 722-30.

Miyagawa, Tomoyuki, et al. (2014b), 'Inhibition of Hsp90 and 70 sensitizes melanoma cells to hyperthermia using ferromagnetic particles with a low Curie temperature', *International Journal of Clinical Oncology,* 19 (4), 722-30.

Miyahara, T., et al. (1993), 'Hyperthermic enhancement of cytotoxicity and increased uptake of cis-diamminedichloroplatinum(II) in cultured human esophageal cancer cells', *Jpn J Cancer Res,* 84 (3), 336-40.

Mocan, L., et al. (2015a), 'Photothermal treatment of liver cancer with albumin-conjugated gold nanoparticles initiates Golgi Apparatus-ER dysfunction and caspase-3 apoptotic pathway activation by selective targeting of Gp60 receptor', *Int J Nanomedicine,* 10, 5435-45.

Mocan, Lucian, et al. (2015b), 'Photothermal treatment of liver cancer with albumin-conjugated gold nanoparticles initiates Golgi Apparatus–ER dysfunction and caspase-3 apoptotic pathway activation by selective targeting of Gp60 receptor', *International Journal of Nanomedicine,* 10, 5435-45.

Mocan, Lucian, et al. (2016), 'Advances in cancer research using gold nanoparticles mediated photothermal ablation', *Clujul Medical,* 89 (2), 199-202.

Mohanty, S. K., Sharma, M., and Gupta, P. K. (2006), 'Generation of ROS in cells on exposure to CW and pulsed near-infrared laser tweezers', *Photochem Photobiol Sci,* 5 (1), 134-9.

Mojica Pisciotti, M. L., et al. (2014), 'In vitro and in vivo experiments with iron oxide nanoparticles functionalized with DEXTRAN or polyethylene glycol for medical applications: magnetic targeting', *J Biomed Mater Res B Appl Biomater,* 102 (4), 860-8.

Monge-Fuentes, V., et al. (2011), 'Biodistribution and biocompatibility of DMSA-stabilized maghemite magnetic nanoparticles in nonhuman primates (Cebus spp.)', *Nanomedicine (Lond),* 6 (9), 1529-44.

Moros, M., et al. (2015), 'Deciphering intracellular events triggered by mild magnetic hyperthermia in vitro and in vivo', *Nanomedicine (Lond),* 10 (14), 2167-83.

Moulin, Maryline and Arrigo, André-Patrick (2008), 'Caspases activation in hyperthermia-induced stimulation of TRAIL apoptosis', *Cell Stress & Chaperones,* 13 (3), 313-26.

Moussa, Marwan, et al. (2016), 'Effect of thermal dose on heat shock protein expression after radio-frequency ablation with and without adjuvant nanoparticle chemotherapies', *International Journal of Hyperthermia,* 32 (8), 829-41.

Mu, Q., Wang, H., and Zhang, M. (2016), 'Nanoparticles for imaging and treatment of metastatic breast cancer', *Expert Opin Drug Deliv*, 1-14.

Muhammad, Z., et al. (2016), 'PEG capped methotrexate silver nanoparticles for efficient anticancer activity and biocompatibility', *Eur J Pharm Sci,* 91, 251-5.

Mujahid, A., et al. (2006), 'Acute heat stress stimulates mitochondrial superoxide production in broiler skeletal muscle, possibly via downregulation of uncoupling protein content', *Poult Sci,* 85 (7), 1259-65.

Muldoon, Leslie L., et al. (2005), 'Imaging, Distribution, and Toxicity of Superparamagnetic Iron Oxide Magnetic Resonance Nanoparticles in the Rat Brain and Intracerebral Tumor', *Neurosurgery*, 785-96.

Multhoff, Gabriele, et al. (2015), 'The role of heat shock protein 70 (Hsp70) in radiation-induced immunomodulation', *Cancer Letters,* 368 (2), 179-84.

Mundra, Vaibhav, et al. (2015), 'Systemic Delivery of Nanoparticle Formulation of Novel Tubulin Inhibitor for Treating Metastatic Melanoma', *Drug delivery and translational research,* 5 (3), 199-208.

Munoz de Escalona, M., et al. (2016), 'Magnetic solid lipid nanoparticles in hyperthermia against colon cancer', *Int J Pharm,* 504 (1-2), 11-9.

Nagarsekar, Ashish, et al. (2008), 'Febrile-range hyperthermia accelerates caspase-dependent apoptosis in human neutrophils', *Journal of immunology (Baltimore, Md. : 1950),* 181 (4), 2636-43.
Naha, P. C., Chhour, P., and Cormode, D. P. (2015), 'Systematic in vitro toxicological screening of gold nanoparticles designed for nanomedicine applications', *Toxicol In Vitro,* 29 (7), 1445-53.
Nakano, Katsunori and Vousden, Karen H. (2001), 'PUMA, a Novel Proapoptotic Gene, Is Induced by p53', *Molecular Cell,* 7 (3), 683-94.
Naqvi, S., et al. (2010a), 'Concentration-dependent toxicity of iron oxide nanoparticles mediated by increased oxidative stress', *Int J Nanomedicine,* 5, 983-9.
Naqvi, Saba, et al. (2010b), 'Concentration-dependent toxicity of iron oxide nanoparticles mediated by increased oxidative stress', *International Journal of Nanomedicine,* 5, 983-89.
Near, Rachel D., Hayden, Steven C., and El-Sayed, Mostafa A. (2013), 'Thin to Thick, Short to Long: Spectral Properties of Gold Nanorods by Theoretical Modeling', *The Journal of Physical Chemistry C,* 117 (36), 18653-56.
Negrini, S., Gorgoulis, V. G., and Halazonetis, T. D. (2010), 'Genomic instability--an evolving hallmark of cancer', *Nat Rev Mol Cell Biol,* 11 (3), 220-8.
Nel, A. E., et al. (2009), 'Understanding biophysicochemical interactions at the nano-bio interface', *Nat Mater,* 8 (7), 543-57.
Ngoune, Romeo, et al. (2016), 'Accumulating nanoparticles by EPR: A route of no return', *Journal of Controlled Release,* 238, 58-70.
Nichols, Joseph W. and Bae, You Han (2014), 'EPR: Evidence and fallacy', *Journal of Controlled Release,* 190, 451-64.
Nikoletopoulou, Vassiliki, et al. (2013), 'Crosstalk between apoptosis, necrosis and autophagy', *Biochimica et Biophysica Acta (BBA) - Molecular Cell Research,* 1833 (12), 3448-59.
Nikoobakht, B; El-Sayed, Mostafa A (2003), 'Preparation and Growth Mechanism of Gold Nanorods (NRs) Using Seed-Mediated Growth Method ', *15*, 1957-62.
Noda, Yuta and Hayakawa, Tomokatsu (2016), 'Systematic control of edge length, tip sharpness, thickness, and localized surface plasmon resonance of triangular Au nanoprisms', *Journal of Nanoparticle Research,* 18 (10), 314.
Noël, Claudie, Simard, Jean-Christophe, and Girard, Denis (2016), 'Gold nanoparticles induce apoptosis, endoplasmic reticulum stress events and cleavage of cytoskeletal proteins in human neutrophils', *Toxicology in Vitro,* 31, 12-22.
Numico, G., et al. (2015), 'Cancer survivorship: long-term side-effects of anticancer treatments of gastrointestinal cancer', *Curr Opin Oncol,* 27 (4), 351-7.
O'Neal, D. P., et al. (2004a), 'Photo-thermal tumor ablation in mice using near infrared-absorbing nanoparticles', *Cancer Lett,* 209 (2), 171-6.
O'Neal, D. Patrick, et al. (2004b), 'Photo-thermal tumor ablation in mice using near infrared-absorbing nanoparticles', *Cancer Letters,* 209 (2), 171-76.
Oberle, C., et al. (2010), 'Lysosomal membrane permeabilization and cathepsin release is a Bax/Bak-dependent, amplifying event of apoptosis in fibroblasts and monocytes', *Cell Death Differ,* 17 (7), 1167-78.
Ogden, Angela, et al. (2014), 'Interphase microtubules: chief casualties in the war on cancer?', *Drug discovery today,* 19 (7), 824-29.
Oh, N. and Park, J. H. (2014), 'Endocytosis and exocytosis of nanoparticles in mammalian cells', *Int J Nanomedicine,* 9 Suppl 1, 51-63.
Oh, Y., et al. (2016), 'In vitro study on apoptotic cell death by effective magnetic hyperthermia with chitosan-coated MnFe(2)O(4)', *Nanotechnology,* 27 (11), 115101.

Orlando, Antonina, et al. (2016), 'Evaluation of gold nanoparticles biocompatibility: a multiparametric study on cultured endothelial cells and macrophages', *Journal of Nanoparticle Research,* 18 (3), 58.

Ortega, D., et al. (2010), 'Size and surface effects in the magnetic properties of maghemite and magnetite coated nanoparticles', *Philosophical Transactions of the Royal Society A: Mathematical, Physical and Engineering Sciences,* 368 (1927), 4407.

Ortega-Ortega, Yolanda, et al. (2011), 'Heat shock protein 60 from Klebsiella pneumoniae protects mononuclear cells from apoptotic cell death induced by dexamethasone', *Microbial Pathogenesis,* 51 (5), 352-59.

Orynbayeva, Zulfiya, Sensenig, Richard, and Polyak, Boris (2015), 'Metabolic and structural integrity of magnetic nanoparticle-loaded primary endothelial cells for targeted cell therapy', *Nanomedicine (London, England),* 10 (10), 1555-68.

Ossowski, Liliana and Aguirre-Ghiso, Julio A. (2010), 'Dormancy of metastatic melanoma', *Pigment cell & melanoma research,* 23 (1), 41.

Ott, M., et al. (2007), 'Mitochondria, oxidative stress and cell death', *Apoptosis,* 12 (5), 913-22.

Ou, J. R., et al. (2014), 'Heat shock protein 90 in Alzheimer's disease', *Biomed Res Int,* 2014, 796869.

Pagani, Olivia, et al. (2010), 'International Guidelines for Management of Metastatic Breast Cancer: Can Metastatic Breast Cancer Be Cured?', *JNCI Journal of the National Cancer Institute,* 102 (7), 456-63.

Pagliari, L. J., et al. (2005), 'The multidomain proapoptotic molecules Bax and Bak are directly activated by heat', *Proc Natl Acad Sci U S A,* 102 (50), 17975-80.

Panariti, A., Miserocchi, G., and Rivolta, I. (2012a), 'The effect of nanoparticle uptake on cellular behavior: disrupting or enabling functions?', *Nanotechnol Sci Appl,* 5, 87-100.

Panariti, Alice, Miserocchi, Giuseppe, and Rivolta, Ilaria (2012b), 'The effect of nanoparticle uptake on cellular behavior: disrupting or enabling functions?', *Nanotechnology, Science and Applications,* 5, 87-100.

Panchapakesan, B., et al. (2011), 'Gold nanoprobes for theranostics', *Nanomedicine (Lond),* 6 (10), 1787-811.

Park, Chang-Jin and Seo, Young-Su (2015), 'Heat Shock Proteins: A Review of the Molecular Chaperones for Plant Immunity', *The Plant Pathology Journal,* 31 (4), 323-33.

Park, J., et al. (2015), 'Multifunctional hollow gold nanoparticles designed for triple combination therapy and CT imaging', *J Control Release,* 207, 77-85.

Park, Y. C., et al. (2014), 'Effect of PEG molecular weight on stability, T(2) contrast, cytotoxicity, and cellular uptake of superparamagnetic iron oxide nanoparticles (SPIONs)', *Colloids Surf B Biointerfaces,* 119, 106-14.

Parmar, Harshida, et al. (2015), 'Size Dependent Heating Efficiency of Iron Oxide Single Domain Nanoparticles', *Procedia Engineering,* 102, 527-33.

Patra, C. R., et al. (2010), 'Fabrication of gold nanoparticles for targeted therapy in pancreatic cancer', *Adv Drug Deliv Rev,* 62 (3), 346-61.

Patra, H. K., et al. (2007a), 'Cell selective response to gold nanoparticles', *Nanomedicine,* 3 (2), 111-9.

Patra, Hirak K., et al. (2007b), 'Cell selective response to gold nanoparticles', *Nanomedicine: Nanotechnology, Biology and Medicine,* 3 (2), 111-19.

Pauksch, Linda, et al. (2014), 'Silver nanoparticles do not alter human osteoclastogenesis but induce cellular uptake', *Toxicology Reports,* 1, 900-08.

Pavlyukov, Marat S., et al. (2011), 'Survivin Monomer Plays an Essential Role in Apoptosis Regulation', *The Journal of Biological Chemistry,* 286 (26), 23296-307.
Pearce, J., et al. (2013a), 'Magnetic Heating of Nanoparticles: The Importance of Particle Clustering to Achieve Therapeutic Temperatures', *J Nanotechnol Eng Med,* 4 (1), 110071-1100714.
Pearce, John, et al. (2013b), 'Magnetic Heating of Nanoparticles: The Importance of Particle Clustering to Achieve Therapeutic Temperatures', *Journal of Nanotechnology in Engineering and Medicine,* 4 (1), 0110071-01100714.
Pelaz, B., et al. (2012), 'Tailoring the synthesis and heating ability of gold nanoprisms for bioapplications', *Langmuir,* 28 (24), 8965-70.
Pelaz, Beatriz and del Pino, Pablo (2012), 'Synthesis Applications of Gold Nanoparticles', 4, 3-33.
Peng, M., et al. (2015), 'Dextran-coated superparamagnetic nanoparticles as potential cancer drug carriers in vivo', *Nanoscale,* 7 (25), 11155-62.
Pennisi, Rosa, Ascenzi, Paolo, and di Masi, Alessandra (2015), 'Hsp90: A New Player in DNA Repair?', *Biomolecules,* 5 (4), 2589-618.
Perciavalle, R. M., et al. (2012), 'Anti-apoptotic MCL-1 localizes to the mitochondrial matrix and couples mitochondrial fusion to respiration', *Nat Cell Biol,* 14 (6), 575-83.
Perez-Hernandez, M., et al. (2015), 'Dissecting the molecular mechanism of apoptosis during photothermal therapy using gold nanoprisms', *ACS Nano,* 9 (1), 52-61.
Pérez-Hernández, Marta, et al. (2015), 'Dissecting the Molecular Mechanism of Apoptosis during Photothermal Therapy Using Gold Nanoprisms', *ACS Nano,* 9 (1), 52-61.
Pérez-Herrero, Edgar and Fernández-Medarde, Alberto (2015), 'Advanced targeted therapies in cancer: Drug nanocarriers, the future of chemotherapy', *European Journal of Pharmaceutics and Biopharmaceutics,* 93, 52-79.
Peter, M. E. and Krammer, P. H. (2003), 'The CD95(APO-1/Fas) DISC and beyond', *Cell Death Differ,* 10 (1), 26-35.
Petrache Voicu, Sorina Nicoleta, et al. (2015), 'Silica Nanoparticles Induce Oxidative Stress and Autophagy but Not Apoptosis in the MRC-5 Cell Line', *International Journal of Molecular Sciences,* 16 (12), 29398-416.
Phung, Y. T., et al. (2011), 'Rapid generation of in vitro multicellular spheroids for the study of monoclonal antibody therapy', *J Cancer,* 2, 507-14.
Pissuwan, D., Valenzuela, S. M., and Cortie, M. B. (2006), 'Therapeutic possibilities of plasmonically heated gold nanoparticles', *Trends Biotechnol,* 24 (2), 62-7.
Pitsillides, Costas M., et al. (2003), 'Selective Cell Targeting with Light-Absorbing Microparticles and Nanoparticles', *Biophysical Journal,* 84 (6), 4023-32.
Prevo, Brian G., et al. (2008), 'Scalable routes to gold nanoshells with tunable sizes and their response to near infrared pulsed laser irradiation', *Small (Weinheim an der Bergstrasse, Germany),* 4 (8), 1183-95.
Prijic, S., et al. (2010), 'Increased cellular uptake of biocompatible superparamagnetic iron oxide nanoparticles into malignant cells by an external magnetic field', *J Membr Biol,* 236 (1), 167-79.
Punsawad, Chuchard, et al. (2015), 'Enhanced expression of Fas and FasL modulates apoptosis in the lungs of severe P. falciparum malaria patients with pulmonary edema', *International Journal of Clinical and Experimental Pathology,* 8 (9), 10002-13.
Puyo, Stéphane, Montaudon, Danièle, and Pourquier, Philippe (2014), 'From old alkylating agents to new minor groove binders', *Critical Reviews in Oncology/Hematology,* 89 (1), 43-61.

Qin, J., et al. (2015), 'Gold nanorods as a theranostic platform for in vitro and in vivo imaging and photothermal therapy of inflammatory macrophages', *Nanoscale,* 7 (33), 13991-4001.
Qiu, Yang, et al. (2010), 'Surface chemistry and aspect ratio mediated cellular uptake of Au nanorods', *Biomaterials,* 31 (30), 7606-19.
Raaphorst, G. P. and Feeley, M. M. (1990), 'Comparison of recovery from potentially lethal damage after exposure to hyperthermia and radiation', *Radiat Res,* 121 (1), 107-10.
Radons, J. (2016), 'The human HSP70 family of chaperones: where do we stand?', *Cell Stress Chaperones,* 21 (3), 379-404.
Radovic, M., et al. (2015), 'Preparation and in vivo evaluation of multifunctional (9)(0)Y-labeled magnetic nanoparticles designed for cancer therapy', *J Biomed Mater Res A,* 103 (1), 126-34.
Raji, V., et al. (2011a), 'Selective photothermal efficiency of citrate capped gold nanoparticles for destruction of cancer cells', *Experimental Cell Research,* 317 (14), 2052-58.
Raji, V., et al. (2011b), 'Selective photothermal efficiency of citrate capped gold nanoparticles for destruction of cancer cells', *Exp Cell Res,* 317 (14), 2052-8.
Ramírez-Labrada, A., et al. (2015), 'Two death pathways induced by sorafenib in myeloma cells: Puma-mediated apoptosis and necroptosis', *Clinical and Translational Oncology,* 17 (2), 121-32.
Reddy, L. H., et al. (2012a), 'Magnetic nanoparticles: design and characterization, toxicity and biocompatibility, pharmaceutical and biomedical applications', *Chem Rev,* 112 (11), 5818-78.
Reddy, L. Harivardhan, et al. (2012b), 'Magnetic Nanoparticles: Design and Characterization, Toxicity and Biocompatibility, Pharmaceutical and Biomedical Applications', *Chemical Reviews,* 112 (11), 5818-78.
Reddy, Utkarsh A., Prabhakar, P. V., and Mahboob, M. (2015), 'Biomarkers of oxidative stress for in vivo assessment of toxicological effects of iron oxide nanoparticles', *Saudi Journal of Biological Sciences*.
Redza-Dutordoir, Maureen and Averill-Bates, Diana A. (2016), 'Activation of apoptosis signalling pathways by reactive oxygen species', *Biochimica et Biophysica Acta (BBA) - Molecular Cell Research,* 1863 (12), 2977-92.
Reeves, Daniel B. and Weaver, John B. (2012), 'Simulations of magnetic nanoparticle Brownian motion', *Journal of Applied Physics,* 112 (12), 124311.
Rehman, J., et al. (2002), 'Ferromagnetic self-regulating reheatable thermal rod implants for in situ tissue ablation', *J Endourol,* 16 (7), 523-31.
Remya, N. S., et al. (2016), 'Toxicity, toxicokinetics and biodistribution of dextran stabilized Iron oxide Nanoparticles for biomedical applications', *International Journal of Pharmaceutics,* 511 (1), 586-98.
Ren, Decheng, et al. (2010), 'BID, BIM, and PUMA Are Essential for Activation of the BAX- and BAK-Dependent Cell Death Program', *Science (New York, N.Y.),* 330 (6009), 1390-93.
Rengan, Aravind Kumar, et al. (2015), 'In Vivo Analysis of Biodegradable Liposome Gold Nanoparticles as Efficient Agents for Photothermal Therapy of Cancer', *Nano Letters,* 15 (2), 842-48.
Repnik, Urška, Česen, Maruša Hafner, and Turk, Boris (2013), 'The Endolysosomal System in Cell Death and Survival', *Cold Spring Harbor Perspectives in Biology,* 5 (1).
Retsky, Michael, et al. (2004), 'Hypothesis: Induced angiogenesis after surgery in premenopausal node-positive breast cancer patients is a major underlying

reason why adjuvant chemotherapy works particularly well for those patients', *Breast Cancer Research,* 6 (4), R372-R74.
Rey, S., et al. (2016), 'Molecular targeting of hypoxia in radiotherapy', *Adv Drug Deliv Rev*.
Ricci, Jean-Ehrland, et al. (2004), 'Disruption of Mitochondrial Function during Apoptosis Is Mediated by Caspase Cleavage of the p75 Subunit of Complex I of the Electron Transport Chain', *Cell,* 117 (6), 773-86.
Richter, K., Haslbeck, M., and Buchner, J. (2010), 'The heat shock response: life on the verge of death', *Mol Cell,* 40 (2), 253-66.
Rivet, C. J., et al. (2012), 'Altering iron oxide nanoparticle surface properties induce cortical neuron cytotoxicity', *Chem Res Toxicol,* 25 (1), 153-61.
Rizzo, L. Y., et al. (2013), 'Recent progress in nanomedicine: therapeutic, diagnostic and theranostic applications', *Curr Opin Biotechnol,* 24 (6), 1159-66.
Robinson, R., Gerlach, W., and Ghandehari, H. (2015), 'Comparative effect of gold nanorods and nanocages for prostate tumor hyperthermia', *J Control Release,* 220 (Pt A), 245-52.
Rodríguez-Vargas, José Manuel, et al. (2012), 'ROS-induced DNA damage and PARP-1 are required for optimal induction of starvation-induced autophagy', *Cell Research,* 22 (7), 1181-98.
Rofe, Adam P. and Pryor, Paul R. (2016), 'Purification of Lysosomes Using Supraparamagnetic Iron Oxide Nanoparticles (SPIONs)', *Cold Spring Harbor Protocols,* 2016 (4), pdb.prot084822.
Roos, W. P., Thomas, A. D., and Kaina, B. (2016), 'DNA damage and the balance between survival and death in cancer biology', *Nat Rev Cancer,* 16 (1), 20-33.
Roti Roti, J. L. (2008a), 'Cellular responses to hyperthermia (40-46 degrees C): cell killing and molecular events', *Int J Hyperthermia,* 24 (1), 3-15.
Roti Roti, Joseph L. (2008b), 'Cellular responses to hyperthermia (40–46°C): Cell killing and molecular events', *International Journal of Hyperthermia,* 24 (1), 3-15.
Ruta, S., Chantrell, R., and Hovorka, O. (2015), 'Unified model of hyperthermia via hysteresis heating in systems of interacting magnetic nanoparticles', *Sci Rep,* 5, 9090.
Rylander, M. N., et al. (2010), 'Measurement and mathematical modeling of thermally induced injury and heat shock protein expression kinetics in normal and cancerous prostate cells', *Int J Hyperthermia,* 26 (8), 748-64.
Sabale, S., et al. (2015), 'Superparamagnetic MFe2O 4 (M = Ni, Co, Zn, Mn) nanoparticles: synthesis, characterization, induction heating and cell viability studies for cancer hyperthermia applications', *J Mater Sci Mater Med,* 26 (3), 127.
Sadeghi, Leila, Tanwir, Farzeen, and Yousefi Babadi, Vahid (2015), 'In vitro toxicity of iron oxide nanoparticle: Oxidative damages on Hep G2 cells', *Experimental and Toxicologic Pathology,* 67 (2), 197-203.
Saelens, X., et al. (2004), 'Toxic proteins released from mitochondria in cell death', *Oncogene,* 23 (16), 2861-74.
Safa, Ahmad R. (2013), 'Roles of c-FLIP in Apoptosis, Necroptosis, and Autophagy', *Journal of carcinogenesis & mutagenesis,* Suppl 6, 003.
Sainz, V., et al. (2015), 'Regulatory aspects on nanomedicines', *Biochem Biophys Res Commun*.
Sajjadi, A. Y., Mitra, K., and Grace, M. (2013), 'Expression of heat shock proteins 70 and 47 in tissues following short-pulse laser irradiation: assessment of thermal damage and healing', *Med Eng Phys,* 35 (10), 1406-14.

Salatin, S., Maleki Dizaj, S., and Yari Khosroushahi, A. (2015a), 'Effect of the surface modification, size, and shape on cellular uptake of nanoparticles', *Cell Biol Int,* 39 (8), 881-90.

Salatin, Sara, Maleki Dizaj, Solmaz, and Yari Khosroushahi, Ahmad (2015b), 'Effect of the surface modification, size, and shape on cellular uptake of nanoparticles', *Cell Biology International,* 39 (8), 881-90.

Samali, A., et al. (2001), 'Hsp27 protects mitochondria of thermotolerant cells against apoptotic stimuli', *Cell Stress Chaperones,* 6 (1), 49-58.

Samanta, Debangshu, et al. (2014), 'Hypoxia-inducible factors are required for chemotherapy resistance of breast cancer stem cells', *Proceedings of the National Academy of Sciences of the United States of America,* 111 (50), E5429-E38.

Sambale, Franziska, et al. (2015), 'Three dimensional spheroid cell culture for nanoparticle safety testing', *Journal of Biotechnology,* 205, 120-29.

Samborski, P. and Grzymislawski, M. (2015), 'The Role of HSP70 Heat Shock Proteins in the Pathogenesis and Treatment of Inflammatory Bowel Diseases', *Adv Clin Exp Med,* 24 (3), 525-30.

Santhosh, P. B. and Ulrih, N. P. (2013), 'Multifunctional superparamagnetic iron oxide nanoparticles: promising tools in cancer theranostics', *Cancer Lett,* 336 (1), 8-17.

Santoro, M. Gabriella (2000), 'Heat shock factors and the control of the stress response', *Biochemical Pharmacology,* 59 (1), 55-63.

Saptarshi, Shruti R., Duschl, Albert, and Lopata, Andreas L. (2013), 'Interaction of nanoparticles with proteins: relation to bio-reactivity of the nanoparticle', *Journal of Nanobiotechnology,* 11, 26-26.

Schug, Zachary T. and Gottlieb, Eyal (2009), 'Cardiolipin acts as a mitochondrial signalling platform to launch apoptosis', *Biochimica et Biophysica Acta (BBA) - Biomembranes,* 1788 (10), 2022-31.

Schwartz, Jon A., et al. (2009), 'Feasibility Study of Particle-Assisted Laser Ablation of Brain Tumors in Orthotopic Canine Model', *Cancer Research,* 69 (4), 1659.

Sessler, Tamas, et al. (2013), 'Structural determinants of DISC function: New insights into death receptor-mediated apoptosis signalling', *Pharmacology & Therapeutics,* 140 (2), 186-99.

Sever, R. and Brugge, J. S. (2015), 'Signal transduction in cancer', *Cold Spring Harb Perspect Med,* 5 (4).

Seyfried, T. N. and Huysentruyt, L. C. (2013), 'On the origin of cancer metastasis', *Crit Rev Oncog,* 18 (1-2), 43-73.

Shah, Saqlain A., et al. (2013), 'PEG-coated folic acid-modified superparamagnetic MnFe2O4 nanoparticles for hyperthermia therapy and drug delivery', *Materials Chemistry and Physics,* 138 (2-3), 703-08.

Sharifi, Ibrahim, Shokrollahi, H., and Amiri, S. (2012), 'Ferrite-based magnetic nanofluids used in hyperthermia applications', *Journal of Magnetism and Magnetic Materials,* 324 (6), 903-15.

Sharma, D. and Masison, D. C. (2009), 'Hsp70 structure, function, regulation and influence on yeast prions', *Protein Pept Lett,* 16 (6), 571-81.

Shellman, Yiqun G., et al. (2008), 'Hyperthermia Induces Endoplasmic Reticulum-Mediated Apoptosis in Melanoma and Non-Melanoma Skin Cancer Cells', *Journal of Investigative Dermatology,* 128 (4), 949-56.

Shetake, N. G., et al. (2015), 'Magnetic nanoparticle-mediated hyperthermia therapy induces tumour growth inhibition by apoptosis and Hsp90/AKT modulation', *Int J Hyperthermia,* 31 (8), 909-19.

Shi, Yigong (2004), 'Caspase activation, inhibition, and reactivation: A mechanistic view', *Protein Science : A Publication of the Protein Society,* 13 (8), 1979-87.
Shin, Dong Yeok, et al. (2009), 'Implication of intracellular ROS formation, caspase-3 activation and Egr-1 induction in platycodon D-induced apoptosis of U937 human leukemia cells', *Biomedicine & Pharmacotherapy,* 63 (2), 86-94.
Shin, Yu Jin, et al. (2013), 'Centrifugal Shape Sorting and Optical Response of Polyhedral Gold Nanoparticles', *Advanced Materials,* 25 (29), 4023-27.
Shuford, K. L., Ratner, M. A., and Schatz, G. C. (2005a), 'Multipolar excitation in triangular nanoprisms', *J Chem Phys,* 123 (11), 114713.
Shuford, Kevin L., Ratner, Mark A., and Schatz, George C. (2005b), 'Multipolar excitation in triangular nanoprisms', *The Journal of Chemical Physics,* 123 (11), 114713.
Silva, A. C., et al. (2011a), 'Application of hyperthermia induced by superparamagnetic iron oxide nanoparticles in glioma treatment', *Int J Nanomedicine,* 6, 591-603.
Silva, André C., et al. (2011b), 'Application of hyperthermia induced by superparamagnetic iron oxide nanoparticles in glioma treatment', *International Journal of Nanomedicine,* 6, 591-603.
Silva, L. H., et al. (2016), 'Labeling mesenchymal cells with DMSA-coated gold and iron oxide nanoparticles: assessment of biocompatibility and potential applications', *J Nanobiotechnology,* 14 (1), 59.
Singh, Ishwar S. and Hasday, Jeffrey D. (2013), 'Fever, hyperthermia and the heat shock response', *International Journal of Hyperthermia,* 29 (5), 423-35.
Singh, Mohan, et al. (2015), 'Application of gold nanoparticles for gastrointestinal cancer theranostics: A systematic review', *Nanomedicine: Nanotechnology, Biology and Medicine,* 11 (8), 2083-98.
Singh, N., et al. (2010a), 'Potential toxicity of superparamagnetic iron oxide nanoparticles (SPION)', *Nano Rev,* 1.
Singh, Neenu, et al. (2010b), 'Potential toxicity of superparamagnetic iron oxide nanoparticles (SPION)', *Nano Reviews,* 1, 10.3402/nano.v1i0.5358.
Singh, Rajesh and Lillard, James W. (2009), 'Nanoparticle-based targeted drug delivery', *Experimental and molecular pathology,* 86 (3), 215-23.
Sinha, Krishnendu, et al. (2013), 'Oxidative stress: the mitochondria-dependent and mitochondria-independent pathways of apoptosis', *Archives of Toxicology,* 87 (7), 1157-80.
Sinha, Pratima, et al. (2005), 'Tumor immunity: a balancing act between T cell activation, macrophage activation and tumor-induced immune suppression', *Cancer Immunology, Immunotherapy,* 54 (11), 1137-42.
Sirenko, O., et al. (2015), 'High-content assays for characterizing the viability and morphology of 3D cancer spheroid cultures', *Assay Drug Dev Technol,* 13 (7), 402-14.
Slimen, I. B., et al. (2014), 'Reactive oxygen species, heat stress and oxidative-induced mitochondrial damage. A review', *Int J Hyperthermia,* 30 (7), 513-23.
Smolkova, Ilona S., et al. (2015), 'Alternating magnetic field energy absorption in the dispersion of iron oxide nanoparticles in a viscous medium', *Journal of Magnetism and Magnetic Materials,* 374, 508-15.
Soenen, S. J., et al. (2009), 'Stable long-term intracellular labelling with fluorescently tagged cationic magnetoliposomes', *Chembiochem,* 10 (2), 257-67.
Soenen, Stefaan J., et al. (2011), 'Cellular toxicity of inorganic nanoparticles: Common aspects and guidelines for improved nanotoxicity evaluation', *Nano Today,* 6 (5), 446-65.
Soenen, Stefaan J., et al. (2012), 'Cytotoxic Effects of Gold Nanoparticles: A Multiparametric Study', *ACS Nano,* 6 (7), 5767-83.

Soenen, Stefaan J. H., et al. (2010), 'High Intracellular Iron Oxide Nanoparticle Concentrations Affect Cellular Cytoskeleton and Focal Adhesion Kinase-Mediated Signaling', *Small,* 6 (7), 832-42.
Song, Alfred S., Najjar, Amer M., and Diller, Kenneth R. (2014), 'Thermally Induced Apoptosis, Necrosis, and Heat Shock Protein Expression in Three-Dimensional Culture', *Journal of Biomechanical Engineering,* 136 (7), 071006-06.
Song, Yuyu and Brady, Scott T. (2015), 'Posttranslational Modifications of Tubulin: Pathways to Functional Diversity of Microtubules', *Trends in cell biology,* 25 (3), 125-36.
Soni, Sanjeev, et al. (2014), 'Investigation on nanoparticle distribution for thermal ablation of a tumour subjected to nanoparticle assisted thermal therapy', *Journal of Thermal Biology,* 43, 70-80.
Sreenivasa, Geetha, et al. (2003), 'Clinical use of the hyperthermia treatment planning system HyperPlan to predict effectiveness and toxicity', *International Journal of Radiation Oncology*Biology*Physics,* 55 (2), 407-19.
Stapf, Marcus, et al. (2015), 'Magnetic thermoablation stimuli alter BCL2 and FGF-R1 but not HSP70 expression profiles in BT474 breast tumors', *International Journal of Nanomedicine,* 10, 1931-39.
Stern, J. M., et al. (2007), 'Efficacy of laser-activated gold nanoshells in ablating prostate cancer cells in vitro', *J Endourol,* 21 (8), 939-43.
Stetler, R. A., et al. (2010), 'Heat shock proteins: cellular and molecular mechanisms in the central nervous system', *Prog Neurobiol,* 92 (2), 184-211.
Stope, M. B., et al. (2016), 'Jump in the fire--heat shock proteins and their impact on ovarian cancer therapy', *Crit Rev Oncol Hematol,* 97, 152-6.
Su, Y., et al. (2011), 'Insulin-like growth factor binding protein 5 suppresses tumor growth and metastasis of human osteosarcoma', *Oncogene,* 30 (37), 3907-17.
Subburaj, Y., et al. (2015), 'Bax monomers form dimer units in the membrane that further self-assemble into multiple oligomeric species', *Nat Commun,* 6, 8042.
Suk, J. S., et al. (2016), 'PEGylation as a strategy for improving nanoparticle-based drug and gene delivery', *Adv Drug Deliv Rev,* 99 (Pt A), 28-51.
Sun, W. and Yang, J. (2010), 'Functional mechanisms for human tumor suppressors', *J Cancer,* 1, 136-40.
Suto, Makoto, et al. (2009), 'Heat dissipation mechanism of magnetite nanoparticles in magnetic fluid hyperthermia', *Journal of Magnetism and Magnetic Materials,* 321 (10), 1493-96.
Tahover, E., Patil, Y. P., and Gabizon, A. A. (2015), 'Emerging delivery systems to reduce doxorubicin cardiotoxicity and improve therapeutic index: focus on liposomes', *Anticancer Drugs,* 26 (3), 241-58.
Taipale, M., Jarosz, D. F., and Lindquist, S. (2010), 'HSP90 at the hub of protein homeostasis: emerging mechanistic insights', *Nat Rev Mol Cell Biol,* 11 (7), 515-28.
Takayama, S., Reed, J. C., and Homma, S. (2003), 'Heat-shock proteins as regulators of apoptosis', *Oncogene,* 22 (56), 9041-7.
Tang, Dan, et al. (2005), 'Expression of heat shock proteins and heat shock protein messenger ribonucleic acid in human prostate carcinoma in vitro and in tumors in vivo', *Cell Stress & Chaperones,* 10 (1), 46-58.
Tang, Y. and McGoron, A. J. (2013), 'Increasing the rate of heating: a potential therapeutic approach for achieving synergistic tumour killing in combined hyperthermia and chemotherapy', *Int J Hyperthermia,* 29 (2), 145-55.
Tang, Y., et al. (2015), 'In vitro cytotoxicity of gold nanorods in A549 cells', *Environ Toxicol Pharmacol,* 39 (2), 871-8.

Tarantola, M., et al. (2011), 'Toxicity of gold-nanoparticles: synergistic effects of shape and surface functionalization on micromotility of epithelial cells', *Nanotoxicology,* 5 (2), 254-68.
Tedeschi, J. N., et al. (2015), 'Increased expression of Hsp70 and Hsp90 mRNA as biomarkers of thermal stress in loggerhead turtle embryos (Caretta Caretta)', *J Therm Biol,* 47, 42-50.
Tennstaedt, Annette, et al. (2012), 'Human High Temperature Requirement Serine Protease A1 (HTRA1) Degrades Tau Protein Aggregates', *The Journal of Biological Chemistry,* 287 (25), 20931-41.
Terentyuk, G. S., et al. (2013), 'Cancer laser therapy using gold nanoparticles', 659-703.
Theumer, Anja, et al. (2015), 'Superparamagnetic iron oxide nanoparticles exert different cytotoxic effects on cells grown in monolayer cell culture versus as multicellular spheroids', *Journal of Magnetism and Magnetic Materials,* 380, 27-33.
Thiesen, Burghard and Jordan, Andreas (2008), 'Clinical applications of magnetic nanoparticles for hyperthermia', *International Journal of Hyperthermia,* 24 (6), 467-74.
Thomas, Luke W., Lam, Connie, and Edwards, Steven W. (2010), 'Mcl-1; the molecular regulation of protein function', *FEBS Letters,* 584 (14), 2981-89.
Thun, Michael J., et al. (2010), 'The global burden of cancer: priorities for prevention', *Carcinogenesis,* 31 (1), 100-10.
Tiwari, Meenakshi, et al. (2015a), 'Apoptosis in mammalian oocytes: a review', *Apoptosis,* 20 (8), 1019-25.
Tiwari, P. M., Bawage, S. S., and Singh, S. R. (2015b), 'Gold nanoparticles and their applications in photomedicine, diagnosis and therapy', 249-66.
Tlotleng, N., et al. (2016), 'Cytotoxicity, intracellular localization and exocytosis of citrate capped and PEG functionalized gold nanoparticles in human hepatocyte and kidney cells', *Cell Biol Toxicol,* 32 (4), 305-21.
Tombacz, E., et al. (2015), 'Magnetic iron oxide nanoparticles: Recent trends in design and synthesis of magnetoresponsive nanosystems', *Biochem Biophys Res Commun,* 468 (3), 442-53.
Tong, Ling and Cheng, Ji-Xin (2009), 'Gold nanorod-mediated photothermolysis induces apoptosis of macrophages via damage of mitochondria', *Nanomedicine,* 4 (3), 265-76.
Tong, S., et al. (2014), 'Nanomedicine: tiny particles and machines give huge gains', *Ann Biomed Eng,* 42 (2), 243-59.
Tonino, S. H., et al. (2011), 'ROS-mediated upregulation of Noxa overcomes chemoresistance in chronic lymphocytic leukemia', *Oncogene,* 30 (6), 701-13.
Toraya-Brown, Seiko and Fiering, Steven (2014), 'Local tumour hyperthermia as immunotherapy for metastatic cancer', *International Journal of Hyperthermia,* 30 (8), 531-39.
Toy, Randall, et al. (2014), 'Shaping cancer nanomedicine: The effect of particle shape on the in vivo journey of nanoparticles', *Nanomedicine (London, England),* 9 (1), 121-34.
Trosko, J. E. (2009), 'Review Paper: Cancer Stem Cells and Cancer Nonstem Cells: From Adult Stem Cells or from Reprogramming of Differentiated Somatic Cells', *Veterinary Pathology Online,* 46 (2), 176-93.
Tseng, Hubert, et al. (2015), 'A spheroid toxicity assay using magnetic 3D bioprinting and real-time mobile device-based imaging', *Scientific Reports,* 5, 13987.

Tseng, Peter, Judy, Jack W., and Di Carlo, Dino (2012), 'Magnetic nanoparticle-mediated massively parallel mechanical modulation of single-cell behavior', *Nat Meth,* 9 (11), 1113-19.
Tsuchiya, Yuichi, Nakabayashi, Osamu, and Nakano, Hiroyasu (2015), 'FLIP the Switch: Regulation of Apoptosis and Necroptosis by cFLIP', *International Journal of Molecular Sciences,* 16 (12), 30321-41.
Tu, S., et al. (2006), 'In situ trapping of activated initiator caspases reveals a role for caspase-2 in heat shock-induced apoptosis', *Nat Cell Biol,* 8 (1), 72-7.
Turk, Boris and Turk, Vito (2009), 'Lysosomes as "Suicide Bags" in Cell Death: Myth or Reality?', *Journal of Biological Chemistry,* 284 (33), 21783-87.
Turk, Vito, et al. (2012), 'Cysteine cathepsins: From structure, function and regulation to new frontiers', *Biochimica et Biophysica Acta (BBA) - Proteins and Proteomics,* 1824 (1), 68-88.
Unfried, Klaus, et al. (2009), 'Cellular responses to nanoparticles: Target structures and mechanisms', *Nanotoxicology,* 1 (1), 52-71.
Untch, Michael, et al. (2014), 'Current and future role of neoadjuvant therapy for breast cancer', *The Breast,* 23 (5), 526-37.
Unterweger, H., et al. (2014), 'Development and characterization of magnetic iron oxide nanoparticles with a cisplatin-bearing polymer coating for targeted drug delivery', *Int J Nanomedicine,* 9, 3659-76.
Valastyan, Scott and Weinberg, Robert A. (2011), 'Tumor Metastasis: Molecular Insights and Evolving Paradigms', *Cell,* 147 (2), 275-92.
Valdiglesias, V., et al. (2015a), 'Effects of iron oxide nanoparticles: cytotoxicity, genotoxicity, developmental toxicity, and neurotoxicity', *Environ Mol Mutagen,* 56 (2), 125-48.
Valdiglesias, Vanessa, et al. (2015b), 'Effects of iron oxide nanoparticles: Cytotoxicity, genotoxicity, developmental toxicity, and neurotoxicity', *Environmental and Molecular Mutagenesis,* 56 (2), 125-48.
Valdiglesias, Vanessa, et al. (2016), 'Are iron oxide nanoparticles safe? Current knowledge and future perspectives', *Journal of Trace Elements in Medicine and Biology,* 38, 53-63.
Vallejo-Fernandez, G., et al. (2013), 'Mechanisms of hyperthermia in magnetic nanoparticles', *Journal of Physics D: Applied Physics,* 46 (31), 312001.
van der Meel, R., et al. (2013), 'Ligand-targeted particulate nanomedicines undergoing clinical evaluation: current status', *Adv Drug Deliv Rev,* 65 (10), 1284-98.
van der Zee, J. (2002), 'Heating the patient: a promising approach?', *Annals of Oncology,* 13 (8), 1173-84.
van Tonder, Alet, Joubert, Annie M., and Cromarty, A. Duncan (2015), 'Limitations of the 3-(4,5-dimethylthiazol-2-yl)-2,5-diphenyl-2H-tetrazolium bromide (MTT) assay when compared to three commonly used cell enumeration assays', *BMC Research Notes,* 8, 47.
van Zijl, Franziska, Krupitza, Georg, and Mikulits, Wolfgang (2011), 'Initial steps of metastasis: Cell invasion and endothelial transmigration', *Mutation Research,* 728 (1-2), 23-34.
Vandenabeele, Peter, et al. (2010), 'Molecular mechanisms of necroptosis: an ordered cellular explosion', *Nat Rev Mol Cell Biol,* 11 (10), 700-14.
Vankayala, R., et al. (2014), 'Gold nanoshells-mediated bimodal photodynamic and photothermal cancer treatment using ultra-low doses of near infra-red light', *Biomaterials,* 35 (21), 5527-38.
Vaupel, Peter W. and Kelleher, Debra K. (2010), 'Pathophysiological and vascular characteristics of tumours and their importance for hyperthermia:

Heterogeneity is the key issue', *International Journal of Hyperthermia,* 26 (3), 211-23.
Velez, Ana Maria Abreu and Howard, Michael S. (2015), 'Tumor-suppressor Genes, Cell Cycle Regulatory Checkpoints, and the Skin', *North American Journal of Medical Sciences,* 7 (5), 176-88.
Venojärvi, Mika, et al. (2013), 'Stress Proteins and Heat Shock Proteins', 229-35.
Vera, Jerry and Bayazitoglu, Yildiz (2009), 'Gold nanoshell density variation with laser power for induced hyperthermia', *International Journal of Heat and Mass Transfer,* 52 (3-4), 564-73.
Verma, A. and Stellacci, F. (2010), 'Effect of surface properties on nanoparticle-cell interactions', *Small,* 6 (1), 12-21.
Vidalino, Laura, et al. (2009), 'SERPINB3, apoptosis and autoimmunity', *Autoimmunity Reviews,* 9 (2), 108-12.
Villanueva, A., et al. (2010), 'Hyperthermia HeLa Cell Treatment with Silica-Coated Manganese Oxide Nanoparticles', *The Journal of Physical Chemistry C,* 114 (5), 1976-81.
Vlad, M., et al. (2010), 'Morphological changes during acute experimental short-term hyperthermia', *Rom J Morphol Embryol,* 51 (4), 739-44.
Vlad, M., et al. (2013), 'Electron microscopy of the morphological changes in rat viscera during experimental hyperthermic shock', *Journal of Medicine and Life,* 6 (1), 55-60.
Vogel, Christine and Marcotte, Edward M. (2012a), 'Insights into the regulation of protein abundance from proteomic and transcriptomic analyses', *Nature reviews. Genetics,* 13 (4), 227-32.
Vogel, Christine. (2012b), 'Insights into the regulation of protein abundance from proteomic and transcriptomic analyses', *Nat Rev Genet,* 13 (4), 227-32.
Vucic, D., Dixit, V. M., and Wertz, I. E. (2011), 'Ubiquitylation in apoptosis: a post-translational modification at the edge of life and death', *Nat Rev Mol Cell Biol,* 12 (7), 439-52.
Wahajuddin and Arora, S. (2012a), 'Superparamagnetic iron oxide nanoparticles: magnetic nanoplatforms as drug carriers', *Int J Nanomedicine,* 7, 3445-71.
Wahajuddin and Arora, Sumit (2012b), 'Superparamagnetic iron oxide nanoparticles: magnetic nanoplatforms as drug carriers', *International Journal of Nanomedicine,* 7, 3445-71.
Wan, Jiali, et al. (2015), 'Surface chemistry but not aspect ratio mediates the biological toxicity of gold nanorods in vitro and in vivo', *Scientific Reports,* 5, 11398.
Wang, Chunxin and Youle, Richard J. (2009), 'The Role of Mitochondria in Apoptosis()', *Annual review of genetics,* 43, 95-118.
Wang, G., et al. (2014a), 'One-step synthesis of water-dispersible ultra-small Fe3O4 nanoparticles as contrast agents for T1 and T2 magnetic resonance imaging', *Nanoscale,* 6 (5), 2953-63.
Wang, Hsiu-Yu, et al. (2013a), 'Hyperthermia Stress Activates Heat Shock Protein Expression via Propyl Isomerase 1 Regulation with Heat Shock Factor 1', *Molecular and Cellular Biology,* 33 (24), 4889-99.
Wang, Jing, et al. (2012a), 'Selective photothermal therapy for breast cancer with targeting peptide modified gold nanorods', *Dalton Transactions,* 41 (36), 11134-44.
Wang, Junyun, et al. (2015), 'Insulin-like growth factor binding protein 5 (IGFBP5) functions as a tumor suppressor in human melanoma cells', *Oncotarget,* 6 (24), 20636-49.
Wang, Kewei and Lin, Bingliang (2013), 'Inhibitor of apoptosis proteins (IAPs) as regulatory factors of hepatic apoptosis', *Cellular Signalling,* 25 (10), 1970-80.

Wang, L. S., Chuang, M. C., and Ho, J. A. (2012b), 'Nanotheranostics--a review of recent publications', *Int J Nanomedicine,* 7, 4679-95.
Wang, S., Yu, H., and Wickliffe, J. K. (2011a), 'Limitation of the MTT and XTT assays for measuring cell viability due to superoxide formation induced by nano-scale TiO2', *Toxicol In Vitro,* 25 (8), 2147-51.
Wang, Shuguang, et al. (2008), 'Challenge in Understanding Size and Shape Dependent Toxicity of Gold Nanomaterials in Human Skin Keratinocytes', *Chemical physics letters,* 463 (1-3), 145-49.
Wang, Sihong, Diller, Kenneth R., and Aggarwal, Shanti J. (2004), 'Kinetics Study of Endogenous Heat Shock Protein 70 Expression', *Journal of Biomechanical Engineering,* 125 (6), 794-97.
Wang, X., et al. (2014b), 'HSP27, 70 and 90, anti-apoptotic proteins, in clinical cancer therapy (Review)', *Int J Oncol,* 45 (1), 18-30.
Wang, Yucai, et al. (2013b), 'A Comparison Study of Gold Nanohexapods, Nanorods, and Nanocages for Photothermal Cancer Treatment', *ACS nano,* 7 (3), 2068-77.
Wang, Z., et al. (2013c), 'The role of mitochondria-derived reactive oxygen species in hyperthermia-induced platelet apoptosis', *PLoS One,* 8 (9), e75044.
Wang, Zhenjia, et al. (2011b), 'Targeting of Nanoparticle-Complexed Drugs across the Vascular Endothelial Barrier via Caveolae', *IUBMB life,* 63 (8), 659-67.
Watanabe, M., et al. (2013), 'Effects of Fe3O4 Magnetic Nanoparticles on A549 Cells', *Int J Mol Sci,* 14 (8), 15546-60.
Wei, A., et al. (2013), 'Gold nanoparticles (GNPs) as multifunctional materials for cancer treatment', 349-89e.
Weissleder, R. (2001a), 'A clearer vision for in vivo imaging', *Nat Biotechnol,* 19 (4), 316-7.
Weissleder, Ralph (2001b), 'A clearer vision for in vivo imaging', *Nat Biotech,* 19 (4), 316-17.
Weiswald, Louis-Bastien, Bellet, Dominique, and Dangles-Marie, Virginie (2015), 'Spherical Cancer Models in Tumor Biology()', *Neoplasia (New York, N.Y.),* 17 (1), 1-15.
Welch, W. J. and Suhan, J. P. (1985), 'Morphological study of the mammalian stress response: characterization of changes in cytoplasmic organelles, cytoskeleton, and nucleoli, and appearance of intranuclear actin filaments in rat fibroblasts after heat-shock treatment', *J Cell Biol,* 101 (4), 1198-211.
Werneburg, Nathan W., et al. (2012), 'Tumor Necrosis Factor-related Apoptosis-inducing Ligand (TRAIL) Protein-induced Lysosomal Translocation of Proapoptotic Effectors Is Mediated by Phosphofurin Acidic Cluster Sorting Protein-2 (PACS-2)', *The Journal of Biological Chemistry,* 287 (29), 24427-37.
Westphal, Dana, et al. (2011), 'Molecular biology of Bax and Bak activation and action', *Biochimica et Biophysica Acta (BBA) - Molecular Cell Research,* 1813 (4), 521-31.
White, Michael G., et al. (2012), 'Mitochondrial dysfunction induced by heat stress in cultured rat CNS neurons', *Journal of Neurophysiology,* 108 (8), 2203-14.
Wicki, A., et al. (2015), 'Nanomedicine in cancer therapy: challenges, opportunities, and clinical applications', *J Control Release,* 200, 138-57.
Wickramasinghe, N. S., et al. (2005), 'Hypoxia alters cathepsin B / inhibitor profiles in oral carcinoma cell lines', *Anticancer Res,* 25 (4), 2841-9.
Wilhelm, Claire and Gazeau, Florence (2008), 'Universal cell labelling with anionic magnetic nanoparticles', *Biomaterials,* 29 (22), 3161-74.
Willers, Henning, et al. (2013), 'Basic Mechanisms of Therapeutic Resistance to Radiation and Chemotherapy in Lung Cancer', *Cancer journal (Sudbury, Mass.),* 19 (3), 200-07.

Willis, Simon N., et al. (2007), 'Apoptosis Initiated When BH3 Ligands Engage Multiple Bcl-2 Homologs, Not Bax or Bak', *Science,* 315 (5813), 856.
Wills, John W., et al. (2016), 'Genetic toxicity assessment of engineered nanoparticles using a 3D in vitro skin model (EpiDerm™)', *Particle and Fibre Toxicology,* 13 (1), 50.
Winter, Evelyn, et al. (2014), 'Involvement of extrinsic and intrinsic apoptotic pathways together with endoplasmic reticulum stress in cell death induced by naphthylchalcones in a leukemic cell line: Advantages of multi-target action', *Toxicology in Vitro,* 28 (5), 769-77.
Wissing, M. D. (2015), 'Chemotherapy- and irradiation-induced bone loss in adults with solid tumors', *Curr Osteoporos Rep,* 13 (3), 140-5.
Wood, William C. (2007), 'Breast surgery in advanced breast cancer: Local control in the presence of metastases', *The Breast,* 16, Supplement 2, 63-66.
Workman, P. and Powers, M. V. (2007), 'Chaperoning cell death: a critical dual role for Hsp90 in small-cell lung cancer', *Nat Chem Biol,* 3 (8), 455-7.
Wu, Qiong, et al. (2015), 'Quantum dots decorated gold nanorod as fluorescent-plasmonic dual-modal contrasts agent for cancer imaging', *Biosensors and Bioelectronics,* 74, 16-23.
Wu, X., et al. (2013), 'The use of femto-second lasers to trigger powerful explosions of gold nanorods to destroy cancer cells', *Biomaterials,* 34 (26), 6157-62.
Wust, P., et al. (2006), 'Magnetic nanoparticles for interstitial thermotherapy--feasibility, tolerance and achieved temperatures', *Int J Hyperthermia,* 22 (8), 673-85.
Wyld, L., Audisio, R. A., and Poston, G. J. (2015), 'The evolution of cancer surgery and future perspectives', *Nat Rev Clin Oncol,* 12 (2), 115-24.
Xia, Tian, et al. (2006), 'Comparison of the Abilities of Ambient and Manufactured Nanoparticles To Induce Cellular Toxicity According to an Oxidative Stress Paradigm', *Nano Letters,* 6 (8), 1794-807.
Xie, H. N., et al. (2013), 'Synthesis and NIR optical properties of hollow gold nanospheres with LSPR greater than one micrometer', *Nanoscale,* 5 (2), 765-71.
Xing, Y., et al. (2014), 'Radiolabeled nanoparticles for multimodality tumor imaging', *Theranostics,* 4 (3), 290-306.
Xu, Xi-bin, et al. (2013), 'Tunable Nanoscale Confinement of Energy and Resonant Edge Effect in Triangular Gold Nanoprisms', *The Journal of Physical Chemistry C,* 117 (34), 17748-56.
Yallapu, M. M., et al. (2011), 'Multi-functional magnetic nanoparticles for magnetic resonance imaging and cancer therapy', *Biomaterials,* 32 (7), 1890-905.
Yamamoto, Shuhei, et al. (2015), 'Three-dimensional magnetic cell array for evaluation of anti-proliferative effects of chemo-thermo treatment on cancer spheroids', *Biotechnology and Bioprocess Engineering,* 20 (3), 488-97.
Yameen, Basit, et al. (2014a), 'Insight into nanoparticle cellular uptake and intracellular targeting', *Journal of Controlled Release,* 190, 485-99.
Yameen, Basit, et al. (2014b), 'Insight into nanoparticle cellular uptake and intracellular targeting', *Journal of controlled release : official journal of the Controlled Release Society,* 190, 485-99.
Yan, Biao (2011), 'Research progress on Livin protein: an inhibitor of apoptosis', *Molecular and Cellular Biochemistry,* 357 (1), 39-45.
Yan, S. Y., et al. (2014), 'Therapeutic mechanism of treating SMMC-7721 liver cancer cells with magnetic fluid hyperthermia using Fe2O3 nanoparticles', *Braz J Med Biol Res,* 0, 0.

Yang, Kai-Lin, et al. (2016), 'In vitro comparison of conventional hyperthermia and modulated electro-hyperthermia', *Oncotarget; Advance Online Publications: Page 4*.
Yang, Lingyan, et al. (2015), 'Photothermal Therapeutic Response of Cancer Cells to Aptamer–Gold Nanoparticle-Hybridized Graphene Oxide under NIR Illumination', *ACS Applied Materials & Interfaces,* 7 (9), 5097-106.
Yang, Qi-Heng and Du, Chunying (2004), 'Smac/DIABLO Selectively Reduces the Levels of c-IAP1 and c-IAP2 but Not That of XIAP and Livin in HeLa Cells', *Journal of Biological Chemistry,* 279 (17), 16963-70.
Yang, X., et al. (2012a), 'Hsp70 promotes chemoresistance by blocking Bax mitochondrial translocation in ovarian cancer cells', *Cancer Lett,* 321 (2), 137-43.
Yang, Xiaokui, et al. (2012b), 'Hsp70 promotes chemoresistance by blocking Bax mitochondrial translocation in ovarian cancer cells', *Cancer Letters,* 321 (2), 137-43.
Yang, Xifei, et al. (2010), 'SiO(2)nanoparticles induce cytotoxicity and protein expression alteration in HaCaT cells', *Particle and Fibre Toxicology,* 7, 1-1.
Yao, M., et al. (2015), 'Uptake of Gold Nanoparticles by Intestinal Epithelial Cells: Impact of Particle Size on Their Absorption, Accumulation, and Toxicity', *J Agric Food Chem,* 63 (36), 8044-9.
Ye, T., et al. (2016), 'Synthesis and optical properties of gold nanorods with controllable morphology', *J Phys Condens Matter,* 28 (43), 434002.
Yin, Perry T., Shah, Birju P., and Lee, Ki-Bum (2014), 'Combined magnetic nanoparticle-based microRNA and hyperthermia therapy to enhance apoptosis in brain cancer cells', *Small (Weinheim an der Bergstrasse, Germany),* 10 (20), 4106-12.
Yoo, D., et al. (2013), 'Magnetically triggered dual functional nanoparticles for resistance-free apoptotic hyperthermia', *Angew Chem Int Ed Engl,* 52 (49), 13047-51.
Yoo, M. K., et al. (2007), 'Superparamagnetic iron oxide nanoparticles coated with galactose-carrying polymer for hepatocyte targeting', *J Biomed Biotechnol,* 2007 (10), 94740.
You, Ying, et al. (2016), 'Silica-coated triangular gold nanoprisms as distance-dependent plasmon-enhanced fluorescence-based probes for biochemical applications', *Nanoscale,* 8 (42), 18150-60.
Yu, B., et al. (2010), 'Receptor-targeted nanocarriers for therapeutic delivery to cancer', *Mol Membr Biol,* 27 (7), 286-98.
Yu, L., et al. (2014), 'Evaluation of hyperthermia of magnetic nanoparticles by dehydrating DNA', *Sci Rep,* 4, 7216.
Yu, M., et al. (2012a), 'Dextran and polymer polyethylene glycol (PEG) coating reduce both 5 and 30 nm iron oxide nanoparticle cytotoxicity in 2D and 3D cell culture', *Int J Mol Sci,* 13 (5), 5554-70.
Yu, Miao, et al. (2012b), 'Dextran and Polymer Polyethylene Glycol (PEG) Coating Reduce Both 5 and 30 nm Iron Oxide Nanoparticle Cytotoxicity in 2D and 3D Cell Culture', *International Journal of Molecular Sciences,* 13 (5), 5554-70.
Zagar, T. M., et al. (2010), 'Hyperthermia combined with radiation therapy for superficial breast cancer and chest wall recurrence: a review of the randomised data', *Int J Hyperthermia,* 26 (7), 612-7.
Zanoni, M., et al. (2016), '3D tumor spheroid models for in vitro therapeutic screening: a systematic approach to enhance the biological relevance of data obtained', *Sci Rep,* 6, 19103.

Zeng, L., et al. (2012), 'Death receptor 6 induces apoptosis not through type I or type II pathways, but via a unique mitochondria-dependent pathway by interacting with Bax protein', *J Biol Chem,* 287 (34), 29125-33.
Zhang, Guandong, et al. (2012), 'Tunability and stability of gold nanoparticles obtained from chloroauric acid and sodium thiosulfate reaction', *Nanoscale Research Letters,* 7 (1), 337.
Zhang, Jian-fu, et al. (2016), 'Molecular mechanisms of synergistic induction of apoptosis by the combination therapy with hyperthermia and cisplatin in prostate cancer cells', *Biochemical and Biophysical Research Communications,* 479 (2), 159-65.
Zhang, Junran and Powell, Simon N. (2005), 'The Role of the BRCA1 Tumor Suppressor in DNA Double-Strand Break Repair', *Molecular Cancer Research,* 3 (10), 531.
Zhang, Liangxuan, Pelech, Steven, and Uitto, Veli-Jukka (2004), 'Bacterial GroEL-like heat shock protein 60 protects epithelial cells from stress-induced death through activation of ERK and inhibition of caspase 3', *Experimental Cell Research,* 292 (1), 231-40.
Zhang, S., Gao, H., and Bao, G. (2015), 'Physical Principles of Nanoparticle Cellular Endocytosis', *ACS Nano,* 9 (9), 8655-71.
Zhang, Shiwen, et al. (2014), 'Photothermolysis mediated by gold nanorods modified with EGFR monoclonal antibody induces Hep-2 cells apoptosis in vitro and in vivo', *International Journal of Nanomedicine,* 9, 1931-46.
Zhang, Weiqi, et al. (2013a), 'Trafficking of Gold Nanorods in Breast Cancer Cells: Uptake, Lysosome Maturation, and Elimination', *ACS Applied Materials & Interfaces,* 5 (19), 9856-65.
Zhang, Yue and Calderwood, Stuart K. (2011), 'Autophagy, Protein Aggregation and Hyperthermia: A Minireview', *International journal of hyperthermia : the official journal of European Society for Hyperthermic Oncology, North American Hyperthermia Group,* 27 (5), 409-14.
Zhang, Z., Wang, J., and Chen, C. (2013b), 'Gold nanorods based platforms for light-mediated theranostics', *Theranostics,* 3 (3), 223-38.
Zhao, J., Wallace, M., and Melancon, M. P. (2014), 'Cancer theranostics with gold nanoshells', *Nanomedicine (Lond),* 9 (13), 2041-57.
Zhao, Qing-Li, Fujiwara, Yoshisada, and Kondo, Takashi (2006), 'Mechanism of cell death induction by nitroxide and hyperthermia', *Free Radical Biology and Medicine,* 40 (7), 1131-43.
Zharov, Vladimir P., Galitovsky, Valentin, and Viegas, Mark (2003), 'Photothermal detection of local thermal effects during selective nanophotothermolysis', *Applied Physics Letters,* 83 (24), 4897-99.
Zheng, J. H., et al. (2015), 'Discoveries and controversies in BCL-2 protein-mediated apoptosis', *FEBS J*.
Zheng, Janet H., et al. (2016), 'Discoveries and controversies in BCL-2 protein-mediated apoptosis', *The FEBS Journal,* 283 (14), 2690-700.
Zhou, Feifan, Yang, Ying, and Xing, Da (2011), 'Bcl-2 and Bcl-xL play important roles in the crosstalk between autophagy and apoptosis', *FEBS Journal,* 278 (3), 403-13.
Zhuang, L., et al. (2015), 'Inhibition of livin expression suppresses cell proliferation and enhances chemosensitivity to cisplatin in human lung adenocarcinoma cells', *Mol Med Rep,* 12 (1), 547-52.
Zunino, B., et al. (2016), 'Hyperthermic intraperitoneal chemotherapy leads to an anticancer immune response via exposure of cell surface heat shock protein 90', *Oncogene,* 35 (2), 261-8.